

# Journal of Marine Technology and Environment

---

Vol.I, year 2010



**ISSN 1844-6116**

**YEAR III, 1/2010**  
**ISSN 1844 – 6116**  
**JOURNAL OF MARINE TECHNOLOGY AND ENVIRONMENT**

This Journal has been founded in 2008 as a biannual publication of  
Constanta Maritime University/ROMANIA

#### **TOPICS**

- Marine Science and Engineering
- Marine Environmental Issues
- Marine Renewable Energy and Sustainability
- Maritime Safety
- Marine Chemistry
- Marine Corrosion and Material Science
- Ship Design, Building Technologies
- Ocean Engineering
- Advanced Technologies for MET
- Advances in numerical methods for marine engineering
- Algorithms for multidisciplinary problems in marine engineering and other related topics

#### **Editor in Chief**

Feiza MEMET (Constanta Maritime University/ROMANIA)

#### **Associate Editors**

Prof.Dumitru DINU, Ph.D. (Constanta Maritime University/ROMANIA)  
Prof. Nicolae BUZBUCHI, Ph.D. (Constanta Maritime University/ROMANIA)  
Prof. Ricardo Rodriguez - MARTOS DAUER, Ph.D. (Departament de Ciencia I Enginyeria Nautiques/ Universitat Politecnica de Catalunya/SPAIN)  
Prof. Osman Kamil SAG, Ph.D. (Piri Reis University/TURKEY)  
Prof. Suleyman OZKAYNAK, Ph.D. (Piri Reis University/TURKEY)  
Prof. Boyan Kirilov MEDNIKAROV, Ph.D. (Naval Academy "Nikola Y Vaptsarov"/BULGARIA)  
Prof. Amable LOPEZ, Ph.D. (Universidad Politecnica de Madrid/SPAIN)  
Prof. Takeshi NAKAZAWA, Ph.D. (World Maritime University/SWEDEN)  
Prof. Razvan TAMAS, Ph.D. (Constanta Maritime University/ROMANIA)  
Prof. Radu MIHALCEA, PH.D. (University of Illinois at Chicago/USA)  
Prof. Gheorghe SAMOILESCU, Ph.D. ("Mircea cel Batrin" Naval Academy/ROMANIA)  
Prof. Remus ZAGAN, Ph.D. ("Ovidius" University of Constanta/ROMANIA)  
Prof. Adriana Teodora MANEA, Ph.D. ("Ovidius" University of Constanta/ROMANIA)

#### **Editorial Secretary**

Ass.Prof Alexandra NITA, Ph.D. (Constanta Maritime University/ROMANIA)  
Ass.Prof.Louis DUMITRACHE, Ph.D. (Constanta Maritime University/ROMANIA)  
Ass.Prof Liviu STAN, Ph.D. (Constanta Maritime University/ROMANIA)  
Ass.Prof Mihaela Barhalescu, Ph.D. (Constanta Maritime University/Romania)

**Secretariate:** Toma Anisoara  
Radu Mirela

**Scientific Board**

Cornel PANAIT (Constanta Maritime University/ROMANIA)  
Paul BOCANETE (Constanta Maritime University/ROMANIA)  
Eugen BARSAN (Constanta Maritime University/ROMANIA)  
George CARUNTU (Constanta Maritime University/ROMANIA)  
Emil OANTA (Constanta Maritime University/ROMANIA)  
Darie TUDOR (Constanta Maritime University/ROMANIA)  
Laurentiu Claudiu MANEA ("Ovidius" University of Constanta/ROMANIA)  
Titi TURCOIU (Romanian-American University/ROMANIA)  
Marin NEDEV (Naval Academy "Nikola Y. VAPTSAROV"/BULGARIA)  
Chavdar ALEXANDROV (Naval Academy "Nikola Y. VAPTSAROV"/BULGARIA)  
Marcel la CASTELLS i SANABRA (Departament de Ciència i Enginyeria Nautiques/Universitat Politecnica de Catalunya/ SPAIN)  
Santiago ORDAS JIMENES (Departament de Ciència i Enginyeria Nautiques/Universitat Politecnica de Catalunya/SPAIN)  
Francesc Xavier MARTINEZ DE OSES (Departament de Ciència i Enginyeria Nautiques/Universitat Politecnica de Catalunya/SPAIN)  
Teresa J.LEO (Universidad Politecnica de Madrid /SPAIN)  
Miguel Angel HERREROS (Universidad Politecnica de Madrid /SPAIN)  
Michael BALDAUF (World Maritime University /SWEDEN)  
Nikolay Angelov ANGELOV (Naval Academy "Nikola Y Vaptsarov"/BULGARIA)  
Blagovest Chanev BELEV (Naval Academy "Nikola Y Vaptsarov"/BULGARIA)  
Ivan Enchev IVANOV (Naval Academy "Nikola Y Vaptsarov"/BULGARIA)  
Nikolai Zhelev KOLEV (Naval Academy "Nikola Y Vaptsarov"/BULGARIA)  
Bohos Rupen APRAHAMIAN (Naval Academy "Nikola Y Vaptsarov"/BULGARIA)

**JOURNAL ADDRESS**

**Journal of Marine Technology and Environment**

Constanta Maritime University, 104, Mircea cel Batran Street, 900663, Constanta,  
Romania

Tel: +40 241 664 740/ 107

Fax: +40 241 617 260

E-mail: [jmte@imc.ro](mailto:jmte@imc.ro)

<http://cmu-edu.eu/jmte/>

**EDITURA NAUTICA**

Constanta Maritime University  
Constanta Maritime University, 104, Mircea Cel Batran Street, 900663, Constanta, Romania

**CONTENTS**

1.	<b>STUDY REGARDING TO THE CORROSIVE ACTION OF THE SEA WATER IN THE SUPERFICIAL LAYERS</b> <sup>1</sup> BARHALESCU MIHAELA, <sup>1</sup> DUMITRACHE CONSTANTIN, <sup>1</sup> SABAU ADRIAN, <sup>1</sup> Constanta Maritime University, Romania.....	9
2.	<b>STRUCTURAL ANALYSES BY X-RAY DIFFRACTION OF SUPERFICIAL LAYERS OBTAINED BY SPARKING PROCESSES</b> <sup>1</sup> BARHALESCU MIHAELA, <sup>1</sup> DUMITRACHE CONSTANTIN, <sup>1</sup> SABAU ADRIAN, <sup>1</sup> Constanta Maritime University, Romania.....	15
3.	<b>OPTIMIZATION OF STATUSES AND HUMAN BEHAVIOUR IN STRESSFUL SITUATIONS BY THE SHIP</b> <sup>1</sup> BACALOV JANTCO, <sup>2</sup> BOYAN MEDNIKAROV, <sup>1</sup> Technical University, Varna, Bulgaria, <sup>2</sup> Nikola Y. Vaptsarov Naval Academy, Varna, Bulgaria.....	21
4.	<b>ENHANCED SIMULATION TECHNOLOGIES TO SUPPORT MARITIME OPERATIONAL RISK MANAGEMENT ONBOARD SHIPS</b> <sup>1</sup> BALDAUF MICHAEL, <sup>1</sup> JENS-UWE SCHRÖDER-HINRICHS <sup>2</sup> KNUD BENEDICT, <sup>2</sup> MATTHIAS KIRCHHOFF, <sup>2</sup> MICHAEL GLUCH <sup>1</sup> World Maritime University Malmö, Sweden, <sup>2</sup> Hochschule Wismar, ISSIMS Warnemünde, Germany.....	25
5.	<b>A POTENTIAL APPLICATION OF ARC FAULT CIRCUIT INTERRUPTERS IN SHIP ELECTRIC SYSTEMS</b> <sup>1</sup> BOHOS APRAHAMIAN, <sup>1</sup> LYUBOMIR DANKOV, <sup>1</sup> Nikola Vaptsarov Naval Academy, Varna, Bulgaria.....	39
6.	<b>STRUCTURAL AND KINEMATIC VIBRATION ON INTERNAL COMBUSTION ENGINE - PART I</b> <sup>1</sup> BUZBUCHI NICOLAE, <sup>1</sup> STAN LIVIU, <sup>2</sup> BERESCU SERBAN, <sup>1</sup> Constanta Maritime University, Romania, <sup>2</sup> Romanian Naval Authority, Romania.....	47
7.	<b>STRUCTURAL AND KINEMATIC VIBRATION ON INTERNAL COMBUSTION ENGINE - PART II</b> <sup>1</sup> BUZBUCHI NICOLAE, <sup>1</sup> STAN LIVIU, <sup>1</sup> MEMET FEIZA, <sup>1</sup> Constanta Maritime University, Romania.....	55
8.	<b>EXPLICIT DYNAMIC SIMULATION OF A PIPE DEBRIS PROJECTILE IMPACT OVER A NUCLEAR HEAVY WATER STORAGE VESSEL</b> <sup>1</sup> CALIMANESCU IOAN, <sup>2</sup> GRIGORESCU LUCIAN, <sup>1</sup> Saipem SpA Italy, <sup>2</sup> Constanta Maritime University, Romania.....	61

9.	<b>EXPLICIT DYNAMIC SIMULATION OF A SPACE DEBRIS PROJECTILE IMPACT OVER A SATELLITE STRUCTURE</b> <sup>1</sup> CALIMANESCU IOAN, <sup>2</sup> GRIGORESCU LUCIAN, <sup>1</sup> Saipem SpA Italy, <sup>2</sup> Constanta Maritime University, Romania.....	71
10.	<b>TRANSITORY PHENOMENONS INTO NAVAL ELECTRICAL EQUIPMENT</b> <sup>1</sup> DELIU FLORENȚIU, <sup>1</sup> BURLACU PAUL, <sup>1</sup> Naval Academy “Mircea cel Batran”, Constanta, Romania.....	81
11.	<b>INTERNATIONAL STANDARDS OF MARITIME ENGLISH AS A MEANS TO IMPROVE SAFETY AT SEA</b> DEMYDENKO N., Kyiv State Maritime Academy, Ukraine.....	91
12.	<b>DETERMINATION OF EXPLOATATION RESOURCES OF SUPPORTING GIRDER FROM RAILWAY</b> <sup>1</sup> DICHEV D., <sup>1</sup> TODOROV B. S., <sup>2</sup> DIMITROVA A. M., <sup>1</sup> LYUTSKANOV, G. K., <sup>1</sup> N.Y Vaptsarov Naval Academy - Varna, Bulgaria, <sup>2</sup> Technical University, Varna, Bulgaria.....	95
13.	<b>HE VELOCITY OF THE LOCK WATER LEVEL AT A LINEAR VARIATION OF THE FLOW IN THE FILLING (EMPTYING) CONDUIT</b> <sup>1</sup> DINU DUMITRU, <sup>1</sup> CUPSA OVIDIU SORIN, <sup>1</sup> Constanta Maritime University, Romania.....	101
14.	<b>SHIP MANOEUVRING BY PMM - MATHEMATICS AND EXPERIMENTS PART I, PART II</b> <sup>1</sup> GANEA B., <sup>1</sup> Safety At Sea Ltd., Glasgow, G2 5rl, U.K., Scotia.....	109
15.	<b>MATHEMATICAL PROPERTIES OF HYPERBOLIC CONSERVATION LAWS FOR SHALLOW WATERS</b> <sup>1</sup> GHERGHINA AUREL, <sup>2</sup> VLADU GABRIEL, <sup>1</sup> Military Staff, Romania, <sup>2</sup> Research Center for Navy, Romania.....	131
16.	<b>MECHANICAL PACKING (AXIAL SEAL WITH SLIDING RINGS) STUDY USING FINITE ELEMENT METHOD – WITH “ANSYS 9 - WORKBENCH” PROGRAM</b> <sup>1</sup> GRIGORESCU LUCIAN, <sup>1</sup> ZIDARU NICOLAE, <sup>1</sup> Constanta Maritime University, Romania.....	141
17.	<b>LASSIFICATION OF THE MARINE SIMULATOR EXERCISES (WORKING SCENARIOS)</b> HINEV VALENTIN, Nikola Vaptsarov Naval Academy, Bulgaria.....	149

18.	<b>DECK CADET AND “ON-LINE TRAINING” ON BOARD OF THE SHIP</b> IORDANOAIA FLORIN, Constanta Maritime University, Romania.....	159
19.	<b>MULTISTATIC SONAR PULSE SIGNALS TIME DELAY ESTIMATION</b> <sup>1</sup> KOLEV N. ZH., <sup>1</sup> IVANOV P. VL., <sup>1</sup> KALOYANCHEV P. ST. Naval Academy, Varna, Bulgaria.....	169
20.	<b>THERMODYNAMIC AND ECOLOGICAL ANALYSIS OF INTERNAL COMBUSTION ENGINES</b> MEMET FEIZA , Constanta Maritime University, Romania.....	181
21.	<b>A POINT OF VIEW ON THE REGASIFICATION OF LNG</b> MEMET FEIZA , Constanta Maritime University, Romania.....	187
22.	<b>FPGA IMPLEMENTATIONS OF CONSTANT FALSE ALARM RATE DETECTORS ( CFAR )</b> <sup>1</sup> MILANOV PETER, <sup>2</sup> ALEXANDROV CHAVDAR, <sup>1</sup> ZMD Bulgaria, <sup>2</sup> N. Vaptsarov Naval Academy, Bulgaria.....	191
23.	<b>MARINE DIESEL ENGINE ENERGY AND ECONOMICAL PARAMETERS DETERMINATION AFTER INDICATOR DIAGRAM DIGITAL PROCESSING</b> <sup>1</sup> MOSKOV JULIAN, <sup>1</sup> ZARKO ILIEV, <sup>1</sup> Naval Academy – Varna, Bulgaria.....	199
24.	<b>ENGINE ROOM SIMULATOR ERS4000 USE FOR ANALISIS OF ENERGY EFFICIENCY OF INTEGRATED SHIP ENERGY SYSTEM</b> <sup>1</sup> NEDEV MARIN, <sup>1</sup> ANGELOV NIKOLAJ, <sup>1</sup> PETKOV PETKO , <sup>1</sup> Nikola Vaptsarov Naval Academy, Varna, Bulgaria.....	205
25.	<b>ANALITIC METHOD FOR THE TEMPEREATURE DISTRIBUTION INSIDE THE CILINDER WALLS</b> <sup>1</sup> OMOCEA ION, <sup>2</sup> TURCOIU TITI, <sup>1</sup> Constanta Maritime University, Romania, <sup>2</sup> Romano-Americana University of Bucharest, Romania.....	213
26.	<b>THE SEAFARERS’S LONELINESS; A FACTOR OF RISK FOR MARITIME SAFETY</b> RODRÍGUEZ-MARTOS RICARDO, Universitat Politecnica de Catalunya, Spania.....	217
27.	<b>ANALYSIS OF TRANSIENT DIESEL- ENGINE</b> <sup>1</sup> SABAU ADRIAN, <sup>1</sup> BARHALESCU MIHAELA, <sup>1</sup> DUMITRACHE CONSTANTIN, <sup>1</sup> Constanta Maritime University, Romania.....	223

28.	<b>SIMULATION OF FUEL INJECTION PIPE PRESSURE</b> <sup>1</sup> SABAU ADRIAN, <sup>1</sup> DUMITRACHE CONSTANTIN, <sup>1</sup> BARHALESCU MIHAELA, <sup>1</sup> Constanta Maritime University, Romania.....	231
29.	<b>APPLIED RESEARCH AIMED AT DESIGNING THE OPTIMAL SOLUTION FOR A SUBMERSIBLE ELECTRIC GENERATOR</b> <sup>1</sup> SAMOILESCU GHEORGHE, <sup>2</sup> SERGIU NICOLAE, <sup>2</sup> DORIAN MARIN, <sup>3</sup> SERGHEI RADU, <sup>1</sup> BARBU ALINA , <sup>1</sup> “Mircea cel Batran” Naval Academy, Romania, <sup>2</sup> National Institute for Research and Development in Electrical Engineering,Romania, <sup>3</sup> Zodiac Company, Romania .....	237
30.	<b>NALYSIS OF ASYNCHRONOUS TRIPHASE ELECTRIC MOTORS USED IN AC PROPULSION SYSTEMS</b> <sup>1</sup> SAMOILESCU GHEORGHE, <sup>2</sup> SAMOILESCU ADELINA, <sup>3</sup> RADU SERGHEI, <sup>1</sup> CIZER LAURA, <sup>1</sup> “Mircea cel Batran” Naval Academy, Romania , <sup>2</sup> Politechnic University of Bucharest, Romania, <sup>3</sup> Zodiac Company, Romania.....	241
31.	<b>CONCEPTS OF REFRIGERATION CYCLES AND CRYOGENICS FOR LNG TANKERS</b> <sup>1</sup> STAN LIVIU, <sup>1</sup> BUZBUCHI NICOLAE, <sup>2</sup> BERESCU SERBAN, <sup>1</sup> Constanta Maritime University, Romania, <sup>2</sup> Romanian Naval Authority, Romania.....	249
32.	<b>INCOMPRESSIBLE MODELS AND LOW MACH NUMBER EXPANSIONS FOR SHALLOW WATERS</b> <sup>1</sup> VLADU GABRIEL, <sup>2</sup> GHERGHINA AUREL, <sup>1</sup> Research Center for Navy, Romania, <sup>2</sup> Military Staff, Romania.....	257
33.	<b>THE IMPACT ON EMISSIONS IN SW EUROPEAN SHORT SEA SHIPPING BASED ON MOPSEA EMISSION MODEL</b> <sup>1</sup> XAVIER MARTÍNEZ DE OSÉS F., <sup>1</sup> MARCEL-LA CASTELLS, <sup>1</sup> Universitat Politècnica de Catalunya, Spania.....	263

## STUDY REGARDING THE CORROSIVE ACTION OF THE SEA WATER IN THE SUPERFICIAL LAYERS

<sup>1</sup>BARHALESCU MIHAELA, <sup>1</sup>DUMITRACHE CONSTANTIN, <sup>1</sup>SABAU ADRIAN

<sup>1</sup>Constanta Maritime University, Romania

The experimental research was made on superficial layers laid-down through electrical sparking on the steel carbon OL 37 probes, the used electrode being made from a corrosion resistant material (Nickel). The corrosion resistance of the obtained experimental layers was determined through gravimetric method. The superficial layers subjected to the corrosion agent (see water) were analysed through optical microscopy, using the computers QX3 Intel Play microscope and through atomic force microscopy.

**Keywords:** corrosion, superficial layers, electrical discharge, nickel

### 1. INTRODUCTION

The superficial treatment through impulse electrical discharges is a procedure through which the properties of the metallic materials can be improved. Process consist in discharges (short period) and the erosion of the cathode takes place a transfer of erosion products on the treated surface.

The properties of the superficial layers obtained through this procedure are the same as the electrodes material being used or very close to this one, the properties resulting from micro alloying and the diffusion of the electrode material in the sample of steel [1].

### 2. EXPERIMENTAL RESEARCH

The experiments were done for the superficial treatment through impulse electrical discharges, made with the ELITRON 22A equipment, using Ni electrodes of some parallelepiped samples with the surfaces of 0,00127512 m<sup>2</sup>, from steel carbon OL 37 brand, the probes plane surfaces were previously prepared. Preparing the surfaces presumes a thorough treatment and degrease with a powerful solvent.

The treatment through electrical discharges were made manually, the active electrode is under a 60° angle with the treated surface.

When making treatment with electrical discharges, a significant importance in the formation of the superficial layer and the quality, has the electrode section surface, influence that will be manifested at the working regime temperature variation and at the current density which passes through the electrode.

In the experiments wasn't specified the electrode vibration amplitude value because this does not influence neither the layer thickness, or the structure, the only importance is to be big enough to prevent the solder of the electrode with the surface which will be treated.

In table 1 are presented the recommended values for the electrode cross section in regard to the work regime of the ELITRON – 22A equipment and the current value at every regime.

**Table 1 The recommended values for the electrode cross section**

Electric work regime ELITRON – 22A	1	2	3	4	5
Electrode cross section value [mm]	4	5	4 ÷ 6	5 ÷ 6	6 ÷ 9
Work current [A]	0,5	0,8	1,3	1,8	2,3

Through the corrosion research process using the gravimetric method, the parallelepiped samples superficial treated with electrical sparking, with the surface of 0,00127512 m<sup>2</sup> where suspended with an synthetic line (nylon) of  $\phi = 0,2\text{ mm}$  in a plastic material tub at 4 cm above the tubes liquid level (see water), being immersed 285 days in static see water at the environments temperature [2].

The samples on which the superficial treatment was made through impulse electrical discharges where individually weighted on the analytic balance at different time intervals, determining the corrosion process speed.

$$v_{cor} = \frac{\Delta m}{S \cdot t}$$

where:  $v_{cor}$  - rate of corrosion  $[g \cdot m^{-2} \cdot day^{-1}]$ ;  
 $\Delta m$  - variation weight  $[g]$ ;  
 $S$  – samples surfaces in contact with see water  $[m^{-2}]$ ;  
 $t$  – time of exposure  $[days]$ .

The research of superficial layers processed with electrical sparking using CuSn10 electrode, immersion 285 days in see water was realized through optical microscopy using QX3 Intel play Computer microscope at 60:1 enlarge power.

The fine determining of the topography surfaces exposed to the action of the corrosive environment was made using the atomic force microscope (AFM).

### 3. RESULTS AND DISCUSSION

The speed corrosion variation results from immersed samples in sea water (285 days), is presented in figure 1.

The samples from OL 37 carbon steel sparking with Ni electrode are corrosion resistant, having the estimated scale of 4 (according to STAS 9684-82), the corrosion speed between

0.21 – 1.0 g/(m<sup>2</sup>.day) in comparison to the steel used as original probe which has the estimated scale 5, and the corrosion speed between 1.0 – 2.1 g/(m<sup>2</sup>.day) [3].

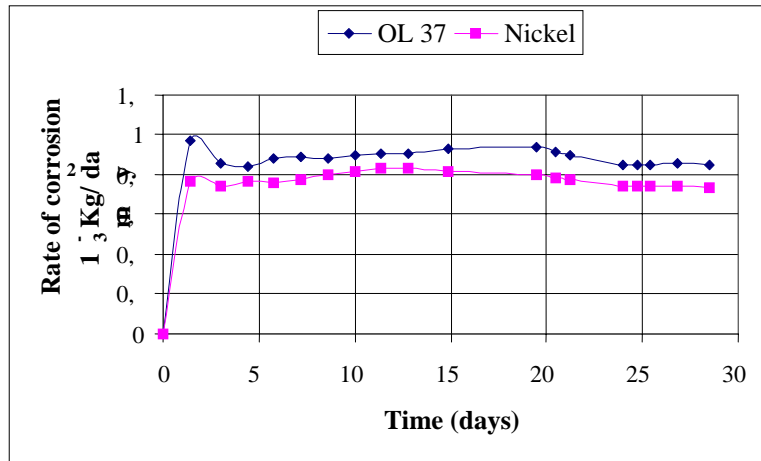


**Fig. 1. Rate of corrosion**

In the first stages of corrosion (0-30 days) corrosion rate increases rapidly and corrosion test results in the short term are inconclusive for the long term corrosion. On the superficial layers subjected to see water, initially you can observe a progressive increase of the corrosion speed, because of the oxygen absorption. After the effect of microorganism, the corrosion drops to an almost stationary value. This is because of the fact that microorganisms eliminate oxygen from the surfaces, but a anaerobic corrosion still persists.

The superficial layers subjected to the corrosion agent (sea water) where analysed through optical microscopy, using the computers QX3 Intel Play microscope and through atomic force microscopy.

The optical metallographic analyses of the original probe from OL 37 steel and sample sparked with nickel electrode are present in figure 2 and 3.

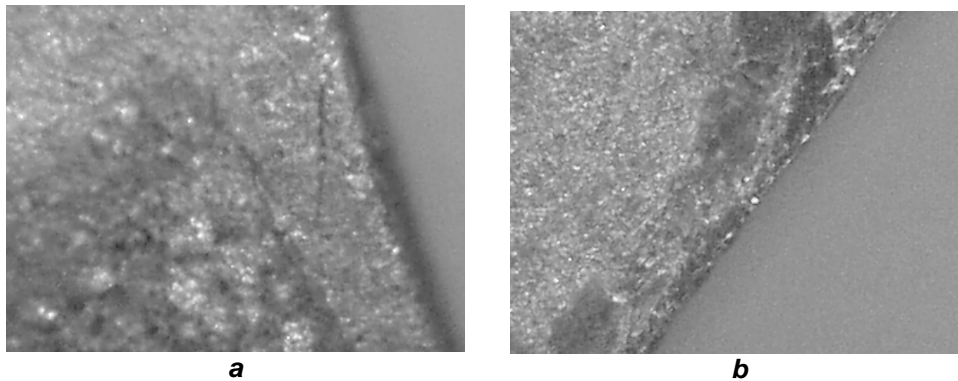


**Fig. 2. OL 37 sample steel - 60:1**

On the original probe from OL 37 steel we can observe corrosion products (iron oxides); it has brown color (figure 2, a). On the side of the sample appear the reaction products, which are blue color (figure 2, b).

Level differences on the surface could be observed as result of the cleaning the corrosion products from the sample.

When used nickel electrode to obtained a compact deposition with few corrosion product which are in brown color zones (figure 3, a).

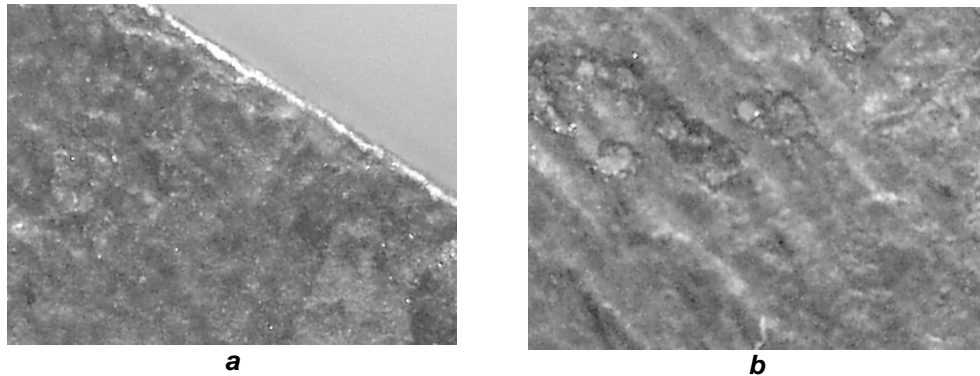


**Fig. 3. OL 37 steel samples sparked with Ni electrode – 60:1  
Work regime 2 - 60:1**

The sample sparked with nickel electrode leads to a uniform superficial layers which good corrosion protection (figure 3, a).

In this sample can be seen that after electrical sparking deposition were obtained zones with a compact layer without discontinuities.

Homogenous structure of the superficial layer leads to the formation of craters corrosion zones (figure 3, b) where the superficial layer has surface defects (pores, discontinuities) and allowed the corrosive agent to attack the base material.

The “wave-mode” from the AFM microscope on the probes superficial treated with the Ni electrode present the surface relief through color tone. The light color zones are the highest ones.

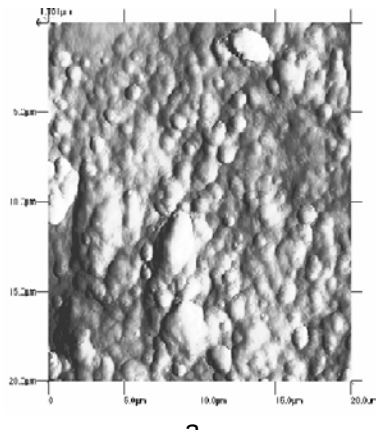


**Fig. 4. Superficial treated sample with Nil electrode**

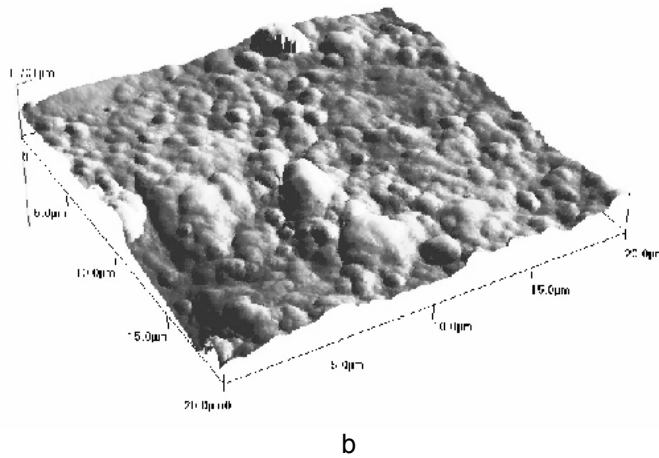


**Fig. 4. Superficial treated sample with Ni electrode**  
**a. "wave mode" image – 2d on an scanned area of 20x20 μm**  
**b. "wave mode" image – 3d on an scanned area of 20x20 μm**

The images presented in figure 4 accentuate the facts that, after the corrosion process in sea water, the deposition layers does not degrade.

The AFM wave mode images on superficial layers obtained from sparking with nickel electrode after the exposure to the corrosive environment action highlight some islands and formations compact from material deposited.

Figure 4,b shows appearance of dark zones that represent points with the lowest height, the difference between the lowest and highest zones reaching value 1.701 μm.

Histogram relief sample surface (figure 5) sparking with Ni electrode shows an uneven layer deposition and possible penetration by corrosive agent to the basic material.

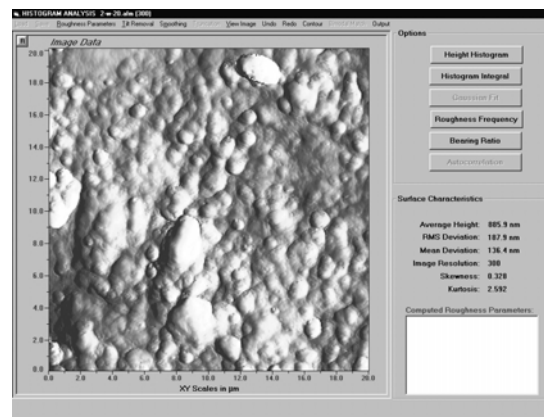


**Fig. 5. The histogram of the untreated probe surface profile after the exposure to the action of the corrosive environment in the same conditions as the superficial treated probes**

#### 4. CONCLUSIONS

The superficial layer laid through Ni electrode sparking a improved corrosion resistance to see water compared to the base steel, at long terms tries the corrosion speed is stabilizing remaining almost constant.

After the optical metallographic analysis on the superficial layers, after the contact with the corrosion agent could be observed zones where the deposited layers is uniform and the corrosion agent could not interact with the basic material, so in these zones is not any effect on the corrosion process.

The investigations through atomic force microscopy made on the samples tested for long term corrosion, accentuate the compact and homogenous surfaces areas, which had not permitted the corrosive agent to interact with the base material.

The wave-mode images present the discontinuities of the superficial laid layers, which represent a possible access way in for the corrosive agent to the samples material.

#### REFERENCES

- [1]. Barhalescu M. - *Cercetari privind obtinerea si analiza structurala a straturilor metalice subtiri rezistente la coroziune*, Teză de doctorat, Facultatea "Știința și Ingineria Materialelor" Iași, 2007;
- [2]. Barhalescu M., Pascu R., Dinescu M. - *Corrosion Protection of Metallic Surfaces by Processing with Impulse Electrical Discharges, Protective coatings and thin films 07* of E-MRS 2007 Spring Meeting, 28 May-1 June, Strasbourg
- [3]. Barankova H., Bardos L., Berg S. - *Surface and Coatings Technology*, No. 94-95, 1997
- [4]. Boian R. - *Corrosion Tests and Standard: Application and Interpretation, ASTM Publication*. 2 nd edition., 2004
- [3]. Zolotih. B. N., Melider. R.R. - *Fiziceskie osnovielektroerozionnoi*, Masinostroenie, Moskva
- \*\*\* *Ustanovska ELITRON 22*, Academia Nauk, Chisinau,1991

## STRUCTURAL ANALYSES BY X-RAY DIFFRACTION OF SUPERFICIAL LAYERS OBTAINED BY SPARKING PROCESSES

<sup>1</sup>BARHALESCU MIHAELA, <sup>1</sup>DUMITRACHE CONSTANTIN, <sup>1</sup>SABAU ADRIAN

<sup>1</sup>Constanta Maritime University, Romania

The superficial layers obtained using electrical discharge technology in impulses is part of surfaces engineering domain.

In this paper we analyze phase quality using X-ray diffraction on superficial layers after the sparking process with wolfram, titanium and aluminum and graphite electrode.

The phase quality analyses through X-ray diffraction for deposition layers with electrical discharge method using wolfram, titanium, aluminum and graphite electrodes on non alloy steel samples suppose the obtain and interpretation of diffraction graphics.

**Keywords:** superficial layers, electrical discharge technology in impulses, X-ray diffraction

### 1. INTRODUCTION

The efficient and rational use of metallic materials is a problem of present interest in most factories. The superior capitalization of metallic materials into products is obtained by application of the most efficient bulk – and/or surface – thermal treatments.

In most cases, the pieces are made by carbon steel and in some cases by irons.

In order to increase the wear resistance and the hardness, major properties of pieces, these are subject to superficial hardening treatments: thermal (superficial chilling), thermo chemical treatments.

For some purpose of increasing the endurance of pieces intensely subject to wear, in the last time a series of unconventional superficial treatments with laser beams and, last but not the least, the PVD and CVD. All these methods confer very high hardness to superficial layers, yielding to a considerable enhancement of the treated piece lifetime.

An important disadvantage of these treatments is the high-price since expensive installations and devices are needed. In the field of surface engineering a new kind of superficial thermal treatment of micro alloying and spark deposition was imposed. Some tests it was made of naval steel.

### 2. EXPERIMENTAL RESEARCH

The structure investigations will be made with X-rays diffraction techniques. This kind of techniques has two components, both are as important: experimental system configuration and the theoretical model for experimental data interpretation. In many case, the fine structure investigations use diffractometric technique with goniometric montage Bragg - Bretano type.

X-ray diffraction, in classic theory, means the interference between electromagnetic waves with waves of length situated within 0.5 – 3.0 Å domain. The interference of waves is produced if they are coherent, then in one direction their phase difference is an integer (number) from  $2\pi$  radians or the wave's way difference is a number of wave lengths. This condition is known as Bragg equation law and has the expression:

$$2d_{hkl}\sin\Theta_i = n\lambda \quad (1)$$

Where:

$d_{hkl}$  is distance between two planes with (hkl) indexes;

$\Theta_i$  is diffraction angle;

$N$  is diffraction order;

$\lambda$  is wave's length for X radiation.

Crystalline phases analysis using X – ray diffraction has the following aspects:

- a. each structure phase will generate a specific diffraction specter because each has its own crystalline network.
- b. geometric form and intensity of diffraction maximums depends on the structure factors and on the phase quantity which generates the maximums.

The diffraction image of metallic sample, polyphases, will be the result of diffraction specters, produced from components phases overlap.

The most used method for quality structure analysis is the comparison of information between the analyzed structure extracted from sample diffractogram (the image of diffraction) and well known crystalline substances, organized in data bases. Usually diffractometers are used for recording of diffraction results. The investigations for superficial layers obtained by using electrical discharge method was made with DRON 3 diffractometer which has a radiation tube with molybdenum anode, under the following working conditions: radiation  $Mo K_{\alpha}$ , with  $\lambda_{Mo} = 0.7107 \text{ \AA}$ ; the acceleration tension on the tube: 40 KV; cathode current supply: 15 mA; sample rotation speed:  $\omega_1 = 4^\circ/\text{min}$  inscription band speed: 1800 mm/h; working slit: 1 mm and 0.5 mm.

The determinations were made on plane surfaces 20x20 mm, of the samples sparking with W, Ti, Al and graphite electrodes.

By using Bragg equation it was determined that the structure interplanes distances, which was generated by the diffraction maximums and the crystalline phases which compose the superficial layers were identified.

### 3. RESULTS AND DISCUSSIONS

The qualitative analysis of phase by x-ray diffraction for superficial layers obtained by the electrical discharge method with W, Ti, Al and graphite electrodes requires obtaining and interpreting diffraction graphics as it results from OLC 45 samples.

Qualitative analysis using X – ray diffractions of obtained layers was made by using a radiation tube with Mo anode and  $\lambda_{Mo} = 0.7107 \text{ \AA}$  on DRON 3 diffractometer.

After the sparking process, new superficial layers were obtained by using 4 regimes an Elitron 22. Diffractometric analysis was made on these layers.

Diffraction dates obtained superficial layers as result of sparking process with W, Ti, Al and graphite electrodes are presented in tables 1,2,3,4.

Qualitative phase analysis using X rays on superficial layers obtained using sparking method with W electrode (table 1) shows the W existence in the layer (the maximum from  $2\Theta_1 = 18.48^\circ$ ,  $2\Theta_2 = 31.90^\circ$  and  $2\Theta_3 = 37.64^\circ$ ) close to C.V.C. structure phase and C.F.C. structure phase.

**Table 1 Diffraction dates obtained superficial layers as result of sparking process with W**

No. peack	$2\Theta_i$ [°]	$d_{hkl}$ calculated [Å]	$d_{hkl}$ standard [Å]	hkl	phase
1	16.88	2.420	2.410	110	Fe <sub>2</sub> N
2	18.48	2.213	2.230	110	W
3	19.93	2.050	2.010	110	M( $\alpha$ CVC)
4	22.48	1.820	1.794	200	A( $\gamma$ CFC)
5	28.33	1.450	1.428	200	M( $\alpha$ CVC)
6	31.90	1.290	1.290 1.268	311 220	W A( $\gamma$ CFC)
7	34.82	1.187	1.166	211	M( $\alpha$ CVC)
8	37.64	1.100	1.110	220	W

During the sparking process on the samples surface there is a melting of the material followed by a faster solidifications. If we consider the diffractometer result we can see that in superficial layers, after the processing using W electrode, martensite and residual austenite is to be found.

At  $2\Theta = 31.50^\circ$  angle there is an overlap on diffraction maximum generated from (211) planes from W, with maximum from (220) planes from  $\gamma$  phase (residual austenite).

We can mention that W can be dissolved in iron till at 7.16%, and then it will form a solid solution which as it grows the W percentage the C.V.C. network constant of the iron will grow. The present of W carbide in the layer it less probable; the W carbide does not appear in X ray diffraction.

Because the discharge between the sample and the electrode takes place in the air, the nitrogen is divided and will form nitrogen compounds in the superficial layers. In this case on diffractograms we can see the maximum at  $2\Theta = 16.88$  which corresponds to Fe<sub>2</sub>N compound, for  $d = 2.42 \text{ \AA}$  between crystalline planes with (110) (020) indexes.

Diffraction dates results in X-ray analysis of superficial layer as result of sparking with titanium electrode on steel sample OLC 45 is shown in table 2.

**Table 2 Diffraction dates obtained superficial layers as result of sparking process with Ti**

Nr. peack	$2\Theta_i$ [°]	$d_{hkl}$ calculated [Å]	$d_{hkl}$ standard [Å]	hkl	phase
1	19.52	2.09	2.09	101	Fe <sub>3</sub> N
2	19.96	2.05	2.01	110	M( $\alpha$ CVC)
3	22.80	1.797	1.794	200	A( $\gamma$ CFC)
4	32.55	1.267	1.261		Fe <sub>2</sub> Ti <sub>4</sub> O
5	33.14	1.246	1.240 1.268	103 220	Fe <sub>3</sub> N A( $\gamma$ CFC)
6	34.48	1.198	1.195	220	Fe <sub>2</sub> N
7	35.37	1.169	1.166	211	M( $\alpha$ CVC)
8	38.25	1.084	1.091	222	TiO <sub>2</sub>
9	39.00	1.06	1.01 1.04	220 202	M( $\alpha$ CVC) Fe <sub>3</sub> N

Superficial processing using titanium electrode in normal atmosphere is very difficult because the Ti interacts with the oxygen in the air, and the titanium oxides are formed very fast.

Then, after the sparking processed in the air using Ti electrode it is possible that it doesn't have free Ti. This was confirmed by diffractometric analysis (table 2) which shows the presence of the Ti oxide layer at  $2\Theta = 38.25^\circ$  with maximum from planes with crystallographic indexes (222) for  $d_{(222)} = 1.89 \text{ \AA}$ .

The diffraction dates from table 2 shows the presence in the layer structure of a new triple chemical compound  $\text{Fe}_2\text{Ti}_4\text{O}$  with a complex cubic structure which appears at  $2\Theta = 32.25^\circ$ . Close to these phases in superficial layer the presence of a "α" type phase with bigger network parameters was detected a phase which is in fact martensite and a "γ" type phase which is residual austenite.

The sparking in the air using Ti electrode when nitrogen is dissociated will determine the forming of the  $\text{Fe}_x\text{N}$  in superficial layer composition. In our sample case after analysis it was shown at angle position  $2\Theta = 19.52^\circ$  for interplanes distance calculated at  $d = 2.09$  Which corresponds to (101) planes. From these planes is the diffraction maximum and  $\text{Fe}_3\text{N}$  phase was identified characterized from interplanes distance  $d_{(101)} = 2.09 \text{ \AA}$ .  $\text{Fe}_x\text{N}$  characterized from diffraction maximum at different angle positions but on sample diffractogram this maximum does not appear or overlap with another diffraction maximum (at  $2\Theta = 33.14^\circ$  maximum for γ phase with  $\text{Fe}_3\text{N}$  compound is overlapped).

X ray diffraction analysis includes the samples from steel OLC 45 sparking with Al electrode. The dates of diffraction from one of these samples are presented in table 3.

**Table 3 Diffraction dates obtained superficial layers as result of sparking process with Al**

Nr. peack	$2\Theta_i$ [°]	$d_{hkl}$ calculated [Å]	$d_{hkl}$ standard [Å]	hkl	faza
1	14.07	2.895	2.89	100	FeAl
2	17.40	2.350	2.33	111	Al
3	20.06	2.04	2.02 2.01	200 110	Al M(α CVC)
4	22.64	1.813	1.794	200	A(γ CFC)
5	28.70	1.433	1.428	200	M(α CVC)
6	32.38	1.27	1.272 1.268	 220	 Fe <sub>2</sub> Al <sub>5</sub> A(γ CFC)
7	35.42	1.168	1.166	211	M(α CVC)
8	38.45	1.079	1.089	311	A(γ CFC)

The principal maximum from diffractogram are from Al and from C.V.C. type structure phase which due to the thermal regime applied to metallic material from superficial layer is martensite. Close to these maximums we can see at  $2\Theta = 14.07^\circ$  maximum for AlFe compound from the planes (100). The maximum which corresponds to "γ" phase (residual austenite) is weak but it can be seen at  $2\Theta_1 = 22.64^\circ$ ,  $2\Theta_2 = 32.38^\circ$  and also at  $2\Theta_3 = 38.45^\circ$ . At angle position  $2\Theta = 20.06^\circ$  where the most intense maximum appears of the diffractogram is an overlap of maximums of diffraction from "α" type phase from planes (110) from Al planes (200) and FeAl compound planes (220). On this diffractogram we can see maximum

of diffraction from compounds as  $Fe_xN$  type, even if the processing through electrical discharge that was made in the air.

The most complex diffractogram from the superficial layer series was recorded from the surface of OLC 45 steel sample processed with graphite electrode. The diffraction dates are presented in table 4.

**Table 4 Diffraction dates obtained superficial layers as result of sparking process with graphite**

Nr. peack	$2\Theta_i$ [°]	$d_{hkl}$ calculated [Å]	$d_{hkl}$ standard [Å]	hkl	faza
1	17.12	2.387	2.380	112	$Fe_3C$
2	18.16	2.251	2.260	200	$Fe_3C$
3	19.92	2.054	2.01 2.07	110 111	M( $\alpha$ CVC) A( $\gamma$ CFC)
4	20.60	1.987	1.971	211	$Fe_3C$
5	22.08	1.855	1.850	122	$Fe_3C$
6	22.70	1.805	1.794	200	A( $\gamma$ CFC)
7	23.21	1.766	1.759	212	$Fe_3C$
8	25.12	1.632	1.682	004	$Fe_3C$
9	26.04	1.577	1.583	130	$Fe_3C$
10	27.37	1.501	1.509	222	$Fe_3C$
11	28.75	1.431	1.428	200	M( $\alpha$ CVC)
12	31.24	1.319	1.327	230	$Fe_3C$
13	32.14	1.280	1.268	220	A( $\gamma$ CFC)
14	34.17	1.209	1.202	141	$Fe_3C$
15	35.45	1.164	1.166	211	M( $\alpha$ CVC)
16	36.99	1.120	1.126	330	$Fe_3C$
17	37.75	1.098	1.089	311	A( $\gamma$ CFC)
18	39.63	1.048	1.01	220	M( $\alpha$ CVC)

For the same angular domain  $2\Theta = 14^\circ - 40^\circ$ , the diffractogram has more diffraction maximums. Thirteen maximums were indicated which come from different cementite crystalline planes. In the layers structure this phase is predominant.

Close to cementite the presence of austenite was found at  $2\Theta = 19.81^\circ$ ,  $2\Theta = 22.70^\circ$ ,  $2\Theta = 32.14^\circ$ ,  $2\Theta = 37.75^\circ$ , and ferrite at  $2\Theta = 20.11^\circ$ ,  $2\Theta = 28.75^\circ$ ,  $2\Theta = 35.45^\circ$ .

The most evident maximum from  $2\Theta = 20^\circ$  is a composed maximum which contains "reflections" from (111) crystalline planes which correspond to austenite.

Because the diffractogram is very complicated it was not possible to identify the maximum from  $Fe_xN$  phases taking into consideration that these phase should appear in the layer.

As conclusion we can assert that after the sparking with graphite electrode on hypereutectoid steel this will harden superficially, as a consequence of a white cast iron layer on the surface of the processed sample that contains cementite

#### 4. CONCLUSIONS

X ray diffraction structural investigations show on diffraction graphics obtained from superficial layers a fund of abnormal radiation because of amorphous metallic material zones from layer structure.

Because in the superficial layer from steel with 0.45 %C the material thaws and is followed by an ultra rapid solidification. If we consider the diffractometric determinations, we will see martensite and residual austenite in the new formed layer.

The diffraction graphics obtained from the superficial layers sparking by Ti electrode don't show the Ti in the layer; this can be found just in combination with oxygen and iron ( $\text{Fe}_2\text{Ti}_4\text{O}$ ;  $\text{TiO}_2$ ).

On the diffractogram obtained from the graphite electrode sparking layer on steel sample a lot of maximums were identified belonging to cementite which explains the forming of white cast iron in new formed layer.

#### REFERENCES

- [1]. Alexandru A., Bulancea V., Pop D., Pop F., Alexandru A. – *Analiza fazica a aliajelor metalice*, Editura Cermi, Iasi, 1998
- [2]. Gheorghies C. – *Controlul structurii fine a metalelor cu radiatii X*, Editura Tehnica, Bucuresti, 1990
- [3]. Morton P.H., Bell T. – *Les procedes technologique des surfaces appliqués au titan, Traitement Thermique*, nr. 241, Paris, 1990
- [4]. Pauleau Y. – *Materials and processes for surface and Interface Engineering*, Kluwer Academic Publ, London, 1994
- [5]. Popescu N. – *Tratamente termice neconventionale*, Editura Tehnica, Bucuresti, 1990

## OPTIMIZATION OF STATUSES AND HUMAN BEHAVIOUR IN STRESSFUL SITUATIONS BY THE SHIP

<sup>1</sup>BACALOV JANTCO, <sup>2</sup>MEDNIKAROV BOYAN

<sup>1</sup>Technical University, Varna, Bulgaria, <sup>2</sup>Nikola Y. Vaptsarov Naval Academy, Varna, Bulgaria

Irrespective of a variety of stressful factors, psychologists study those consequences, which they cause on physiological, psychological and behavior levels. With rare exceptions, these consequences are negative. There are emotional shifts, the sphere is deformed motivation, the course of processes of recognition and thinking changes, the impellent and speech behavior is broken. There are bases to assert, that the influence of particularly strong disorganization on human activity by the ship is made with emotional stresses achieved degrees frustration. The force frustrations are the ones that are capable of breaking any other mental processes. Moreover, frustrations impose on man certain stereotyped ways „of an emergency output" from an extreme situation adequate to the form of the displayed frustration

Presumably, the optimization of the mental condition and behavior of each crew member in extreme situations should provide the appropriate psychological preparation. Otherwise, there is nothing to hope that the individual, staying in a stressful condition, will work rationally, vigorously, quickly, with perseverance.

**Keywords:** extreme situation; stress factors; crew; well-being; emotional shifts; frustration; practical importance

The psychology of extreme situations is one of dynamically developing directions of applied psychology. It investigates problems connected to rating, prediction in stressful situations. Taking into account the high probability of occurrence of stressful situations by the ships of the modern merchant marine fleet, it is necessary to pay appropriate attention to all accessible ways and mechanisms of management under conditions of crisis and risk.

Depending on the type of stress factor and the nature of its influence the modern science of psychology allocates various kinds of stress, in the most general classification - physiological and psychological which in turn, is subdivided into information and emotional. They both have their places in sea practice concerning the ship crew members in long sailing and their frequent being in hostile environment.

The information stress by the ship as a rule arises in situations of information overloads, for example when the captain, the log officer or the operator of technical control systems who bear the responsibility for consequences of the decisions made have no time to bring in corrective amendments, or correct their own mistakes or make the right decisions in due time.

The emotional stress usually takes place in situations menacing safety of the ship and each crew member as well as their economic well-being, social status, interpersonal relations (including family problems) etc.

Irrespective of a variety of stress factors, psychologists study those consequences, which they cause on physiological, psychological and behavior levels. With rare exceptions, these consequences are negative. In psychological science the evidence is presented to prove that usually there are emotional shifts, the sphere is deformed motivationally, the

course of processes of perception and thinking changes, the impellent and speech behavior is broken. Besides, the practice gives the bases to approve, that especially strong confusion that influences human activity by the ship is made with emotional stresses achieved degrees affect in one way or another (impulse, brake or generalization ). The effect of the forces is so strong that they are capable of breaking any other mental processes. Moreover, the effect imposes on the member of crew the certain stereotyped ways "of an emergency output" from an extreme situation appropriate to the form of displayed affect.

The assumption, that the optimization of mental statuses and behavior of each crew member in extreme situations should provide the appropriate psychological preparation is not perceived as deprived sense. Practice is convincing, that otherwise there is nothing to hope that the individual, staying in a stressful status, will work rationally, vigorously, fast and with perseverance.

In view of the unconditional practical importance of the problem it is necessary to note, that the psychology of extreme situations should have the appropriate status, for example at sea schools, both at selecting the future seamen, and during their complex professional preparation. Unfortunately, it is not always so. The offered report gives an opportunity to the readers who are familiar with sea business to make rather clear performance and about psychological features of activity of man in typical situations by the ship connected to difficulties and to increased danger to his existence.

Frequently the concept used concerning stress, "the extreme factors" assumes that they are not indifferent for the organism and for the human behavior. Occurrence of the special situations promotes revealing of adequacy or non-adequacy of functional and mental opportunities of the seaman during performance of different activities. For sea activity more often negative sensations are shown as a result of monotony, long sailing, constraints of conditions (in household, or in especially the professional plan), bad weather, approaching of powerful physical weariness, or occurrences of real threat to health and life from failures, malfunctions, disorganization etc. As rule aspirations of the psychologists to define what precisely limits physiological and psychological adaptation of transformations have had no success. This is largely due to the big and unequal opportunities of adaptation of man which complicate the definition of this limit. But, clear business, in reality is invalid to be guided on an extreme limit of existing organism, beginning of destruction.

Each limiting status of destruction is preceded by a number and an actability status, original protective mechanisms, directed to avoidance of action of the dangerous factor. In a number of these statuses it is possible to determine some kind of a secondary limiting status, in the middle between norm and illness. It can have gradation from poorly appreciable unpleasant sensations up to feeling intolerable overload and pains. It is necessary to note, that the concept "extreme conditions" covers all strong influences of environments which are taking place on endurance and inducing infringement of adaptation. The adaptation of man in many respects is determined by the existing adaptive psychological and physiological levels. The application is caused by the man concrete adaptive strategy.

Due to the process of adaptation the preservation homeostasis is achieved at interaction organism with the external world. In this connection processes of adaptation include not only optimization of functioning organism, but also maintenance of equation in the system "organism -environment"("organism - conditions of ability to live"). The process of adaptation is realized every time, when essential changes arise in the system "organism-environment" and provide the formation of a new status, which allows to achieve a peak efficiency of physiological functions and behavior reactions. As the organism and the environment are not in static or in dynamic balance, their parities vary constantly, and consequently, the process of adaptation is carried out constantly.

The above mentioned refers equally to both animals and men. However, the essential difference about the man is the main role during maintenance of the adequate relations in

the system "individual - environment", during which all parameters of system can change. Mental adaptation plays a special role here.

Mental adaptation is considered as a result of activity of complete self-controlled system (at a level "of operative rest"), emphasizing thus its system organization. But by such a consideration a picture remains incomplete. There will be the greatest possible satisfaction of urgent needs. Hence, the mental adaptation can be determined and as a process of establishing optimum conformity to the person and environments during realization of activity, peculiar to the man, which process allows an individual to satisfy urgent needs and in connection with them to realize the importance of the purpose, providing at the same time conformity to the maximal activity of man, its behavior, requirements of the environment.

The mental adaptation is a continuous process, which, alongside with the actual mental adaptation (that is maintenance mental homeostasis), includes two aspects: optimization of constant influence of an individual with an environment and establishment of adequate conformity between the mental and physiological characteristics.

The views of many authors on the essence of influence of psychological stress factor assume, that bringing to a stress situation results to the man of the requirements recognizing as outstripping of its opportunity to resist to overcome, to render resistance to survive, that conducts to distress. But it is also possible to apprehend stress factor as an opportunity to realize potential and thus to reach desirable consequences. Hence, it seems possible, to determine stress factor in connection with conformity of components of system "man - environment". The discrepancies of the requirements of environment to the man or man by environment conduct to distress, their satisfaction promotes occurrence eustress.

H. Selie for the first time has developed the concepts of intensity and specificity of the stress forming factors, specifying, that stress factor small intensity, not capable of causing stressful status, raises stability constitution to some or any other strong stress factor. In his opinion any stimulus, bringing to adaptivity reaction, has specific and non-specific action. However, growing on intensity the stress factor can cause generallity stress. During the development of the biological system on the basis precedents of collision about environment accumulates fund complexes of adaptive reactions.

Paramount event, inducing the change homeostasis\at the systems menacing with infringement of its integrity is a dangerous, extreme change of environment. Threshold of sensitivity to dangerous event is the sensitivity of system to minimally dangerous change of environment. Active reaction of system we can apprehend it reaction, directed to liquidation of danger of environment by liquidation of the carrier of danger or leaving from him (increase distances between it and reacting system). The reaction of adaptive system (man in an extreme situation) by expectation or disappearance of danger, or end of adaptive reorganization, as a result of which the dangerous factor will cease to be stimulated for the given system can be referred to as stability. Then more repeatedly there was a biological system with similar events, its adaptive opportunities for preservation of its integrity and resistance independently to influence of environment. Besides, it is necessary to note, that the dangerous changes of environment include active emotional - impellent protective reaction, and at impossibility events is included passive emotional - impellent reaction. If in the first case the vegetative system of man has secondary protective value, in the second case the significant activation vegetative of sphere gets primary value.

Naturally, there is a question: whether it is possible to overcome influences of stress forming factor of the purposeful psychology correction of work by systematic occurrences adaptability reactions of the specified type. It is known, that the experience in that sense is saved in the armed forces in many countries, but while the methodically proved system of psychological preparation of the seamen of civil fleet is not known to us.

The basic directions of psychological preparation of the experts (seamen) are: formation of the proved knowledge about real conditions of work, readiness for difficulty at work, increase of a level of psychological stability and endurance, development of unpretentiousness, moderation in desires and requirements; inculcation of trust to the administrative board, installation on the disciplined behavior, obedience, reduction of mental traumas, increase of a level of professional skills and physiological and psychological endurance.

The efficiency of the work done in many respects will depend on, as far as the principles of psychological modeling of an antagonism difficulties will be observed punctually; professional conditionality of the contents of psychological preparation to soluble tasks, safety of actions during performance of exercises and trainings. Besides, it is very important to observe psychological conformity of educational and real tasks; problematic of created educational situations.

Naturally there is a question - who will carry out similar substantial work on organization of psychological preparation and where? The experience gained so far in this area shows, that the productivity is higher on main faculty, at sea faculty, where the basic attention is focused on realization of the psychological analysis of kinds of professional activities; on the development of the recommendations for the formation of necessary professionally important qualities during study; on the development of psychological models of employment and development of the offers on creation of optimum levels of mental intensity of trained structure by means of imitation of the psychological factors of sea work.

Taking into account the importance and insufficient work on the approaches to organization of psychological preparation in education at sea school there is a necessity for a detailed development of a technique of its realization, having paid special attention to the question of introduction of psychological elements during complex preparation.

The psychological model of modern sea business is generally created by:

1. Using various means of imitation - in laboratories, on ranges, on training machines, etc.
2. Modeling fires, collapses, holes, breadboard models of the damaged engineering, every possible problem points and obstacles, including set suddenly.
3. Organizing real counteraction to dangers during preparation.

Carrying out various compositions of the above mentioned means, depending on soluble tasks, the instructor can introduce into the process of educational activity the various psychological factors capable of causing positive activity of the individual, and negative mental phenomena. The conditional creation of threat to life and well-being of personal structure of a vessel is accompanied by the action of the factor of danger, real negative influence - suddenness, lack of information about uncertainty, the realization of actions not planned - novelty of conditions, etc. Skilful balanced introduction in educational process of the specified factors allows really to simulate separate elements challenge of modern sea work and consequently to solve tasks of psychological preparation.

## REFERENCES

- [1] Achkova, M., **Applied Psychology in medicine and healthcare**, Sofia, 2001, (in Bulgarian).
- [2] Bakalov, Y. **Introduction to military psychological knowledge**, Sofia, 1997, (in Bulgarian).
- [3] Clark, D.M. **A cognitive approach to panic**, Behavior Research and Therapy, 29, 1996.
- [4] Freud, S. **Introduction to the psychology of the war neuroses**, London, 1919.
- [5] Hristozov, H. **Mechanisms of individual development**, "Social Medicine", issue. 3, 2000.
- [6] Popov, H., **Post-traumatic stress**, Sofia, 2003 (in Bulgarian).
- [7] Selie, H. **Stress without distress**, Sofia, 1999, (in Bulgarian).
- [8] Stoyanov, V. **Organizational Psychology**, Sofia, 2008 (in Bulgarian).
- [9] Temkov, I., H. Popov, **Stress and personal crises**, Sofia, 1987 (in Bulgarian).
- [10] Uzunov, N. **Stress and psychotrauma**, Stara Zagora, 2000. (in Bulgarian).

## ENHANCED SIMULATION TECHNOLOGIES TO SUPPORT MARITIME OPERATIONAL RISK MANAGEMENT ONBOARD SHIPS

<sup>1</sup>BALDAUF MICHAEL, <sup>1</sup>JENS-UWE SCHRÖDER-HINRICHS,  
<sup>2</sup>KNUD BENEDICT, <sup>2</sup>MATTHIAS KIRCHHOFF, <sup>2</sup>MICHAEL GLUCH

<sup>1</sup>World Maritime University Malmö, Sweden, <sup>2</sup>Hochschule Wismar, ISSIMS Warnemünde, Germany

Approximately 90 per cent of global trade is realized via ships and seaways: a world without shipping is therefore unimaginable. Consequently, hazards and accidents in shipping have negative effects on the world-wide economy and have to be avoided by adequate safety related measures. As the United Nations specialised agency in the maritime field, the International Maritime Organisation (IMO) is responsible for improving maritime safety and preventing pollution from ships. One of the most important regulatory measures to achieve these aims is the International Safety Management Code. Additionally, based on IMO conventions and performance standards as i.a. for Integrated Navigation and Integrated Bridge Systems (INS/IBS), many new devices and sophisticated systems are these days installed onboard to support the bridge team and the pilot in handling a ship safely and in managing operational risks. However, accidents still occur and further improvement of risk management is needed. This paper deals with investigations into the application of simulation techniques to enhance onboard operational risk management. A concept for a real-time simulation-based tool using an innovative combination of mandatory technical and navigational equipment will be introduced, and a sample for applying such a module for the purpose of collision avoidance is described.

**Keywords:** Vessel Manoeuvring, Collision Avoidance, Maritime System Modeling, Simulation

### 1. INTRODUCTION

Safety, in very general terms, can be defined as condition or status with the absence of hazards and conditions where the risk is negligible or at least in a tolerable (ALARP-as low as reasonably practicable) range. Risk is defined as a combination of the frequency of a hazard and its consequences. The so called 'acceptable risk' can be seen as the borderline between a safe and an unsafe status of a system or process. With respect to maritime safety, according to available statistics, the risks of collision and grounding are the two predominant maritime operational risks. That is why collision and grounding avoidance are main tasks of the navigating officer when he is on duty on the bridge. Several technical especially dedicated to these tasks are installed on the bridge in order to assist the human operator.

Modern ship bridges are highly-automated man-machine systems. Safety and efficiency of the ship operations are dependent, as in all other complex man-machine systems, on the

communication between humans and machines during the accomplishment of tasks. Human operators can fulfil their assigned monitoring, control, and decision tasks most effectively, if the information flow between them and machines is adapted to their skills and abilities (e.g. Bainbridge (1983) [1] and Lützhöft, 2004) [11]).

In recent years, to improve maritime safety a strong increase of installations of modern information systems on the ship bridges can be observed. Simple displays and control systems were supplemented or replaced by complex decision support systems. Information of different sensors and systems are combined in integrated navigation and integrated bridge systems (INS, IBS). Furthermore, modern ship engine control systems today are equipped e.g. with highly sophisticated diagnosis systems to also online monitor engine conditions and support condition based maintenance regimes.

However, according to numerous investigations e.g. by insurance companies and classification societies, there are still a high number of accidents with serious damages and injuries. The majority of total losses in shipping is due to collisions, groundings and contacts although there are high sophisticated navigation systems integrated on board providing the officer of the watch with facilities to warn him if a dangerous situation has to be expected. But not only accident figures are of importance. Moreover, it has to be considered, that according to investigation and statistical analysis in the maritime field i.a. [13] every serious casualty corresponds on average to 30 less serious casualties, 300 near-miss accidents and 3,000 unsafe actions. Furthermore, detailed analysis of marine accident investigation reports dealing with collisions, performed by the Nautical Institute (see [8]), showed that nearly 50% of all collisions happened due to the fact that one of the involved vessels even had not seen the other vessel. In this respect, other investigations dealing with alert management on board modern vessels ([3], [12]) have shown that there is a superfluous of alarming from several systems. With respect to collision and grounding avoidance looking at the presently implemented collision warnings, lacks and shortcomings regarding the adjustment of the thresholds were identified especially. Officers tend more to switch off alarm functions than to adjust the thresholds for collision warnings (CPA - Distance at closest point of approach, and time to this point - TCPA as well as bow crossing range and time BCR/BCT) manually.

Obviously, in order to enhance the onboard operational risk management there is a compelling need for task- and situation-dependent triggering of alarms and warnings. That is why investigations were started into an approach to make use of the potential of the new equipment for implementation of simulation technologies in order to reach a new quality level in risk management. For this purpose data available from ARPA and AIS as well as the use of data recorded by a SOLAS conform Voyage Data Recorder (VDR) and an engine diagnosis system will be taken into account and be combined with fast-time simulation techniques.

## **2. DRAFT CONCEPT FOR SIMULATION-BASED OPERATIONAL RISK MANAGEMENT ONBOARD SHIPS**

The role of computer based simulation is increasing on the ships bridge, especially for manoeuvre planning and for collision and grounding avoidance. Simulation based prediction tools are very helpful and already in use on ships for a long time. Well known is the so called Trial Manoeuvre mode in ARPA radars to be used in order to analyse future encounter situation for selected relevant course and speed alternatives to check potential collision avoidance strategies.

With the emerging Electronics Chart and Information Systems (ECDIS) new tools were introduced for supporting voyage planning by means of principle manoeuvring

characteristics. For controlling the ship on her route the future track of the ship was shown as a so called "curved headline" overlay in ECDIS.

However, prediction functions and tools, implemented so far, are very simple and only based either on new constant course and speed values as in the ARPA trial function or on estimated future courses & tracks based on the simple integration of the current ship motion parameters as rate of turn and speed components to be considered as constant.

The simplification of these predictions allows restricted use only. That is why new concepts for on board displays and simulation tools were developed using an innovative approach which includes the immediate response on changes of rudder and engine commands for the display of the future track.

This approach was investigated in research projects, dedicated on the one hand to the further development of user interfaces on ships navigational bridges and to investigations into potential improvements for manoeuvring assistance on the other hand.

A simulation based prediction tool was developed to simulate the ships motion with complex dynamic models in fast time and to display the ships track immediately for the intended or actual rudder or engine manoeuvre (Benedict, Baldauf et al [4]). Generally there are two areas of application of such a tool. It can be seen both as training tool for ship manoeuvres and to be used as assistance tool on board vessels. Predictions as elements of on board displays can be used as in the loop control elements to steer the ship manually but supported by the future track or speed indication in the ECDIS interface.

One crucial problem for the prediction is the accuracy of the simulation. A very sophisticated approach was used to represent the ships' dynamic by very extensive equations very similar to those used in Full Mission ship handling simulators. The parameters of the equation of motion will be estimated by an extra fast time simulation program and a data analyser already used for tuning of the hydrodynamic models in a ship handling simulator. These methods will be described in the following chapters.

The input output relations of the developed concept are shown in Fig. 1. The inputs consist of controls, the states and the data for the environmental conditions (depicted in the three blocks on the left side). The core module Simulation/Prediction is in the centre of the figure. Additionally there is an input of the Ships condition parameters. They are normally fixed but in case of malfunctions they might change, e.g. reducing the rudder turning rate or maximum angle. Relevant information should be delivered to the simulation module by means of status and condition information monitored by the engine diagnosis system. The results from the simulation block are transferred to a dedicated display unit of an INS or IBS and are displayed preferably in ECDIS (for grounding avoidance purposes) or Radar (for collision avoidance purposes).

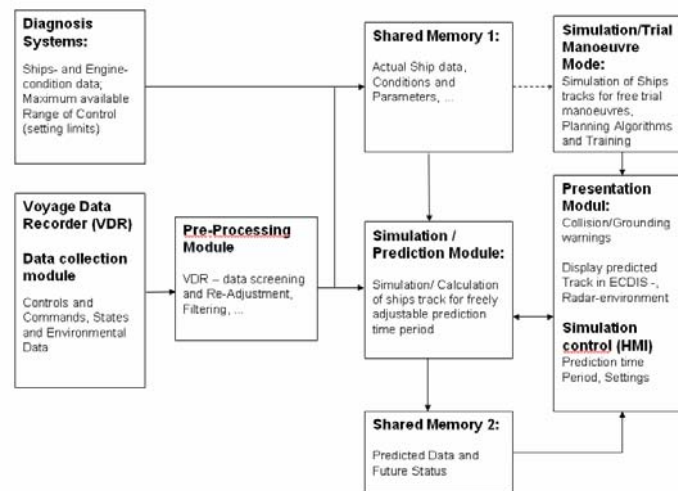


**Fig. 1. Generic modular Concept of a simulation-based Prediction System (data sources, flows and functional modules)**

The figure also illustrates the aspects of the more technological setup of the structure of the modules. A commercial IMO-proven VDR plays the role of a data collector for the controls, states and environmental parameters measured by the ship sensors. After pre-processing these data will be stored in Shared Memory 1, together with parameters of the technical conditions which will be provided by a diagnosis system. This system continuously checks the ships and engine conditions. In this way it can be ensured that also remaining manoeuvring reserves, e.g. the maximum available rudder angle or maximum available engine, thruster power can be taken into account for the collision and grounding risks.

Such a simulation-based prediction system and the technical setup may be used preferably to support grounding avoidance by pilots, captains and navigating officers when manoeuvring in narrow waters. However it also can be applied for the improvement of the on board collision avoidance process (see also [2]). There are ongoing investigations to enhance the existing collision warnings by using predicted manoeuvring characteristic data for dynamic adaptation of alarm thresholds in contrary to conventional fixed limit values for CPA/TCPA used for every encounter situation without any distinction regarding the prevailing circumstances. The following Figure 2 shows the principal structure of the simulation-based module applied to support the onboard management of risk of collision.

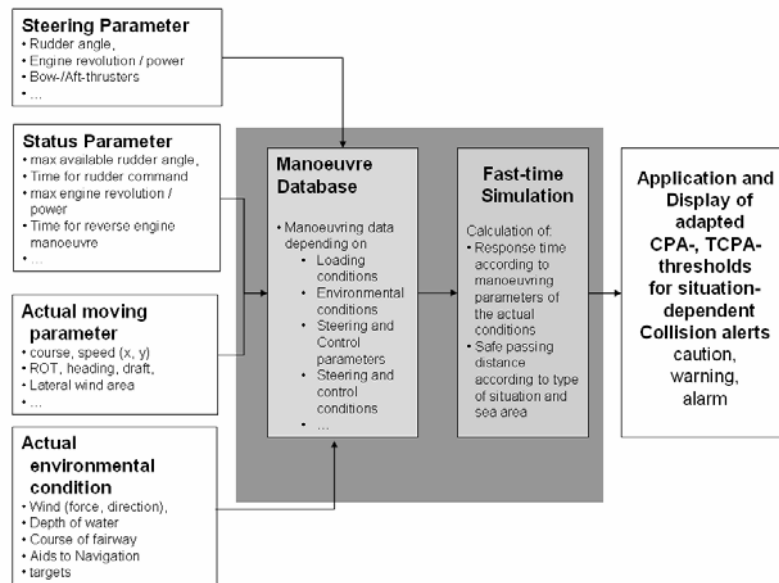


**Fig. 2. Principal Structure of a Fast-time-Simulation Module to support advanced Management of Risk of Collision**

Regarding collision avoidance the described module is planned to deliver specific manoeuvring data valid for a concrete situation of the ship status and the environmental condition at the time an encounter situation occurs. Especially the response times for a potential course change manoeuvre, may be taken from extracted processed VDR recordings and used for automatic adaptation of the TCPA related limits of the dangerous target alarms. Either they may be taken directly from a database or calculated by using the fast time simulation algorithm. The response times for turning manoeuvre are fundamental for collision avoidance actions. Such response times are seldom available to captains on board. And even if so, then only for some standard manoeuvres valid under selected environmental and loading conditions as well. They are usually neither exactly known nor applicable to the prevailing circumstances of a concrete dangerous encounter situation. Especially this gap can be reduced by using predictions basing on a full simulation model as it will be described in the next chapter.

### 3. SHIP DYNAMIC MODEL FOR FAST TIME SIMULATIONS

The following equation of motion was used as math model for the ships dynamic:

$$\begin{aligned}
 X &= m(\dot{u} - rv - x_G r^2) \\
 Y &= m(\dot{v} + ru + x_G \dot{r}) \\
 N &= I_z \dot{r} + mx_G(\dot{v} + ru)
 \end{aligned}
 \tag{1}$$

On the right side are the effects of inertia where u and v represent the speed components in longitudinal and transverse direction x and y, r is the rate of turn of the ship.

The ships mass is  $m$  and  $x_G$  is the distance of centre of gravity from the origin of the co-ordinate system,  $I_z$  is the moment of inertia around the z-axis.

The ships hull forces  $X$  and  $Y$  as well as the yawing moment  $N$  around the z-axis are on the left side. Their dimensionless coefficients are normally represented by polynomials based on dimensionless parameters, for instance in the equation for transverse force  $Y$  and yaw moment  $N$  given as the sum of terms with linear components  $N_r$ ,  $N_v$ ,  $Y_r$  and  $Y_v$  and additional non-linear terms depending on speed components  $u$ ,  $v$ , rate of turn  $r$ , revolution  $n$  and rudder angle  $\delta$ . Other forces as for instance rudder forces and wind forces are expressed as look up tables. There are additional equations for the engine model, additionally with look-up tables to represent automation systems characteristics.

The solution of this set of differential equations is calculated every second; some internal calculations are even done with higher frequency. This equation of motion (1) can be written in the form:

$$x'(t) = f(x, u_c, t) \quad (2)$$

Where:

state spaces with track co-ordinates  $\zeta$ - $\eta$ , heading  $\psi$ :

$$x = [u, v, r, \xi, \eta, \psi, \delta, n_{ME}, n_{TH}, \dots]$$

Conrols with commanded values (Cmd) for main engine (ME) and thrusters (TH):

$$u_c = [\delta_{Cmd}, n_{ME\_Cmd}, n_{TH\_Cmd}, \dots]$$

with initial conditions at  $t = t_0$ :  $x(t_0) = x_0$ ;  $u(t_0) = u_{c0}$ :

$$x_0 = [u_0, v_0, r_0, \xi_0, \eta_0, \psi_0, \delta_0, n_{ME0}, n_{TH0}, \dots]$$

$$u_{c0} = [\delta_{Cmd0}, n_{ME\_Cmd0}, n_{TH\_Cmd0}, \dots]$$

This equation of motion (2) can be solved by numerical integration for the prediction time period  $t_0$  to  $t_1$  in the form of the general solution:

$$x(t) = x(t_0) + \int_{t_0}^{t_1} x'(t) dt$$

i.e. for the full set of states and controls:

$$x(t) = x_0 + \int_{t_0}^{t_1} f(x, u_c, t) dt \quad (3)$$

A simplified solution for a simplified prediction could be used by integration of track and heading assuming constant speed  $u_0$ ,  $v_0$  and rate of turn  $r_0$ , and would results always in a circular motion with constant speed:

$$x(t) = x_0 + \int_{t_0}^{t_1} f(u_0, v_0, r_0) dt \quad (4)$$

In Figure 3 the results of both the methods are depicted for a PORT-rudder manoeuvre.

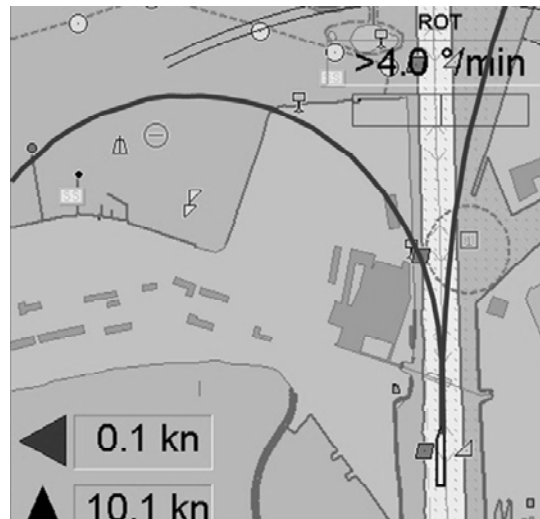


**Fig. 3. Presentation of different track predictions for an identical rudder manoeuvre**

The simplified prediction resulting from integration Eq. (4) of current constant motion parameters delivers the right track with a small turning to STB. At the same time the enhanced simulation is showing a turning circle to port. This track belongs to the sophisticated dynamic prediction based on full math model Eq. (3) considering the change of rudder angle to PORT (left track with turning to port). The sample shows, that the chosen rudder angle is too large with respect to grounding avoidance a smaller rudder angle can be used instead.

The advantage of the full simulation is clearly demonstrated, because the navigator is immediately and nearly without any delay, informed about where the ship will go and how the risk of grounding would be developing without a correcting rudder command.

#### **4. PROVISION OF DATA AND PARAMETER TUNING FOR MODELLING SHIPS DYNAMIC BEHAVIOUR**

The quality of the math model for the simulation and the parameters in the equations are of high importance for the effectiveness and accuracy of the dynamic prediction. There is a great need for fast and effective modeling and tuning processes. This is valid not only for the simulation-based prediction module but e.g. also for full mission ship handling simulators where clients from shipping companies need to be trained on their specific ship types. This is the same procedure as we need for tuning the ship model parameters in the prediction module.

If this modeling process is done manually by conventional tuning methods then there is substantial time consumption, which depending on the level of detail and accuracy of a model may take up to one month or longer, because manoeuvre simulation has to be done in real time at a SHS. Even when using the simulator in „fast mode“- which is up to ten times faster – it's still to slow. Commonly there are no effective tools for supporting the modeling



achieve an Optimised Ship Model-Parameter file which has to be applicable as ship model file for the dynamic predictor on the bridge of a ship. The biggest problem is that there are up to 200 parameters and the effect of the changes are not very clear; some changes may even have effects which counteracts the results of the others. Therefore it is very important to know about those parameters which have a clear impact on the manoeuvring characteristics.

One example is given to indicate the effect of tuning of one hull parameter; here the variation of ships moment of inertia  $I_z$  is given in Fig. 5.

For the demonstration a parameter-series of turning circles with Hard Rudder to starboard was simulated varying the value of the factor  $k_{zz}^2$  which was initially 0.16 between 0.1 and 0.2 in steps of 0.01. During the simulation process the status of the execution is shown by means of coloured bars in the relevant data windows.

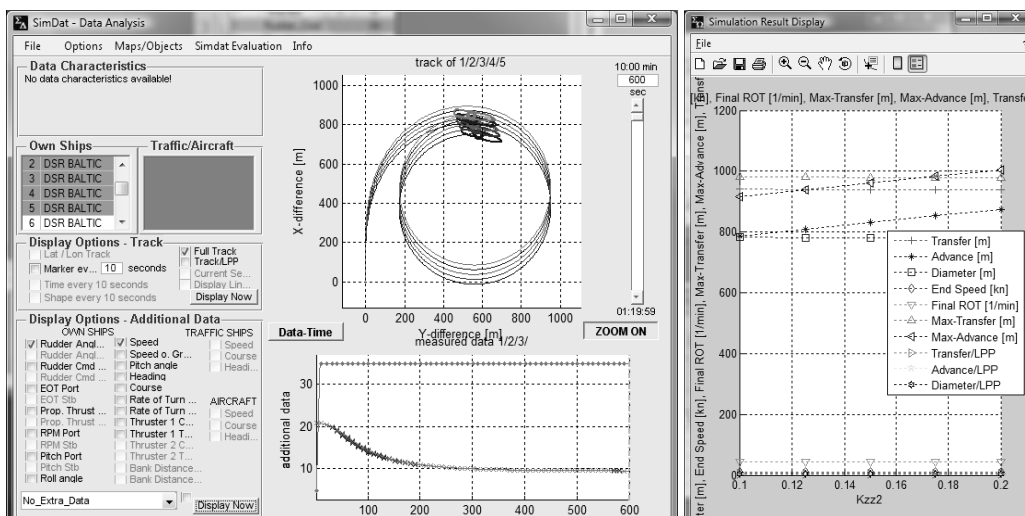


**Fig. 5. Model tuning - Parameter series for changing Moment of Inertia for Turning circle tracks and speed plots (left); extract of characteristic manoeuvring data for turning circle in table format (right)**

The result in Fig. 5 shows a clear effect on the advance of the turning circle whereas the diameter and the speed loss did not change. The optimization window shows parameters which can be set as target values for the optimization process.

## 5. APPLICATION OF SIMULATION TECHNOLOGIES TO MANAGE THE OPERATIONAL RISK OF COLLISION

In principle the process of collision avoidance consists of the following elements:

- Situation assessment
- Decision finding
- Initiate an action to avoid a dangerous encounter
- Monitoring the effect of the measure and modify if necessary.

During the process of situation assessment the Officer of the Watch (OOW) has to

evaluate and assess the results of his permanent observations of the sea area in order to detect any risk of collision with other objects in the vicinity of his own ship. In case a developing or existing risk of collision is detected, the OOW has to decide when and by taking which measure – usually a manoeuvre to increase the expected passing distance in due time – the potential danger can be avoided. Finally, the action has to be taken, its consequences and effects has to be monitored. If necessary, the manoeuvre has to be corrected or adjusted, so that the risk is acceptable. After a safe passing, the ship has to be brought back to the original path and course respectively.

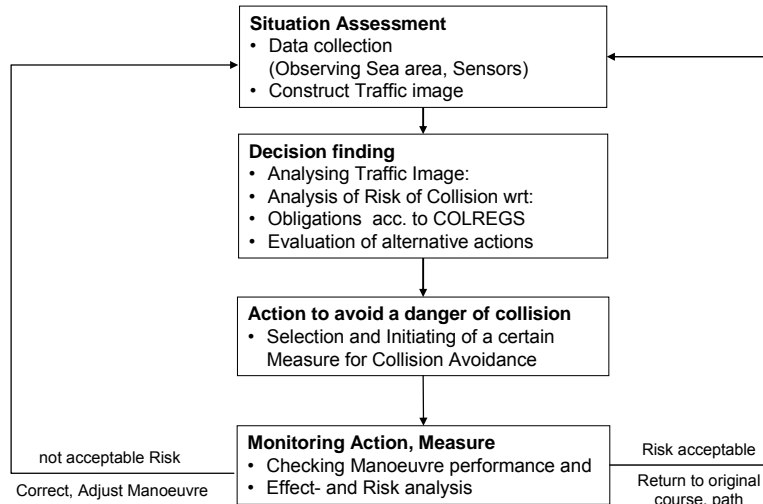


**Fig. 6. Model of the onboard Collision Avoidance Process**

The basics for actions to avoid collisions are laid down in the "International Rules for Preventing Collisions at Sea" (COLREGS). The rules presently valid were adopted by the IMO as a convention in 1972 and set into force in 1977. With respect to manoeuvres to avoid collision especially Part C "Sailing and Steering Rules" is valid. This part again is divided into three sections which contains rules that have to be applied by vessels

- (1) in any condition of visibility
- (2) when in sight of another or
- (3) in restricted visibility.

In the specific rules different actions are defined e.g. in Rule 7 how to determine a risk of collision. With respect to the avoidance of a potential collision different actions are described for good and for restricted visibility. Except Radar, no specific link regarding technical equipment to be used for situation assessment is made in the rules. Moreover it is stated, that all available means shall be used and consequently new technologies should also be integrated within the frame of this process (se e.g. [7]).

As already mentioned shortly in the second chapter, the the technical setup shall be applied for the improvement of on board collision avoidance by the development and implementation of an algorithm which provides situation-dependent alarm thresholds for CPA/TCPA – limit settings.

Core element of this approach is a risk model for situation assessment, developed by Hilgert & Baldauf [9], defining three types of encounter situations and considering the two conditions of visibility as laid down in the COLREGS as well. Furthermore the concept also corresponds to the new IMO's definition for alerts given in the new performance standards for INS [10]. It allows the implementation of situation dependent collision alert categories "Caution", "Warning" and "Alarm" as well. Cautions and warnings may be switched off by the operator, but alarms may not.

For self adaptation of thresholds different CPA limits are foreseen for different types of encounters. They will be calculated and set automatically according to the hydrodynamic safe passing distance related to the dimensions of the involved ships, the actual sea area and visibility conditions as well. As suggestion for initial basic values CPA limits were determined by detailed empirical field study.

**Table 1: Recommendation for basic values to calculate situation dependent thresholds to trigger a collision warning**

Type of encounter	$f_x$	$f_x$
	good visibility	restricted visibility
Head-on and Meeting port-port	2.5	5
Overtaking and Meeting stb/stb	2.5	5
Crossing	5	10

To ensure a wide range of user acceptance, within the study, one emphasis was laid on the navigators' behaviour and taken into account. From the point of view of well experienced navigators it is rather more practical to determine the safe passing distance with respect to usual data. Under pragmatic aspects and according to the investigations performed it can be assumed that the nominal safe passing distance have to be in relation to the ship's length of the largest vessel  $L_{max}$  involved in an encounter situation (but  $L_{max}$  should not be less than 1 cbl). Consider different kinds of encounter situations as defined in the COLREGS a factor " $f_x$ " is necessary which depends on the kind of situation "x" and the Limit is then to be calculated as to Safe Passing Distance (nominal) =  $f_x \cdot L_{max}$ . with  $f_x$  values as given in table 1.

Manoeuvring data corresponding to the actual ship and environmental conditions have to be used for automatic adaptation of the TCPA related limits of the dangerous target alarms, either by taking them directly from a database or by calculations using the fast time simulation algorithms. A sample of a standard set of response times for a usual sized 5.000 TEUs container vessel is given in Table 2. As mentioned before, such manoeuvring data are today not available at all onboard the ships and the application of a module as developed and described here would therefore substantially contribute to the improvement of this situation.

**Table 2: Predicted response times for turning manoeuvre depending on own ships speed and rudder angles**

Own Speed [kt]	Rudder angle [deg]	Time for 90 course alteration [min]	Covered distance [nm]
24	Hard starboard	2:25 min	0,97
24	Starboard 15	3:51 min	1,54
22	Starboard 20	3:24 min	1,25
22	Starboard 15	4:10 min	1,53

As stated before, when applying the drafted concept for situation dependent adaptation of alarm thresholds the relevant limit values should be determined from either direct recordings of the continuously working VDR or by calculations using the simulation-based prediction module.

For the situation dependent adaptation of a TCPA limit the module is further developed, so that it can be used to calculate the rudder response times and manoeuvring parameters for the actual loading conditions of the own ship and the prevailing environmental conditions (wind, current). The figure below depicts the results of the fast-time simulation for relevant advance and transfer ways as well as times of 90° course changes to starboard using 10°, 20° and hard rudder angle which is suggested as utmost minimum TCPA-Limit for alarming.

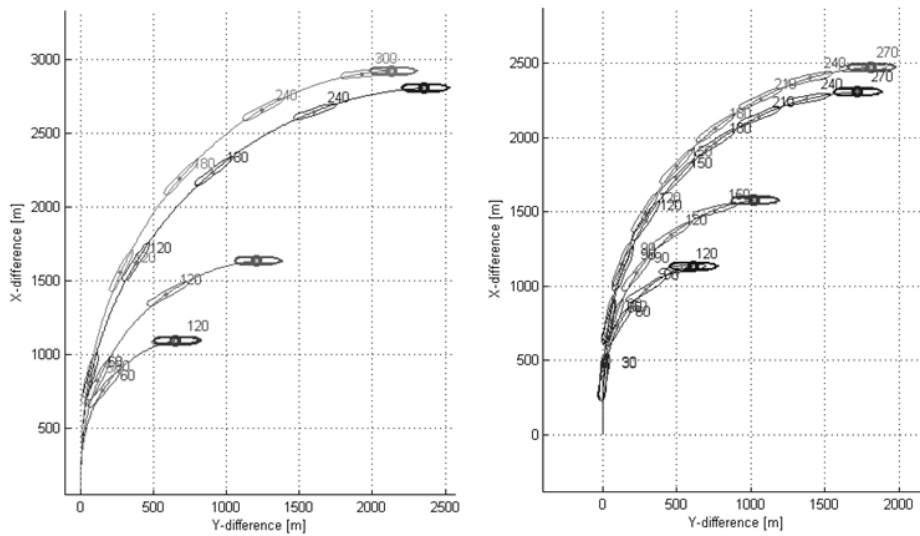


**Fig. 7. Samples of fast-time simulation results for course changes of a 5.000 TEU container ship for different loading and environmental conditions (left –ballast, right – loaded)**

Exemplarily the fast-time-simulation results are shown for the underlying course change using rudder starboard 10 with additional consideration of assumed wind (direction 45° and force 45 kn).

Such comprehensive calculations and predictions are possible today, when the simulation module is linked to an VDR, which collects the actual own ship's and environmental conditions and provide them to the relevant collision avoidance device (as e.g. ARPA/Radar) with a situation dependent minimum TCPA-limit. First studies applying the situation dependent thresholds for detection of dangerous encounter situations in overall traffic scenarios in sea areas off the coast monitored by VTS leads to a reduction of the number of collision alerts by 40%.

## 6. SUMMARY AND CONCLUSION

To improve onboard operational risk management investigations into the application of simulation techniques to collision and grounding avoidance were performed. A concept for an enhanced real-time simulation based module basing on innovative combination of

mandatory technical and navigational equipment is drafted and a sample for applying such a module for purposes of potential automatic situation-dependent adaptation of thresholds for collision warnings is described. The simulation-based prediction tool show immediately results of rudder and engine control changes in an electronic chart environment to be used for manual correction of steering actions and to support grounding avoidance by the bridge team and the pilot especially when manoeuvring in narrow waters. The parameters for the ship model equations can be found using fast simulation techniques. For the future it is planned to use optimization methods and parameter estimation technologies for ship dynamic model parameters.

For enhanced support of onboard collision avoidance automatic adaptation of thresholds that trigger collision warnings are suggested. Therefore the simulation techniques are applied to predict the rudder response time valid for actual ship status and environmental conditions for a manoeuvre to avoid a collision.

The research results presented in this paper were partly achieved in research projects funded by the German Federal Ministry of Economics and Technology and the Ministry of Education and Research of Mecklenburg-Pomerania.

## REFERENCES

- [1]. Bainbridge, L. - ***Ironies of Automation***. Automatica 19 (1983): pp. 775-779
- [2]. Baldauf, Benedict, Wilske, Grundevik, Klepsvik - ***Combination of Navigational Equipment and VDR Based Information to Enhance Alert Management***. In Weintrit, A. (Ed.): Advances in Marine Navigation and Safety of Transportation. Monograph Gdynia Maritime University and The Nautical Institute London (UK), Gdynia, June 2007, pp. 315-320
- [3]. Baldauf, M.; Benedict, K.; Motz, F.; Höckel, S. - ***Investigations into enhanced alert management for collision avoidance in ship borne integrated navigation systems***, in: Cordeiro, J.; Filipe, J. (eds): Proceedings of the 11<sup>th</sup> International Conference on Enterprise Information Systems – Human Computer Interaction. Setubal (Portugal) 2009, pp. 169-174.
- [4]. Benedict, Kirchhoff, Baldauf, Gluch, Fischer - ***Concept for On-board Prediction Displays based on actual Ship Condition and Manoeuvring Simulation for Navigation and Shiphandling***. Paper at IMSF Conference 2007, August 20 – 24, 2007 Busan / Korea
- [5]. Benedict, K. et al - ***Combining Fast-Time Simulation and Automatic Assessment for Tuning of Simulator Ship Models*** MARSIM - International Conference on Marine Simulation and Ship Manoeuvrability, Terschelling, Netherlands, 2006 Proceedings, M-Paper 19 pp. 1-9
- [6]. Clarke & Horn - ***Estimation of Hydrodynamic Derivatives***, Proceedings of the 11th Ship Control Systems Symposium, Southampton 1997, Vol. 3, pp. 275-289
- [7]. Cockroft A.,N.; Lameijer I.N.F. - ***A guide to the Collision Avoidance Rules: International Regulations for Preventing Collisions at Sea***. 6<sup>th</sup> edition, Elsevier Butterworth-Heinemann, Oxford, 2004
- [8]. Gale H.; Patraiko D. - ***Improving navigational safety***, Seaways, London, July 2007 pp. 4-8
- [9]. Hilgert H., Baldauf M. - ***A common risk model for the assessment of encounter situations onboard ships***. Maritime Collision and Prevention, Chiavari Publishing, Surrey, England. 1996 pp.136-148
- [10]. IMO 2007 - ***Revised performance standards for integrated navigation systems (INS)***. MSC.252(83). London: International Maritime Organization.
- [11]. Lützhöft, M. - ***Maritime Technology and Human Integration on the Ship's bridge***. Dissertation No. 907, Linköping Studies in Science and Technology. Sweden, 2004.
- [12]. Motz F., Baldauf, M. ***Investigations into Ship borne Alarm Management - Conduction and Results of Field Studies***, Proceedings of the 9<sup>th</sup> International Conference on Enterprise Information Systems, Volume Human Computer Interaction Funchal, Portugal, September 2007, pp. 136-141.

- [13]. Schröder, J.-U.: **Data collection of causes and underlying factors of marine casualties.** (in German) Schriftenreihe der Bundesanstalt für Arbeitsschutz und Arbeitsmedizin Dortmund/Berlin/Dresden, 2004
- [14]. Schröder, J.-U., Baldauf, M. & Ghirxi, K.T.: **Accident reporting deficiencies related to Human Factors in engine room fires on board ships**, in Bris, R., Guedes Soares, C. & Martorell, S. (eds.): Reliability, Risk and Safety – Theory and Applications. Proceedings of the European Safety and Reliability Conference 2009 (ESREL 2009), Prague, Czech Republic, 7-10 September 2009, Leiden: CRC Press/Balkema, 2009, pp. 261-268.
- [15]. Oltmann **Identification of Hydrodynamic Damping Derivatives – a Pragmatic Approach**, MARSIM - International Conference on Marine Simulation and Ship Manoeuvrability, Kanazawa, Japan, 2003

## A POTENTIAL APPLICATION OF ARC FAULT CIRCUIT INTERRUPTERS IN SHIP ELECTRIC SYSTEMS

<sup>1</sup>BOHOS APRAHAMIAN, <sup>1</sup>LYUBOMIR DANKOV

<sup>1</sup>*Nikola Vaptsarov Naval Academy, Varna, Bulgaria*

The arc-fault circuit interrupter (AFCI) is emerging as a new device in the US National Electrical Code (NEC) and in residential installations to enhance electrical safety. New technology generally fosters questions and concerns about the workings and application of the technology and this article will address some of the most frequently asked questions surrounding AFCI:

- How does the AFCI work? and,
- What is the state of the potential application of AFCIs in ship electric systems?

This article addresses both questions.

**Keywords:** electric arc detection, AFCI, electrical safety

### 1. INTRODUCTION

Developments of arc fault circuit protection are introduced to protect the United States Navy ships from serious fires caused by electric arcs. In the early seventies of the twentieth century the fires caused by the electric systems of the US submarines are recognised as one of the main technical problems endangering the safety of their crews. This type of problems exist in all vessels but in navy ships is most dangerous. The current of a middle sized electric generator can bore a large hole in the box of the electricity distribution panel and fire objects outside the box.

Most of the electricity distribution panels and the cable network on the ships are protected by large automatic breakers with rated currents in the magnitude of hundreds of amperes. Therefore the large currents of an electric arc does not actuate the interrupters of the automatic breakers. The electric arc is not a short circuit connection but is an active load releasing a big amount of heat. The electric arcs are caused by corrosive damages decreasing the distance between the electric rims and damages of the mounting and in the insulation caused by the vibrations. Among other, reasons for the formation of electric arcs are external object and the pollution of the electricity distribution panels.

Arc faults may occur for many reasons such as worn electrical insulation or damaged wire, misapplied or damaged appliance cords and equipment, loose electrical connections, receptacle leakage, neutral leads pinched to grounded metal box, wet connections or conduit, shorted wires, wires or cords in contact with vibrating metal, overheated or stressed electrical cords and wires.

The crucial consumers in the electricity distribution systems are supplied by several electricity sources. When an electric arc is formed in such electricity distribution panel the power must be switched off from all the electricity supplying sources.

In 1979 the US Navy introduced a special program for investigation of the electric arc and creation of sensors and devices for protection of the electric systems of the ships. The Applied Physics Laboratory (APL) of the John Hopkins University has been joint to this program. The developed sensors and systems are intended to protect only the electricity

distribution panels in the US submarines. To avoid false tripping a combination of optical and pressure sensors is used. Thermal sensors are also included in the latest systems [1], [2], [3].

## 2. HOW THE AFCI WORKS

Conventional circuit breakers only respond to overloads and short circuits; so they do not protect against arcing conditions that produce erratic current flow. An AFCI is selective so that normal arcs do not cause it to trip.

The AFCI circuitry continuously monitors current flow through the AFCI. AFCIs use unique current sensing circuitry to discriminate between normal and unwanted arcing conditions. Once an unwanted arcing condition is detected, the control circuitry in the AFCI trips the internal contacts, thus de-energizing the circuit and reducing the potential for a fire to occur. An AFCI should not trip during normal arcing conditions, which can occur when a switch is opened or a plug is pulled from a receptacle.

When an arc fault occurs, AFCI opens the circuit and stops the flow of electricity in a fraction of a second [1]. While connected loads, such as fluorescent lighting, motors, dimmers and switches, may have inherent arcing as a normal mode of operation, the AFCI is designed to distinguish these arcing faults from hazardous arcing faults by monitoring the intensity, duration and frequency of the arcing fault.

Presently, AFCIs are designed into conventional circuit breakers combining traditional overload and short-circuit protection with arc fault protection – figure 1. AFCI circuit breakers (AFCIs) have a test button and look similar to ground fault circuit interrupter (GFCI) circuit breakers. Some designs combine GFCI and AFCI protection. Additional AFCI design configurations are anticipated in the near future.

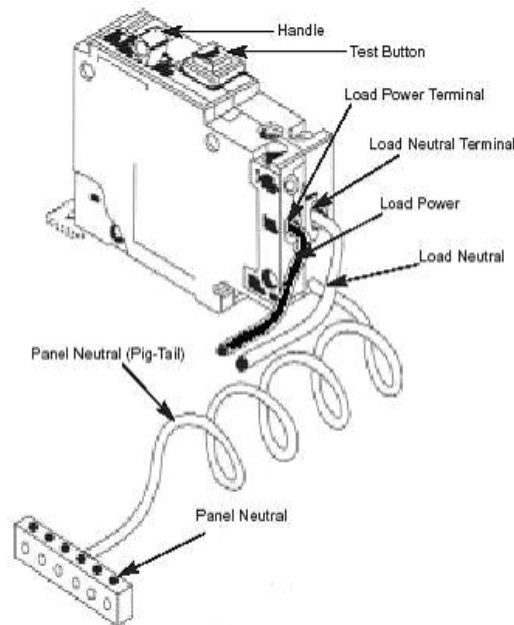


**Figure 1 Typical design of an AFCI.**

AFCIs typically comprise a pair of separable contacts that open (trip) upon sensing an arcing current from line to ground, and/or from line to neutral. AFCIs typically use a differential transformer to measure arcing from line to ground. Detecting arcing from line to neutral is accomplished by detecting rapid changes in load current by measuring voltage drop across relatively constant resistance, usually a bimetallic element (bimetal). Additionally, during over current conditions (i.e. above rated current) the bimetal heats up and flexes a predetermined distance to engage a primary tripping mechanism and trip the circuit breaker.

It is important to note that AFCIs are designed to mitigate the effects of arcing faults but cannot eliminate them completely. In some cases, the initial arc may cause ignition prior to detection and circuit interruption by the AFCI.

The AFCI circuit breaker serves a dual purpose – not only will it shut off electricity in the event of an “arcing fault”, but it will also trip when a short circuit or an overload occurs. The AFCI circuit breaker provides protection for the branch circuit wiring and limited protection for power cords and extension cords.

AFCI Protection Features are [3]:

1. Parallel Protection– direct contact of two wires with opposite polarity (example: damaged extension cords),
2. Ground Protection – arc between a single conductor and ground (example: improperly installed wall receptacles),
3. Series Protection – arc across the break in a single conductor, which progresses to a ground or parallel arc (example: cable pierced by a nail from a wall hanger),
4. Overload Protection,
5. Short Circuit Protection.

The AFCI should not be confused with the GFCI or ground fault circuit interrupter. The GFCI is designed to protect people from severe or fatal electric shocks while the AFCI protects against fires caused by arcing faults. The GFCI also can protect against some electrical fires by detecting currents caused by arcing and other faults to ground but cannot detect hazardous across-the-line arcing faults that can cause fires.

A ground fault is an unintentional electric path diverting current to ground. Ground faults occur when current leaks from a circuit. How the current leaks is very important. If a person's body provides a path to ground for this leakage, the person could be injured, burned, severely shocked, or electrocuted.

A combination AFCI and GFCI can be used to satisfy the NEC requirement for GFCI protection only if specifically marked as a combination device.

Hazardous arcing faults may occur in any of three configurations:

1. Line-to-neutral,
2. Series (such as in a broken or frayed wire or at a loose connection),
3. Line-to-ground.

Voltage and current signals can be taken by an AFCI unit connected as indicated in figure 2. The connections and current transformer coils indicated in figure 2 constitute one method of obtaining the circuit information for the unit. There may be many other means of obtaining the same information. The AFCI unit will use the circuit information to perform an analysis to determine whether an arc is present and whether it is an arc that should be interrupted. It will very likely be looking for several simultaneous indications of arc presence and persistence in order to verify that the signal is from a hazardous arc. On determining that a hazardous arc is in the circuit, the unit signals interruption of the circuit [4], [5].

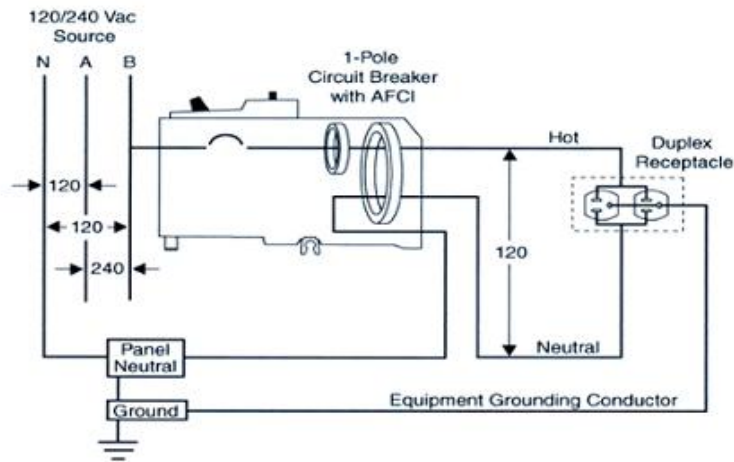


**Figure 2 Connections to an AFCI.**

The various manufacturers of today's AFCIs use different methods of obtaining circuit information and analyzing it. The descriptions in this article provide a generic overview and are not intended to represent exact methods employed for a specific product. The signals may be captured by variations of the configuration of figure 2. Also, some of the units use a microprocessor to perform the analysis, while others use electronic circuitry to perform a direct analysis. The characteristics presented in this article are indications of available characteristics and are not necessarily those used by the various manufacturers. However, all of the units perform an analysis of circuit signals to identify the arc.

In older arc fault protection systems, used widely in US Navy ships, operating signal is formed by arc detection system using the arc lighting effects or the abrupt change of the pressure. The sensors are mounted in the spots with heightened probability of arc fault formation like electric panels, junction boxes, etc. Supplementary thermal sensors are added for detection of serial arc faults caused by damages of the mounting and in the insulation. The sensors turn on the signalization systems, giving a warning of needed prevention operations before damages and failures of the electric systems occur.

### 3. APPLICATION OF AFCIs IN SHIP ELECTRIC SYSTEMS

#### 3.1. Arc Fault Protection Technology at Applied Physics Laboratory (APL) of the John Hopkins University [2]

Electrical fires are of even greater concern onboard ships, where the means of escape are limited. Historical data show that major electrical fires occur on Navy ships at a rate greater than 6 times per year. These fires damage equipment and place the lives of personnel and the survival of the ship at risk. APL investigated the causes and propagation of the high-energy arcs that produce damaging fires and created the Arc Fault Detection (AFD) system to detect and quench these fires. In addition, the Continuous Thermal Monitoring (CTM) system was created that can predict more than 60% of the arcs before they occur and thus prevent arcing damage. These systems, which are installed in all US submarines and nuclear aircraft carriers, are credited with saving nine submarines from catastrophic electrical fires and directly saving two lives. With the advent of electric

propulsion, the generation of electricity on ships is slated to increase many fold, potentially increasing the severity and frequency of electrical fires. APL took the arc problem from basic research into characterizing arc behavior to sensor research and development. A complete system was developed around the sensors and integrated into submarine and ship power systems. New level production drawings were created and delivered to the Navy, and systems were mass produced via competitive bids. More than 15 000 photosensors, 4000 pressure sensors, and 175 control units have been built and deployed on each ship of all classes of submarines. More than 50 control units and 1700 sensors have been deployed on nuclear aircraft carriers. AFD systems are approved by the Navy for connection to all types of power systems including nuclear systems. AFD protection is being planned for all new classes of ships. Although this technology has progressed to the point where it is appropriate for protecting the AC power for commercial ships and critical land-base applications, it presently is a stand-alone capability and work is needed to make it a fully integrated, generalized solution to power quality issues.

A new type of power distribution architecture, the Integrated Power System (IPS), was proposed for the next generation Navy ships. Such electricity distribution systems are also widely used in big passenger ships, build the last decade. The IPS system focused on the integration of electric propulsion into an all-electric ship. With the design of conventional ships, the screw (propeller), shaft, and drive unit (steam turbine, gas turbine, or diesel engine) are first placed in alignment and then all other elements are installed around the propulsion items. With electric drive, the generation of the power and the screw do not have to be coupled by a shaft and so they no longer drive the layout of the ship. However, the use of electric propulsion greatly increases the amount of electricity that must be generated and distributed and increases the risk of electrical fires. In 2000, APL evaluated the IPS and found that it was as susceptible to arcing faults as any other electrical distribution system.

Today, the AFD/CTM system protects switchboards against arcing failures, but not against other types of electrical failures. The present design does not protect the ship's cables against battle damage, nor does it protect any electrical loads from internal failures. As the naval and marine industry move toward allelectric ships, new challenges are appearing. Electric motors of many megawatts are used for main propulsion and as side thrusters. A new challenge would be to miniaturize the AFD sensors so that they could be used to protect these large loads. Ships experience considerable vibration, which can abrade insulation and loosen connections. The mechanical spaces containing the switchboards and large electrical motors are frequently not air-conditioned, but rather cooled only by large amounts of fresh air. This exposes the equipment to large swings in temperature, a salt-laden atmosphere, and humidity. Temperature swings, salt, humidity, and vibration combine to reduce the reliability of the electrical systems. AFD/CTM sensors each contain temperature sensors for correction of onboard data. It may be possible to use these sensors as part of the condition-based maintenance of the switchboards. Small, inexpensive current sensors need to be designed and integrated into the sensor network. The combination of continuous current and temperature measurements within the switchboards, along with artificial intelligence software, could be used to furnish predictive diagnostic information (e.g., when motors become overloaded) to the crew at an early stage. Preventative maintenance is expensive and laborintensive, and as the Navy moves toward reduced manning, such maintenance is becoming a major issue. Turning the AFD/CTM system from just arc fault protection into a predictive electrical condition-based maintenance system has large potential payoffs for the Navy in enabling staff reductions. Techniques to protect large motors on land have proved to be too large and expensive for Navy shipboard use. Thus far, electrical loads on Navy ships are only protected by breakers. Breakers give protection against fires caused by gross overloads and failures but furnish little protection to the actual equipment. Further development of the AFD/CTM sensors could miniaturize them

for mounting at critical locations inside existing motors and generators, bringing protection and predictive information to these potential trouble spots. Critical land-based installations, such as a military computing and communication center or major online credit card processing center, must be supplied with electrical power from two separated substations. Power from both enters the plant through an automatic power source selector called an automatic bus transfer. Frequently, power is also available from a third source such as a large battery-backed uninterruptible power supply. While there are multiple independent power sources, each one enters the common switchboards and is then distributed to the loads. The presence of multiple power sources does not protect against failures within the power distribution network. The addition of current sensors to the AFD/ CTM system would allow it to sense power disturbances other than those caused by arcing in the switchboards (e.g., arcing on supply cables). By knowing the direction of current flow, one can more selectively remove power from arcs and minimize the loss of power to other areas, keeping the majority of the power distribution network online.

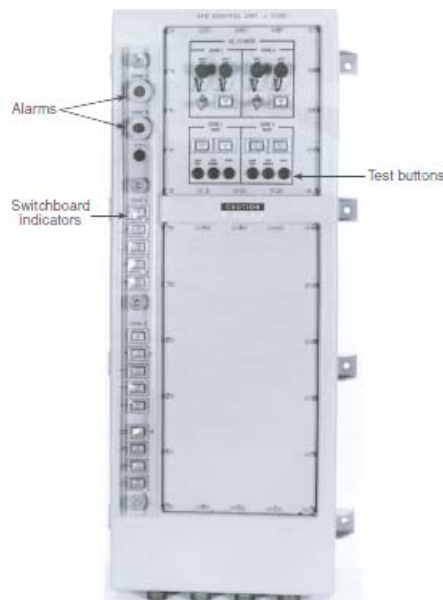


**Figure 3 Submarine AFD/CTM control unit.**

### **3.2. ARCON Arc Fault Protection System on Ships, proposed by MOELLER [6]**

In the event of an arc fault, the air pressure and temperature reach their maximum values within 10-15 ms so that the arc fault can very well be compared to an explosion. As the electrical characteristics depend on the conditions at hand, such as generator output or the length of the connection cables, only the duration of the arc fault is a controllable variable. ARCON quenches the arc fault in only two milliseconds – long before any serious damage to persons or to the switchboard can occur.

The function of ARCON is quickly described: The light emitted from the arc fault, as well as its short-circuit current, can be detected very easily. Special sensors connected to fibre-optic cables are laid along the active switchboard sections for detecting the light. Some of

the extremely bright light of the arc fault enters the fibre optic cable radially and is transferred to the evaluation device where this information is processed. ARCON uses the current transformers present in the incomers to detect the second variable. If both detection variables exceed certain specified threshold values at the same time the evaluation unit triggers the quenching device. The device produces a three-phase bolted short-circuit as close as possible to the incoming supply and parallel to the fault location. The current takes the path of least resistance and the arc fault is quenched. The entire process - consisting of detection, evaluation and quenching - is completed within two milliseconds. The value of the arc fault current is not important. The incoming circuit-breaker also only isolates the section of the system that is affected by the arc fault. All unaffected areas are kept in operation. As a backup measure and to prevent automatic restarts, ARCON triggers all shunt releases of the circuit-breakers feeding this area. ARCON fully meets here the selectivity requirements in marine power supply systems. Once the causes of the fault have been rectified and the quenching device replaced, the switchboard is ready for service without any restriction.

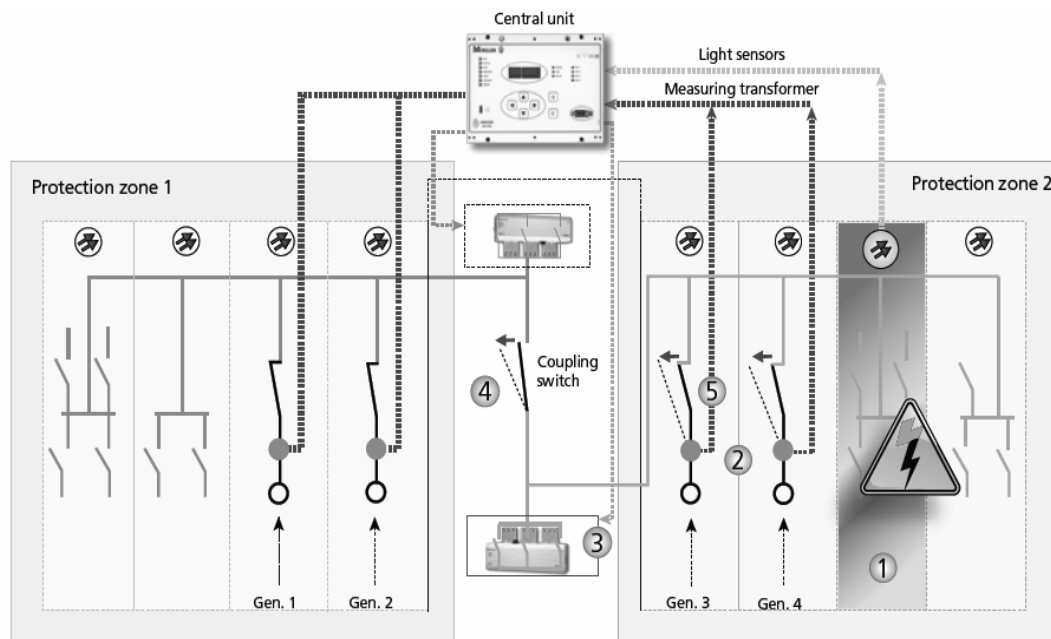


**Figure 4 Function of ARCON arc fault protection system scenario:**  
**1. Arc fault in protection zone 2 -> Signal of light sensors to central processing unit**  
**2. Incoming supply current transformers -> Signal to central unit**  
**3. Quenching device is activated -> Arc fault is quenched after 2ms**  
**4. Coupling switch opened first by the short-circuit current according to selectivity**  
**5. Incoming supply circuit-breakers in protection zone 2 open as a result of the short-circuit current Protection zone 1 stays in operation.**

#### 4. CONCLUSIONS

The AFCIs react to the electromagnetic noise, created by the electric arc. False trips are possibly caused by electromagnetic noises, formed during the normal operation of the electric systems. Such noises are formed by the brushes of the universal motors, used in hand electric tools, by the electric discharge lamps and by the electric switches. AFCIs work properly in living conditions, but their application in the surroundings of the industry with powerful electromagnetic noises is not yet recommended by the AFCI manufacturers.

Considering the importance of this new technology for the safety of the electric systems of the Navy and the Air Force, the US Congress every year grants several millions of dollars for scientific investigations in this realm [7]. The powerful electromagnetic noises on board of the US Navy ships are an obstacle for the auspicious application of the AFCIs, but their experimental application in US Air Force planes is very successful.

The sophistication of the digital systems for signal collection and processing in real time reassure that AFCIs will very soon be reliable enough and applicable in the ships of the navy and the mercantile marine. Their testing in ship premises without powerful electromagnetic noise is applicable right now.

#### REFERENCES

- [1] Gregory G. D. and G. W. Scott, -**The Arc-Fault Circuit Interrupter, An Emerging Product**, IEEE Transactions on Industry Applications, September-October 1998, pp. 928-933
- [2] H. Bruce Land III, C. L. Eddins, and J. M. Klimek, -**Evolution of Arc Fault Protection Technology at APL**, Johns Hopkins APL Technical Digest, Vol. 25, Number 2, 2004, pp. 140-153
- [3] Gregory G. D. and A. Manche, -**Arc Detection with the AFCI**, *IAEI Magazine Online*, July 2000
- [4] Single Pole Arc Fault Circuit Breaker, US Design Patent #450660, November, 2001
- [5] Arc Fault Circuit Breaker, World Intellectual Property Organization Patent #WO 01/20634 A2, March, 2001
- [6] [www.moeller.com](http://www.moeller.com)
- [7] [www.thomas.gov](http://www.thomas.gov)

## STRUCTURAL AND KINEMATIC VIBRATION ON INTERNAL COMBUSTION ENGINE - PART I

<sup>1</sup>BUZBUCHI NICOLAE, <sup>1</sup>STAN LIVIU, <sup>2</sup>BERESCU SERBAN

<sup>1</sup>Constanta Maritime University, Romania, <sup>2</sup>Romanian Naval Authority, Romania

Computational methods to predict the vibration of an internal combustion engine have become more important as demands for matching the lighter weight with low vibration levels and for reducing the development period have been increasing. The former studies of engine vibration are categorized into two groups. One deals with structural vibration (elastic vibration) in relatively higher frequencies. The other deals with kinematic vibration (rigid body motion) in low frequencies. Recently, it is becoming more important to analyze structural and kinematic coupled vibration in middle range frequencies. In this study, we developed an engine vibration analysis system for a computer aided design software, which can comprehensively analyze structural and kinematic coupled vibration in a wide range. A new formulation using a local observer frame and eigenmodes was proposed to efficiently calculate the structural and kinematic coupled vibration of the moving elastic body. In addition, some types of force elements were developed to express the transmitting force from a body to another body or the boundary conditions. The developed program was applied to a real engine model and verified by experiment under running conditions

**Keywords:** engine vibration analysis, body and force element, shafting torsional vibrations

### 1. INTRODUCTION

As the demands for low fuel consumption in automotive engines and the reduction of engine development period increase, calculational methods of engine vibration are becoming more important in structural design to match lighter weight with lower vibration. Previous studies of engine vibration analysis are categorized into two groups. One deals with structural vibration (elastic vibration) in relatively higher frequencies. Generally, this is calculated by a finite element analysis solver such as CATIA, ADINA, NASTRAN, etc. under the assumption that the vibration is infinitesimal. In this case, the coupled vibration between the crankshaft and cylinder block through main bearings is analyzed using a rotational coordinate system for the crankshaft and an inertial coordinate system for the cylinder block. The other deals with kinematic vibration (rigid body motion) in very low frequencies, which is solved by multibody dynamics theory using differential algebraic equations.

On the other hand, to reduce the vibration in a middle frequency range, it is also becoming more important to analyze the structural and kinematic coupled vibration. In this frequency range, the crankshaft rotates with elastic vibration that includes many torsional and bending modes. The cylinder block vibrates elastically with large rigid motion caused by the combustion force of the cylinder and the inertia force of the piston-connecting rod system. In addition, as the vibration of the crankshaft is transmitted to the cylinder block

through the oil film bearings, the nonlinear dynamic characteristics of the oil film significantly influences the interaction between the crankshaft and the cylinder block.

From these features, it is impossible to solve the structural and kinematic coupled vibration by the linear finite element analysis method. On the other hand, a multibody solver deals with structural and kinematic coupled vibration by adding the elastic mode to the rigid body. However, this method is not always practical because such a solver includes three kinds of coordinates (Cartesian coordinates, Euler parameters and modal parameters) and many complicated coupling terms are derived from the coupling between the rigid body motion and the elastic vibration. In addition, the simple constraint equation of differential algebraic equations, such as for a revolutionary joint, is not sufficient to express the nonlinear characteristics of the oil film bearing.

From this background, in [6] the authors proposed a new formulation that is more practical than differential algebraic equations for the structural and kinematic coupled vibration. In this study, they developed the engine vibration analysis system based on its formulation for a computer aided design tool. In engine vibration analysis, the important engine components such as the crankshaft and cylinder block are modeled by body elements whose motion and vibration are solved by its formulation. In addition, several types of force elements are introduced to express the boundary conditions of each component and the interaction between components. The developed system was applied to an inline four-cylinder engine and verified by experiment under running conditions.

## 2. OUTLINE OF ENGINE VIBRATION ANALYSIS SYSTEM (EVAS)

Figure 1 shows the system schematic of the inline 4-cylinder engine as shown in Fig. 2. The system is composed of body elements and force elements. The body element is expressed by a finite element model and is used for the moving elastic body such as a crankshaft and a cylinder block. The force elements express the boundary condition of body elements and the interaction between body elements. According to the connecting condition and function, the force elements are categorized as piston-conrod element, journal bearing element, motor element, engine mount element, thrust bearing element and belt element.

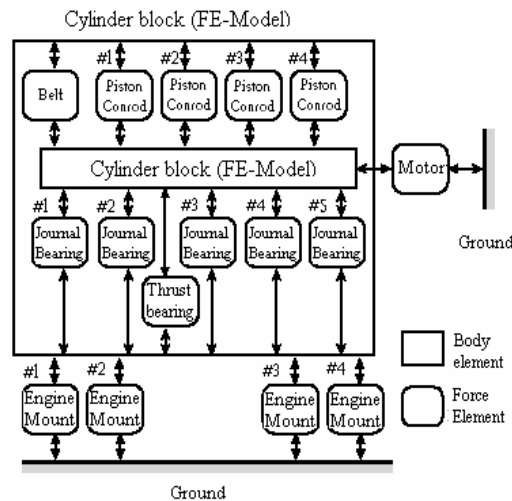


Fig. 1. Schematic of EVAS

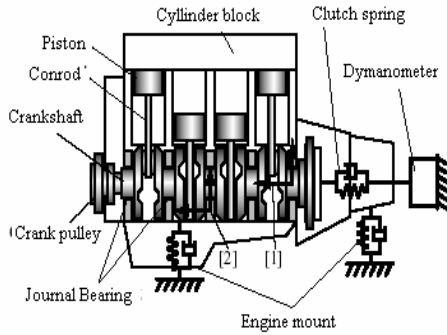


Fig. 2. Model of inline 4 cylinder engine

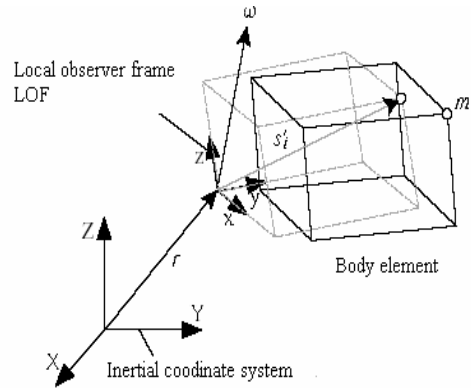


Fig. 3. Local observer frame

### 3. FORMULATION OF EVAS

#### 3.1. Body element

The motion and vibration of a body element are calculated by the equation of motion formulated using a local observer frame (LOF) and both rigid and elastic modes of the body. The equations of motion are written by modal coordinate  $q_k$  as follows:

$$\ddot{q}_k + \sum_{i=1}^N m_i \Phi_{ik}^T A^T a + \sum_{i=1}^N m_i \Phi_{ik}^T A^T (\ddot{\alpha} + \ddot{\omega} \tilde{\omega}) A \left( s'_i + \sum_{j=1}^N \Phi_{ij} q_j \right) + 2 \sum_{i=1}^N m_i \Phi_{ik}^T A^T \tilde{\omega} A \sum_{j=1}^N \Phi_{ij} \dot{q}_j + \lambda_k q_k + c_k \dot{q}_k = \sum_{j=1}^N \Phi_{ik}^T A^T F_j \quad (1)$$

Refer to the above-mentioned paper [6], for details about the derivation of Eq.(1) and the LOF. In Eq.(1),  $a$  is the acceleration of the LOF,  $\tilde{\omega}$  is the skew-symmetric matrix of the angular velocity  $\omega$ ,  $\ddot{\alpha}$  is the angular acceleration ( $=\dot{\omega}$ ), and  $A$  is the direction cosine matrix. The eigenvalue  $\lambda_k$  and the eigenvector  $\Phi_{ik}$  of the body are obtained by modal analysis of a finite element solver. The modal proportional viscous damping coefficient  $c_k$  is estimated by experimental modal analysis. Eq.(1) is calculated by time integration method, as mentioned later.

The LOF observes the motion of the body locally while being located in the vicinity of the body, as shown in Fig. 3. At each time step in the calculation, the LOF is updated appropriately so that the modal coordinate  $q_k$  should be infinitesimal in Eq.(1). In Fig. 2, the LOF for the crankshaft is coordinate [1], and that of the cylinder block is coordinate [2]. Though the LOF can be set at the arbitrary position of the body element, for a rotating body such as a crankshaft the LOF should be attached to the rotating axis for simplification of the calculation.

### 3. 2 Force element

The force elements acquire the state values such as displacement and velocity of body elements at each time step, and calculate the force  $F_i$  in Eq.(1) using the state values. The calculated force is given to the body elements. The calculational method differs depending on the kind of force element. Figure 4 shows a piston-conrod element. This element generates the combustion force  $F_c$ , the piston side force  $F_s$ , the friction force  $F_f$  between a piston and cylinder, and the crankpin input force  $F_{py}$  and  $F_{pz}$  according to the crank angle  $\theta$ . The combustion force  $F_c$  is calculated by the measured or predicted cylinder gas pressure. From the combustion force, other forces are calculated by kinematic method. For example, the piston side force  $F_s$  is calculated by the following equation using the piston mass  $m_p$  and the equivalent reciprocating mass  $m_1$  of the conrod.

$$F_s = - \left\{ F_c - R\dot{\theta}^2 (m_p + m_1) \left( \cos \theta + \frac{R}{L} \cos 2\theta \right) \right\} \tan \phi \quad . (2)$$

Figure 5 and Figure 6 show the journal bearing element. This element generates the oil film force  $F_b$  and moment  $M_b$  from the eccentricity  $e$  of the journal center, the eccentricity velocity  $\dot{e}$ , the attitude angle  $\psi$  and the attitude angular velocity  $\dot{\psi}$  based on hydrodynamic lubrication theory. The oil film pressure  $p$  is approximately calculated using the next equation from Reynold's equation:

$$p = \frac{6\eta x(x-B)}{h^3} \left\{ \frac{\bar{\omega}}{2} \frac{\partial \bar{h}}{\partial \varphi} + \left( \frac{\bar{\omega}}{2} - \dot{\psi} \right) e \sin \delta - \dot{e} \cos \delta \right\} \quad (3)$$

where  $\eta$  is the viscosity coefficient of the oil,  $\bar{h}$  is the radial clearance when the journal center is at the bearing center,  $h$  is the radial clearance when the journal center is eccentric, and  $\bar{\omega}$  is the spin angular velocity of the journal. The oil film force  $F_{bx}$  and  $F_{by}$  are calculated by the integration of Eq.(3) in the bearing surface where the pressure  $p$  becomes positive. In addition, two journal elements are arranged as shown in Fig. 6 to express the moment  $M_b$  by the force  $F_{b1}$  and  $F_{b2}$ .

Figure 7 shows the motor element which simulates the power transmission from the dynamometer to the clutch in engine bench tests [6].

Disk 1 is a rotational driver and it rotates as

$$\dot{\theta} = \omega t + \theta_0 \quad . (4)$$

where  $\omega$  is the angular velocity of disk 1, and  $\theta_0$  is the initial phase. Disk 2 expresses the clutch. The torque  $T_r$  acting on the clutch is calculated by the rotational spring coefficient  $K_r$  and damping coefficient  $C_r$  which simulate a torsional clutch spring as follows:

$$\dot{T} = -K_r (\theta_2 - \theta_1) - C_r (\dot{\theta}_2 - \dot{\theta}_1) \quad (5)$$

The engine mount element expresses the support force of engine mounts. The thrust bearing element expresses the constraint of the crankshaft in the axial direction. These elements are composed of a nonlinear spring and damper. The belt element expresses the timing belt which connects a crank pulley and accessory pulleys as shown in Fig. 8. Here, the forces  $F_{B1}$ ,  $F_{B2}$ ,  $F_{B3}$ ,  $F_{B4}$  acting on each pulley center are calculated on the assumption that the belt tension  $T_B$  is constant.

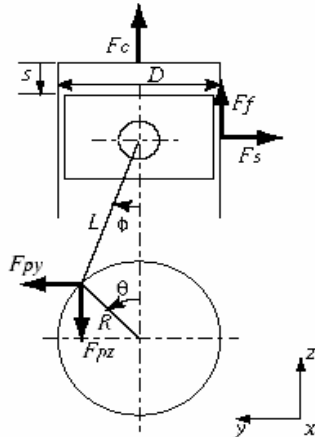


Fig. 4. Piston-crank element

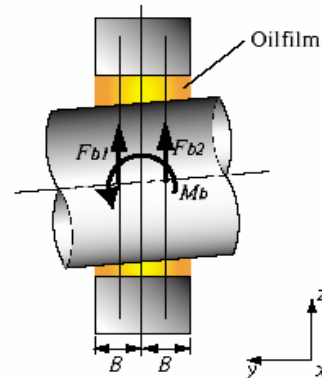


Fig. 5. Journal Bearing element (side view)

#### 4. NUMERICAL CALCULATION OF EVAS

In EVAS, the vibration response of the engine system is calculated by a time integration method. Figure 9 shows the entire flow of the calculation. In Step <1> in Fig. 9, the eigenvalue  $\lambda_j$  and eigenvector  $\Phi_{ij}$  calculated beforehand by a finite element solver, are set to the body elements. In Step <2>, the time is set up in the start time  $sT$  and the body elements, and the force elements are set to the initial condition. Steps <3> to <6> are the procedure series for calculating the response at the time  $t$ . In Step <3> the forces determined explicitly by the function of time are calculated, such as the combustion force  $F_c$  and the crankpin input  $F_{py}$  and  $F_{pz}$ . In Step <4>, the response of each body element is calculated according to the acting force. In Step <5>, each force element acquires the state values of the body elements and calculates provisionally the unknown forces such as the journal bearing force  $F_{by}$  and  $F_{bz}$ , the driving torque  $T_r$  of the motor element and the support force of the mount element. The time integration of Step <4> is performed by a linear acceleration method. The convergence calculation is carried out by the numerical feedback loop from steps <4> to <6> as the balance error of Eq.(1) becomes 0.1% or less at the time  $t$ . If the calculation converges, the time  $t$  is advanced  $dt$  and the step returns to <3>. Below, steps <3> to <7> are repeated to the end time  $eT$ .

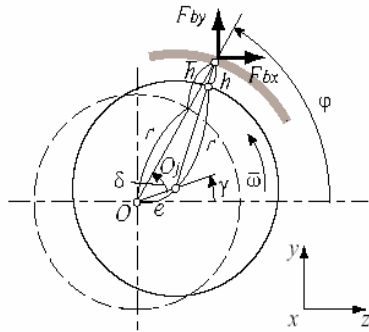


Fig. 6. Journal Bearing element (cross section)

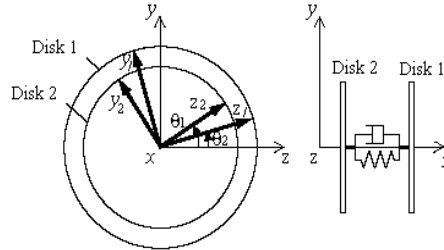


Fig. 7. Motor element

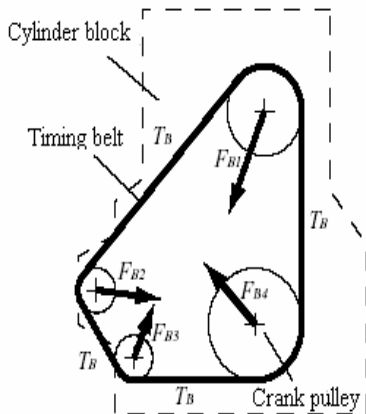


Fig. 8. Belt element

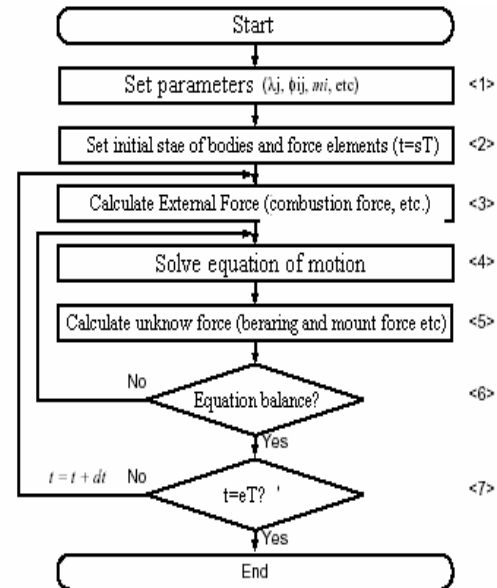


Fig. 9. Flowchart of calculation

## 5. MARINE SHAFTING TORSIONAL VIBRATIONS

Shafting torsional vibrations are characterized by shafting variable speed of rotation. In contrast to some other, easily visible or perceptible kind of vibration like axial or lateral vibrations, shafting torsional vibrations are "invisible". However, this kind of shafting vibration may become, under certain circumstances, a cause of serious damages, even fractures of shafting.

Torsional vibrations are the characteristic of nearly all rotational machines and devices. However, torsional vibrations of internal combustion engines and their shafting are especially significant. These vibrations appear as the result of variable revolution of rotating parts, invisible to human eye.

Torsional vibrations are the consequence of a number of processes. The most common are:

- Variable gas pressure in the cylinder of an engine;
- Inertial forces of a crank mechanism;
- Fluctuation of sea water flow around the propeller.

The excitation of torsional vibrations is significantly determined by the piston's stroke and the mean effective pressure. The ongoing increase of these characteristics is the cause of increased vibration excitation in the recent propulsion plants.

The variable torque, generated in the engine's cylinder is transmitted through the shafting up to the propeller. This torque initiates the vibration movement of the propulsion plant components.

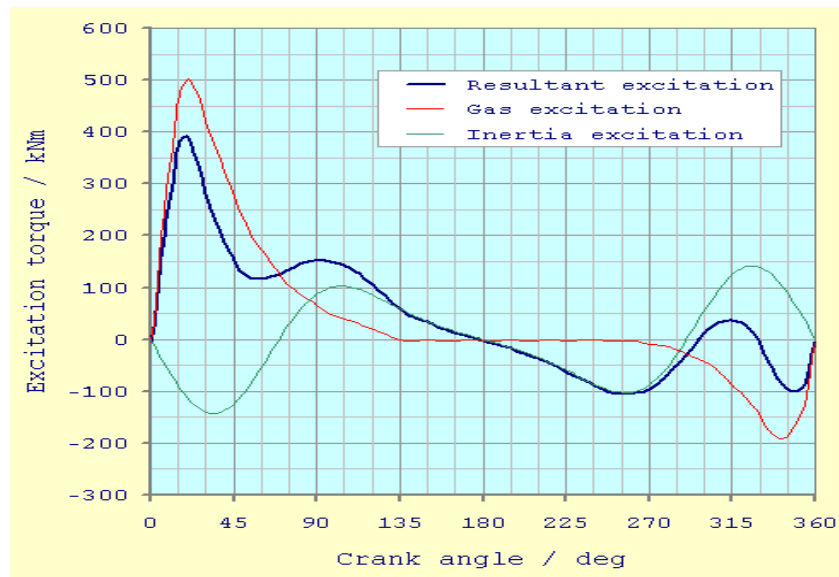


**Fig.10. Excitation torque generated in cylinder of a typical low-speed diesel engine during crankshaft's full revolution (360 degrees). The resultant excitation combines the influences of the gas pressure and the crank mechanism inertial forces**

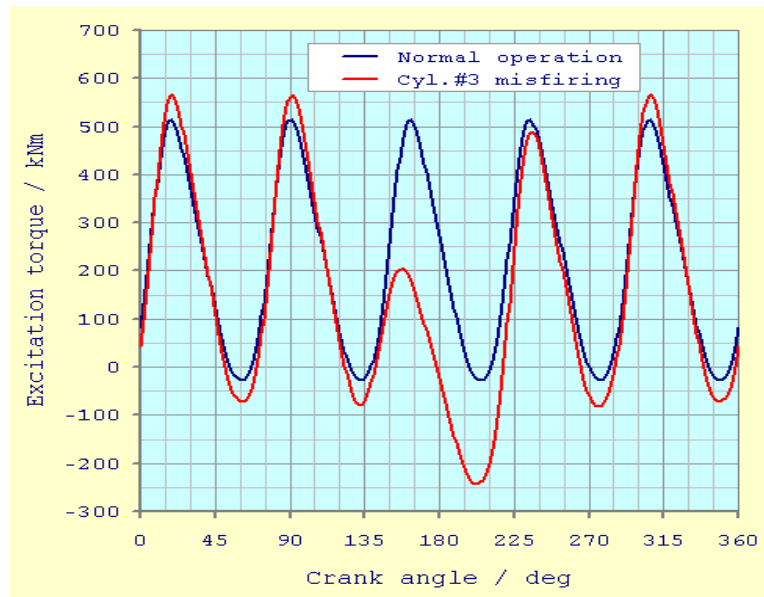


**Fig. 11. Cumulative excitation torque generated in a typical five-cylinder low-speed diesel engine during crankshaft's full revolution (360 degrees). The blue line represents the case when all cylinders work properly (normal operation). The red line represents the case when cylinder no. 3 lacks ignition (misfiring operation)**

## REFERENCES

- [1]. Buzbuchi N., Taraza D., Lyridis D. - **Theoretical and Experimental Study of the Torsional, Bending and Axial Coupled Vibration of Marine Diesel Engine Shafting System**, Bull. of the Mar. Eng-ing Soc. in Japan (MESJ), the Fifth International Symposium on Marine Engineering ISME, Yokohama, 1995.
- [2]. Buzbuchi N. - **Fundamentals Effect Between Torsional and Longitudinal Shafting Vibration**, ISSN 1224-6077, A X-a Conferință Națională de Vibrații Mecanice, Timișoara, 1999.
- [3]. Buzbuchi N., Boianjiu M., Șoloiu V.A. - **Simulation of Coupled Vibrations in Two-Stroke Engine Crank Shafting**, Buletinul Tehnic al Registrului Naval Român, nr. 3-4, București, ISSN-1220-7357, 1998.
- [4]. Jenzer J., Welte Y. - **Coupling Effect between Torsion and Axial Vibration in Installations with Two - Stroke Diesel Engines**, New Slugger Diesel, 1991.
- [5]. Shimoyamanda K., Wakabayashi K., Kodana T., Honda Y., Iwamoto, S., - **Technical Series Paper No 930197**, SAE International Congress & Exhibition, 1993.
- [6]. Kawamoto A., Inagaki M., Aoyama T., Mori, N. - **Vibration of Moving Flexible Body**, ASME DETC'99 Proc., VIB-8232, (1999), ASME.

## STRUCTURAL AND KINEMATIC VIBRATION ON INTERNAL COMBUSTION ENGINE - PART II

<sup>1</sup>BUZBUCHI NICOLAE, <sup>1</sup>STAN LIVIU, <sup>1</sup>MEMET FEIZA

<sup>1</sup>Constanta Maritime University, Romania

As presented in the title, the present paper is a sequel of the previous one, dedicated to the general study of the engine dynamic system. For this engine we developed a structural and kinematic model. The main purpose is now the study of the marine engine dynamic behaviour, including the system response, stress limits, the influence of one missfiring cylinder, system resonance and counteracting shafting torsional vibrations. The main conclusions have been presented in Part I

**Keywords:** engine vibration analysis, marine shafting torsional vibrations, resonance

### 1. THE RESPONSE OF A SYSTEM

Mechanical systems, as a whole, possess some vibration properties denoted as *natural frequencies* and corresponding *modes of vibration*.

If the frequency of excitation, expressed as the number of impulses per second, is sufficiently different from the system's natural frequency, the system will vibrate "moderately". If, however, the frequency of excitation is equal, or nearly equal, to the system's natural frequency, the system will respond by strong, even severe vibrations, Figure 1.

The propulsion plant, composed of the propulsion engine, the shafting and the propeller, denotes a vibration system. This system, determined by the inertia of its components, as well as by the stiffness between them, possesses its own natural frequencies and corresponding modes of vibration.

The propulsion shafting, composed of the crankshaft, the intermediate shaft and the propeller shaft, will start to vibrate when excited by variable torque.

The main consequence of propulsion shafting torsional vibration is the occurrence of torsional vibration stresses in the components of the system, Figure 2. The total torsional stress in each component of a shafting system is then determined as the sum of a vibration stress component and a static stress component. As mentioned earlier, the static stress component is a product of power transmission.

### 2. STRESS LIMITS

Classification societies prescribe the amount of allowable torsional vibration stresses for engine crankshafts, intermediate shafts and propeller shafts. These stress limits are determined by the purpose, shape, material selected, dimensions and intended operation of

shafting. Moreover, the stress limits are not constant; instead they are a function of engine speed.

At the engine's low speeds, the stress limits increase, whereas at the engine's high speeds, the stress limits decrease. When the engine's speed rise, the static stress component rise and it is necessary that the total stress level remain within some acceptable limits.

For the each shaft type, classification societies prescribe two values of stress limits - the lower and the higher, Figure 2.

The lower stress limit is applicable for the entire speed range of a propulsion plant. This limit determines the maximum stress level allowed for the continuous engine operation.

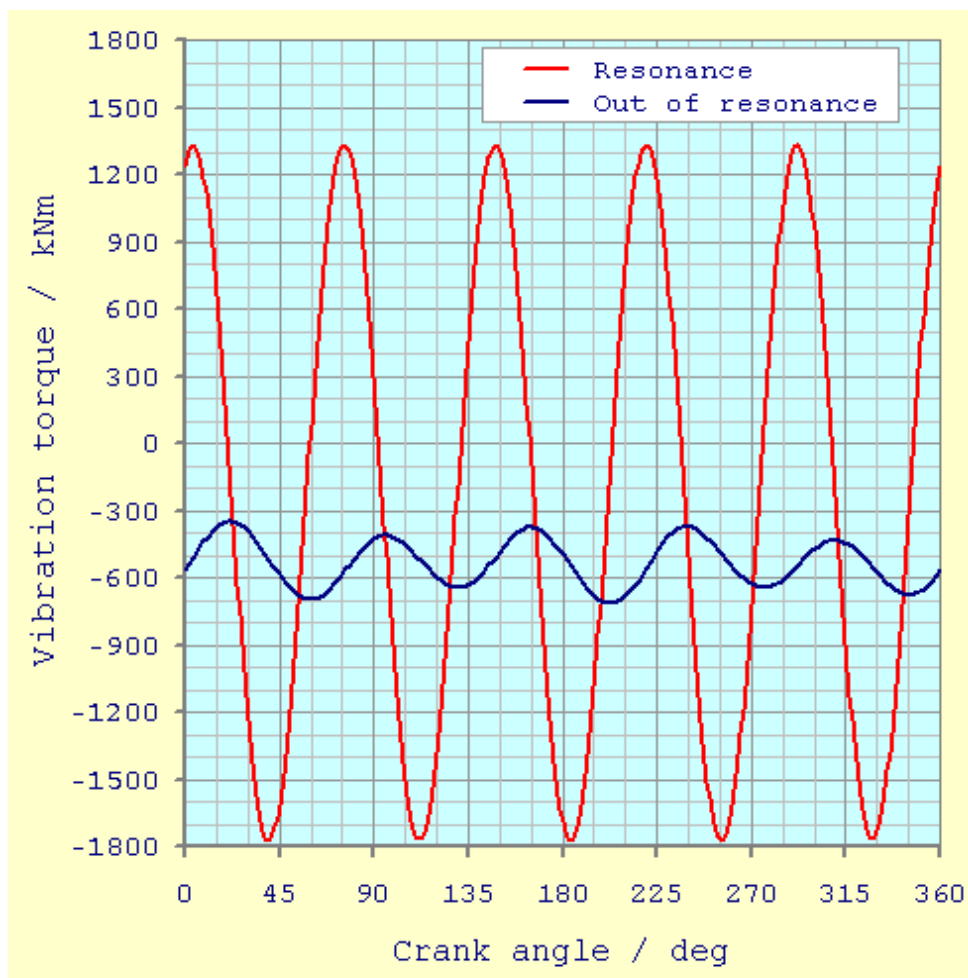


**Fig. 1. Typical vibration torque variation in a propeller shaft of a conventional low-speed diesel engine propulsion plant. The blue line corresponds to system out-of-resonance running condition, while the red line corresponds to system resonance running condition**

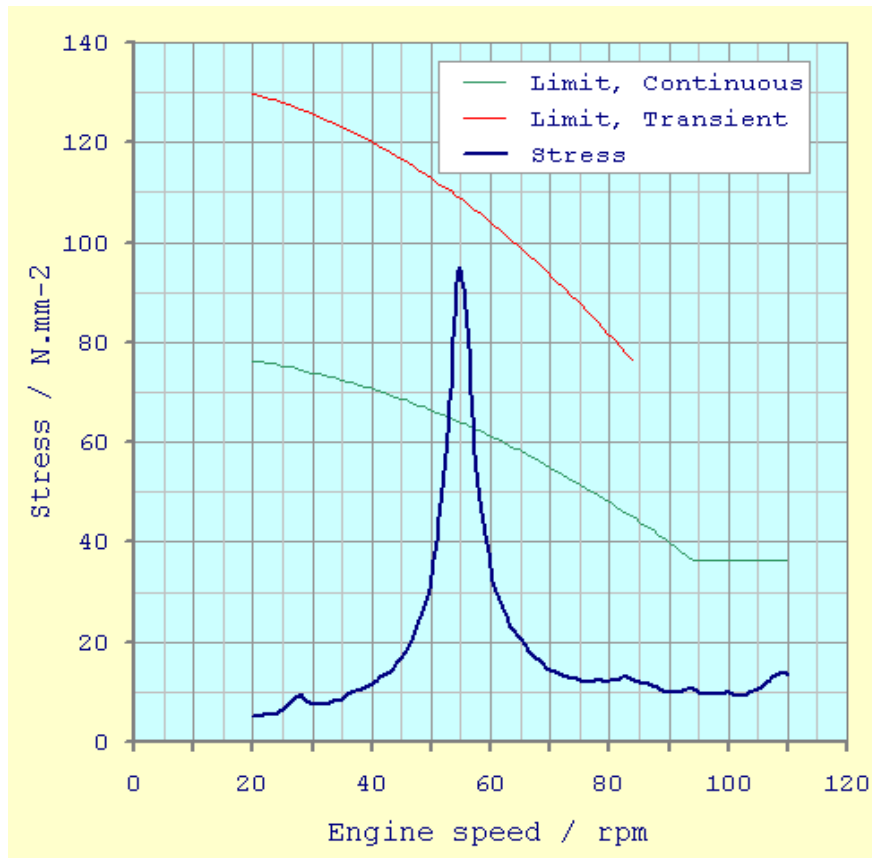


**Fig. 2. Typical torsional vibration stress response for intermediate shaft during normal operation of a conventional low-speed diesel engine propulsion plant. Stress limits for engine continuous as well as transient running are also included**

The higher stress limit is applicable only for a fraction of the entire speed range, i.e. up to 80% of engine maximum continuous speed. This stress limit represents the stress level which, in any case, should not be exceeded.

In the events when actual vibration stresses exceed the lower stress limit, but not the higher stress limit, the so-called barred speed range is introduced.

The barred speed range has to be passed through rapidly. Actually, torsional vibrations need some time to be fully developed and, if the barred speed range is passed sufficiently fast, there is a great possibility that the full stress level will never be reached.

The barred speed range is clearly noted in red on the tachometer, as well as on notice boards. Moreover, the recent propulsion plants are equipped with special devices that ensure that this range should be passed through rapidly.

The intermediate shaft vibratory stress variation, as shown in Figure. 2, exhibits some interesting points deserving more clarification.

- Engine speed ranges below 40 rpm and over 70 rpm are characterized by moderate, even low stress levels. Torsional vibration stress is exceptionally low in the engine

speed range above 90 rpm, i.e. in the vicinity of an engine service speed that amounts to 105 rpm. Fortunately, the static torsional stress component is the largest in this region.

- The peak vibration stress is reached at 55 rpm, when the engine output is less than 15% of the maximum continuous rating. At the same time, the static stress component amounts to approximately one third of the shaft static stress at the nominal engine speed. This is due to the resonance between the excitation torque and the system's natural frequency. Therefore, this engine speed is usually called the critical speed.
- In the engine speed range between 53 and 57 rpm the actual vibration stress is higher than the stress limit for continuous running and the barred speed range is introduced. For the safety reasons, the actual restricted speed range is usually imposed in a slightly wider interval.

### 3. THE INFLUENCE OF ONE CYLINDER NOT FIRING

In general, any kind of irregularity in cylinder firings usually produces enlarged vibratory stresses in the components of a propulsion plant. As shown in Figure 3, the absence of firing in one of the cylinders significantly changes the whole picture of propulsion plant torsional vibration behavior.

Misfiring in any one cylinder causes the rise of resonances that are small, even negligible, during the engine's normal operation. Moreover, these resonances are usually placed in the vicinity of an engine's rated speed and, therefore, they are the cause of an additional operation limitation. Fortunately, these operation limitations are not permanent, but only applicable until the resolution of the problem.

In the case of an intermediate shaft shown in Figure 3, the additional speed restrictions would be, alongside with the previous one, in the interval from 80 rpm to 86 rpm, as well as in the region above 102 rpm. Since no one classification society allows barred speed ranges in the region above 80% of the rated speed, the operation limitation will read: "*in the event of one cylinder misfiring the maximum engine speed is not to exceed 80 rpm*". The note of this or a similar meaning should be included in the propulsion plant operation manual.

### 4. RESONANCE

The resonance is a state of movement when system vibrates in phase with an externally applied load. The excitation torque is built of a number of single harmonic excitations. Each single harmonic excitation has its own frequency, which is a multiple of the shaft rotation frequency. This multiple is called *order*. There exists the first order excitation, the second order excitation, etc. Of course, the  $n$ -th order excitation produce the  $n$ -th order response. Finally, the system response, Figure 4, is also built of a number of single harmonic responses.

Each single harmonic response has its own system resonance. Various peaks on the diagram in Figure 4 correspond to such system resonances.

The main resonance, usually denoted as a system main critical speed, is a resonance when the system vibrates in phase with the  $n$ -th order excitation. If the propulsion plant is powered by a two-stroke engine,  $n$  is equal to the number of engine cylinders. If, on the other hand, the propulsion plant is powered by a four-stroke engine,  $n$  is equal to the one half of the number of engine cylinders.

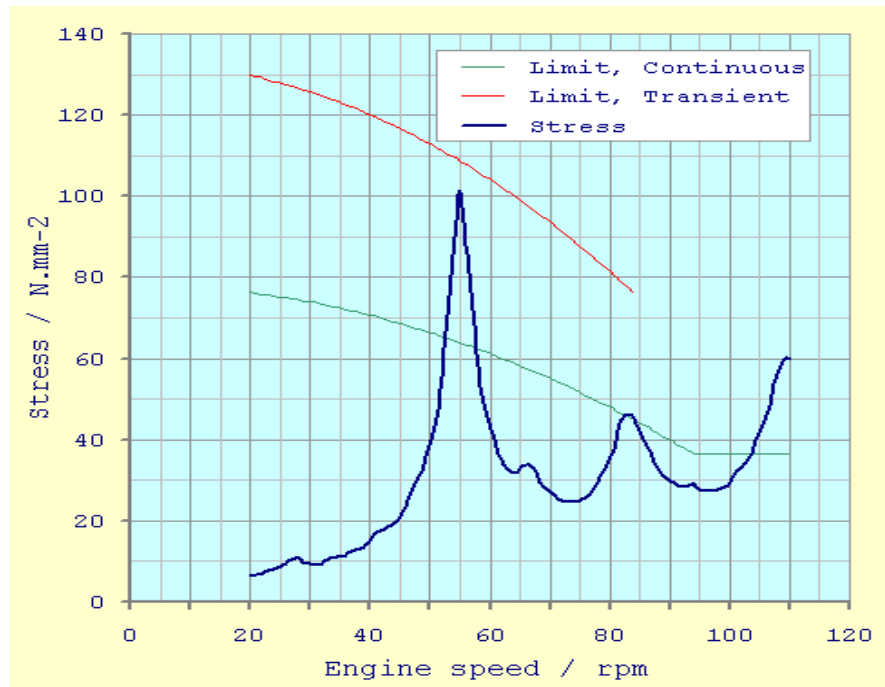


**Fig. 3. Typical torsional vibration stress response for intermediate shaft during one cylinder misfiring operation of a conventional low-speed diesel engine propulsion plant. Stress limits for engine continuous as well as transient running are also included**

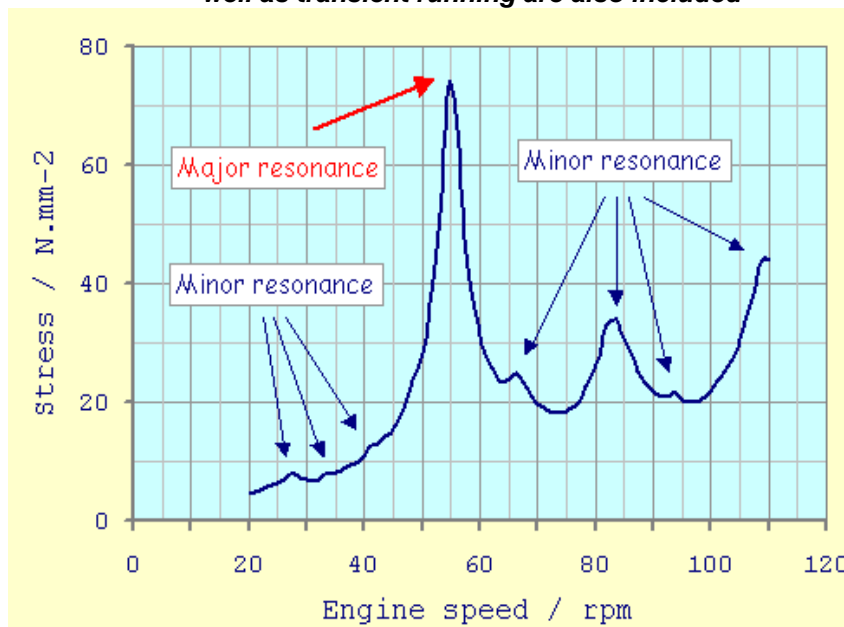


**Fig. 4. Resonances**

## 5. COUNTERACTING SHAFTING TORSIONAL VIBRATIONS

The easiest, the fastest and the most cost-effective way to counteract shafting torsional vibrations is in the propulsion shafting design phase. Later, when the propulsion shafting is finished and put in operation, the satisfactory solutions are rare and more expensive.

During propulsion shafting design phase it is possible by proper design to keep vibration responses within the allowable limits. The most usual measures are:

- selection of appropriate dimensions and materials;
- selection of appropriate turning wheel;
- selection of engine appropriate location, if applicable.

Minor torsional vibration problems of an existing propulsion plant may be resolved by appropriate operations, i.e. by the rapid pass through the hazardous speed ranges. If this is not applicable, the only possible solutions are the propulsion shafting redesign, or mounting of a torsional vibration damper.

The torsional vibration damper is a device that should be mounted on the fore end crankshaft flange. It absorbs some vibration energy from the system and in that way saves the propulsion shafting components from the unacceptable stress levels. However, it should be clearly realized that this solution may be prohibitively costly - the cost of a large torsional vibration damper may be in excess of US\$ 100.000 per piece.

## REFERENCES

- [1]. Buzbuchi N., Taraza D., Lyridis D. - **Theoretical and Experimental Study of the Torsional, Bending and Axial Coupled Vibration of Marine Diesel Engine Shafting System**, Bull. of the Mar. Eng-ing Soc. in Japan (MESJ), the Fifth International Symposium on Marine Engineering ISME, Yokohama, 1995.
- [2]. Buzbuchi N. - **Fundamentals Effect Between Torsional and Longitudinal Shafting Vibration**, ISSN 1224-6077, A X-a Conferință Națională de Vibrații Mecanice, Timișoara, 1999.
- [3]. Buzbuchi N., Boianciu M., Șoloiu V.A. - **Simulation of Coupled Vibrations in Two-Stroke Engine Crank Shafting**, Buletinul Tehnic al Registrului Naval Român, nr. 3-4, București, ISSN-1220-7357, 1998.
- [4]. Jenzer J., Welte Y. - **Coupling Effect between Torsion and Axial Vibration in Installations with Two - Stroke Diesel Engines**, New Slugger Diesel, 1991.
- [5]. Shimoyamanda K., Wakabayashi K., Kodana T., Honda Y., Iwamoto S. - **Technical Series Paper No 930197**, SAE International Congress & Exhibition, 1993.
- [6]. Kawamoto, A., Inagaki, M., Aoyama, T., Mori, N. **Vibration of Moving Flexible Body**, ASME DETC'99 Proc., VIB-8232, (1999), ASME.
- [7]. Wang, P.C.- **Numerical and Matrix**

## EXPLICIT DYNAMIC SIMULATION OF A PIPE DEBRIS PROJECTILE IMPACT OVER A NUCLEAR HEAVY WATER STORAGE VESSEL

<sup>1</sup>CALIMANESCU IOAN, <sup>2</sup>GRIGORESCU LUCIAN

<sup>1</sup>Saipem SpA Italy, <sup>2</sup>Constanta Maritime University ,Romania

The purpose of this article is to numerically investigate the dynamic response of a heavy water nuclear storage vessel subjected to an impact with high speed debris (pipe fragment). The pipe fragment has a mass of 31 kg. There were employed 5 different simulation scenarios, where the projectile was supposed to have speeds from 10 to 50 m/sec. The used simulation code was ANSYS/LS-DYNA, taking advantage of its explicit dynamics facilities and capability to model a solid/fluid interface. The impact was studied for the vessel wall which was simulated involving Shell 163 type finite elements and also the effect of the fluid on response was considered, the vessel being considered filled with radioactive heavy water at atmospheric pressure.

**Keywords:** FEA, Explicit Dynamic, Simulation, Projectile, Impact, Nuclear, Vessel.

### 1. INTRODUCTION

Under the UK Nuclear Installations Act (1965), the safety of a nuclear plant is the responsibility of the operator, or licensee. The latter is required to submit to the Nuclear Installations Inspectorate (NII) “a written demonstration of safety, the safety case, which is periodically updated to reflect changing conditions”. The Safety Case is then assessed by the NII to determine whether it is “adequate”, within the framework of a set of principles called.

The purpose of this article is to investigate the dynamic response of a heavy water nuclear storage vessel subjected to an impact with high speed debris (pipe fragment).

The pipe fragment has a mass of 31 kg. There were employed 5 simulation scenarios, where the projectile was supposed to have speeds from 10 to 50 m/sec. The used simulation code was ANSYS/LS-DYNA using its explicit dynamics facilities. The impact was studied for the vessel wall which was simulated involving Shell 163 type finite elements and also the effect of the fluid on response was considered, the vessel being considered filled with fluid at atmospheric pressure.

ANSYS/LS-DYNA combines the LS-DYNA explicit finite element program with the powerful pre- and post-processing capabilities of the ANSYS program. The explicit method of solution used by LS-DYNA provides fast solutions for short-time, large deformation dynamics, quasi-static problems with large deformations and multiple non-linearity, and complex contact/impact problems.

## 2. NUMERICAL INVESTIGATION

### 2.1 CAD-FEA Model

The CAD geometry of the vessel and the projectile, with all their dimensions and relative positions (in meters) at the time 0 seconds of simulation, are given in the figure below:

The Vessel wall is supposed to be made out of 1018 Steel plate with the thickness of 8 mm and with a Plastic Kinematic material behavior. The finite elements type used were Shell 163.

The plastic Kinematic type of material in ANSYS definition may be isotropic, kinematic, or a combination of isotropic and kinematic hardening models with strain rate dependency and failure. Isotropic and kinematic contributions may be varied by adjusting the hardening parameter  $\beta$  between 0 (kinematic hardening only) and 1 (isotropic hardening only). Strain rate is accounted for using the Cowper-Symonds model which scales the yield stress by the strain rate dependent factor as shown below: where  $\sigma_0$  is the initial yield stress,  $\dot{\epsilon}$  is the strain rate, C and P are the Cowper-Symonds strain rate parameters,  $\epsilon_p^{eff}$  is the effective plastic strain, and  $E_p$  is the plastic hardening modulus.

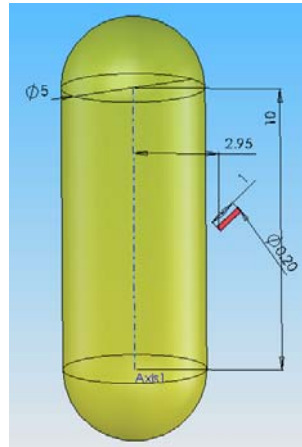


**Fig.1.CAD geometry of Vessel and Projectile.**

$$\sigma_y = \left[ 1 + \left( \frac{\dot{\epsilon}}{C} \right)^{\frac{1}{P}} \right] \left( \sigma_0 + \beta E_p \epsilon_p^{eff} \right) \quad (1)$$

$$E_p = \frac{E_{tan} E}{E - E_{tan}}$$

The Vessel is filled with radioactive heavy water at atmospheric pressure. The fluid domain was modeled using the Solid 164 type of finite elements in which the material model was deemed to be the Elastic Fluid Material Model. By using this option to modeled vessel, filled with fluid, the impact will be more realistically treated by the software. The fluid model requires that the bulk modulus be specified, (which is 2.2e9 Pa) and the density of 1002 kg/m<sup>3</sup>. Between the vessel wall domain and the fluid domain a contact surface was established in order to have the loading effects transferred from wall to the fluid and back. This will allow simulating the dynamic response of the system vessel-fluid as a whole.

The projectile itself was modeled with Solid 164 finite elements type and the Rigid type of material was involved.

The boundary conditions were imposed to the lower part of the Vessel by restricting the degrees of freedom of certain nodes. No other loads as internal pressure of the fluid or temperatures were imposed to the model.

The adaptive meshing setting was on for the vessel wall finite elements mesh.

## 2.2 Simulation Scenarios

The study comprised 5 different scenarios, in which the Vessel was supposed to stay fixed and the speed of impact projectile was varied from 10; 20; 30; 40 and 50 m/sec. Some selected results are shown below.

### Projectile speed 10 m/sec

The time for impact with the given projectile speed is considered to be 0.041 seconds after simulation start.

At the impact time the program calculated some results both for vessel wall and the fluid domain and they are given below.

The von Mises equivalent stress reaches a maximum value of 8.71 MPa at the impact area. The impact energy is absorbed by the structure and converted in deformation energy, this changing the stress state all over the vessel wall. Also the fluid inside the vessel contributes to disseminate the impact energy in the structure, this contributing to the stress distribution as shown in the Figure 2.

The distribution of pressures due to the impact, inside the fluid, will be different of those of vessel wall structure, both as shape and as magnitude. The maximum value is reached away from the impact point, at the upper side of the vessel, due to the geometric configuration of the vessel, and the value is 5192 Pa, as may be seen in the Figure 3.

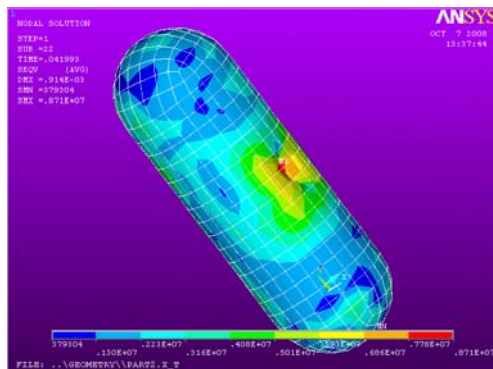


**Fig.2. Von Mises Equivalent Stress distribution at impact time on the vessel wall-Impact Speed 10 m/sec.**

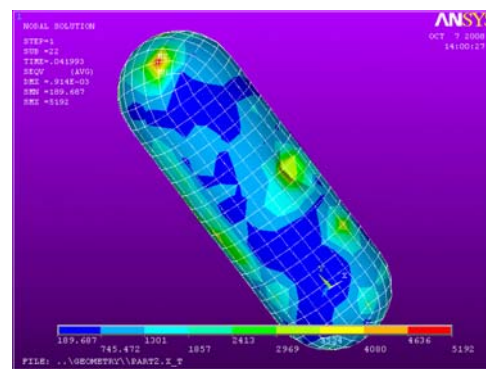


**Fig.3. Pressure distribution at impact time in the fluid-Impact Speed 10 m/sec.**

By studying the Time History of the von Mises stress for a vessel wall finite element node situated very close to the impact area, the graph below was deduced:

The two peaks seen in the graph are due to the fact that the projectile is hitting the vessel first with one end and secondly with the other end before being repulsed back.

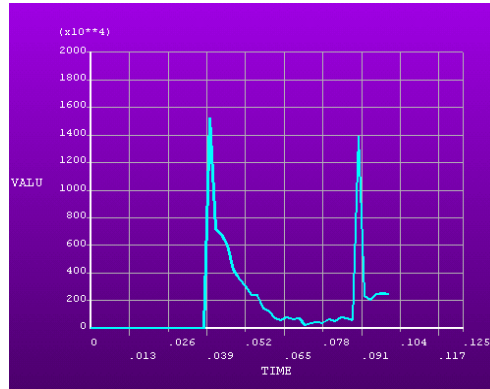


**Fig.4. Time History of von Mises Equivalent Stress for impact area-Impact Speed 10 m/sec.**

The maximum vessel wall acceleration of  $673 \text{ m/sec}^2$  is located in the upper side, having almost the same magnitude and distribution as the acceleration of the fluid (Figures 5 and 6).

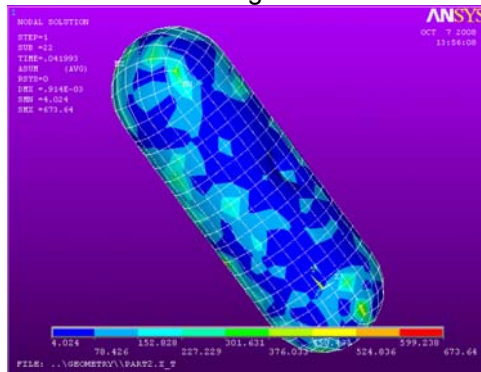


**Fig.5. Acceleration distribution at impact time on the vessel wall-Impact Speed 10 m/sec.**

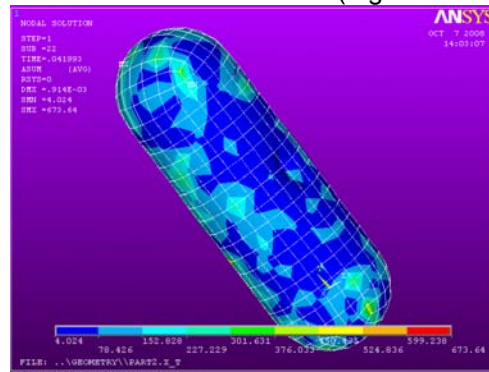


**Fig.6. Acceleration distribution at impact time within the fluid-Impact Speed 10 m/sec**

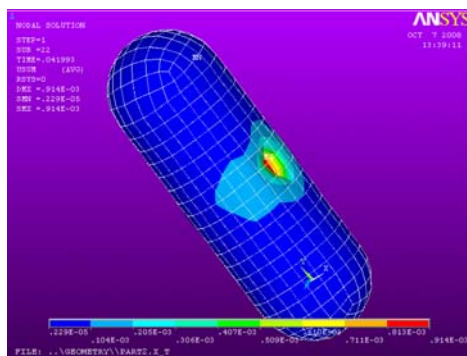


**Fig.7. Displacement distribution at impact time of the vessel wall -Impact Speed 10 m/sec.**

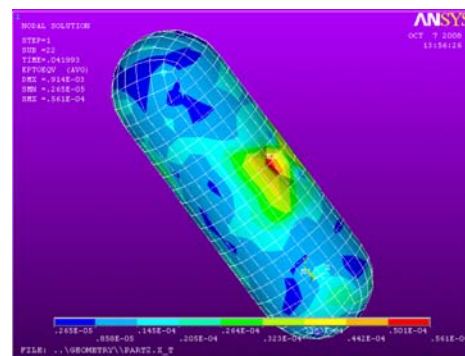


**Fig.8. Total Strain distribution at impact time of the vessel wall -Impact Speed 10 m/sec.**

The maximum displacement of vessel wall is 0.93 mm in the impact area as shown in the Figure 7. The total strain, as expected, reaches its maximum value of  $0.561e-4$  at the impact region having a pattern very similar to those of the equivalent stress.

Projectile speed 30 m/sec

The time for impact with the given projectile speed is considered to be 0.0159 seconds after simulation start. At the impact time the program calculated some results both for vessel wall and the fluid domain and they are given below.

The von Mises equivalent stress reaches a maximum value of 91.9 MPa at the impact area (Fig.9).

The distribution of pressures due to the impact, inside the fluid, will be different of those of vessel wall structure as well. The maximum value is reached away from the impact point, at the upper side of the vessel, due to the geometric configuration of the vessel, and the value is 364579 Pa, many times bigger that those of the previous scenario, as may be seen in the Figure 10.

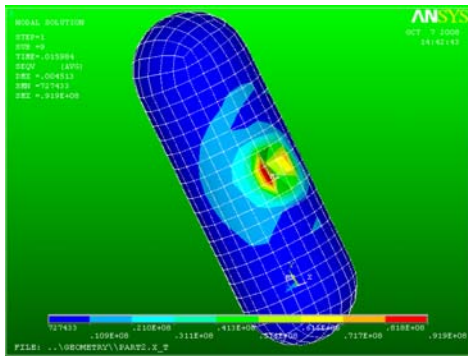


**Fig.9. Von Mises Equivalent Stress distribution at impact time on the vessel wall-Impact Speed 30 m/sec.**

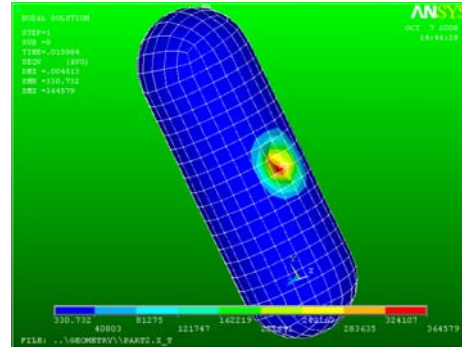


**Fig.10. Pressure distribution at impact time in the fluid-Impact Speed 20m/sec.**

Considering the Time History of the von Mises stress for a finite element node (vessel wall) situated very close to the impact area, the graph below was deduced:

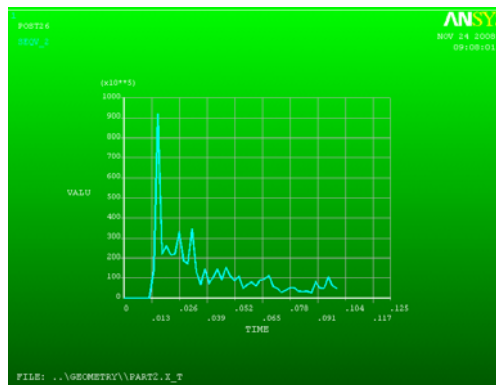


**Fig.11. Time History of von Mises Equivalent Stress for impact area-Impact Speed 30 m/sec.**

Also it may be seen the two peaks in the graph which are due to the fact that the projectile is hitting the vessel first with one end and secondly with the other end before being repulsed back, are different as magnitude, the projectile being massively decelerated after the first blow, the second one being a low energy hit.

The maximum vessel wall acceleration of  $41827 \text{ m/sec}^2$  is located this time at the impact region, having almost the same magnitude and distribution as the acceleration of the fluid, which is normal since the fluid and the wall share a common boundary (Figures 12 and 13).

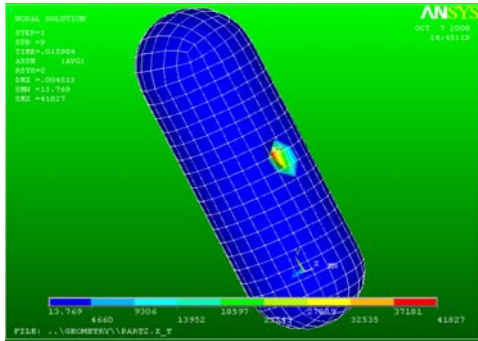


**Fig.12. Acceleration distribution at impact time on the vessel wall-Impact Speed 30 m/sec.**

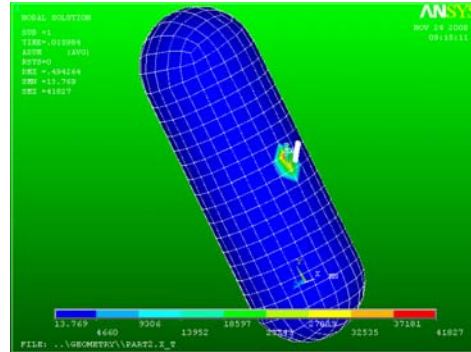


**Fig.13. Acceleration distribution at impact time within the fluid-Impact Speed 30 m/sec.**

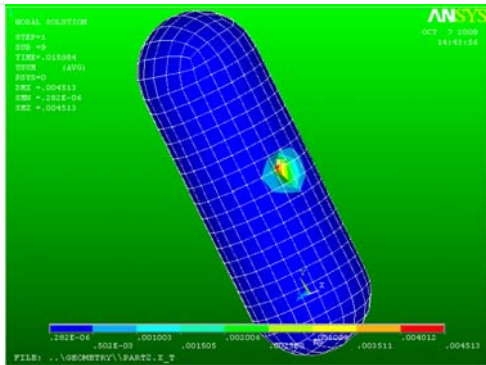


**Fig.14. Displacement distribution at impact time of the vessel wall -Impact Speed 30 m/sec.**

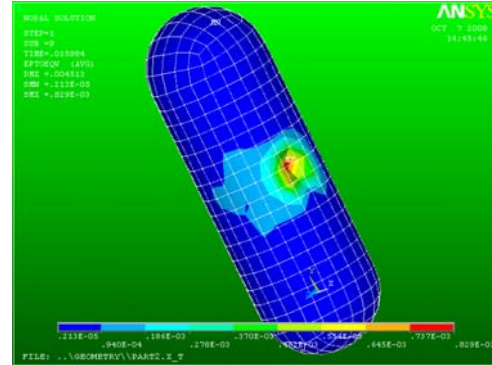


**Fig.15. Total Strain distribution at impact time of the vessel wall -Impact Speed 30 m/sec.**

The maximum displacement of vessel wall is 4.5 mm in the impact area, much greater than those of the previous scenario as shown in the Figure 14.

The total strain reaches its maximum value of  $0.829 \times 10^{-3}$  at the impact region having a pattern very similar to those of the equivalent stress.

Projectile speed 50 m/sec

The time for impact with the given projectile speed is considered to be 0.0139 seconds after simulation start.

The von Mises equivalent stress reaches a maximum value of 209 MPa at the impact area (Fig.16), in this scenario the stress being near the yield toughness (310 MPa). We may

conclude that further increasing the projectile speed, the local stresses at the impact region, will reach and surpass the yield and ultimate toughness of the material. For the time being the vessel still resists to the impact.

The distribution of pressures due to the impact, inside the fluid, will be different of those of vessel wall structure as well. The maximum value is reached away from the impact point, at the upper side of the vessel, due to the geometric configuration of the vessel, and the value is 163808 Pa, as may be seen in the Figure 17.

Considering the Time History of the von Mises stress for a finite element node situated very close to the impact area, the graph below was deduced (Fig.18).

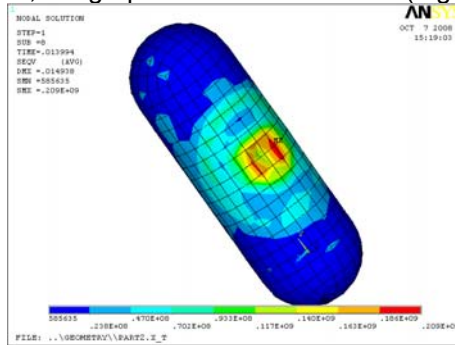


**Fig.16.Von Mises Equivalent Stress distribution at impact time on the vessel wall-Impact Speed 50 m/sec.**

The maximum vessel wall acceleration of  $131490 \text{ m/sec}^2$  is located this time at the impact region, having almost the same magnitude and distribution as the acceleration of the fluid ( $176769 \text{ m/sec}^2$ ), which is normal since the fluid and the wall share a common boundary.

The maximum displacement of vessel wall is this time 14 mm in the impact area, much grater that those of the previous scenario as shown in the Figure 20.

The total strain reaches its maximum value of 1.378% at the impact region very near to the yielding strain of 2%. The vessel is still deforming in the elastic region even at projectile sped of 50 mps (Figure 21).

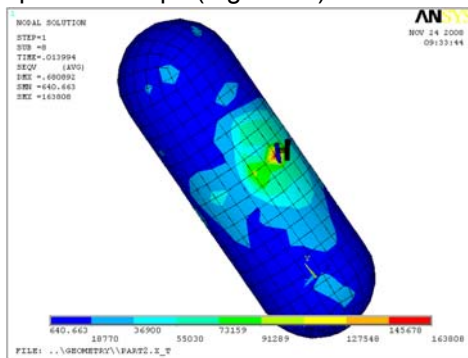


**Fig.17.Pressure distribution at impact time in the fluid-Impact Speed 50 m/sec.**

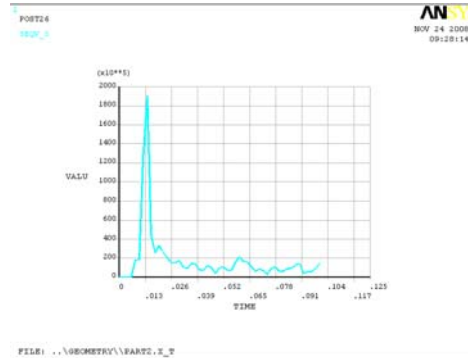


**Fig.18.Time History of von Mises Equivalent Stress for impact area-Impact Speed 50 m/sec.**

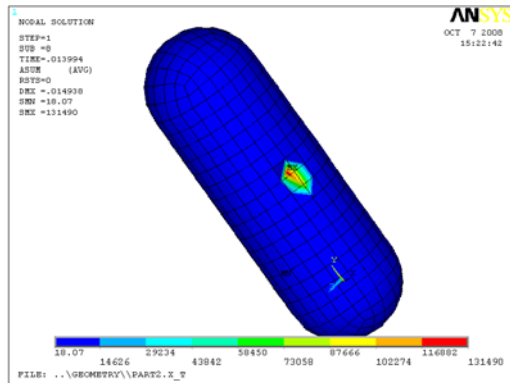


**Fig.19. Acceleration distribution at impact time on the vessel wall-Impact Speed 50 m/sec.**

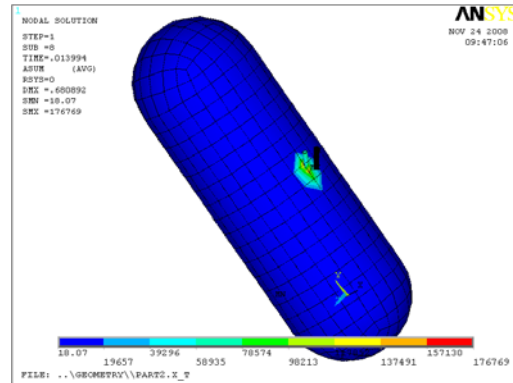


**Fig.20. Acceleration distribution at impact time within the fluid-Impact Speed 50 m/sec.**

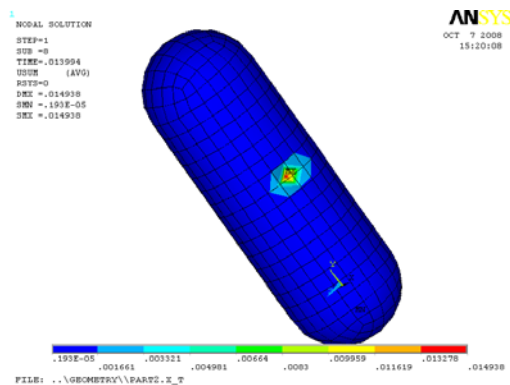


**Fig.21. Displacement distribution at impact time of the vessel wall –Impact Speed 50 m/sec.**

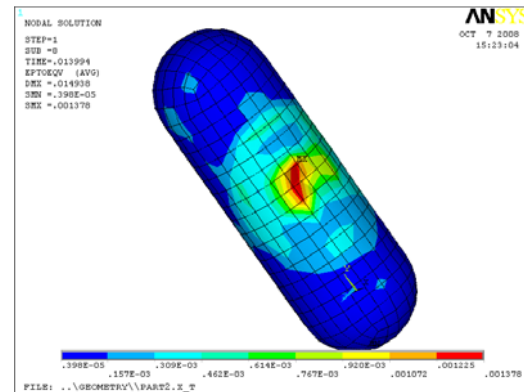


**Fig.22. Total Strain distribution at impact time of the vessel wall –Impact Speed 50 m/sec.**

As already seen, all the dynamic response values are increasing as the projectile speed is increasing, which is somehow in accordance with an elementary technical commonsense conclusion. In order to be more explicit, the maximum values for some of those values, for all the simulated scenarios, were inserted into some graphs, as shown below.

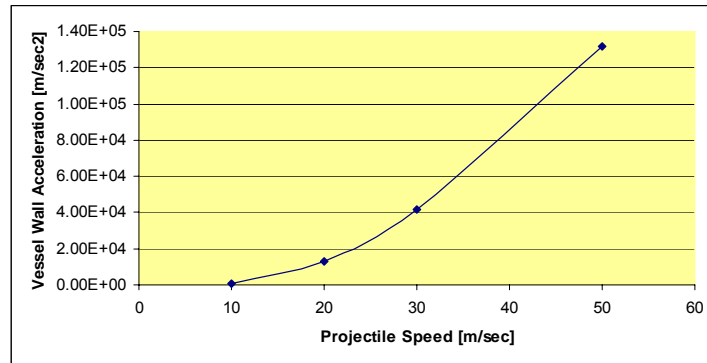


**Fig.23. Vessel wall maximum acceleration progress for all 5 scenarios.**

The dependency between the projectile speed and the vessel wall maximum acceleration at the impact area is almost linear (Fig.23).

The same think may be stated for the progress of von Mises Equivalent stress (Fig.24), the slight difference between the values for 20 against 30 mps speed of the projectile are due to the considered impact time, being known that the calculation step time in the explicit dynamic are discrete and the impact time is somehow approximate.

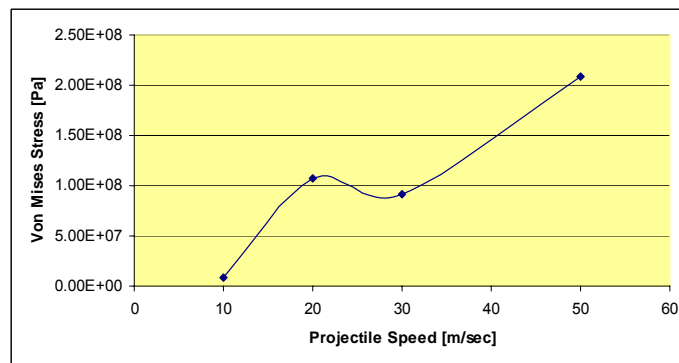


**Fig.24. Von Mises Equivalent Stress in the vessel wall progress for all 5 scenarios.**

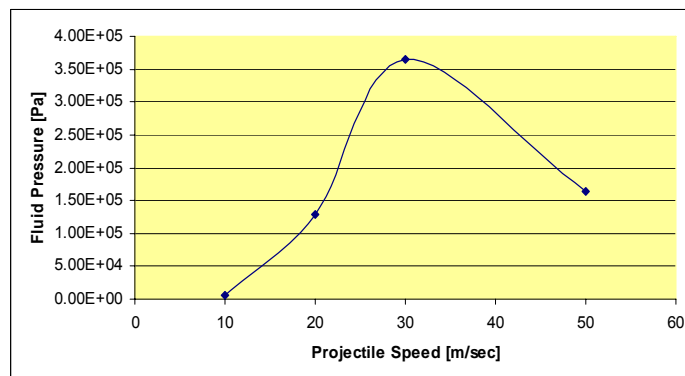


**Fig.25. Fluid pressure progress for all 5 scenarios.**

The fluid pressure progress shown in Figure 25 shows a steady growth until projectile speed of 30 mps followed by a sharp decrease for 40 and 50 mps. This is due the inertial decoupling between the vessel wall and fluid domain for high speed impact and high values of the vessel wall acceleration.

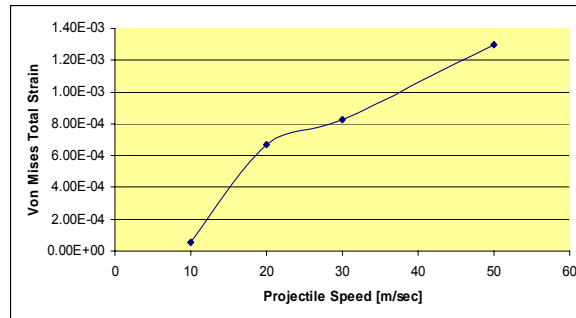


**Fig.26. Total Strain progress for all 5 scenarios**

Finally, the total strain follows almost a linear growing pattern as the projectile speed is increased form 10 to 50 mps.

### 3. CONCLUSIONS

Based on the analysis and results presented some conclusions are to be made.

The ANSYS/LS-DYNA model provides a consistent and reasonable result for vessel-projectile impact analysis. Its results are comparable with other approaches. The collision process is complex and must be evaluated on a case-by-case basis.

Compared with other vessel-projectile impact models, ANSYS/LS-DYNA provides much more information such as detailed time history curves, animation of the collision process, a series of damage pictures for any part of the vessel, velocity and displacement histories. These are very helpful for better understanding this kind of phenomena.

The results obtained from the finite element simulation, may be used for the assessment of the of vessel behavior under the defined projectile impact scenario, for the relative comparison of structural arrangements, and for the validation of analytical techniques for structural/fluid dynamic response and impact analysis.

The presence of fluid can be a significant factor in terms of the vessel capacity to absorb the energy of the projectile, due to the impact.

### REFERENCES

- [1]. ANSYS, ANSYS - **Structural Analysis Guide**, ANSYS, Inc., Houston, 2004
- [2]. Grimes, R.G., Lewis, J.G. and Simon, H.D. - **A Shifted Block Lanczos Algorithm for Solving Sparse Symmetric Generalized Eigenproblems**, SIAM Journal on Matrix Analysis and Applications, Vol.15, No.1, pp.228-272, 1994
- [3]. LSTC, LS-DYNA - **Theoretical Manual**, Livermore Software Technology Corporation, Livermore, 1998
- [4]. UK Aircraft Accident Investigation Board - **Report on the Accident to Boeing 737-236, G-BGJL at Manchester International Airport on 22 August 1985**, Aircraft Accident Report No. /88(EW/C929), British Department of Transport, 1985
- [5]. Yu, S.O., Jo, J.C., Kim, H.J., Yune, Y.G. and Jhung, M.J. - **Transient piping pressure and force caused by high pressure steam flow disturbances**, Transactions of the Korean Society of Pressure Vessels and Piping, Vol.1, No.1, pp.41-54, 2005

## EXPLICIT DYNAMIC SIMULATION OF A SPACE DEBRIS PROJECTILE IMPACT OVER A SATELLITE STRUCTURE

<sup>1</sup>CALIMANESCU IOAN, <sup>2</sup>GRIGORESCU LUCIAN

<sup>1</sup>*Saipem SpA Italy*, <sup>2</sup>*Constanta Maritime University, Romania*

The purpose of this article is to investigate numerically the dynamic response of a satellite structure subjected to an impact with high velocity space debris. Satellites provide numerous services for modern society. They perform essential duties for military, governmental, and commercial organizations. The missions of these spacecraft include science ventures such as earth observation, interplanetary exploration, astronomy, and solar physics. They also include commercial endeavors such as television signal transmission, data transmission, and satellite telephone communication. In one of the currently considered designs of the satellite, its outer skin is planned to be constructed from two-ply composite material panels. Their structure may be subjected to impacts with space debris (mass 0.0014 kg). In the present work a transient non-linear-dynamics based analysis is carried out in order to predict the extent of damage of satellite panels during potential hypervelocity impact with space debris. The used simulation code was ANSYS/LS-DYNA, taking advantage of its explicit dynamics facilities and capability to model the impact phenomenon.

**Keywords:** FEA, Explicit Dynamic, Simulation, Projectile, Impact, Satellite.

### 1. INTRODUCTION

#### 1.1 *Satellite structure and materials*

Aerospace structures generally require lightweight designs. The goal of these designs is to optimize the strength per weight, or efficiency of the design. Satellite structural design has evolved greatly over the past four decades. Traditionally, efficiency has been accomplished using a combination of various structural designs and materials.

Primary structures are designed using several criteria that depend on the mission requirements. Conventional spacecraft incorporate 4 basic primary structural designs: skin-frame structures; truss structures; monocoque cylinders; and skin-stringer structures.

The skin-frame structural design uses an interior skeletal network of axial and lateral frames to mount exterior skin panels using fasteners or rivets. The frames support bending, torsional, and axial forces. The skin reinforces the structure by supporting the shear forces introduced by the interior member connections. The skin is sometimes minimized to save mass, even though the thin skin leads to some structural instability. When the skin buckles due to shear, it transfers all additional shears loading to in-plane tension forces at 45° which must be supported by the connections. The buckling modes of the skin exhibit large deformations that make it insufficient for exterior mounted components such as solar cells. The buckling strength of the assembly is typically increased by adding intermediate members.

The Isogrid end panels use an array of equilateral triangle cutouts to increase the stiffness per weight of a structure. The pattern may be manufactured by machining a metallic panel, or it may be constructed using fiber composite materials. The concept began in the early 1960s using metal structures and development continues today with research focusing primarily on composite applications. The satellite structural configuration is designed to accommodate all of the mission components (see Figure 2).

The spacecraft uses body-mounted solar cells for power generation, torque coils for attitude control, digital cameras for attitude determination, micro-pulsed plasma thrusters for orbit control and several other components for data processing and communications. All of the electronics components connect to the isogrid at web intersection points, known as nodes. The isogrid pattern is configured with two inch node spacing. This pattern allows for convenient mounting of the components while increasing the structural performance.

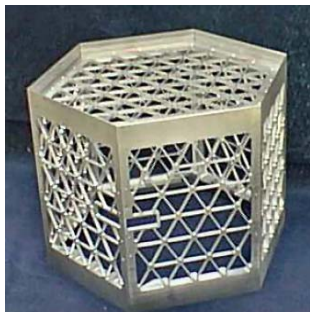


**Fig.1. Isogrid structure of a satellite**

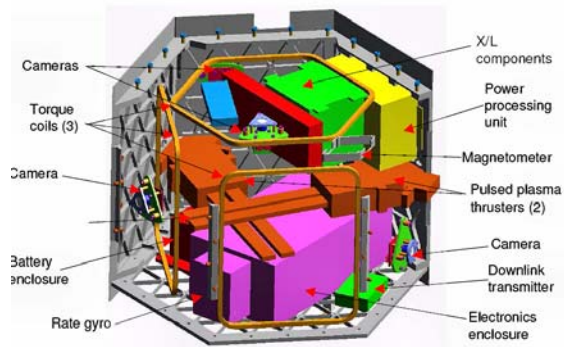


**Fig.2. Internal Configuration of satellite**

The external configuration of a satellite is given below:

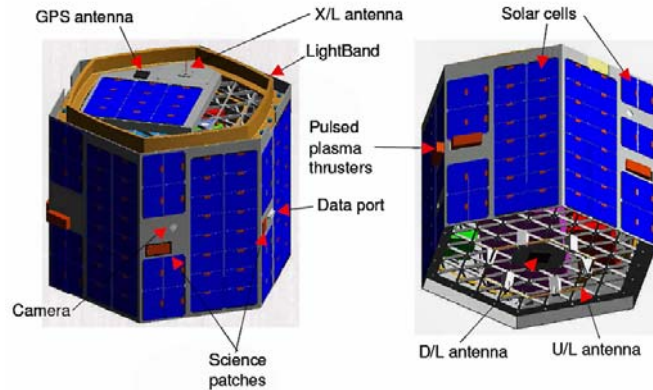


**Fig.3. External Configuration of satellite**

Satellite structural designs also use several different materials. Materials are chosen based on their properties, cost, and complexity. There are two typical materials used in spacecraft.

*Composite materials* used in satellite structures consist of a matrix and reinforcement. The matrix (metal, epoxy) binds the reinforcing fibers (carbon, graphite) together into a continuous system. The efficiency of composite structures is due its high specific modulus and unique load path. The flexural shear loads are transferred from the matrix to axial loads

on the high-strength fibers, creating a structure 3 to 5 times as stiff as aluminum at 60% of the mass.

*Aluminum alloys* are the most widely used metallic materials in spacecraft manufacturing. The advantages include high strength to weight ratios, high ductility and ease of machining. The stiffness to weight ratio is comparable to steel; however, the strength to weight ratio is typically higher. The disadvantages include low hardness and a high coefficient of thermal expansion (CTE). The alloys are typically tempered to increase the material strengths. Two typical alloys used in manufacturing are 6061-T6 and 7075-T7. Aluminum 6061-T6 contains silicon and magnesium which strengthens the alloy during tempering. This alloy has good machinability and corrosion resistance. Aluminum 7075-T7 contains zinc and trace amounts of magnesium. The alloy exhibits higher strength than 6061-T6, but is more difficult to machine.

### **1.2 Impact scenario hypothesis**

It is known that hypervelocity impacts of natural meteoroids and man-made space debris can significantly affect the performance and even the integrity of a satellite. Hypervelocity impacts associated with sub-micron and micron size space-debris particles can degrade sensitive satellite devices like mirrors, optical sensors and thermal control surfaces. Larger particles with diameters in a range between tens and hundreds of microns can penetrate, during impact, the outer skin of a satellite as well as cause a substantial damage to the solar cells. Still larger, millimeter-size, particles can penetrate the walls of exposed fuel/oxidizer tanks and cause a serious damage to some interior devices/equipment. Finally, hypervelocity impacts associated with the largest particles could potentially lead to a complete failure of the impacted satellite component and jeopardize the integrity of the whole satellite. In addition to the aforementioned structural damage, hypervelocity impact typically creates plasma that can lead to the electromagnetic interference. In addition, when the satellite surfaces are already electrically charged by the surrounding aerodynamic plasma, the impact-induced plasma can give rise to substantial electrical discharges, which can result in a major structural damage to the satellite. Other impact induced effects include the generation of light flashes and the attitude changes in the satellite. The extent of structural damage caused by hypervelocity impacts depends on a number of parameters associated with the impactor (a meteoroid or a space-debris particle) and the target (the outer skin of the satellite). Among these, the most important are the size, the shape, the impact velocity, the impact angle and the material density of the impactor. The extent of damage caused by a given impactor also depends on the dynamic-load bearing capability of the target which is controlled by the target design, its thickness and the material or materials used to construct the target. It should be noted, however, that equally important may be the level of sensitivity of the target to the damage of a particular type. For example, a small impact-induced dimple may have no significant effect on the aerodynamic performance of a satellite or the operation of a solar array but can seriously degrade the function of a sensor, a mirror or a window. The type of structural damage imparted to a satellite is greatly controlled by the magnitude of the momentum of the impactor. At smaller values of the impactor momentum, the damage consists mostly of craters created during the initial impact and by the ejection of surrounding material. As the impactor momentum increases, the damage becomes more pronounced, becomes to include, in addition to the front-face craters and spalling, also back-face spalling.

At the largest of levels of the impactor momentum, a complete penetration of the target takes place. The last mode of structural damage to a satellite is generally considered as fatal and a satellite must be design so that such damage will not occur.

## 2. NUMERICAL INVESTIGATION

### 2.1 CAD-FEA Model

The CAD geometry of the satellite panel structure, with all its dimensions (in meters) at the time 0 seconds of simulation, is given in the figure below:

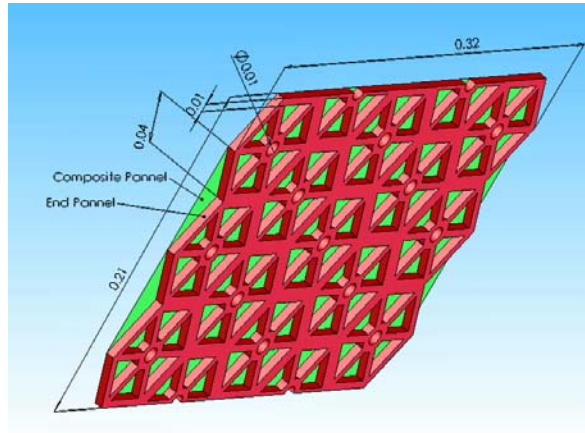


**Fig.4.CAD geometry of satellite panel**

After generation, the CAD geometric model was exported in the software ANSYS/LS-DYNA.

ANSYS/LS-DYNA combines the LS-DYNA explicit finite element program with the powerful pre- and post-processing capabilities of the ANSYS program. The explicit method of solution used by LS-DYNA provides fast solutions for short-time, large deformation dynamics, quasi-static problems with large deformations and multiple non-linearity, and complex contact/impact problems.

The export of the CAD geometry was targeting the implicit dynamic module of the software, in the first step, this for the composite panel was supposed to be modeled using finite elements Shell 181 which has such of capabilities (see Fig.5). The composite panel was deemed to have 2 layers (thickness 0.125 mm each layer) with composite fibers oriented at  $\pm 45^\circ$  as shown below:

The RCC panel material was considered to be orthotropic with the proprieties as below:  
 $E_x = 11.981 \text{ GPa}$ ,  $E_y = 11.981 \text{ GPa}$ ,  $E_z = 45.166 \text{ GPa}$ ,  $G_{xz} = 4.583 \text{ GPa}$ ,  $G_{yz} = 4.583 \text{ GPa}$ ,  
 $G_{xy} = 1.289 \text{ GPa}$ ,  $\nu_{yz} = 0.238$ ,  $\nu_{xz} = 0.238$ ,  $\nu_{xy} = 0.325$ ,  $\rho = 834 \text{ kg/m}^3$ .

The isogrid was modeled using Solid 185 type of finite elements, and was deemed to be made out of Aluminum alloy with the proprieties:

$E_x = 1.75 \text{ e9 Pa}$ ,  $\nu = 0.28$ ,  $\rho = 1275 \text{ kg/m}^3$ .

By switching the implicit dynamic option to explicit dynamic one, the finite elements changed (Shell 181 switched in Shell 163 and Solid 185 in Solid 184) but preserving their previous real constants and thus being ready to be treated under LS-Dyna solver. Also the space debris impact projectile made out of Aluminum alloy, as well, was defined at this stage. The resulting FE mesh is depicted below:

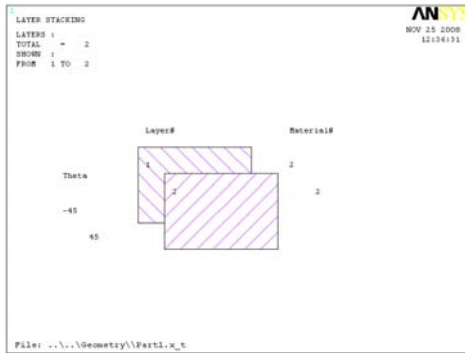


**Fig.5.Composite panel modeling layers using Shell 181 elements**

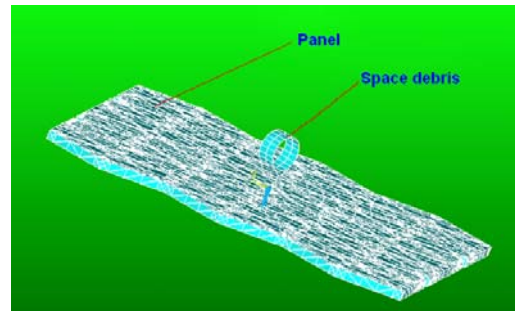


**Fig.6.Finite Elements mesh for Panel and Space debris Projectile**

To such obtained model proper boundary conditions and contact conditions were imposed. The projectile was considered to impact with the speeds  $V_x=V_z=200$  m/sec so that the absolute speed of the projectile is  $V=282$  m/sec impacting the satellite structure from an oblique direction. Projectile has cylindrical shape and its mass is 0.0014 kg.

**2.2 The impact simulation results for the Composite panel**

After running the program, the time when the biggest magnitude of stresses in the satellite panel structure is calculated to be 0.3 e-3 seconds. The calculated impact time is 0.041 e-3 sec after starting simulation.

The composite panel is suffering relatively big displacements and deformations following the collision. For instance the calculated total displacements are shown in Fig.8.

The maximum value to be reached at time 0.3 e-3 sec is 0.297 mm, at and near the impact zone. Looking to the Displacement time history for node 3998, it may be seen that in the first phase the displacement will be positive in Oz direction reaching a maximum of 0.175 mm at time 0.3 e-3 sec followed by a reverse displacement which will reach -0.3 mm at the end of the simulation (Fig.9).

The velocity induced by the space debris upon composite panel is calculated as 0.9 m/sec at the same impact area (Fig.10) and at the considered time. At the same node (3998) the time history (Fig.11) will show that the maximum velocity (for the Oz direction) will be reached at time 0.25 e-3 sec and will have the value of 1.75 m/sec. Then the velocity will oscillate until of the end of the simulation (1 sec).

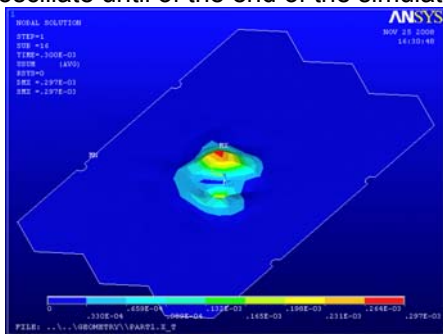


**Fig.7.Displacement distribution for composite panel following collision (0.3e-3 sec)**

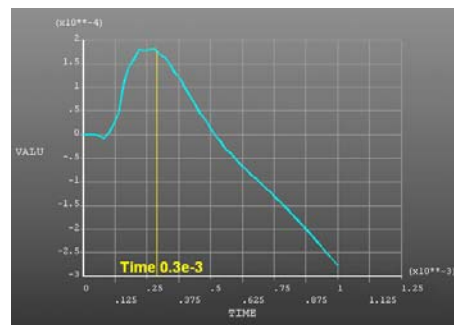


**Fig.8.Displacement time history variation at node 3998**

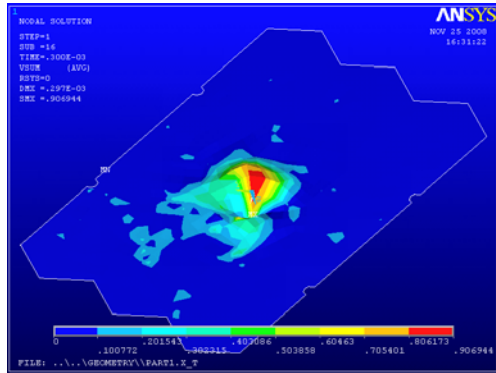


**Fig.9. Velocity distribution for composite panel following collision (0.3e-3 sec)**

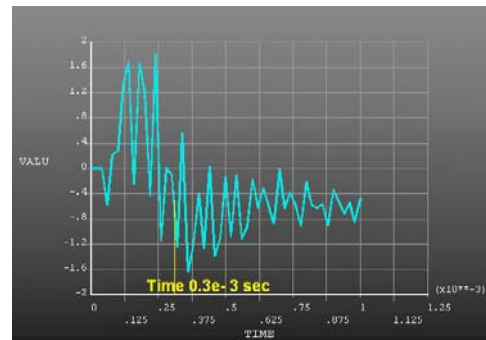


**Fig.10. Velocity time history variation at node 3998**

The acceleration distribution in the composite panel will reach an astonishing  $672,832 \text{ m/sec}^2$ , on an area near the impact zone, as seen in the Figure 11. The acceleration for node 3998 will oscillate around the point zero reaching the biggest magnitude of  $0.8 \text{ e}6 \text{ m/sec}^2$  at time  $0.2 \text{ e-}3 \text{ sec}$  after the start of simulation (Fig.12).

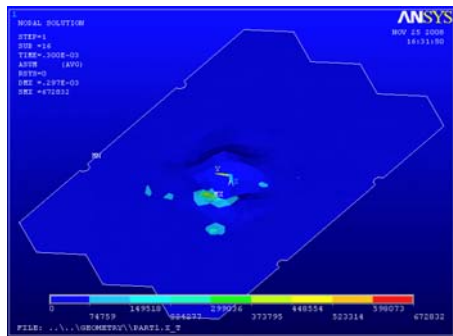


**Fig.11. Acceleration distribution for composite panel following collision (0.3e-3 sec)**

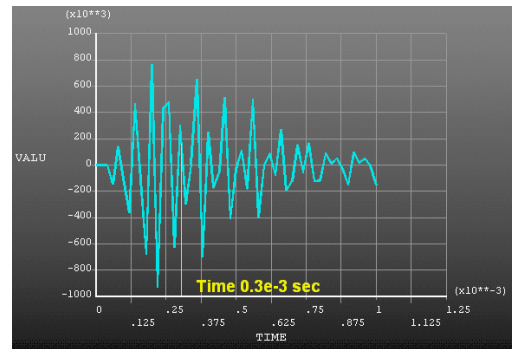


**Fig.12. Acceleration time history variation at node 3998**

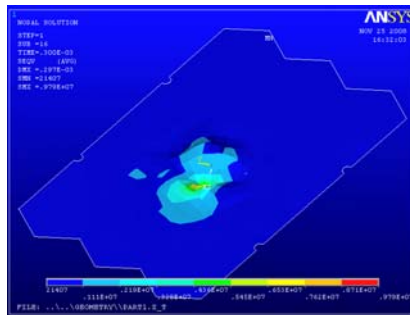


**Fig.13. Von Mises equivalent stress distribution for composite panel following collision (0.3e-3 sec)**

In Figure 14 it is shown the distribution of von Mises equivalent stress which will reach its peak value at the node 3998 of finite elements mesh and at considered time 0.3 e-3 seconds after starting of simulation. The calculated value is 0.979 e7 Pa, which leads us to the conclusion that the composite panel will resist to the collision with the given space debris having near sound speed. The time history for the node 3998 is given below. It may be seen the maximum value of stress reached at time 0.3e-3 sec.

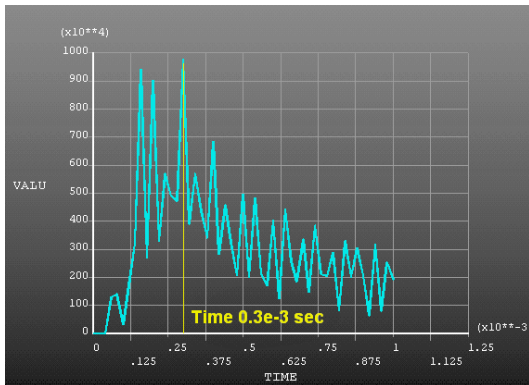


**Fig.14. Von Mises equivalent stress time history variation at node 3998**

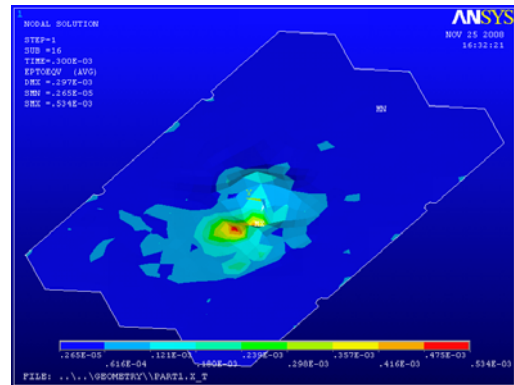


**Fig.15. Von Mises equivalent strains distribution for composite panel following collision (0.3e-3 sec)**

Figure 15 is showing the von Mises equivalent strains as calculated by the program at time 0.3 e-3 sec. The biggest magnitude is reached at the impact area (0.534 e-3).

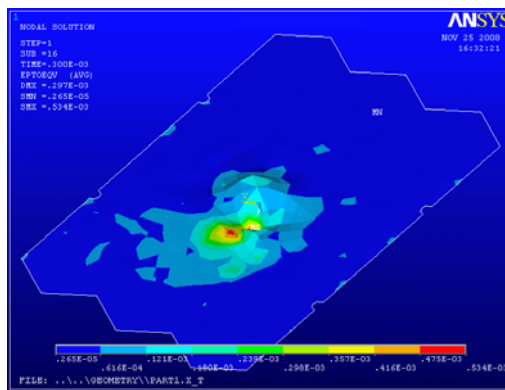


**Fig.15. Von Mises equivalent strains distribution for composite panel following collision (0.3e-3 sec)**

### 2.3 The impact simulation results for the Isogrid (End) panel

The isogrid panel is suffering as expected, the same relatively big displacements and deformations following the collision. For instance the calculated total displacements are shown in Fig.16.

The maximum value to be reached at time 0.6 e-4 sec is 0.177 mm, at the impact zone. By taking a look to the Displacement time history for node 24, it may be seen that the biggest

value of displacement shall be reached at time 1 sec and it will be  $0.8e-4$  m, which is much less than the composite panel's displacement (Fig.17).

The velocity induced by the space debris upon isogrid panel is calculated as 2.4 m/sec at the same impact area (Fig.18) and at the considered time. At the same maximum stress condition node (24) the time history graph (Fig.19) will show that the maximum velocity (for the Oz direction) will be reached at time  $0.6 e-4$  sec and will have the value of 1.06 m/sec. Then the velocity will decrease until the end of the simulation (1 sec.).

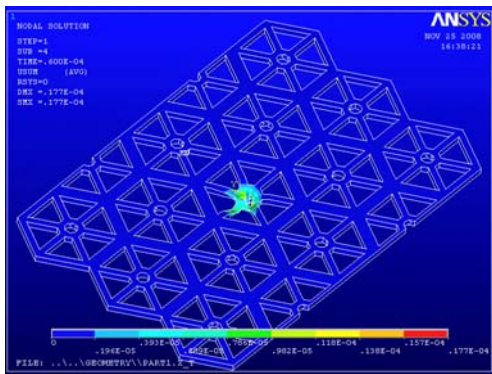


**Fig.16.** Displacement distribution for isogrid panel following collision ( $0.6e-4$  sec)

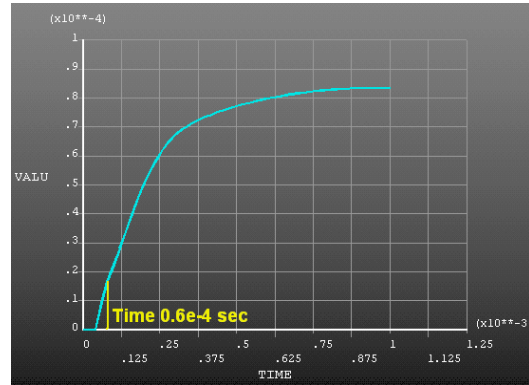


**Fig.17.** Displacement time history variation at node 24

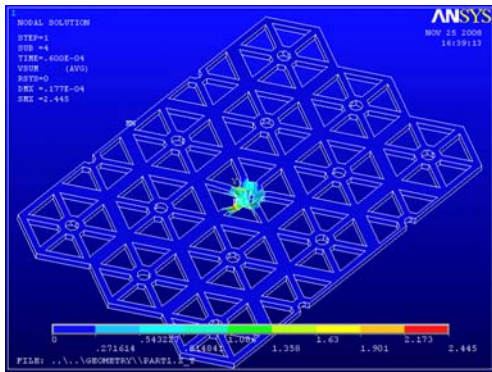


**Fig.18.** Velocity distribution for isogrid panel following collision ( $0.6e-4$  sec)

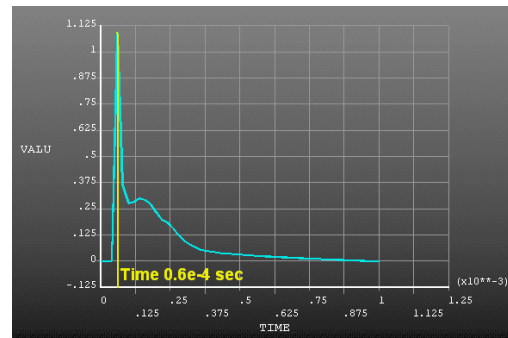


**Fig.19.** Velocity time history variation at node 24

The acceleration distribution in the isogrid panel will reach the value of  $1.23 e6$  m/sec<sup>2</sup>, on an area near the impact zone, as seen in the Figure 20.

The acceleration for node 24 is reaching the biggest magnitude of  $5.6 e5$  m/sec<sup>2</sup> at time  $0.6 e-4$  sec after the start of simulation (Fig.21).

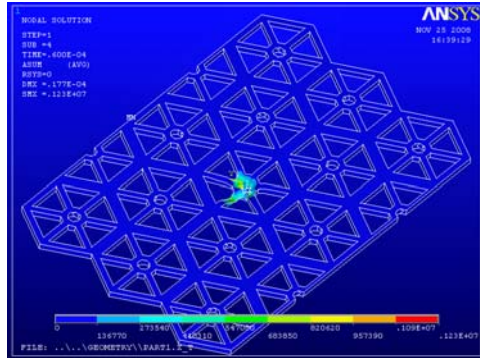


**Fig.20. Acceleration distribution for isogrid panel following collision (0.6e-4 sec)**

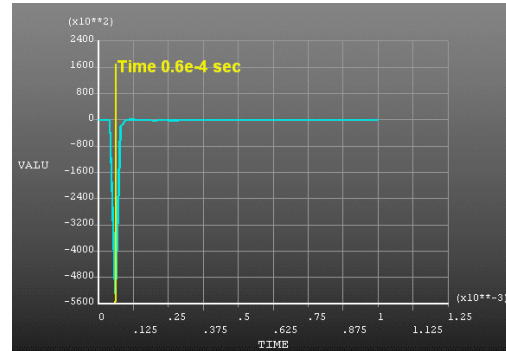


**Fig.21. Acceleration time history variation at node 24**

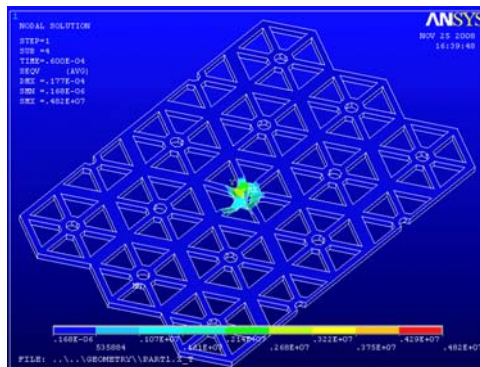


**Fig.22. Von Mises equivalent stress distribution for isogrid panel following collision (0.6e-4 sec)**

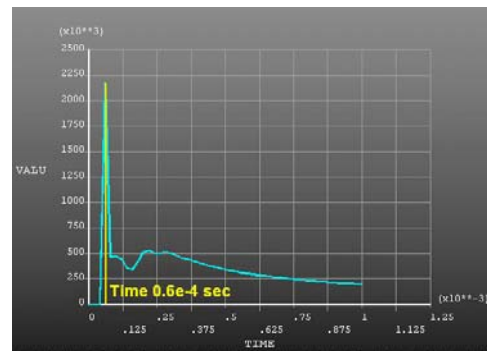


**Fig.23. Von Mises equivalent stress time history variation at node 24**

In Figure 22 it is shown the distribution of von Mises equivalent stress which will reach its peak value at the node 24 of finite elements mesh and at considered time 0.6 e-4 seconds after starting of simulation. The calculated value is 0.482 e7 Pa, less than the maximum stress calculated for the composite panel. The isogrid panel is having an important role in upholding the composite panel and dissipating the impact energy of collision. The time history for the node 24 is given below.

Figure 24 is showing the von Mises equivalent strains as calculated by the program at time 0.6 e-4 sec. The biggest magnitude is reached at the impact area (0.0035). As expected the time history for node 24 and for von Mises strains will follow the same pattern as the one of stresses, the maximum being 1.9 e-3 (Fig.25).

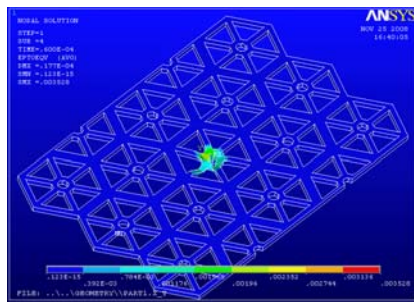


**Fig.24. Von Mises equivalent strains distribution for isogrid panel following collision (0.6e-4 sec)**

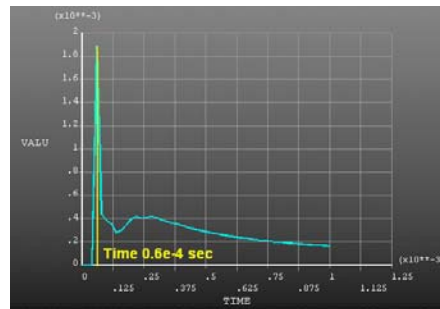


**Fig.25. Von Mises equivalent strains time history variation at node 24**

### 3. CONCLUSIONS

The ANSYS/LS-DYNA model provides a consistent and reasonable result for satellite structure-projectile impact analysis. Its results are comparable with other approaches. The collision process is complex and must be evaluated on a case-by-case basis.

Compared with other impact models, ANSYS/LS-DYNA provides much more information such as detailed time history curves, animation of the collision process, a series of damage pictures for any part of the vessel, velocity and displacement histories. These are very helpful for better understanding this kind of phenomena.

The results obtained from the finite element simulation, may be used for the assessment of the of satellite structure behavior under several defined projectile impact scenario, for the relative comparison of structural arrangements, and for the validation of analytical techniques for structural dynamic response and impact analysis.

Based on the results obtained in the present work, the following main conclusions can be drawn:

- the composite RCC panel will resist near sound speed collision with the given Aluminum space debris, the distribution and magnitude of damages remaining at relatively low levels.
- not the same may be stated for small space debris; the smaller the dimension of impactor may lead to grater/different stress distribution which, eventually, may damage the satellite.
- the isogrid panel shows an essential contribution to the dissipation of impact energy being key player in the overall toughness of the satellite structure.

### REFERENCES

- [1]. Berthoud L., Mandeville J.-C., - **Empirical impact equations and marginal perforation, in: Proceedings of the First European Conference on Space Debris**, Darmstadt, 5–7 April 1993, ESA SD-01, 1993, pp. 459–464.
- [2]. Grujicic M., Zhao C.L., Biggers S.B., Kennedy J.M., Morgan D.R. - **Suitability of a coal-derived carbon-based foam for use, in thermal protection systems of common aero vehicles, in press.**
- [3]. McDonnell J.A.M., (Ed.) - **Meteoroid and Debris Flux and Ejecta Models**, Final and Summary Reports of ESA contr. 11887/96/NL/JG, 1998.
- [4]. McDonnell J.A.M. (Ed.) - **Cosmic Dust**, Wiley, 1987.
- [5]. NASA SP-8042 - **Meteoroid Damage Assessment**, 1970
- [6]. Paul K.G., Berthoud L., - **Empirical scaling laws for crater dimensions for impacts into solar cells, in: Physics, Chemistry and Dynamics of Interplanetary Dust**, Proc. IAU Colloq. No. 150, Gainesville, FL, 1995.
- [7]. Rival M., Mandeville J.-C., - **Modeling of ejecta produced upon hypervelocity impacts**, Space Debris 1 (1999) 45–57.

## TRANSITORY PHENOMENONS INTO NAVAL ELECTRICAL EQUIPMENT

<sup>1</sup>DELIU FLORENTIU, <sup>1</sup>BURLACU PAUL

<sup>1</sup>Naval Academy "Mircea cel Batran", Constanta, Romania

The analysis is based on a naval power with synchronous generator and consumers of various powers. The paper presents a systemic approach to naval power systems based on mathematical models of specific generators and consumers.

**Keywords:** transitional arrangements, electric power system, synchronous generator, mathematical models, the shock load

### 1. INTRODUCTION

Naval power system usually contains type synchronous generators driven by a Diesel engine. Consumers are various electric power and importance of different steps (eg communications system is crucial in ensuring the safety of the vessel). Occurring in ship operation can appear a random event (short-circuit, connecting disconnect of important loads), which should be evaluated in a professional and controlled so that the ship's safety is not affected. Based on mathematical models of generator and consumer examines the transitional operation of the naval power in the stable and unstable conditions.

### 2. MATHEMATICAL MODELS USED IN SIMULATION

Mathematical model of synchronous generator (GS) is characterized by the equations:

$$\left. \begin{aligned} -U\sqrt{3} \cos \theta &= \omega L_d I_d + R_q I_q + L_q \frac{dI_q}{dt} + \omega M_E I_E + \omega M_D I_D + M_Q \frac{dI_Q}{dt} \\ U_E &= M_E \frac{dI_d}{dt} + R_E I_E + L_E \frac{dI_E}{dt} + M_{ED} \frac{dI_D}{dt} \\ 0 &= M_D \frac{dI_d}{dt} + M_{ED} \frac{dI_E}{dt} + R_D I_D + L_d \frac{dI_d}{dt} \\ 0 &= M_Q \frac{dI_q}{dt} + R_Q I_Q + L_Q \frac{dI_Q}{dt} \\ J \frac{d\omega}{dt} &= p_f \left[ (L_d - L_q) I_d I_q + M_E I_q I_E - M_Q I_d I_Q + M_D I_d I_D \right] - M_{motor} \end{aligned} \right\} \quad (1)$$

Dynamic stability are analyzed with this system of differential equations in the original terms are derived from solving an algebraic system. Machine parameters are:

$R_E = 40 \text{ } [\Omega]$  resistance of excitation inolution  
 $R_D = 7.95 \text{ } [\Omega]$  resistance depreciation inolution of the axis d  
 $R_Q = 30.22 \text{ } [\Omega]$  inolution resistance depreciation of inolution q axis  
 $L_D = 0.07 \text{ } [H]$  own inductance depreciation of the axis d  
 $M_{ED} = 0.56 \text{ } [H]$  mutual inductance between excitation and inolution D  
 $M_D = 0.05 \text{ } [H]$  mutual inductance between inolution and stator d  
 $L_Q = 0.25 \text{ } [H]$  own inductance depreciation of q axis  
 $M_Q = 0053 \text{ } [H]$  Mutual inductance between stator q and inolution Q  
 $R_J = 1.6 \text{ } [H]$  stator resistance  
 $L_d = 0.08 \text{ } [H]$  own inductance of stator d-axis  
 $L_q = 0.07 \text{ } [H]$  own inductance of stator q axis  
 $M_{Ed} = 1 \text{ } [H]$  mutual inductance between excitation and inolution d  
 $L_E = 18.51 \text{ } [H]$  own inductance of excitation inolution  
 $\psi_{2N} = 0.7 \sqrt{3} \text{ } [W b]$  nominal stator flux We noted:  
 $I_d = X$  -stator current from axis d,  
 $I_Q = Z$  -stator current of axis q,  
 $I_E = Y$  current excitation,  
 $I_D = D$  current depreciation of the axis d,  
 $I_Q = Q$  current depreciation of the axis q.  
 Analyzing 2 cases of operation:  
 - stable operation to a variable load  
 - unstable operation at short.

### 3. STABLE OPERATION OF MARINE POWER SYSTEM

Presented in the following operation for a stable connection to a major consumer of the ship (the fire pump, ballast pump). The results presented below are for 3 cases for grant of voltage regulators, current frequency and excitation. The system of differential equations is:

$$\left. \begin{aligned}
 &1,6 X + 0,08 \frac{dx}{dt} - 0,07 \omega Z - 0,053 \omega Q + \frac{dy}{dt} = -U \sin \theta \\
 &0,008 \omega X + \omega y + 0,05 \omega D + 0,053 \frac{dQ}{dt} + 1,6 Z + 0,07 \frac{dz}{dt} = U \cos \theta \\
 &\frac{dX}{dt} + 40 Y + 18,51 + 0,56 \frac{dD}{dt} = E \\
 &0,053 \frac{dx}{dt} + 7,95 D + 0,07 \frac{dD}{dt} + 0,56 \frac{dy}{dt} = 0 \\
 &2(0,01 X Z + Z Y - 0,053 D Z) - 15 = 0,01 \frac{d\omega}{dt} \\
 &\frac{d\theta}{dt} + \omega - Q = 0 \\
 &\frac{dE}{dt} = 5000(52 - E) \\
 &\frac{dQ}{dt} = 10000(209,3 - Q) \\
 &\frac{dU}{dt} = 10000(263,36 - U) \\
 &X(0) = -0,95 \\
 &E(0) = 50 \\
 &U(0) = 223,6 \sqrt{3} \\
 &Q(0) = 314 \\
 &Y(0) = 1,25 \\
 &Z(0) = 4 \\
 &\omega(0) = 314 \\
 &\theta(0) = 0,25 \\
 &D(0) = 0
 \end{aligned} \right\} \quad (2)$$

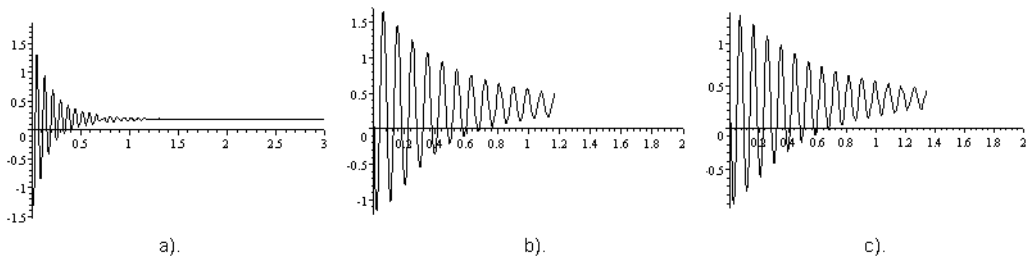


**Fig.1. Load angle variation in the three cases**

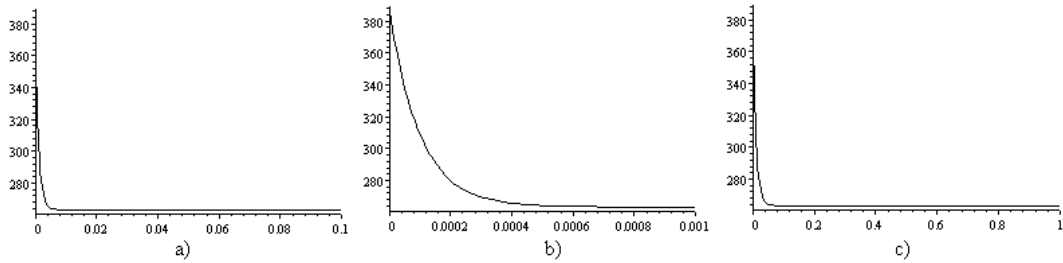


**Fig.2. Statoric tension variation over time**

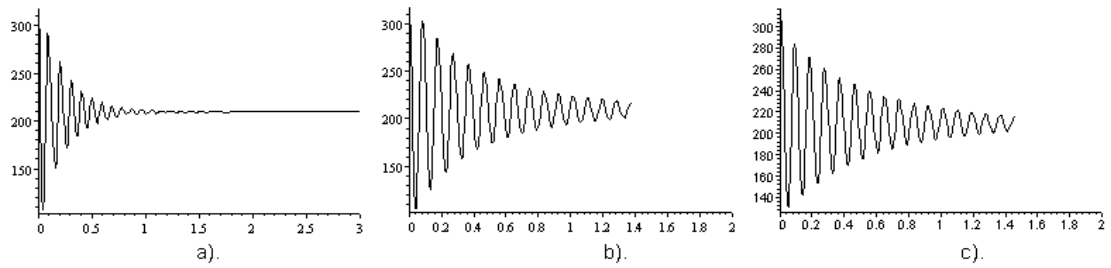


**Fig.3. Changes in time of mechanical angular velocity**

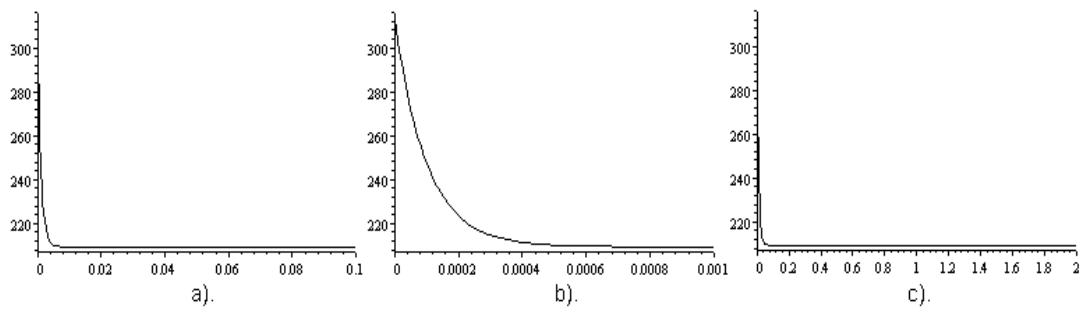


**Fig.4. Variation in time of tension  $U_E$**

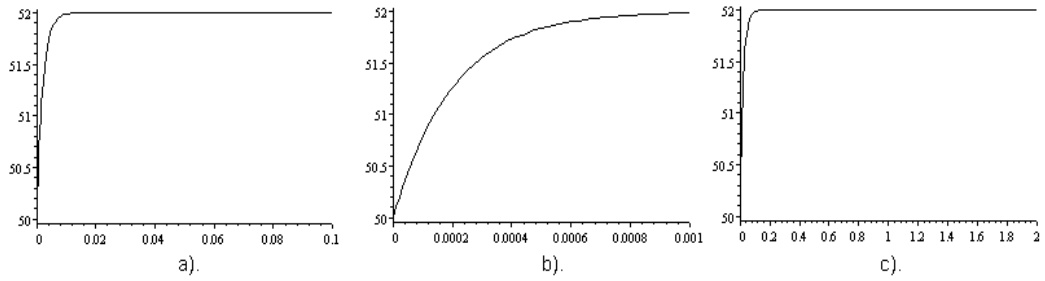


**Fig.5. Changes in time of angular stator pulse  $\omega_1$**

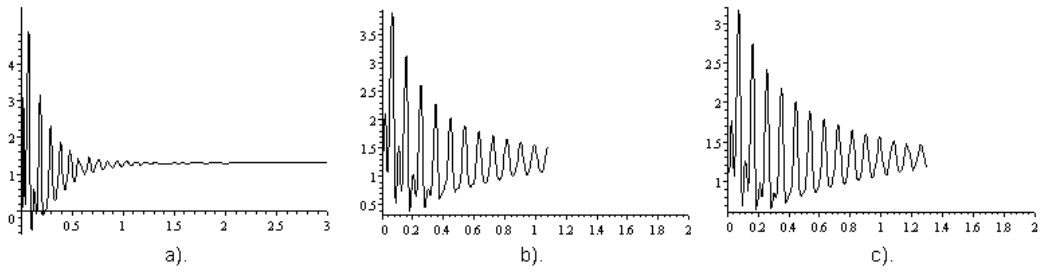


**Fig.6. Variation in time of excitation current**

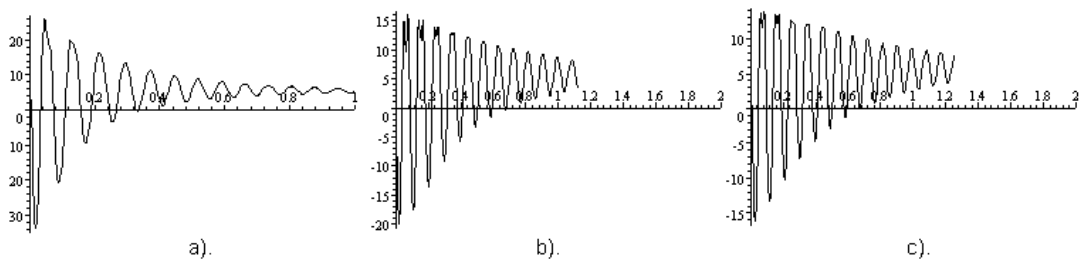


**Fig.7. Variation in time of stator current in q axis**

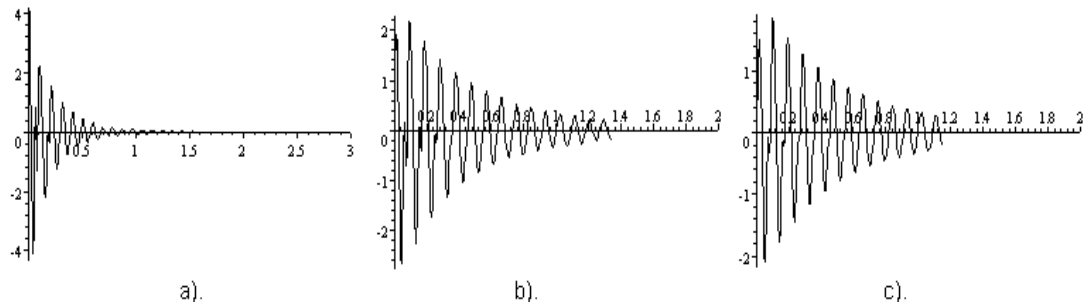


**Fig.8. Variation in time of current  $I_q$**

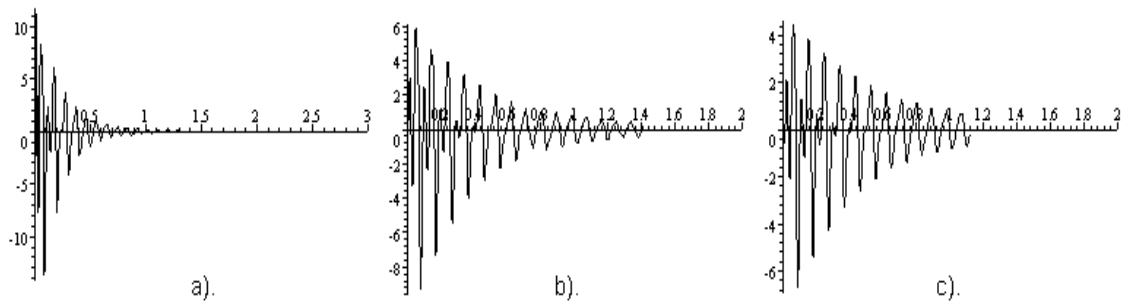


**Fig.9. Variation in time of current  $I_D$**

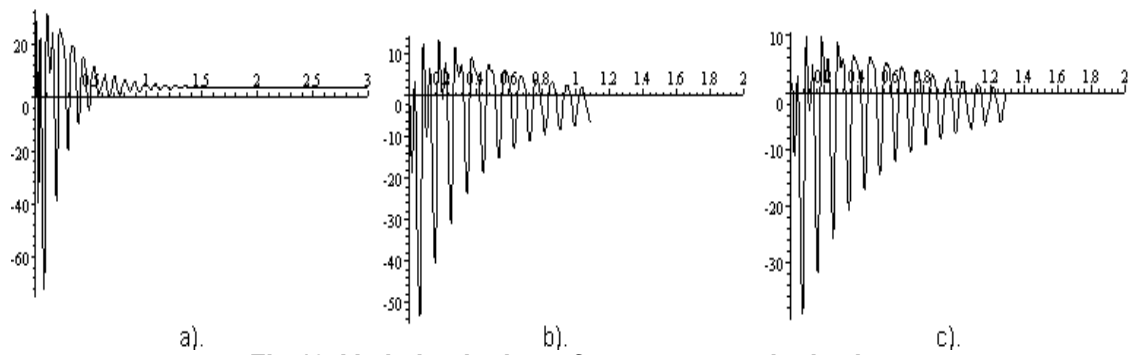


**Fig.10. Variation in time of stator current in d axis**

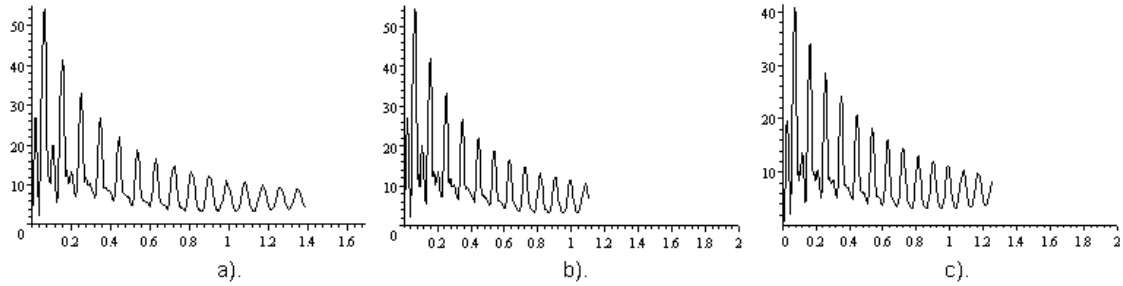


**Fig.11. Variation in time of current stator  $\sqrt{X^2 + Z^2}$**

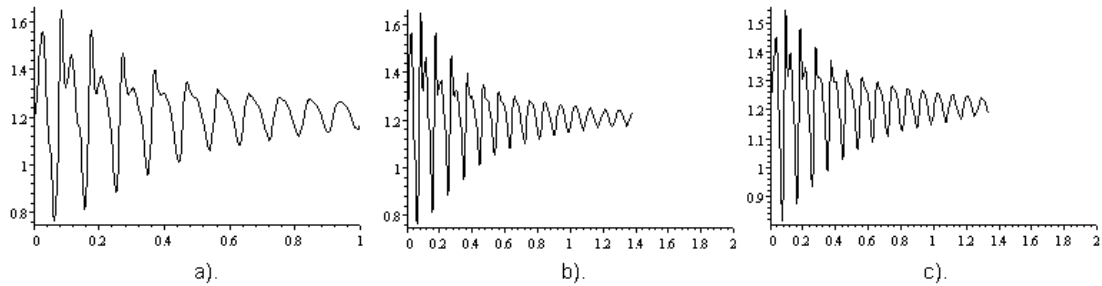


**Fig.12. Variation in time of stator flux  $\sqrt{(L_q I_q)^2 + (L_d I_d + M_E I_E)^2}$**

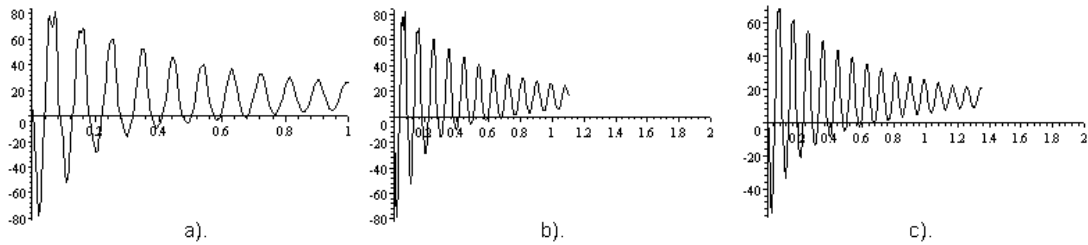


**Fig.13. Variation in time of the electromagnetic torque**

The system is dynamically stable in numerical simulations the results above, in the sense that:

1. load angle  $\theta$  oscillating is stabilized at 1 in the end [s] or 1.5 [s] -2 [s];
2. stator voltage decreases from 380 [V] to 263 [V] the same;
3. frequency / pulsation stator has an oscillating character and tend to the value  $\omega = 209.3$  [rad / s] [f = 209.3 / 6.28 Hz];
4. curenul excitation oscillates towards the 1.3 [A];
5. current stator oscillates him in the same timing for the 30 [A];
6. currents involution of depreciation is "sting" in 1 [s], 1.5 [s], 3 [s].

7. Magnetical flux finally reach face value after the same time; 8.torgue electromagnetic generator is amended over time as see in figure 13. Magnetic coupling between stator and rotor does not "break" when the system is dynamically stable.

#### 4. OPERATION UNSTABLE OF NAVAL POWER

If below operation unstable to the emergence of short-circuit the system, the differential equations in this case is:

$$\left. \begin{aligned} 1,6X + 0,08 \frac{dx}{dt} - 0,07\omega Z - 0,053\omega Q + \frac{dy}{dt} &= -U \sin \theta \\ 0,008\omega X + \omega y + 0,05\omega D + 0,053 \frac{dQ}{dt} + 1,6Z + 0,07 \frac{dz}{dt} &= U \cos \theta \\ \frac{dX}{dt} + 40Y + 18,51 + 0,56 \frac{dD}{dt} &= E \\ 0,053 \frac{dx}{dt} + 7,95D + 0,07 \frac{dD}{dt} + 0,56 \frac{dy}{dt} &= 0 \\ 2(0,01XZ + ZY - 0,053DZ) - 15 &= 0,01 \frac{d\omega}{dt} \\ \frac{d\theta}{dt} + \omega - Q &= 0 \\ \frac{dQ}{dt} &= 10000(209,3 - Q) \\ \frac{dU}{dt} &= 100 \left[ 1,47 - 0,0049Z^2 - (Y + 0,08X)^2 \right] - 0,098z \frac{dz}{dt} - 20(Y + 0,08X) \left( \frac{dY}{dt} + 0,08 \frac{dX}{dt} \right) \end{aligned} \right\} (3)$$

cases, by simulation, they obtained the following results

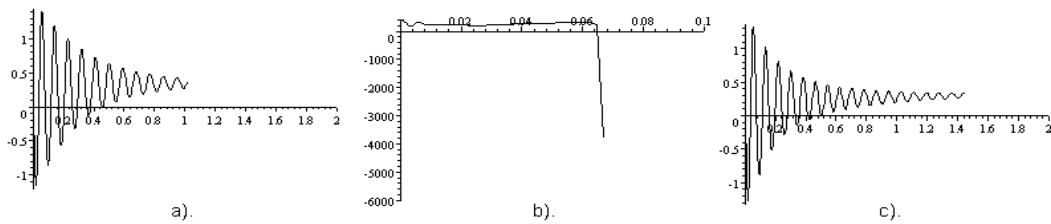


**Fig.14. Changes during pregnancy angle  $\theta$**

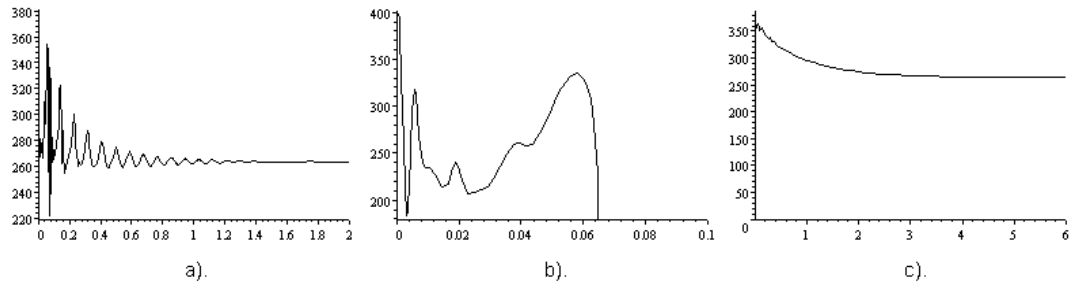


**Fig.15. Variation of stator voltage  $U$  while**

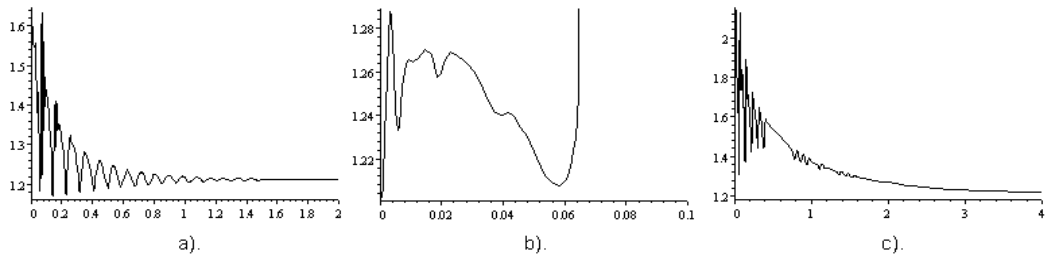


**Fig.16. Variation in time of current stator  $\sqrt{X^2 + Z^2}$**

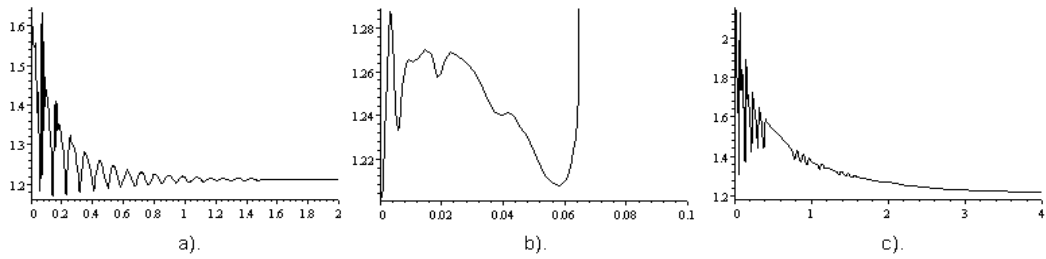


**Fig.17. Variation of stator flux  $\sqrt{(L_q I_q)^2 + (L_d I_d + M_E I_E)^2}$  in 3 cases**

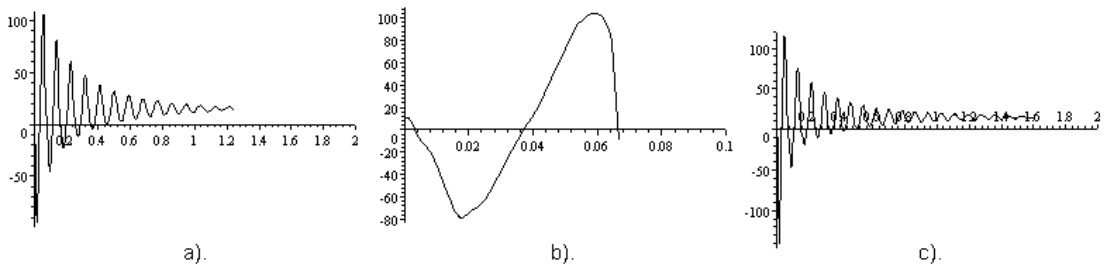


**Fig.18. Variation in time of the electromagnetic torque**

Following the analysis of simulations above operation became unstable after approximately 0.065 s, resulting in this:

1. unghiul load becomes, in absolute value greater than 180;
2. tensiunea stator becomes null;
3. curentul stator is unreliable and very large;
4. Stator flux exceeds the nominal value;
5. cuplul electromagnetic change meaning, magnetic coupling between stator and rotor tip is asynchronous.

In this case the generator loses synchronism in the operation and protection of current maximum and minimum voltage is offline from the system.

## 5. CONCLUSIONS

In the paper there were 2 types of dynamic function: stable and unstable. If stable operation of the basic dimensions of the system reached the final after a finite time interval. If unstable operation, operation in synchronism of the generator is no longer possible and this can be seen from the analysis of variations over time, mainly the electromagnetic torque, voltage and load angle.

In numerical simulations given in the paper used orthogonal model. Equation of motion is achieved rapid change in frequency over time. Using the voltage regulators and frequency lead to a stabilization which depends on constants regulators.

## REFERENCES

- [1]. Andreescu D. **Estimated in control systems of electrical drives**, Ed. Politehnica Timișoara.
- [2]. Babescu M., Paunescu D., **Electrical Machines - mathematical analysis of the transitional arrangements**, Ed. Politehnica, Timișoara, 2001
- [3]. Boldea I., Nasar S.A., **Vector Control of AC Drives**, CRC Press, Florida, 1992
- [4]. Jiao S., Hunter G., Ramsden V., Patterson D.—**Control system design for a 20 KW wind turbine generator with a boost converter and battery bank load**, in Proc. IEEE PESC, Vancouver, BC, Canada, Jun. 2001, pp. 2203-2206
- [5]. Kana C. L., Thamodharan M., Wolf A.—**System management of a wind energy converter**, IEEE Trans. Power Electron., vol. 16, no. 3, pp. 375-381, May, 2001
- [6]. Karlsson P.—**DC distributed power systems-Analysis, design and control for a renewable energy system**, Ph. D. dissertation, Lund Univ., Lund, Sweden, 2002
- [7]. Lane N., Boesch D. F.—**Vision 2033, part 6: Energy, the environment, and global change**. The American Association of the Advancement of Science [Online], 2004
- [8]. Park. **J.K Control of state-constrained linear dynamical systems: Antireset windup approach**, IEEE Proc. Control Theory Appl. Vol.147, No.2 February, 2000

## INTERNATIONAL STANDARDS OF MARITIME ENGLISH AS A MEANS TO IMPROVE SAFETY AT SEA

DEMYDENKO N.

*Kyiv State Maritime Academy, Ukraine*

This article gives background information about MarTEL Project and its achievements. The MarTEL Project is being developed by several European countries within the frameworks of European Union Leonardo da Vinci educational programme in order to establish international standards in Maritime English. In 2009 Ukraine – Kyiv State Maritime Academy, in particular, joined the project. Ukraine occupies the 5<sup>th</sup> place in the world in manpower for different ranks and classes of seafarers working on multi-national and multi-flagged vessels. The participation of the Ukrainian higher educational institution in this project is one indication that Ukraine is interested and involved with international co-operation in order to reduce merchant vessels incidents and accidents caused by the human factor relating to Maritime English communication failure on board ships and in ports.

**Keywords:** Maritime English, international standards, safety of shipping, Leonardo projects.

### 1. INNOVATION PROJECT MARTEL (UK/07/LLP-LdV/TOI-049)

The purpose of MarTEL (Maritime Tests of English Language) is creating of world-wide supported Maritime English standards as well as offering a comprehensive set of guidelines, teaching/learning and assessment materials. The goals of the Project also include the establishment of Maritime English standards sets similar to those existing in General English such as TOEFL, IELTS and so forth. In other words, the project aims to create a system of Maritime English proficiency assessment tests on the basis of the model course developed by IMO (IMO Standard Marine Communication Phrases) for all types and ranks of merchant vessel crews. Shipping is considered to be one of the most important and dangerous sectors of world economy; therefore, the safety of seafarers, cargoes and vessels are of utmost priority for the shipping industry. Communication failure on board a vessel is one of the major reasons of incidents and accidents (Ziarati, 2006, Ziarati et al, 2009). Elimination or reduction of risk in shipping accidents and how the Maritime English standards are observed by all participants of this significant economy's sector: government, shipowners, crewing companies, etc is and should be an important consideration by all concerned. The MarTEL Project partners have been working at Maritime English tests and associated documents for both deck and engineering departments (ratings and officers including cadet officer as well as senior ranks). Much attention is being paid to dissemination of the standards, the problem of training of the teachers, provision for distance and e-learning in the system of Maritime English teaching/learning practical activities, implementation of the pilot project for the establishment of Maritime English Certification

Centre, etc. More details on the project can be found in [www.maritime-tests.org](http://www.maritime-tests.org) and [www.martel.pro](http://www.martel.pro).

## 2. PRACTICAL ASPECTS OF TEACHING MARITIME ENGLISH: LINGUISTIC, METHODOLOGICAL, PSYCHOLOGICAL AND SOCIAL

Participation in the MarTEL Project gives the partners and those associated with project the opportunity to analyse all aspects of Maritime English content and delivery in teaching and to draw the conclusion about the necessity of taking them into account when developing national and international standards.

**Linguistic aspect.** Researchers emphasize on the global nature of English (*Global English, International English*) and call English *lingua franca*. For the people who work in multinational working environment, Maritime English is considered to be *an operational language*, the language with some restrictions if the functional characteristics are concerned in the specific area of merchant marine transportations (Ziarati, 2008). The linguistic analysis indicates the availability of considerable lexical "burden" of special terms, quite a short list of grammar structures, strikingly serious set of phonetic peculiarities in Maritime English use. Specific features of Maritime English cause certain difficulties in mastering the system of maritime terms in which a term is not only a language unit but represents a notion belonging to the special sphere of knowledge. In case all these linguistic factors are taken into account in university curricula, it is possible to foresee that they have a chance of being successfully used for effective training of would-be deck and engineering crew members. Still, as many professionals think, Maritime English is not the whole English language which is required for communication in different spheres of life. The problem of co-relationship of General English and Maritime English emerges when developing the assessment and various teaching/learning materials (studybooks, in particular) that meet all vital needs of the learners at different levels of proficiency. There are also methodological, psychological and social issues related to the efficiency and effectiveness of language learning. Some aspects of these are noted in Roenig and Uriasz work (2009) and the following are summary of the main findings in the research which led to this article.

**Methodological aspect.** The most serious platform for practical researches nowadays is ESP (English for Specific Purposes). After the revolution in linguistics, when it was found out that any language analysis presumes the study of actual communication materials, it became obvious that the methodological aspirations should be focused exceptionally on the learners' needs, meaning that the professional needs acquire priority (development of skills for a given vocation/employment). Learners' language skills, viz., listening, speaking, writing, reading combine the competence which is defined sufficient or insufficient for their professional activities. The MarTEL Project partners have been working out the system of tests which takes into account real communication needs of seafarers. Thus, the project concentrates on the coordination in work of Maritime specialists and language teachers. This is the area of mutual interests where training of teaching staff in rather specific sphere - shipping - appears to be a great challenge.

**Psychological aspect.** Discussions on the problem of proper method selection have proven that the best one is the method which is the most adequate for the learners and their vital interests. Variety of tasks, learning materials, study packs as well as sufficient level of the learner's motivation guarantee the openness of both the student and the teacher, evoke the response to real communication and the interest to the future profession.

**Social aspect.** It is known, that the labour market is the best factor for motivating students in the process of their studies. In the industry of water transportation this problem is being solved through acquiring by students and graduates of real communication experience working in multinational environments when some incidents of intercultural and interconfessional nature may take place. Moreover, sociolinguistic and sociocultural aspects combined with specific labour conditions on a merchant vessel, climatic and weather factors in everyday work of seafarers, pressure of working conditions, isolation in long voyages, health problems, together with the special seafarers' status require extreme concentration and hard work in the course of their professional training including Maritime English proficiency, thus, making them achieve the highest level of professional competency in order to be safe at sea, avoid risks of endangering others and reducing the chances of damaging property.

### **3. UNIFICATION OF NATIONAL AND INTERNATIONAL MARITIME ENGLISH STANDARDS**

The practice of deck and engineering crew training in Maritime English is carried out in close connection with the development of national and international standards. A standard serves as a model, a sample. It is established by professional administrations, and represents a level of quality or achievement used for judging someone or something. Even when the national standards in Maritime English are available, they still differ in various countries. National Maritime English standards in detailed form do not exist in Ukraine. The National Standard of Maritime Education for Bachelor and Master Degrees both deck and engineering departments suggest only general instructions and notions. The achievements of Ukrainian Maritime English specialists are significant (Ivasyuk, 2007); still they haven't yet crowned with job-related standards. At the same time, international organisations and all parties involved demand global standards of Maritime English purposing to remove the differences between the seafarers trained in English speaking countries and those who receive Maritime education in non-English speaking countries. Therefore, the MarTEL Project partners are greatly interested in dissemination of both ideas of international standards and materials developed to support them. In this situation it is expected that the international Maritime English standards will positively influence the creation and further development of national Maritime education standards and help to unify requirements of all institutions dealing with recruiting and certification of seafarers.

### **4. TESTS IN THE SYSTEM OF INTERNATIONAL MARITIME ENGLISH STANDARDS**

Testing is an integral part of any specialists' education. It is an objective, effective tool, simple in use when defining the level of the professional competences. Still, the contents of tests series demand thorough analysis of correct assessment of students' skills as well as clear differentiation of professional specialist tests and professional language tests. MarTEL is a language (including oral) test system which should be adopted by representatives of international shipping industry to certify seafarers' professional competences of all ranks, specialities and nationalities in Maritime English. The concept of MarTEL foresees the development of assessment materials in case a new position is introduced on a merchant vessel. The international standard MarTEL is a software interactive test system which can be

easily used in any educational establishment; for more information in the Internet platform refer to [www.martel.pro](http://www.martel.pro).

## 5. CONCLUSION

Adaptation and approbation of the tests in different Maritime institutions of Europe will take place according to the MarTEL pilot project aiming to evaluate and improve professional language skills of ratings, junior and senior officers. It is expected that the project will radically improve the level of Maritime education since competence in Maritime English not only will improve the communication skills of seafarers but also their learning potential. It also is expected to make the merchant navy a more professional service, make it more efficient and effective and, hence, more competitive. Maritime English as acquired the special status for professional achievements enlarges the basis for successful merchant navy operation.

## REFERENCES

- [1]. IMO, *International Convention of Standards of Training, Certification and Watchkeeping for Seafarers*, 1978
- [2]. *IMO Standard Marine Communication Phrases. International Maritime Organization*, London, 2002.
- [3]. Ivasyuk N.A. - *Quality Standards in Maritime English Education in Ukraine*. – World Maritime Excellence =Світове Морське Вдосконалення . Під ред. Д.Жукова. - О.: АО Бахва, 2007.
- [4]. *MarTEL* – <http://www.maritime-tests.org>; [www.martel.pro](http://www.martel.pro)
- [5]. *Merriam Webster's Dictionary*.- Encyclopaedia Britannica 2008.
- [6]. Roenig J., Urisz J. - *Competence Standards for Maritime English*. Economical, Social and Legal Challenges of Maritime Country in European Union , Kolobrzeg, 2009
- [7]. Ziarati, R. - *Safety At Sea – Applying Pareto Analysis*. Proceedings of World Maritime Technology Conference (WMTTC 06), Queen Elizabeth Conference Centre, 2006.
- [8]. Ziarati M., Ziarati R., Calbas B., Mousley L. - *Improving safety at sea by developing standards for Maritime English*, IMLA, 2008.
- [9]. Ziarati et al. - *Developing Standards for Maritime English*, Bridge Conference 2009, Finland.

## DETERMINATION OF EXPLOITATION RESOURCES OF SUPPORTING GIRDER FROM RAILWAY

<sup>1</sup>DICHEV D., <sup>1</sup>TODOROV B. S., <sup>2</sup>DIMITROVA A. M., <sup>1</sup>LYUTSKANOV, G. K.  
<sup>1</sup>Vaptsarov Naval Academy - Varna, Bulgaria, <sup>2</sup>Technical University – Varna, Bulgaria

The aim of present article is to determine the possibility of further exploitation of the supporting girders of an under-crane way in "Varna - West" port before pressing repair. For this purpose destructive mechanical and metalography testing of samples cuted from those girders were made.

**Keywords:** destructive mechanical testing, tensile test, charpy impact test, fatigue strength

### 1. INTRODUCTION

The main purpose of the present work is to investigate and to determine the state of under-crane girders railway of 20t crane in raw materials (port "Varna - West") [1], [2].

The worn out rail (more than 30 years exploitation) is shown on Fig.1. Scheme of the construction is shown on Fig.2. It is clearly seen that the rail is well worn out and have to be replaced (Fig.1). Before the repair the working capacity of the supporting girders has also to be checked (Fig.2).



**Fig. 1. Wear out rail after many years of exploitation**

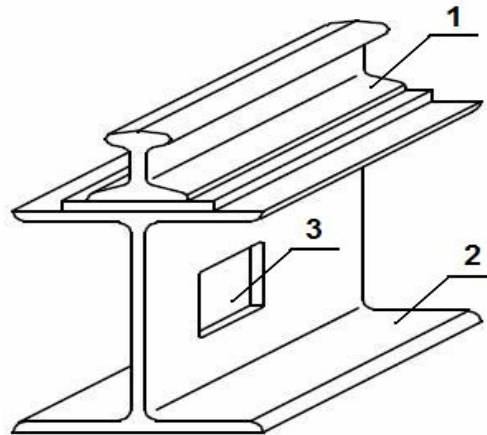


**Fig. 2. Scheme of the construction**  
 1-rail; 2-supporting girder; 3-cutted sample from the supporting girder

## 2. CHEMICAL AND MICROSTRUCTURAL ANALISES

Chemical composition of girder material is shown in Tabl.1

**Table 1: Chemical composition of under-crane girder material**

Chemical element	C	Si	Mn	C r	Ni
Composition, wt. %	0,168	0,165	0,460	0,176	0,095

From chemical composition in Tabl.1 can be seen that the girder material responds to “steel 20” – BDS 5785-83.

Figure 3 shows the microstructure of investigated steel.



**Fig. 3. Microstruvture of investigated steel**

Metalography analysis shows that there are no traces of pores, nonmetal inclusions, surface crackes and other defects in material structure. No changes in material state

resulted from its exploitation can be seen. This is typical for the rolled materials structure with pronounced texture of perlitic areas and well formed between them ferritic areas with clear boundaries of particular fine ferritic grains, [7], [6], [4], [5].

### 3. MECHANICAL TESTING

Main Standard BDS 1086-78 samples were used. Tests were carried out using mechanical testing machine ZDM-5. Results are presented in Tabl.2.

**Table 2: Mechanical characteristics of tested materials**

Mechanical characteristics	Tensile strength, $R_m$ /MPa/	Yield strength, $R_e$ /MPa/	Elongation, $A$ /%/	Reduction of area, $Z$ /%/	Hardness HB
Value	457	347	37	70	128

According to BDS EN 10083-2-A1 mechanical characteristics of “steel 20” have to be as follows

- $R_m$  410-480MPa
- $R_e$  230-320MPa
- $A$  32-37%
- $Z$  59-64%
- HB 101-140

Comparison with experimental results shows:

- Yield strength ( $R_e=347$ MPa) -7% higher than standard requirement;
- Tensile strength ( $R_m=457$ MPa) – fits the standard requirement;
- Elongation ( $A=37\%$ ) - fits the standard requirement;
- Reduction of area ( $Z=70\%$ ) - 8% higher than standard requirement;
- Hardness (128 HB 10/3000/10  $\pm 5$ ) - fits the standard requirement.

From tensile test can be seen that the main metal of the girder is with high ductility and comparatively not so high strength and pronounced yielding offset.

For impact toughness test standard samples were used (Fig.4). Tests were carried out using Charpy hammer with pendulum impact energy  $KU=294.3$ J.

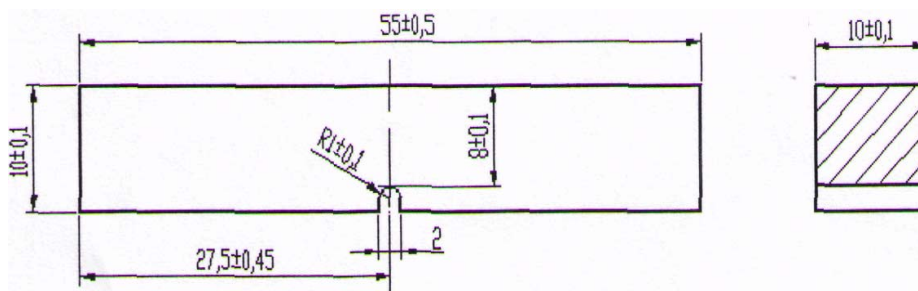


**Fig. 4 Impact testing sample.**

- Samples were longitudinally cut and transverse to the rolling direction. Results are:
- KCV=250 J/cm<sup>2</sup> for longitudinal samples
  - KCV=176 J/cm<sup>2</sup> for transverse samples

The broken samples have typical fracture surfaces (Fig.5) on longitudinal samples the fractured surface lines coincided with perlitic texture can be seen. On the transverse samples fractured surface pronounced cracks can be seen.

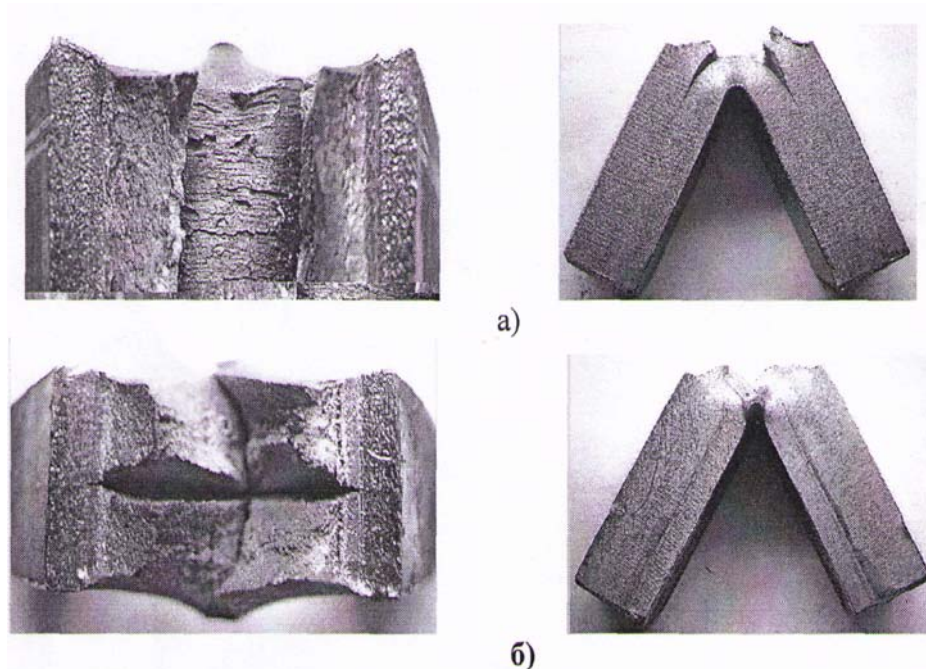


**Fig. 5 Broken impact testing samples fractured surfaces.  
a/ longitudinal to the rolling direction  
b/ transverse to the rolling direction**

On Fig.6 fatigue testing sample is shown.

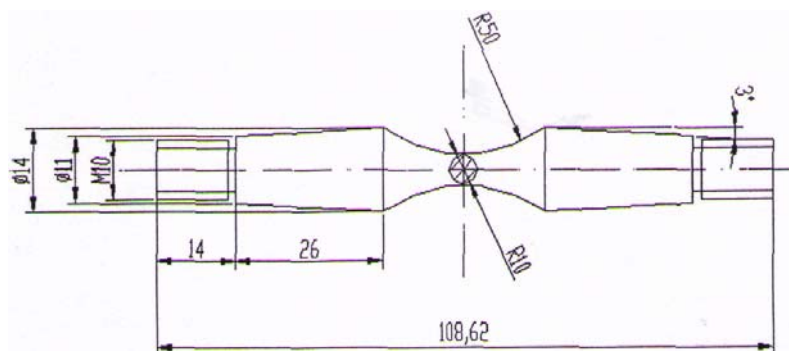


**Fig. 6 Fatigue testing sample.**

Fatigue testing machine MUI-6000 (for fatigue testing under bending with rotation of the sample) was used.

Results from fatigue tests are presented in Tabl.3.

**Table 3: Fatigue testing results**

Fatigue strength, $\sigma_{-1}$ , MPa	380	370	345	325	295	290	250	225	220	200
Cycles , N	$2,44 \cdot 10^4$	$1,8 \cdot 10^4$	$5 \cdot 10^4$	$1,5 \cdot 10^5$	$2,6 \cdot 10^5$	$3,6 \cdot 10^6$	$1,3 \cdot 10^6$	$3,5 \cdot 10^6$	♂	♂

From these experimental results fatigue diagram was drawn (Fig.7). From the diagram fatigue strength value  $\sigma_{-1}=224\text{MPa}$  is found.

This result fits the standard requirement 200-260 MPa (BDS EN 10083-2-A1).

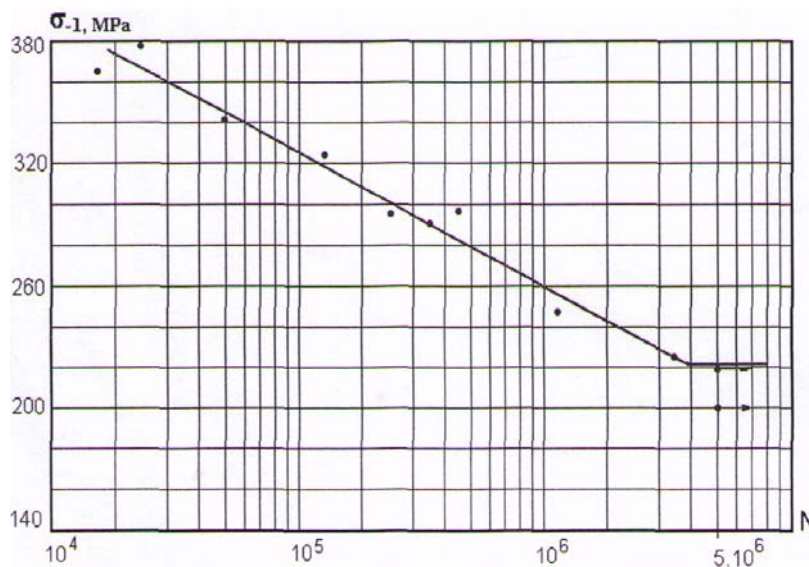


**Fig. 6 Fatigue diagram (Wöhler curve).**

#### 4. CONCLUSIONS

From experiments on samples of girder from under-crane way in carried out raw material shop, can be concluded that steel properties were not changed as a result of many years of exploitation.

#### REFERENCES

- [1]. Arzamasov B. N., Solowev T.V., *Spravochnik po konstrukcionnim materialom*, Moskva, Izdatelstvo MGTU imeni N.E.Baumana, 2005.-637s.(Russian)
- [2]. Bljumenhauer H., *Ispitanie materialov.*, M., Metalurgija, 1979. – 447s. (Russian)
- [3] Efimenko L.A. i dr., *Metalovedenie i termicheskaja obrabotka svarnih soedinenij.*, Moskva, „Logos”, 2007.-455s.(Russian)

- [4]. Harionovskij V.V., **Nadegnost i resurs konstrukcij gazoprovodov**, M., Nedra, 200 – 476s. (Russian)
- [5]. Lalev B. I., Kopchev M. I., **Modelirane na toplinnite procesi pri plosko shlifovane s kinematichno promenlivi parametric na regime na rjazane**, Godishnik na TU-Varna, 2004.tom4, 937 – 946s. (Bulgarian)
- [6.] Plavskij Ju. N., Artemev Ju. G., **Tverdost staly kak funkcia ee protshnostnogo i strukturnogo sostojanija**, Zavodskaja laboratoria, 1989, No5-88-91s. (Russian)
- [7] Romanov O.H., **Vjazkost razrushenija konstrukcionnih stalej**, M., Metalurgija, 1979.-175s. (Russian)

## THE VELOCITY OF THE LOCK WATER LEVEL AT A LINEAR VARIATION OF THE FLOW IN THE FILLING (EMPTYING) CONDUIT

<sup>1</sup>DINU DUMITRU, <sup>1</sup>CUPSA OVIDIU SORIN

<sup>1</sup>Constanta Maritime University, Romania

The paper presents a mathematical model of the filling (emptying) of the lock chamber in a transition period, when the valves are opening or shutting. In this situation, we can consider a linear variation of the flow. We shall study the flow of the viscous fluid, no compressible, in an unsteady regime, through the lock chamber filling (emptying) conduits with the help of the general equation of Navier-Stokes and the equation of continuity. To solve these equations we used the potential vector, which has a physical significance: the circulation of the potential vector on the perimeter of the conduit section is equal to the flow through this conduit. By approximation we established a hyperbolic variation of the velocity of the liquid level to an asymptote.

**Key words:** lock chamber, level velocity, linear variation of the flow, potential vector.

### 1. INTRODUCTION

An accuracy mathematical model of the filling (emptying) reservoir phenomena with liquid, in our case the lock chamber, presume the solving of the movement equations in the conditions very near to the reality (Fig. 1). We refer to the transition periods when the valves are opening or shutting, one to one or all together, and also to the fact that between pool I and the lock chamber (between the lock chamber and the II) are the conduits, sometimes long enough, which influence the filling (emptying) process.

The vector potential is a term taken from electrical engineering, in fact a symbol used to facilitate the mathematical calculation (for the solenoidal field  $\nabla \bar{v} = 0$ , which involve  $\bar{v} = \text{rot} \bar{A}$ ,  $\bar{A} = \bar{A}(x, y, z, t)$  being the potential vector of the field if  $\nabla \bar{A} = 0$ ) apparently without physical significance. The physical significance of the potential vector was put into evidence in the paper [2]: the circulation of the potential vector on the perimeter of the conduit section is equal to the flow through this conduit. The potential vector helps us to solve the Navier –Stokes equations to establish the velocity distribution in the conduit.

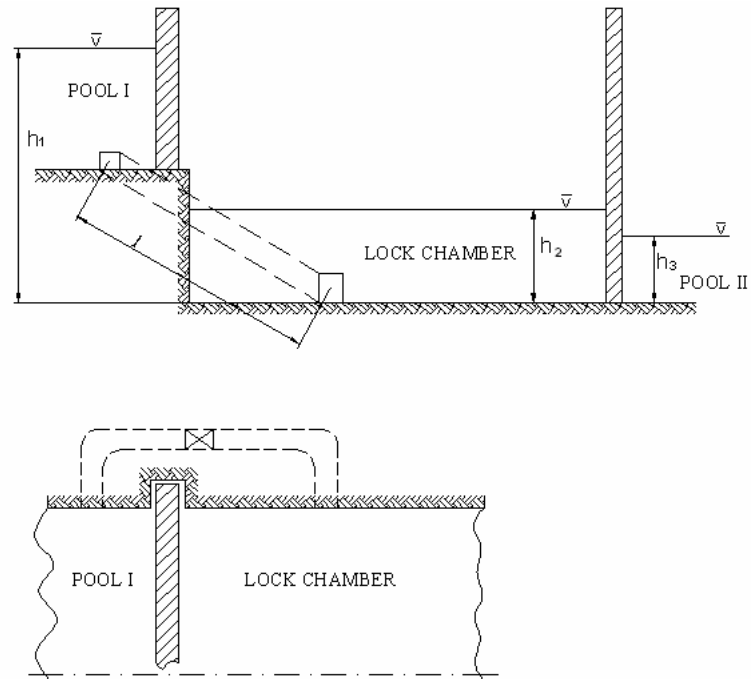


Fig. 1 The lock

For the transitory regimes we can consider a linear variation of the flow. In this situation, we calculated the pressure gradient on the length of the filling (emptying) conduit of the lock chamber. Having this gradient, we could establish the variation of the hydrostatic pressure and the velocity of the lock chamber water level respectively.

## 2. THE USE OF POTENTIAL VECTOR IN THE STUDY OF FLUID MECHANICS

We shall study the flow of the viscous fluid, no compressible, in an unsteady regime, through the lock chamber filling (emptying) conduits with the help of the general equation of Navier-Stokes and the equation of continuity.

In our theoretical study we shall use the transcription of these equations in cylindrical coordinates  $(r, \theta, z)$ .  $Oz$  being the axe of the conduit (Fig. 2):

$$\frac{\partial v_r}{\partial t} + v_r \frac{\partial v_r}{\partial r} + \frac{v_\theta}{r} \frac{\partial v_r}{\partial \theta} + v_z \frac{\partial v_r}{\partial z} - \frac{v_\theta^2}{r} =$$

$$= \nu \left( \frac{\partial^2 v_r}{\partial r^2} + \frac{1}{r^2} \frac{\partial^2 v_r}{\partial \theta^2} + \frac{\partial^2 v_r}{\partial z^2} + \frac{1}{r} \frac{\partial v_r}{\partial r} - \frac{2}{r^2} \frac{\partial v_\theta}{\partial \theta} - \frac{v_r}{r^2} \right) - \frac{1}{\rho} \frac{\partial p}{\partial r};$$

$$\begin{aligned}
 & \frac{\partial v_\theta}{\partial t} + v_r \frac{\partial v_\theta}{\partial r} + \frac{v_\theta}{r} \frac{\partial v_\theta}{\partial \theta} + v_z \frac{\partial v_\theta}{\partial z} + \frac{v_r v_\theta}{r} = \\
 & = v \left( \frac{\partial^2 v_\theta}{\partial r^2} + \frac{1}{r^2} \frac{\partial^2 v_\theta}{\partial \theta^2} + \frac{\partial^2 v_\theta}{\partial z^2} + \frac{1}{r} \frac{\partial v_\theta}{\partial r} + \frac{2}{r^2} \frac{\partial v_r}{\partial \theta} - \frac{v_\theta}{r^2} \right) - \frac{1}{\rho r} \frac{\partial p}{\partial \theta}; \\
 & \frac{\partial v_z}{\partial t} + v_r \frac{\partial v_z}{\partial r} + \frac{v_\theta}{r} \frac{\partial v_z}{\partial \theta} + v_z \frac{\partial v_z}{\partial z} = v \left( \frac{\partial^2 v_z}{\partial r^2} + \frac{1}{r^2} \frac{\partial^2 v_z}{\partial \theta^2} + \frac{\partial^2 v_z}{\partial z^2} + \frac{1}{r} \frac{\partial v_z}{\partial r} \right) - \frac{1}{\rho} \frac{\partial p}{\partial z}; \\
 & \frac{\partial v_r}{\partial r} + \frac{1}{r} \frac{\partial v_\theta}{\partial \theta} + \frac{\partial v_z}{\partial z} + \frac{v_r}{r} = 0.
 \end{aligned} \tag{1}$$

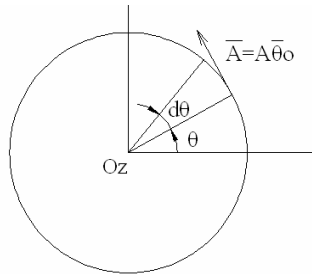


**Fig. 2 The conduit in the cylindrical coordinates**

The movement is axial-symmetric and the axe of the conduit coincides, as we already said, with the axe Oz. The components of velocity will be:

$$\begin{aligned}
 v_r &= v_\theta = 0, \\
 v_z &= v(r, t).
 \end{aligned} \tag{2}$$

As we know, the solenoidal (rotational) fields are characterized by  $\nabla \cdot \bar{v} = 0$ , which involve:

$$\bar{v} = \text{rot} \bar{A}, \tag{3}$$

where  $\bar{A}$  is a function of point and time, which represents the potential vector of the velocities field if  $\nabla \bar{A} = 0$ .

The potential vector of our movement will be:

$$\bar{A} = A(r, z) \theta_0 \tag{4}$$

and it can be determinated with the relation:

$$\Delta \left( \frac{\partial \bar{A}}{\partial t} - \nu \Delta \bar{A} \right) = 0, \tag{5}$$

a particularization for the axial-symmetric movement of the flow of real, no compressible fluids, written using the potential vector of the velocities field.

Solving the equation (5) using the Laplace transformation and taking into account that the circulation of the potential vector on the perimeter of the conduit section is equal to the flow through this conduit we shall obtain [ ]:

$$A(r,t) = \frac{1}{2\pi i} \int_{b-i\infty}^{b+i\infty} e^{st} \frac{Q^*}{2\pi r_0} \frac{2I_1(p) - pI_0(p_0)}{2I_1(p_0) - p_0I_0(p_0)} ds,$$

(6)

when  $I_0$  and  $I_1$  are the Bessel modify functions, rank 0, respectively 1, first sort,

$$p = r\sqrt{\frac{s}{\nu}} \text{ and } p_0 = r_0\sqrt{\frac{s}{\nu}}.$$

$Q^*$  is the Laplace transformation of the flow.

Knowing that the velocity is:

$$v = v_z = (\text{rot } \vec{A})_z, \tag{7}$$

we shall obtain the relation of the velocity:

$$v(r,t) = \frac{1}{2\pi i} \int_{c-i\infty}^{c+i\infty} e^{st} \frac{Q^*}{\pi r_0} \sqrt{\frac{s}{\nu}} \frac{I_0(p) - I_0(p_0)}{2I_1(p_0) - p_0I_0(p_0)} ds. \tag{8}$$

### 3. THE PRESSURE GRADIENT IN THE CASE OF LINEAR VARIATION OF THE FLOW

We consider a linear variation of the flow in the filling (emptying) conduit [1]. In this case, we propose to evaluate the variation of the level in the lock chamber.

So, the flow has a linear variation:

$$Q(t) = k_1 t + k_2. \tag{9}$$

By applying Laplace transformation, we'll obtain:

$$Q^*(s) = \frac{k_1}{s^2} + \frac{k_2}{s} = \frac{k_1 + k_2 s}{s^2}. \tag{10}$$

The expression of the potential vector becomes:

$$A(r,t) = \frac{1}{2\pi i} \frac{1}{2\pi r_0} \int_{b-i\infty}^{b+i\infty} e^{st} \frac{k_1 + k_2 s}{s^2} \frac{2I_1(p) - pI_0(p_0)}{2I_1(p_0) - p_0I_0(p_0)} ds. \tag{11}$$

Solving the integrative, we'll have:

$$A(r,t) = 2\pi i \frac{1}{2\pi i} \frac{1}{2\pi r_0} \sum \text{Re } z = \frac{1}{2\pi r_0} \sum \text{Re } z. \tag{12}$$

The poles of the function under integrative are:

$$s = 0, \text{ double pole and } s = -\frac{\nu}{r_0^2} \alpha_n^2 (n \in N^*, \alpha \in R), \text{ where } \pm i\alpha_n = r_0 \sqrt{\frac{s_n}{\nu}}$$

represent the non-nil solutions of the equation:

$$2I_1(p_0) - p_0I_0(p_0) = 0. \tag{13}$$

Knowing that:

$$I_k(w) = i^{-k} J_k(w) \tag{14}$$

we can write:

$$I_k(iw) = i^{-k} J_k(w) \tag{15}$$

and

$$I_0(iw) = J_0(w). \tag{16}$$

Replacing  $w = p_0 = i\alpha$  in equation (13), we'll have:

$$2J_1(\alpha) = J_0(\alpha), \tag{17}$$

$J_0(\alpha)$  and  $J_1(\alpha)$  being the Bessel functions, rank 0, respectively 1, first sort.

Knowing that the non-nil solutions of this equation,  $\pm \alpha_n$ , can be determined graphically, we obtain:

$$\alpha_1 = 5,15; \alpha_2 = 8,40; \alpha_3 = 11,61; \alpha_4 = 14,83 \text{ etc.}$$

The residuum of double pole,  $s=0$ , is given by the formula:

$$reziduu(0) = \frac{d}{ds} \left[ s^2 e^{st} \frac{k_1 + k_2 s}{s^2} \frac{2I_1(p) - pI_0(p)}{2I_1(p_0) - p_0 I_0(p_0)} \right]. \tag{18}$$

For simple pole  $s = s_n = -\frac{v}{r_0^n} \alpha_n^2$  the residuum of the function under the integrative (11)

will be:

$$reziduu(s_n) = s \frac{\frac{v\alpha^2}{r_0^2} k_1 - k_2 \frac{v\alpha_n^2}{r_0^2} 2I_1\left(i\frac{r}{r_0}\alpha_n\right) - i\frac{r}{r_0}\alpha_n I_0(i\alpha_n)}{\frac{v^2}{r_0^4} \alpha_n^4} \frac{d}{ds} [2I_1(p_0) - p_0 I_0(p_0)]_{s=s_n}. \tag{19}$$

Finally we shall obtain the expression of the potential vector and velocity in the case of linear variation of the flow:

$$A(r,t) = \frac{1}{2\pi r_0} \left[ (k_1 t + k_2) \frac{r}{r_0} \left( 2 - \frac{r^2}{r_0^2} \right) - k_1 \frac{r(r^2 - r_0^2)^2}{24vr_0^3} - 2 \frac{r_0^2}{v} \sum_{n=1}^m e^{\frac{v}{r_0^2} \alpha_n^2 t} \frac{k_1 - k_2 \frac{v}{r_0^2} \alpha_n^2 2J_1\left(\frac{r}{r_0} \alpha_n\right) - \frac{r}{r_0} \alpha_n J_0(\alpha_n)}{\alpha_n^4 J_1(\alpha_n)} \right]; \tag{20}$$

$$v(r,t) = \frac{1}{\pi r_0} \left[ (k_1 t + k_2) \frac{1}{r_0} \left( 1 - \frac{r^2}{r_0^2} \right) - k_1 \frac{r(r^2 - r_0^2)^2 (3r^2 - r_0^2)}{48vr_0^3} - \frac{r_0^2}{v} \sum_{n=1}^m e^{\frac{v}{r_0^2} \alpha_n^2 t} \frac{k_1 + k_2 \frac{v}{r_0^2} \alpha_n^2 J_0\left(\frac{r}{r_0} \alpha_n\right) - \frac{r}{r_0} \alpha_n J_0(\alpha_n)}{\alpha_n^3 J_1(\alpha_n)} \right]; \tag{21}$$

To verify we'll replace  $v(r,t)$  given by (21) in the flow formula:

$$Q(t) = \int_0^{r_0} 2\pi r v(r,t) dr \tag{22}$$

and we'll obtain:

$$Q(t) = k_1 t + k_2, \quad (23)$$

the beginning expression of linear flow.

To determine the pressure gradient, we shall use the Navier-Stokes equation, written in cylindrical coordinates, neglecting the mass forces (the third equation (1)) in which  $v_r = v_\theta = 0, v_z = v(r, t)$ :

$$-\frac{\partial p}{\partial z} = \rho \frac{\partial v}{\partial t} - \eta \left( \frac{\partial^2 v}{\partial t^2} + \frac{1}{r} \frac{\partial v}{\partial r} \right). \quad (24)$$

Taking into account that:

$$2J_1(\alpha) = J_0(\alpha); J_1'(w) = \frac{J_1(w)}{w} + J_0(w); J_0'(w) = -J_1(w); \quad (25)$$

will finally obtain the pressure gradient in the case of known linear variation of the flow:

$$-\frac{\partial p}{\partial z} = \frac{4\rho}{\pi r_0^2} \left[ \frac{1}{3} k_1 + \frac{2v}{r_0^2} (k_1 t + k_2) - \sum_{n=1}^m e^{-\frac{v}{r_0^2} \alpha_n^2 t} \frac{k_1 - k_2 \frac{v}{r_0^2} \alpha_n^2}{\alpha_n^2} \right]. \quad (26)$$

#### 4. LIQUID LEVEL VARIATION

We have established the pressure gradient formula in the case of linear variation of the flow. Now we are interested in the variation of the lock chamber liquid level. We want to know the velocity of this level when the pumps fill the lock chamber. For this, denoting with  $f(t)$  the left part of the relation (26) we can write:

$$dp = -f(t) dz. \quad (27)$$

By integration the relation (27) on the length of the filling conduit, we shall obtain:

$$p_2 - p_1 = -f(t)(z_2 - z_1) \quad (28)$$

or

$$p_1 - p_2 = f(t)l, \quad (29)$$

$l$  being the length of the conduit.

If  $p_1$  is the constant hydrostatic pressure from pool I and  $h_2$  the level of the lock chamber liquid we'll have successively:

$$\begin{aligned} p_1 - \rho g h_2 &= f(t)l; \\ \rho g h_2 &= p_1 - f(t)l; \\ u(t) = \frac{h_2}{t} &= \frac{1}{\rho g t} [p_1 - f(t)l]; \end{aligned} \quad (30)$$

$u(t)$  represents the rising velocity of the level.

By replacing  $f(t)$ , we'll have:

$$u(t) = \frac{p_1}{\rho g t} - \frac{4l}{\pi g r_0^2} \left[ \frac{1}{t} \left( \frac{k_1}{3} + \frac{2\nu k_2}{r_0^2} \right) + \frac{2\nu k_1}{r_0^2} - \sum_{n=1}^m \frac{1}{t} e^{-\frac{\nu}{r_0^2} \alpha_n^2 t} \frac{k_1 - k_2 \frac{\nu}{r_0^2} \alpha_n^2}{\alpha_n^2} \right].$$

(31)

We can easily demonstrate that the two last terms of the square bracket of the relation (31) – those under the sign of sum – are far less than the first two:

$$\frac{\frac{k_1}{3t}}{k_1} = \frac{\sum_{n=1}^m e^{-\frac{\nu}{r_0^2} \alpha_n^2 t}}{3} \gg 1 \quad \text{and} \quad \frac{\frac{2\nu k_2}{r_0^2 t}}{\nu k_2} = 2 \sum_{n=1}^m e^{-\frac{\nu}{r_0^2} \alpha_n^2 t} \gg 1,$$

$$t \sum_{n=1}^m e^{-\frac{\nu}{r_0^2} \alpha_n^2 t} \quad r_0^2 t \sum_{n=1}^m e^{-\frac{\nu}{r_0^2} \alpha_n^2 t}$$

because  $\alpha_n$  has the over unit values (5.15; 8.4; 11.61; 14.83 etc.)

By approximation we can write:

$$u(t) \cong \frac{C_1}{t} + C_2,$$

(32)

where

$$C_1 = \frac{p_1}{\rho g} - \frac{4l}{\pi g r_0^2} \left( \frac{k_1}{3} + \frac{2\nu k_2}{r_0^2} \right) \quad \text{and} \quad C_2 = \frac{8\nu k_1}{\pi g r_0^4},$$

a hyperbolic variation of the liquid level to the asymptote  $u = \frac{8\nu k_1}{\pi g r_0^4}$ .

In the case of emptying the lock chamber by free fall, admitting that the exit of the water is at atmospheric pressure, we'll have:

$$\rho g \frac{h_2 - h_3}{t} = \frac{f(t)}{t} l, \tag{33}$$

$h_2$  – the variable level of the lock chamber water,  $h_3$  – the constant level of pool II.

$$u(t) = \frac{h_2 - h_3}{t} = \frac{l}{\rho g t} f(t); \tag{34}$$

$$u(t) = \frac{4l}{\pi g r_0^2} \left[ \frac{1}{t} \left( \frac{k_1}{3} + \frac{2\nu k_2}{r_0^2} \right) + \frac{2\nu k_1}{r_0^2} - \sum_{n=1}^m \frac{1}{t} e^{-\frac{\nu}{r_0^2} \alpha_n^2 t} \frac{k_1 - k_2 \frac{\nu}{r_0^2} \alpha_n^2}{\alpha_n^2} \right]. \tag{35}$$

We observe that:

$$\lim_{t \rightarrow 0} u(t) = 0 \quad \text{and} \quad \lim_{t \rightarrow \infty} u(t) = \frac{8\nu k_1}{\pi g r_0^4}.$$

## 5. CONCLUSIONS

The mathematical model allows us to solve a quite delicate problem: the variation of the liquid level in the lock chamber in a transition period - the opening of a valve for example. The valve opening can be made so that the flow linear is. Solving Navier-Stokes equations using the potential vector, we have been able to establish the velocity variation in the conduit and the liquid level variation in the lock chamber.

The problem can be formulated conversely: taking a certain velocity, constant, of the liquid level, we'll determine the necessary flow for this level variation. In this situation the pressure gradient has a linear variation  $\frac{\partial p}{\partial z} = at$ , where  $a$  is a dimensional constant.

## REFERENCE

- [1]. DINU D., ***Considerations regarding the Flow through Circular Conduits in the case of Linear Time Variation of Pressure Gradient***, The 5<sup>th</sup> International Scientific Conference on Naval Technologies TEHNONAV, Constanta, 2006.
- [2]. VASILESCU AL.A., PETREA F. ***Sur l'emploi du potentiel vectoriel du champ des vitesses dans la mécanique des fluides***, Buletinul Universității din Galați, Fascicol II, 1984.

## SHIP MANOEUVRING BY PMM - MATHEMATICS AND EXPERIMENTS PART I, PART II

<sup>1</sup>GANEA BOGDAN

<sup>1</sup>*Safety at Sea Ltd., Glasgow, G2 5RL, U.K., Scotia*

The early 2000's saw the revitalisation of the ship manoeuvring activity of the Ship Hydrodynamics Department of Icepronav. Mathematical modelling of the ship manoeuvring was approached on a new basis. The Abkowitz model, although classical, was found suitable for the available experimental gear - the planar motion mechanism (PMM), installed on the carriage of the main towing tank, length×beam×depth: 280×12×6m. Software for the experimental data processing and basic IMO manoeuvres simulation was written. Till mid 2008, this procedure was used for both contractual and research work.

**Keywords:** Ship manoeuvring, planar motion mechanism, IMO manoeuvres simulation

### 1. INTRODUCTION

Even when studied in calm water, the ship manoeuvring abilities assessment is difficult due to the complexity of the flow involved. While the total ship resistance and the propeller characteristics are determined, either theoretically or experimentally, mainly in an 0 incidence flow, during the manoeuvres the fluid flow past all the ship's parts, below and above waterline, is oblique.

Briefly, although the ship manoeuvring is part of classical ship hydrodynamics, predicting ship manoeuvring remains a challenging task.

### 2. SHIP MANOEUVRING MATHEMATICAL MODEL

The mathematical modelling is intended to capture the ship evolution over a wide area. The ship is considered a rigid body. Her evolution is due to the action of the following main forces: inertial, hydro/aerodynamic, propulsion and governing. Two right-handed reference frames are used, as in figure 1:

- global,  $O_0x_0y_0z_0$ , earth related, to report the ship evolution;
- local,  $Oxyz$ , ship related, to express the forces and water/air velocities acting on/past the whole ship.

Here, the local reference frame is located at midship, baseline, CL, due to the assumed longitudinal ship symmetry. This assumption is not always true. For example, in a barge convoy, the barges are not necessarily symmetrically arranged.

3 parameters are used to report the ship evolution on a calm water surface to the global reference frame: the centre of gravity position,  $x_0$ ,  $y_0$  and the head angle,  $\psi$ , figure 1. Roll, heave and pitch motions are neglected since they cannot be measured by the available

experimental gear. Even in calm water, this assumption is not always true, even for a low Froude number.

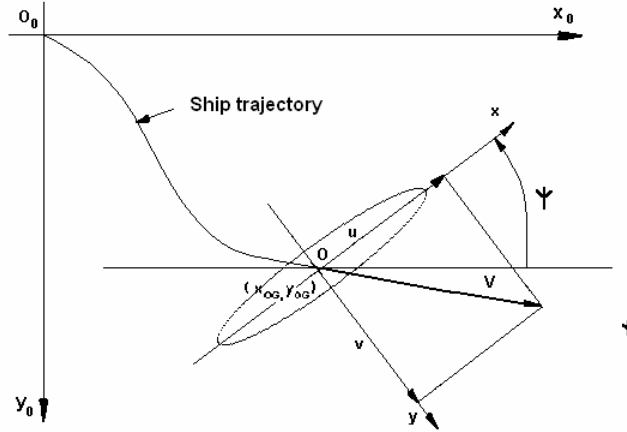


Figure 1. Right-handed reference frames

The mathematical model is composed of 2 groups of equations, initially expressed in the global reference frame:

- 2 force equations, derived from the Newton's 2<sup>nd</sup> law;
- 1 moment equation, derived from the moment-angular momentum relationship.

$$\begin{cases} m \frac{d\vec{V}_G}{dt} = \vec{F}_G \\ \frac{d\vec{H}_G}{dt} = \vec{M}_G \end{cases} \quad (1)$$

- $m$  : ship mass;
- $\vec{V}_G$  : ship centre of gravity, G, velocity;
- $\vec{F}_G$  : force on G;
- $\vec{H}_G$  : angular momentum about G;
- $\vec{M}_G$  : moment about G .

The total vectorial derivative of  $\vec{V}_G$  and  $\vec{H}_G$  will be expressed in the local mobile reference frame. By notation  $r = \dot{\psi}$  and taking into account the ship longitudinal symmetry, the equations (1) become in the local reference frame:

$$\begin{cases} m(\dot{u} - v r - x_G r^2) & = X(u, v, r, \dot{u}, \dot{v}, \dot{r}, \delta) \\ m(\dot{v} + u r + x_G \dot{r}) & = Y(u, v, r, \dot{u}, \dot{v}, \dot{r}, \delta) \\ J_{zz} \dot{r} + m(\dot{v} + u r) x_G & = N(u, v, r, \dot{u}, \dot{v}, \dot{r}, \delta) \end{cases} \quad (2)$$

X, Y, N : torsor of all actions on the ship;

$J_{zz}$  : ship polar moment of inertia about Oz axis;  
 $\delta$  : rudder angle.

There are 2 main approaches to determine the (X, Y, N) torsor:

- by empirical regression type formulae, e.g.: Nomoto, [3], Japanese Manoeuvring Group, [4], [5], SNAME, [6];
- by Taylor series decomposition of X, Y, N about a particular point  $(u, v, r, \dot{u}, \dot{v}, \dot{r}, \delta)$ .

The Taylor series decomposition is valid in just a small interval about the decomposition point. The particular point is chosen to be a constant speed rectilinear trajectory region, i.e.  $(u_0, 0, 0, 0, 0, 0, 0)$ . The ship longitudinal symmetry assumption is used to reduce the number of terms. The higher order acceleration terms and those being a combination of velocities and accelerations are discarded too.

With all these assumptions, the 3<sup>rd</sup> order torsor's decomposition is presented in the relationships: (3)-(6). In order to express the correlation between the effect of the odd number of propellers and the ship velocity, the supplementary terms:  $Y_{0u}$ ,  $Y_{0uu}$ ,  $N_{0u}$ ,  $N_{0uu}$  were added in (4) and (5), although they do not appear in the Taylor decomposition.

$$\begin{aligned}
 X = & X_u \dot{u} + X_0 + X_u \Delta u + \frac{1}{2} X_{uu} \Delta u^2 + \frac{1}{6} X_{uuu} \Delta u^3 + \\
 & + \frac{1}{2} X_{vv} v^2 + \frac{1}{2} X_{rr} r^2 + X_{\delta\delta} \delta^2 + \\
 & + \frac{1}{2} X_{vuu} v^2 \Delta u + \frac{1}{2} X_{rru} r^2 \Delta u + \frac{1}{2} X_{\delta\delta u} \delta^2 \Delta u + \\
 & + X_{vr} vr + X_{v\delta} v\delta + X_{r\delta} r\delta + \\
 & + X_{vru} vr\Delta u + X_{v\delta u} v\delta\Delta u + X_{r\delta u} r\delta\Delta u
 \end{aligned} \tag{3}$$

$$\begin{aligned}
 Y = & Y_v \dot{v} + Y_r \dot{r} + Y_0 + Y_{0u} \Delta u + Y_{0uu} \Delta u^2 + \\
 & + Y_v v + \frac{1}{6} Y_{vvv} v^3 + \frac{1}{2} Y_{vrr} vr^2 + \frac{1}{2} Y_{v\delta\delta} v\delta^2 + Y_{vu} v\Delta u + \frac{1}{2} Y_{vuu} v\Delta u^2 + \\
 & + Y_r r + \frac{1}{6} Y_{rrr} r^3 + \frac{1}{2} Y_{rvv} rv^2 + \frac{1}{2} Y_{r\delta\delta} r\delta^2 + Y_{ru} r\Delta u + \frac{1}{2} Y_{ruu} r\Delta u^2 + \\
 & + Y_\delta \delta + \frac{1}{6} Y_{\delta\delta\delta} \delta^3 + \frac{1}{2} Y_{\delta vv} \delta v^2 + \frac{1}{2} Y_{\delta rr} \delta r^2 + Y_{\delta u} \delta\Delta u + \frac{1}{2} Y_{\delta uu} \delta\Delta u^2 + \\
 & + Y_{vr\delta} vr\delta
 \end{aligned} \tag{4}$$

$$\begin{aligned}
 N = & N_v \dot{v} + N_r \dot{r} + N_0 + N_{0u} \Delta u + N_{0uu} \Delta u^2 + \\
 & + N_v v + \frac{1}{6} N_{vvv} v^3 + \frac{1}{2} N_{vrr} vr^2 + \frac{1}{2} N_{v\delta\delta} v\delta^2 + N_{vu} v\Delta u + \frac{1}{2} N_{vuu} v\Delta u^2 + \\
 & + N_r r + \frac{1}{6} N_{rrr} r^3 + \frac{1}{2} N_{rvv} rv^2 + \frac{1}{2} N_{r\delta\delta} r\delta^2 + N_{ru} r\Delta u + \frac{1}{2} N_{ruu} r\Delta u^2 + \\
 & + N_\delta \delta + \frac{1}{6} N_{\delta\delta\delta} \delta^3 + \frac{1}{2} N_{\delta vv} \delta v^2 + \frac{1}{2} N_{\delta rr} \delta r^2 + N_{\delta u} \delta\Delta u + \frac{1}{2} N_{\delta uu} \delta\Delta u^2 + \\
 & + N_{vr\delta} vr\delta
 \end{aligned} \tag{5}$$

$$\Delta \mathbf{u} = \mathbf{u} - \mathbf{u}_0 \quad (6)$$

The expressions (3)-(5) are those of Strøm-Tejsen and Cislett [7] because they are used by many studies, proving their reliability through decades. However, the calculation process could be carried out also in different ways, leading to different forms of the torsor decomposition. So, the equations (2) could be rewritten in a matrix form:

$$\begin{bmatrix} m - X_{\dot{u}} & 0 & 0 \\ 0 & m - Y_{\dot{v}} & mX_G - Y_{\dot{r}} \\ 0 & mX_G - N_{\dot{v}} & J_{zz} - N_{\dot{r}} \end{bmatrix} \begin{Bmatrix} \dot{u} \\ \dot{v} \\ \dot{r} \end{Bmatrix} = \begin{Bmatrix} f_1 \\ f_2 \\ f_3 \end{Bmatrix}. \quad (7)$$

(7) is a constant coefficients differential equation system. The simple Euler method and the Runge-Kutta type algorithms are frequently applied. Adams-Bashforth methods could also be considered, Ixaru [8]. To obtain the ship trajectory, the resulting ship velocities  $u$ ,  $v$ ,  $r$  are reported to the global reference frame by the same particular Tien-Bryan rotations and then integrated with respect to time. The rotational velocity  $r$  is integrated first, then the linear ones.

### 3. PMM EXPERIMENTS

#### 3.1. General Description

The experiments are intended for the determination of the coefficients (hydrodynamic derivatives) of the system (7). The available experimental gear was a Scotch yoke type planar motion mechanism (PMM). Its kinematics is described in Chislett and Wagner Smitt, [9]. A PMM imposes a set of simple ship trajectories to the self-propelled ship model. During such an evolution, the generated hydrodynamic and inertial forces depend on a small number of coefficients of system (7), which could be so determined. There are 2 kinds of such evolutions:

- non-inertial - the model is moved by PMM with a constant speed on a straight line course;
- inertial – the model is moved by PMM with the same constant speed in the longitudinal direction of the towing tank, while a harmonic transversal movement is imposed too. Both movements are considered with respect to the global reference frame. It results a harmonic acceleration, allowing the determination of the dynamic coefficients too.

The similitude criteria are those used for resistance and self propulsion experiments. The longitudinal speed of the model corresponds to that of the real ship speed for which the ship manoeuvring abilities are to be predicted. The model propeller rpm is determined from the self propulsion experiment results to correspond to this speed. Unfortunately, during the PMM experiments, the additional force, used in the self propulsion experiment to compensate the different ship-model frictional resistance, cannot be imposed. This affects the value of  $X_0$  coefficient, which can no longer be 0. A more advanced experimental setup might electronically compensate this difference.

Once the PMM experiments are finished and the hydrodynamic derivatives computed, the last step is their full scale extrapolation in order to allow the real ship manoeuvring abilities to be predicted. Although in PMM experiments occurs the same scale effect as in the better mastered resistance and self propulsion experiments, due to the flow complexity it

is impossible to cope with it in the same manner and it is almost fully neglected. This leads to a lower accuracy than that the ship speed performance could be predicted.

In the followings, the typical PMM experiments are briefly described.

### 3.2 Non-Inertial PMM Experiment

It is named also static or straight line experiment but it would be better to name it as a *steady* experiment since it is not static at all. The model has a constant speed in the longitudinal direction of the towing tank and various drift and ruder angles, Figure 2. Therefore, there is no model acceleration but hydrodynamic forces generated by the oblique flow past the hull and the rudder.

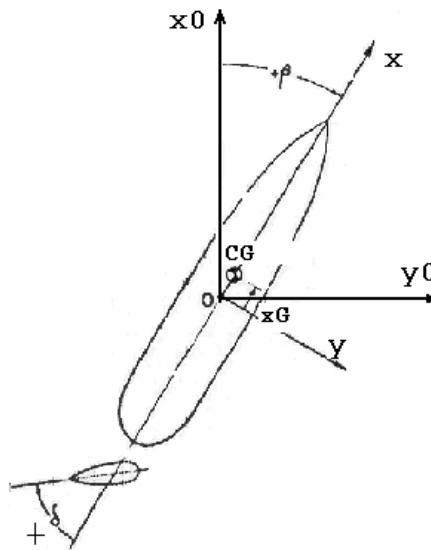


**Figure 2. Non Inertial PMM experiment**

These forces and the moment about the vertical axis, reported to the local reference frame, are recorded as a matrix, for a number of drift and ruder angles. For each drift angle, there are several rudder angles between maximum possible rudder deflection, port and starboard, usually  $35^\circ$ . The range of the drift angles is usually limited by the dynamometer range of measurement. It seems the drift angle could not exceed  $10^\circ$ , obviously depending on the model displacement and its speed.

Due to the drift angle, Figure 2, the constant longitudinal speed  $U_0$  of the model in the global reference frame is reported to the local reference frame by:

$$\begin{aligned} u_0 &= U_0 \cos(\beta) \\ v_0 &= -U_0 \sin(\beta) \end{aligned} \quad (8)$$

It creates an oblique flow past the model hull. This particular movement is characterised by:

$$\begin{aligned} u &= u_0 & \dot{u} &= 0 \\ v &= v_0 & \dot{v} &= 0 \\ r &= 0 & \dot{r} &= 0 \end{aligned} \quad (9)$$

Consequently, there is no inertial force and the torsor (3)-(5) becomes:

$$\begin{aligned} X &= X_0 + \frac{1}{2} X_{vv} v^2 + X_{v\delta} v\delta + \frac{1}{2} X_{\delta\delta} \delta^2 \\ Y &= Y_0 + Y_v v + \frac{1}{6} Y_{vvv} v^3 + \frac{1}{2} Y_{v\delta} v^2 \delta + \frac{1}{2} Y_{\delta\delta} v \delta^2 + \frac{1}{6} Y_{\delta\delta\delta} \delta^3 + Y_\delta \delta \\ N &= N_0 + N_v v + \frac{1}{6} N_{vvv} v^3 + \frac{1}{2} N_{v\delta} v^2 \delta + \frac{1}{2} N_{\delta\delta} v \delta^2 + \frac{1}{6} N_{\delta\delta\delta} \delta^3 + N_\delta \delta \end{aligned} \quad (10)$$

Its coefficients are determined by the least square method over the matrix of the measured data described above.

### 3.3 Inertial PMM Experiments

These are also named dynamic experiments due to the acceleration involved in the model movement. The acceleration is achieved by imposing a harmonic movement to the model. This particular movement has 3 main advantages:

- it is easy to be produced by a constant rotational speed mechanism, allowing easy control of its kinematics;
- it is cyclic, allowing repetitive data to be achieved;
- its velocity and acceleration are in opposite phases, allowing the separation of the effects of viscosity and inertia.

Relating to the main harmonic movement, there are basically 2 such experiments: pure sway and pure yaw, which are described below.

#### 3.3.1 Pure sway experiment

While the model is moved with the same constant speed in the longitudinal direction of the towing tank,  $U_0$ , the PMM imposes a harmonic transversal motion too, always keeping the model parallel with the initial longitudinal direction, figure 3. The rudder is always kept amidships.

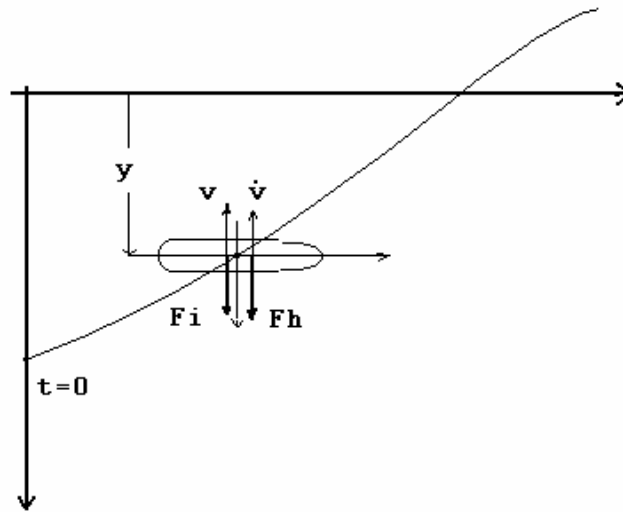


**Figure 3. The harmonic transversal movement**

The transversal harmonic displacement is expressed in the local reference frame by:

$$y = a_0 \cos(\omega t) , \quad (11)$$

$a_0$  : sway amplitude;

$\omega$  : pulsation.

Consequently, the kinematical parameters for this particular movement, expressed in the local reference frame, are:

$$\begin{aligned} u &= U_0 & \dot{u} &= 0 \\ v &= -a_0 \omega \sin(\omega t) = v_0 \sin(\omega t) & \dot{v} &= -a_0 \omega^2 \cos(\omega t) = \dot{v}_0 \cos(\omega t) , \\ r &= 0 & \dot{r} &= 0 \end{aligned} \quad (12)$$

For various amplitudes and pulsations of the harmonic movement, the longitudinal and transversal forces, reported to the local reference frame, are measured and recorded. In order to determine the hydrodynamic derivatives, the measured forces will be equated to their analytical expressions. Theoretically, the measured forces and their moment are composed of an inertial and a hydrodynamic part.

By the left side of (2) and together with (12), the inertial part of the measured torsor is:

$$\begin{aligned} X_i &= 0 \\ Y_i &= -m\dot{v} \\ N_i &= -m x_G \dot{v} \end{aligned} \quad (13)$$

The inertial force is opposed to the direction of the imposed acceleration by PMM, Figure 3.

The hydrodynamic part is expressed by retaining only the 1<sup>st</sup> order terms of the relationships (3)-(5). This is a linear approach. By (15), the hydrodynamic part is:

$$\begin{aligned}
 X_h &= X_0 \\
 Y_h &= Y_0 + Y_v v + Y_{\dot{v}} \dot{v} \\
 N_h &= N_0 + N_v v + N_{\dot{v}} \dot{v}
 \end{aligned} \quad (14)$$

By (12), (13) and (14), the measured torsor is theoretically expressed by:

$$\begin{aligned}
 X_T &= X_0 \\
 Y_T &= Y_0 + (Y_v v_0) \sin(\omega t) + [(Y_{\dot{v}} - m\dot{v})\dot{v}_0] \cos(\omega t) \\
 N_T &= N_0 + (N_v v_0) \sin(\omega t) + [(N_{\dot{v}} - m x_G)\dot{v}_0] \cos(\omega t)
 \end{aligned} \quad (15)$$

The experimental torsor could be expressed by a 1<sup>st</sup> order trigonometric Fourier series:

$$\begin{aligned}
 X_E &= X_{0E} \\
 Y_E &= Y_{0E} + Y_{1a} \cos(\omega t) + Y_{1b} \sin(\omega t) \\
 N_E &= N_{0E} + N_{1a} \cos(\omega t) + N_{1b} \sin(\omega t)
 \end{aligned} \quad (16)$$

Finally, (18) and (19) yield:

$$\begin{aligned}
 X_0 &= X_{0E} \\
 Y_0 = Y_{0E} \quad Y_v &= \frac{Y_{1b}}{v_0} \quad Y_{\dot{v}} - m\dot{v} = \frac{Y_{1a}}{\dot{v}_0} \\
 N_0 = N_{0E} \quad N_v &= \frac{N_{1b}}{v_0} \quad N_{\dot{v}} - m x_G = \frac{N_{1a}}{\dot{v}_0}
 \end{aligned} \quad (17)$$

Since there are several amplitudes and pulsations for which the hydrodynamic derivatives are computed by (17), their final value is determined by a linear regression on the Fourier series coefficients as depending on  $v_0$  and  $\dot{v}_0$ , Figures 4 and 5. Actually, the hydrodynamic derivatives are the gradient of the regression lines.

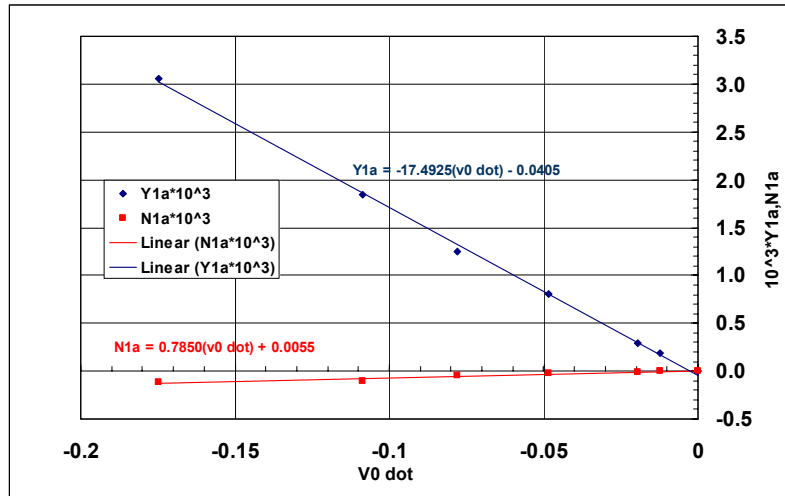


Figure 4. Pure sway. Fourier 1a coefficients linear regression

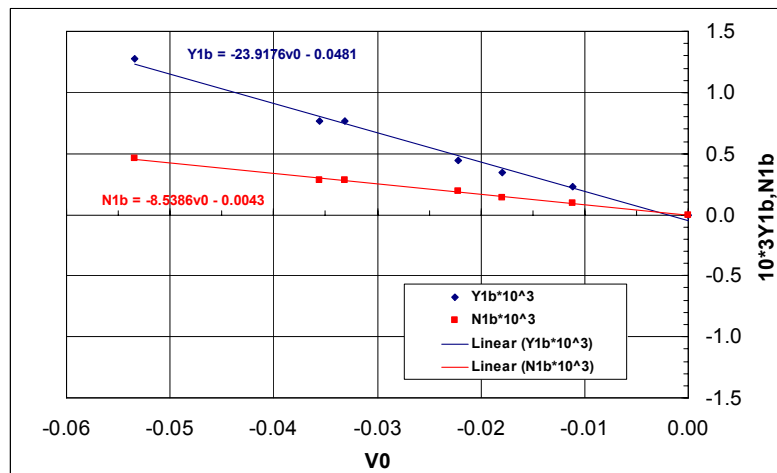


Figure 5. Pure sway. Fourier 1b coefficients linear regression

Usually, only the hydrodynamic derivatives  $Y_{\dot{v}} - m$  and  $N_{\dot{v}} - mX_G$  are retained. The others are preferred from the non-inertial experiment.

In a non-linear approach, the terms of (3)-(5) are considered through the 3<sup>rd</sup> order. However, it is understood that the derivatives computed by this method are not reliable.

### 3.3.2 Pure yaw experiment

The PMM imposes the same  $U_0$  constant velocity longitudinal movement and harmonic transversal movement given by (11), both considered in the global reference frame. While the longitudinal speed is the same for all PMM experiments, the amplitudes and pulsations of the harmonic transversal movement are not necessarily the same for the pure sway and yaw

experiments. To impose a pure yaw movement, PMM keeps the longitudinal axis of the model always tangent to its trajectory. Consequently, its heading angle is always:

$$\operatorname{tg}\psi = \frac{V}{U_0} = -\frac{a_0\omega}{U_0}\sin(\omega t) \quad (18)$$

Because this angle is very small, it could be assumed:

$$\psi \cong \operatorname{tg}\psi = \psi_0 \sin(\omega t) \quad (19)$$

Although it is a matter of intuition that, by keeping the model CL tangent to its trajectory, a pure yaw movement occurs, it is not so easy to prove this rigorously, due to the complex trigonometry involved. It becomes easier if a very small  $\psi$  is assumed. By the particularised Tien-Bryan rotations, the local velocities are:

$$\begin{aligned} u &= U_0 \cos\psi + V \sin\psi \\ v &= -U_0 \sin\psi + V \cos\psi \end{aligned} \quad (20)$$

Since  $\psi$  is assumed very small, there is also:

$$\begin{aligned} \cos\psi &\cong 1 \\ \sin\psi &\cong \psi = \psi_0 \sin(\omega t) \end{aligned} \quad (21)$$

Then, by considering the harmonic expression of  $V$ , involved also in (26), it results:

$$\begin{aligned} u &\cong U_0 + U_0 \sin^2\psi \cong U_0 \\ v &\cong a_0 \sin(\omega t) - a_0 \sin(\omega t) = 0 \end{aligned} \quad (22)$$

The assumption of a very small  $\psi$  appears twice in  $u$  calculation and just once in  $v$  calculation. In the absence of a rigorous demonstration of a constant advancing speed  $u=U_0$ , this might suggest that there are actually still harmonic  $u$  fluctuations, depending on the values of the longitudinal velocity, amplitude and pulsation.

Thus, it is recommended to choose appropriate amplitudes and pulsations before the experiment is performed, by rigorously computing the  $u$  harmonic fluctuations. For the available PMM amplitudes and pulsations and usual longitudinal speeds of the model, these fluctuations are negligible.

Thus, the kinematical parameters of this movement are:

$$\begin{aligned} u &\cong U_0 & \dot{u} &\cong 0 \\ v &= 0 & \dot{v} &= 0 \\ r &\cong \psi_0 \omega \cos(\omega t) = r_0 \cos(\omega t) & \dot{r} &\cong -\psi_0 \omega^2 \sin(\omega t) = \dot{r}_0 \sin(\omega t) \end{aligned} \quad (23)$$

The measured forces and their moments are also composed by an inertial and a hydrodynamic part.

By the left side of (2) and (23), the inertial part of the measured torsor is:

$$\begin{aligned} X_i &= mx_G r^2 \\ Y_i &= -mU_0 r - mx_G \dot{r} \\ N_i &= -J_{zz} \dot{r} - mU_0 x_G r \end{aligned} \quad (24)$$

In a linear approach, just the first order terms of (3)-(5) are considered. By (23), the hydrodynamic part of the measured torsor is:

$$\begin{aligned} X_h &= X_0 \\ Y_h &= Y_0 + Y_r r + Y_{\dot{r}} \dot{r} \\ N_h &= N_0 + N_r r + N_{\dot{r}} \dot{r} \end{aligned} \quad (25)$$

By (23), (24), (25) and neglecting the quadratic term of  $X_i$ , the measured torsor is theoretically expressed by:

$$\begin{aligned} X_T &= X_0 \\ Y_T &= Y_0 + [(Y_r - mU_0)r_0] \cos(\omega t) + [(Y_{\dot{r}} - mx_G)\dot{r}_0] \sin(\omega t) \\ N_T &= N_0 + [(N_r - mU_0 x_G)r_0] \cos(\omega t) + [(N_{\dot{r}} - J_{zz})\dot{r}_0] \sin(\omega t) \end{aligned} \quad (26)$$

The experimental torsor is now expressed by a 1<sup>st</sup> order trigonometric Fourier series:

$$\begin{aligned} X_E &= X_{0E} \\ Y_E &= Y_{0E} + Y_{1a} \cos(\omega t) + Y_{1b} \sin(\omega t) \\ N_E &= N_{0E} + N_{1a} \cos(\omega t) + N_{1b} \sin(\omega t) \end{aligned} \quad (27)$$

(26) and (27) yield:

$$\begin{aligned} X_0 &= X_{0E} \\ Y_0 = Y_{0E} \quad Y_r - mU_0 &= \frac{Y_{1a}}{r_0} \quad Y_{\dot{r}} - mx_G = \frac{Y_{1b}}{\dot{r}_0} \\ N_0 = N_{0E} \quad N_r - mU_0 x_G &= \frac{N_{1a}}{r_0} \quad N_{\dot{r}} - J_{zz} = \frac{N_{1b}}{\dot{r}_0} \end{aligned} \quad (28)$$

## SHIP MANOEUVRING BY PMM - MATHEMATICS AND EXPERIMENTS PART II

Finally, like for the pure sway experiment, the hydrodynamic derivatives are the gradient of the regression lines of  $Y_{1b}$  and  $N_{1b}$  depending on  $r_0$ , respectively  $Y_{1a}$  and  $N_{1a}$  depending on  $\dot{r}_0$ , Figures 6 and 7.

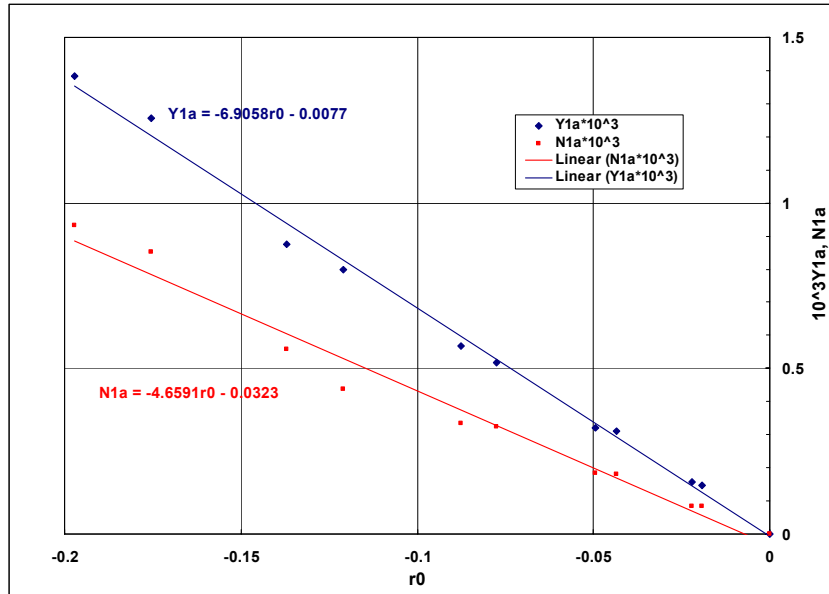


Figure 6. Pure yaw. Fourier 1a coefficients linear regression

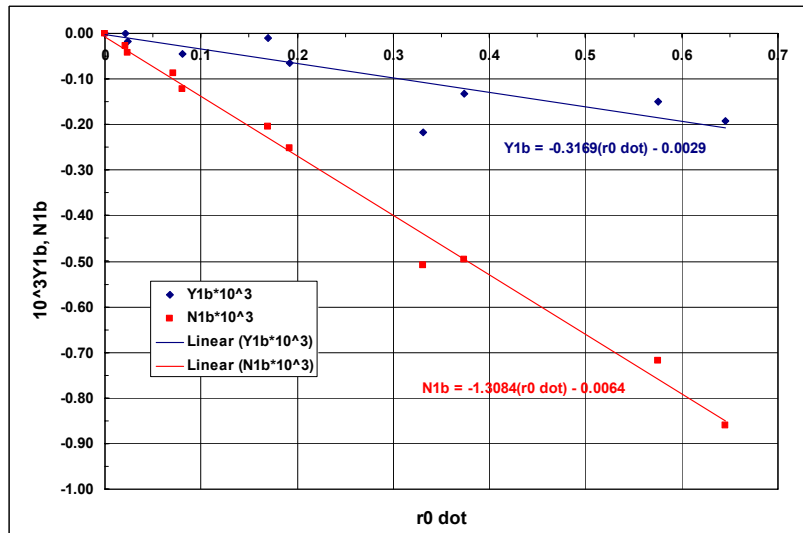


Figure 7. Pure yaw. Fourier 1b coefficients linear regression

All the hydrodynamic derivatives are determined for the model. Of interest is the simulation of the ship manoeuvres. The hydrodynamic derivatives including the mass displacement,  $m$ , can be directly scaled, since the model displacement, the centre of gravity and the speed are rigorously scaled down. The derivative involving the polar moment of inertia,  $J_{zz}$ , cannot be directly scaled, unless its actual value for the ship is known at the moment of the PMM experiments. Otherwise, it is recommended to measure the model  $J_{zz}$  and to scale only  $N_r$ . This incertitude affects on the accuracy of the prediction.

In a non-linear approach, the terms of (3)-(5) are considered through the 3<sup>rd</sup> order. Together with (23), the hydrodynamic part of the measured torsor is:

$$\begin{aligned} X_h &= X_0 + \frac{1}{2} X_{rr} r^2 \\ Y_h &= Y_0 + Y_r \dot{r} + Y_r r + \frac{1}{6} Y_{rrr} r^3 \\ N_h &= N_0 + N_r \dot{r} + N_r r + \frac{1}{6} N_{rrr} r^3 \end{aligned} \quad (29)$$

By (23), (24) and (25), the measured torsor is theoretically expressed by:

$$\begin{aligned} X_T &= X_0 + \left( m x_G + \frac{1}{2} X_{rr} \right) r_0^2 \cos^2(\omega t) \\ Y_T &= Y_0 + (Y_r - m x_G) \dot{r}_0 \sin(\omega t) + (Y_r - m U_0) r_0 \cos(\omega t) + \frac{1}{6} Y_{rrr} r_0^3 \cos^3(\omega t) \\ N_T &= N_0 + (N_r - J_{zz}) \dot{r}_0 \sin(\omega t) + (N_r - m U_0 x_G) r_0 \cos(\omega t) + \frac{1}{6} N_{rrr} r_0^3 \cos^3(\omega t) \end{aligned} \quad (30)$$

Both the theoretical expressions (30) and the measured data are further integrated over a period of the harmonic movement, analytically and respectively numerically. The envisaged hydrodynamic derivatives are separated by choosing the integration limits as below:

$$\begin{aligned} I_X &= \int_0^T X dt \\ I_Y &= \int_0^{\frac{T}{4}} Y dt - \int_{\frac{T}{4}}^{\frac{3T}{4}} Y dt + \int_{\frac{3T}{4}}^T Y dt \\ I_N &= \int_0^{\frac{T}{4}} N dt - \int_{\frac{T}{4}}^{\frac{3T}{4}} N dt + \int_{\frac{3T}{4}}^T N dt \end{aligned} \quad (31)$$

The result of this analytical integration is:

$$\begin{aligned}
 I_{XT} &= X_0 T + \frac{1}{2} T \left( m x_G + \frac{1}{2} X_{rr} \right) r_0^2 \\
 I_{YT} &= T \frac{2}{\pi} (Y_r - m U_0) r_0 + T \frac{4}{3\pi} \left( \frac{1}{6} Y_{rrr} \right) r_0^3 \\
 I_{NT} &= T \frac{2}{\pi} (N_r - m U_0 x_G) r_0 + T \frac{4}{3\pi} \left( \frac{1}{6} N_{rrr} \right) r_0^3
 \end{aligned} \quad (32)$$

By equating the results of the analytical and numerical integration, quadratic and cubic expressions in  $r_0$  are obtained, having as coefficients the hydrodynamic derivatives:

$$\begin{aligned}
 \left( m x_G + \frac{1}{2} X_{rr} \right) r_0^2 &= 2 \frac{(I_{XE} - X_0 T)}{T} \\
 (Y_r - m U_0) r_0 + \frac{2}{3} \left( \frac{1}{6} Y_{rrr} \right) r_0^3 &= \frac{I_{YE}}{T} \frac{\pi}{2} \\
 (N_r - m U_0 x_G) r_0 + \frac{2}{3} \left( \frac{1}{6} N_{rrr} \right) r_0^3 &= \frac{I_{NE}}{T} \frac{\pi}{2}
 \end{aligned} \quad (33)$$

Finally, the hydrodynamic derivatives are computed by regression according to polynomials (33), on the data corresponding to the experimented amplitudes and pulsations.

Appreciated by early works as of a major importance,  $\frac{1}{2} X_{rr}$  must be carefully used later during the ship maneuvering simulations, because its determination might be affected by the non constant speed  $u$ , discussed early in this subchapter and by the lack of the additional frictional force as well. The main hydrodynamic derivatives here determined are:  $\frac{1}{6} Y_{rrr}$  and  $\frac{1}{6} N_{rrr}$ . Although the early works describe them as unimportant, this seems to be not always true. A graphical representation of the polynomials (33) could be an indication of how reliable these derivatives are.

An example of the experimental values of the integrals (32) as function of  $r_0$  and their averaging polynomials (33) is given in the figures 8 and 9, as dimensionless values.

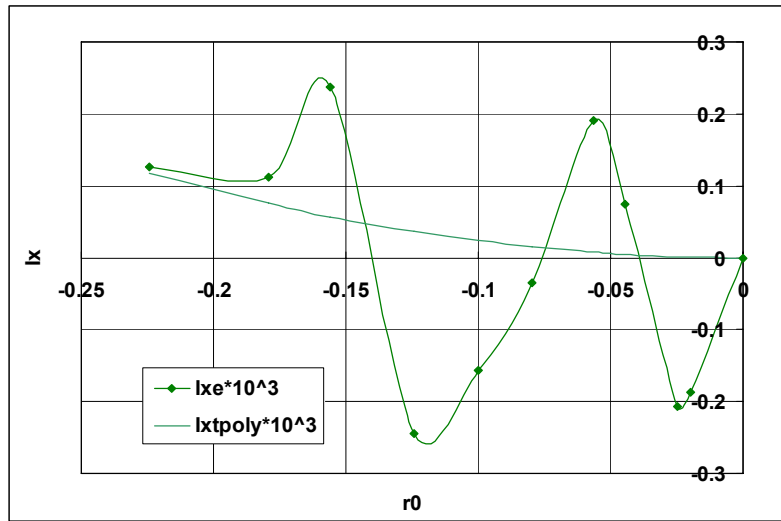


Figure 8. Pure yaw.  $I_x$  values – experimental and averaged by the polynomial (33)

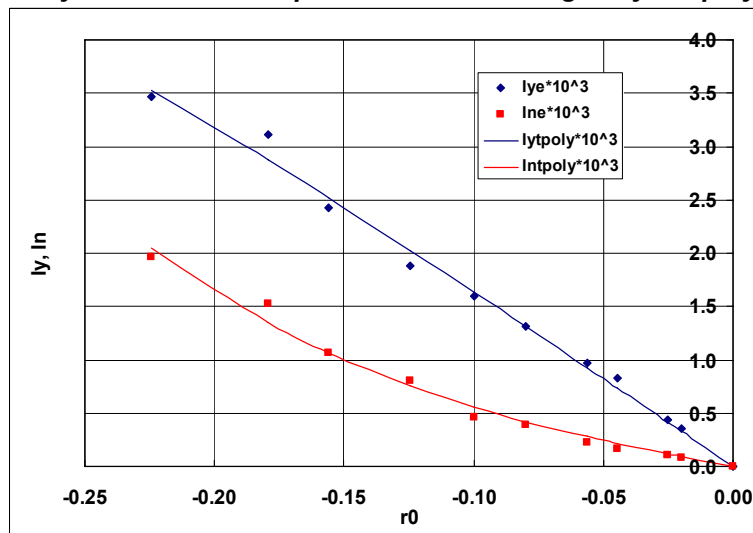


Figure 9. Pure yaw.  $I_y$  and  $I_N$  values – experimental and averaged by the polynomials (33)

### 3.3.3 Yaw and drift angle experiment

This experiment is similar to that of pure yaw but the model longitudinal axis now has a constant drift angle,  $\beta$ , with the tangent of the trajectory. The drift velocity allows the determination of the cross-coupled derivatives in  $r$  and  $v$ . All these derivatives are non-linear. The kinematical parameters of this movement are:

$$\begin{aligned}
 u &\cong U_0 \cos(\beta) & \dot{u} &\cong 0 \\
 v &\cong -U_0 \sin(\beta) & \dot{v} &\cong 0 \\
 r &\cong \psi_0 \omega \cos(\omega t) = r_0 \cos(\omega t) & \dot{r} &\cong -\psi_0 \omega^2 \sin(\omega t) = \dot{r}_0 \sin(\omega t)
 \end{aligned}
 \tag{34}$$

By the left side of (2) and (34), the inertial part of the measured torsor is:

$$\begin{aligned}
 X_i &= mvr + mx_G r^2 \\
 Y_i &= -mur - mx_G \dot{r} \\
 N_i &= -J_{zz} \dot{r} - mux_G r
 \end{aligned}
 \tag{35}$$

By (34) and (3)-(5), the hydrodynamic part of the measured torsor is:

$$\begin{aligned}
 X_h &= X_0 + \frac{1}{2} X_{vv} v^2 + \frac{1}{2} X_{rr} r^2 + X_{vr} vr \\
 Y_h &= Y_0 + Y_i \dot{r} + Y_v v + \frac{1}{6} Y_{vvv} v^3 + \frac{1}{2} Y_{vrr} vr^2 + Y_r r + \frac{1}{6} Y_{rrr} r^3 + \frac{1}{2} Y_{rvv} rv^2 \\
 N_h &= N_0 + N_i \dot{r} + N_v v + \frac{1}{6} N_{vvv} v^3 + \frac{1}{2} N_{vrr} vr^2 + N_r r + \frac{1}{6} N_{rrr} r^3 + \frac{1}{2} N_{rvv} rv^2
 \end{aligned}
 \tag{36}$$

By (34), (35) and (36), the measured torsor could be expressed theoretically by:

$$\begin{aligned}
 X_T &= X_0 + \frac{1}{2} X_{vv} v^2 + (m + X_{vr})vr + \left( mx_G \frac{1}{2} X_{rr} \right) r^2 \\
 Y_T &= Y_0 + Y_v v + \frac{1}{6} Y_{vvv} v^3 + (Y_i - mx_G) \dot{r} + \left( Y_r - mu + \frac{1}{2} Y_{rvv} v^2 \right) r + \frac{1}{2} Y_{vrr} vr^2 + \frac{1}{6} Y_{rrr} r^3 \\
 N_T &= N_0 + N_v v + \frac{1}{6} N_{vvv} v^3 + (N_i - J_{zz}) \dot{r} + \left( N_r - mux_G + \frac{1}{2} N_{rvv} v^2 \right) r + \frac{1}{2} N_{vrr} vr^2 + \frac{1}{6} N_{rrr} r^3
 \end{aligned}
 \tag{37}$$

Since v is constant and by (34), (37) becomes:

$$\begin{aligned}
 X_T &= C_X + (m + X_{vr})v r_0 \cos(\omega t) + \left( mx_G \frac{1}{2} X_{rr} \right) r_0^2 \cos^2(\omega t) \\
 Y_T &= C_Y + (Y_i - mx_G) \dot{r}_0 \sin(\omega t) + \left( Y_r - mu + \frac{1}{2} Y_{rvv} v^2 \right) r_0 \cos(\omega t) + \\
 &\quad + \frac{1}{2} Y_{vrr} v r_0^2 \cos^2(\omega t) + \frac{1}{6} Y_{rrr} r_0^3 \cos^3(\omega t) \\
 N_T &= C_N + (N_i - J_{zz}) \dot{r}_0 \sin(\omega t) + \left( N_r - mux_G + \frac{1}{2} N_{rvv} v^2 \right) r_0 \cos(\omega t) + \\
 &\quad + \frac{1}{2} N_{vrr} v r_0^2 \cos^2(\omega t) + \frac{1}{6} N_{rrr} r_0^3 \cos^3(\omega t)
 \end{aligned}
 \tag{38}$$

(38) and the measured data are integrated over a period, analytically and numerically:

$$I_X = \int_0^T X dt - \int_{\frac{T}{4}}^{\frac{3T}{4}} X dt + \int_{\frac{3T}{4}}^T X dt , \quad (39)$$

$$I_{Y1} = \int_0^{\frac{T}{4}} Y dt - \int_{\frac{T}{4}}^{\frac{3T}{4}} Y dt + \int_{\frac{3T}{4}}^T Y dt , \quad (40)$$

$$I_{Y2} = \int_0^T Y dt . \quad (41)$$

$$\begin{aligned} I_{XT} &= (m + X_{vr})vr_0 \frac{2}{\pi} T \\ I_{Y1T} &= \left( Y_r - \mu v + \frac{1}{2} Y_{rvv} v^2 \right) \frac{2}{\pi} T r_0 + \left( \frac{1}{6} Y_{rrr} \right) \frac{2}{3} \frac{2}{\pi} T r_0^3 \\ I_{Y2T} &= C_Y T + \left( \frac{1}{2} Y_{vrr} \right) v \frac{T}{2} r_0^2 \\ I_{N1T} &= \left( N_r - \mu v x_G + \frac{1}{2} N_{rvv} v^2 \right) \frac{2}{\pi} T r_0 + \left( \frac{1}{6} N_{rrr} \right) \frac{2}{3} \frac{2}{\pi} T r_0^3 \\ I_{N2T} &= C_N T + \left( \frac{1}{2} N_{vrr} \right) v \frac{T}{2} r_0^2 \end{aligned} \quad (42)$$

By equating the results of the analytical and numerical integration, polynomial expressions in  $r_0$  are obtained, (43). The derivatives  $Y_r$ ,  $N_r$  and those in respect with  $v$ , implied in the constants, must be previously known.

$$\begin{aligned} (m + X_{vr})r_0 &= \frac{I_{XE}}{\frac{2}{\pi} vT} \\ \left( Y_r - \mu v + \frac{1}{2} Y_{rvv} v^2 \right) r_0 + \frac{2}{3} \left( \frac{1}{6} Y_{rrr} \right) r_0^3 &= \frac{I_{Y1}}{\frac{2}{\pi} T} \\ \left( \frac{1}{2} Y_{vrr} \right) r_0^2 &= \frac{I_{Y2} - C_Y T}{\frac{1}{2} vT} \\ \left( N_r - \mu v x_G + \frac{1}{2} N_{rvv} v^2 \right) r_0 + \frac{2}{3} \left( \frac{1}{6} N_{rrr} \right) r_0^3 &= \frac{I_{N1}}{\frac{2}{\pi} T} \\ \left( \frac{1}{2} N_{vrr} \right) r_0^2 &= \frac{I_{N2} - C_N T}{\frac{1}{2} vT} \end{aligned} \quad (43)$$

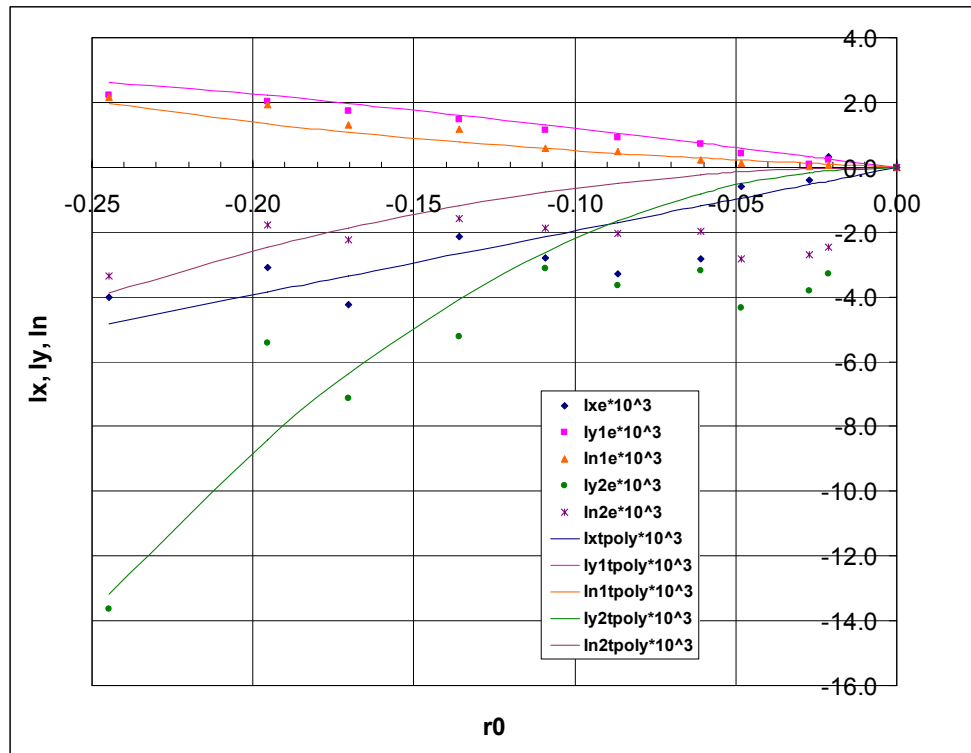


**Figure 10. Yaw and drift angle.  $I_x$ ,  $I_y$  and  $I_N$  values – experimental and averaged by the polynomials (43)**

### 3.3.4 Yaw and rudder angle experiment

This experiment is performed to determine the cross coupled hydrodynamic derivatives with respect of  $r$  and  $\delta$ . Similarly to the pure yaw experiment, the PMM drives the model keeping always its CL tangent to the trajectory. A constant the rudder angle is also present for all amplitudes and pulsation of the harmonic transversal movement.

Because the calculation is similar to the previous experiment one, only the final regression polynomials are given, (44).

$$\begin{aligned}
 (m + X_{\delta r})r_0 &= \frac{I_{XE}}{\frac{2}{\pi}\delta T} \\
 \left( Y_r - mU_0 + \frac{1}{2}Y_{r\delta\delta}\delta^2 \right)r_0 + \frac{2}{3}\left( \frac{1}{6}Y_{rr} \right)r_0^3 &= \frac{I_{Y1}}{\frac{2}{\pi}T} \\
 \left( \frac{1}{2}Y_{\delta r} \right)r_0^2 &= \frac{I_{Y2} - C_Y T}{\frac{1}{2}\delta T} \\
 \left( N_r - mU_0 X_G + \frac{1}{2}N_{r\delta\delta}\delta^2 \right)r_0 + \frac{2}{3}\left( \frac{1}{6}N_{rr} \right)r_0^3 &= \frac{I_{N1}}{\frac{2}{\pi}T} \\
 \left( \frac{1}{2}N_{\delta r} \right)r_0^2 &= \frac{I_{N2} - C_N T}{\frac{1}{2}\delta T}
 \end{aligned} \tag{44}$$

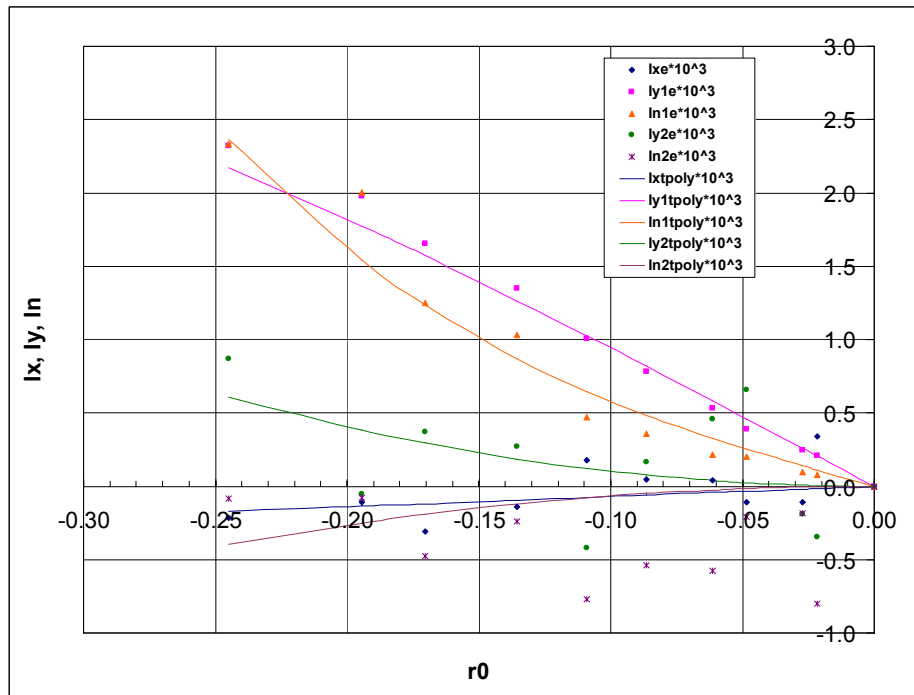


Figure 11. Yaw and rudder angle.  $I_x$ ,  $I_y$  and  $I_N$  values – experimental and averaged

### 3.4 The X Derivatives with Respect of u

The coefficients  $X_u$ ,  $\frac{1}{2}X_{uu}$ ,  $\frac{1}{3}X_{uuu}$  are determined from the results of the resistance and self propulsion experiments. On a straight course and constant ship speed  $U_0$ , there is:

$$X = T(1-t) - R_S = 0 \tag{45}$$

T : propeller impingement;  
 t : thrust deduction factor;  
 R<sub>s</sub> : ship resistance.

During the ship evolution, the actual ship speed  $u$  may differ from the cruise constant speed  $u_0$  and then  $X$  is not 0. According to Strøm-Tejsen and Cissett [7],  $X$  could be expressed by a 3<sup>rd</sup> order polynomial function of  $\Delta u$ :

$$X = a_0 + a_1\Delta u + a_2\Delta u^2 + a_3\Delta u^3 . \quad (46)$$

The coefficients  $a_0, a_1, a_2, a_3$  are determined by regression of  $X$  computed by (45) on several points close to  $u_0$ . The envisaged coefficients are computed by deriving (46) with respect of  $u$  in point  $u_0$ , i.e.  $\Delta u=0$ .

However, this method does not always produce reliable results because a 3<sup>rd</sup> order polynomial imposes 2 inflexion points. Thus, a more versatile spline interpolation was preferred, since the effect of these coefficients is not negligible.

#### 4. RESULTS

The theory explained above was transposed in an in-house-built software. The software process the data acquired during the PMM experiments and finally simulate the basic IMO manoeuvres, according to the resolutions MSC 137(76) and MSC/Circ. 1053.

The graphic results of the simulation of: turning circle, zigzag (10°/10°) and direct spiral manoeuvres for a 32kdwt bulk carrier are here presented.

The model weight is 2000kg and its speed 1.4 m/s. The main parameters of the PMM experiments are:

- Non-inertial experiment  
 Drift angles: -7°; -5°; -3°; 0°; 3°; 5°; 7°.  
 Rudder angles: -35°; -30°; -20°; -10°; 0°; 10°; 20°; 30°; 35°.  
 Sampling time step: 4 ms.
- Inertial experiments  
 The same harmonic parameters for all:  
 Amplitudes: 40; 50 mm.  
 Sway/yaw frequencies: 4; 6; 8; 10; 12 min<sup>-1</sup>.  
 Yaw and drift angle experiment: Drift angle: 4°.  
 Yaw and rudder angle tests: Rudder angle: 20°.  
 Sampling time step: 12 ms for all the experiments.

For ship manoeuvres simulation, the maximum rudder angle is 35° and its rotational speed is 0.1018 s<sup>-1</sup>. The simulation time step is 0.5 s. All the manoeuvres are initiated to starboard. The results are graphically presented here below. The ship satisfies the IMO requirements about the ship manoeuvring abilities, as they are specified in [11]

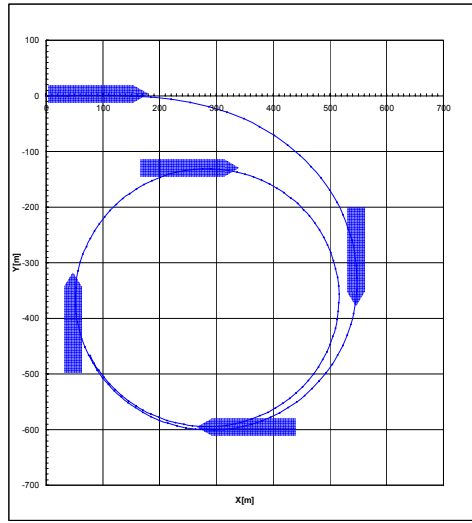


Figure 12. Turning circle on a 100m spaced grid

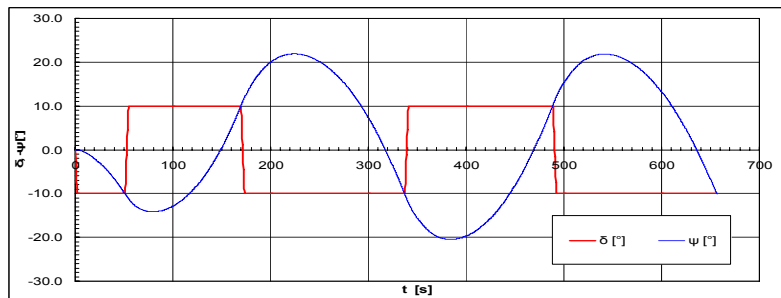


Figure 13. Zigzag 10°/10°

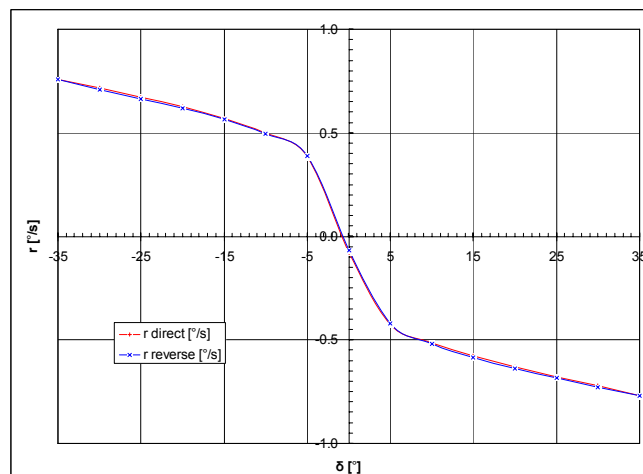


Figure 14. Direct spiral

## 5. CONCLUSIONS

The Abkowitz mathematical model for ship manoeuvring simulation by PMM experiments was here analysed and revised.

The main revision was on the theory of the experimental data processing in order to obtain the hydrodynamic derivatives of the differential system of equations, further used for ship manoeuvring simulation.

Based on this revised theory, in-house-built software for the basic IMO manoeuvres simulation was written. The results were checked against those presented in the early works based on the Abkowitz model. Results on a new ship are here presented too.

## ACKNOWLEDGEMENTS

The present work has been done under the self supported developing programme Ac4592 of Icepronav. The detailed reports are: Ac4592.1.7.1, Ac4592.1.7.2 and Ac4592.1.7.3.

The author expresses special thanks to Prof. Valeriu Ceangă and Dr. Radu Voinescu for their scientific support, advises and experience sharing. The initiative of Dr. Roman Pîrvulescu, head of the Ship Hydrodynamics Department, to extend and revitalise the department activity, boosted the author to approach the ship manoeuvring domain. The cooperation of M. Eng. Adrian Simion, head of the Resistance, Self Propulsion and Sea Keeping Basin, was invaluable, as well as the effort of all involved in the PMM experiments.

We together were once part of the Ship Hydrodynamics Department which was once part of Icepronav - Research and Design Institute for Shipbuilding, Galați, Romania.

## REFERENCES

- [1]. Abkowitz, M.A. - **Lectures on ship Hydrodynamics – Steering and Manoeuvrability**, Hydro and Aerodynamics Laboratory Report No. Hy-5, May 1964, Lyngby, Denmark
- [2]. Lewandowski, E.M. - **The Dynamics of Marine Craft Maneuvering and Seakeeping**, World Scientific Publishing Co. Pte. Ltd., Singapore, 2004
- [3]. Nomoto, K. - **On the Steering Qualities of Ship**, International Shipbuilding Progress, Vol.4, No.35, 1957
- [4]. Inoue, S., Hirano, M., Kijima, K. - **Hydrodynamic derivatives on ship manoeuvring**, International Shipbuilding Progress 28 (321), 1981
- [5]. Inoue, S., Hirano, M., Kijima, K., Takashina, J. - **A practical calculation method of ship manoeuvring**, International Shipbuilding Progress 28 (324), 1981
- [6]. SNAME, Panel H-10 - **Design Workbook on Ship Maneuverability**, New Jersey, 1993
- [7]. Strøm-Tejsen, J., Chislett, M., S. - **A Model Testing Technique and Method of Analysis for the Prediction of Steering and Manoeuvring Qualities of Surface Vessels**, Hydro and Aerodynamics Laboratory Report No. Hy-7, September 1966, Lyngby, Denmark
- [8]. Ixaru, L., Gr. - **Metode pentru ecuații diferențiale cu aplicații**, Editura Academiei RSR, București, 1979
- [9]. Chislett, M., S.; Wagner Smitt, L. – **A Brief Description of the HyA Large Amplitude PMM System**, Hydro and Aerodynamics Laboratory Report No. Hy-16, April 1973, Lyngby, Denmark
- [10]. site [www.statistics.com](http://www.statistics.com)
- [11] MSC/Circ. 1053 - **Explanatory Notes to the Standards for Ship Manoeuvrability**, December, 2002.

## MATHEMATICAL PROPERTIES OF HYPERBOLIC CONSERVATION LAWS FOR SHALLOW WATERS

<sup>1</sup>GHERGHINA AUREL, <sup>2</sup>VLADU GABRIEL

<sup>1</sup>*Military Staff, Romania*, <sup>2</sup>*Research Center for Navy, Romania*

The purpose of this paper is to provide the reader with a presentation of some mathematical properties of hyperbolic conservation laws. We restrict our attention to those properties thought to be essential to the development and application of numerical methods for conservation laws.

**Keywords:** conservation law, flow, wave break

### 1. INTEGRAL FORMS OF CONSERVATION LAWS

In this chapter, we restrict ourselves to simple model problems involving two independent variables, namely the time  $t$  and the spatial coordinate  $x$ . The formal definition of a **system of  $m$  conservation laws** is:

$$U_t + F(U)_x = 0, \quad (1)$$

where  $U$  is the vector of conserved variables and  $F(U)$  is the vector of fluxes. This system is hyperbolic if the Jacobian matrix

$$A(U) = \frac{\partial F}{\partial U}$$

has real eigenvalues  $\lambda_i(U)$  and a complete set of linearly independent eigenvectors  $K^{(i)}(U), i = 1, \dots, m$ . We assume the eigenvalues and the corresponding eigenvectors to be ordered as

$$\lambda_1(U) < \lambda_2(U) < \dots < \lambda_m(U), \\ r^{(1)}(U), r^{(2)}(U), \dots, r^{(m)}(U).$$

It is important to note that now eigenvalues and eigenvectors depend on  $U$ , although sometimes we shall omit the argument  $U$ .

Conservation laws may be expressed in differential and integral form. There are at least two arguments for considering the integral form (s) of the conservation laws:

1. The derivation of the governing equations is based on physical conservation principles expressed as integral relations on control volumes, and
2. The integral formulation requires less smoothness of the solution.

We notice that the last argument  $U$  opens the way to extend the class of admissible solutions of (1) to include discontinuous solutions.

Consider a one-dimensional time dependent system, such as the Euler equations. Choose a control volume  $V = [x_L, x_R] \times [t_1, t_2]$  on the  $x$ - $t$  plan. The integral form of the equation for conservation of mass in one space dimension is

$$\frac{d}{dt} \int_{x_L}^{x_R} \rho(x,t) dx = f(x_L,t) - f(x_R,t), \quad (2)$$

where  $f = \rho u$  is the mass flux. Following this example, for the complete system we have

$$\frac{d}{dt} \int_{x_L}^{x_R} U(x,t) dx = F(U(x_L,t)) - F(U(x_R,t)). \quad (3)$$

This is the **Integral Form I** of the integral form of the conservation laws. Another version of the integral form of the conservation laws is obtained by integrating (3) in time between  $t_1$  and  $t_2$ , with  $t_1 \leq t_2$ :

$$\int_{t_1}^{t_2} \left[ \frac{d}{dt} \int_{x_L}^{x_R} U(x,t) dx \right] dt = \int_{x_L}^{x_R} U(x,t_2) dx - \int_{x_L}^{x_R} U(x,t_1) dx. \quad (4)$$

Using (4) the Integral Form I becomes

$$\int_{x_L}^{x_R} U(x,t_2) dx = \int_{x_L}^{x_R} U(x,t_1) dx + \int_{t_1}^{t_2} F(U(x_L,t)) dt - \int_{t_1}^{t_2} F(U(x_R,t)) dt. \quad (5)$$

This is the **Integral Form II** of the hyperbolic conservation laws.

Another version of the integral form of the conservation laws is obtained by integrating in any domain  $V$  in  $x$ - $t$  space and using Green's theorem. The result is the **Integral Form III** of the conservation laws:

$$\oint [U dx - F(U) dt] = 0, \quad (6)$$

where the line integration is performed along the boundary of the domain  $V$ .

Note that **Integral Form II** of the conservation laws is a special case of **Integral Form III**, in which the control volume  $V$  is the rectangle  $[x_L, x_R] \times [t_1, t_2]$ .

A fourth integral form results from adopting a more mathematical approach for extending the concept of solution to include discontinuities. Thus, a weak or generalized solution  $U$  is required to satisfy the integral relation

$$\int_0^{+\infty} \int_{-\infty}^{+\infty} [\phi_t U + \phi_x F(U)] dx dt = - \int_{-\infty}^{+\infty} \phi(x,0) U(x,0) dx \quad (7)$$

for all **test functions**  $\phi(x,t)$  that are continuously differentiable and have **compact support**.

We recall here that a function  $\phi(x,t)$  has compact support if it vanishes outside some bounded set. Note that the derivatives of  $U(x,t)$  and  $F(U)$  have been passed on to the test function  $\phi(x,t)$ , which is assumed to be sufficiently smooth to admit these derivatives.

There are many interesting and useful examples of hyperbolic conservation laws, see (LeVeque, 1992) and (Toro, 1997). The first one is the so-called scalar conservation law ( $m = 1$ ), which in differential form reads:

$$u_t + f(u)_x = 0. \tag{8}$$

To be able to solve for the conserved variable  $u(x, t)$  the flux function  $f(u)$  must be a completely determined algebraic function of  $u(x, t)$ , and possibly some extra parameters of the problem. The linear advection equation is the simplest example, in which the flux function is  $f(u) = au$ , a linear function of  $u$ . The in viscid Burgers' equation has flux  $f(u) = \frac{1}{2}u^2$ , a quadratic function of  $u$ .

Another example of a conservation law is the traffic flow equation:

$$\rho_t + f(\rho)_x = 0, f(\rho) = u_m \left( 1 - \frac{\rho}{\rho_m} \right) \rho. \tag{9}$$

Here the conserved variable  $\rho(x, t)$  is a density function (density of motor vehicle),  $u_m$  and  $\rho_m$  are parameters of the problem, namely the maximum speed of vehicles and the maximum density, both positive constants.

Another example of practical interest in oil-reservoir simulation is the **Buckley-Leverett equation**:

$$u_t + f(u)_x = 0, f(u) = \frac{u^2}{u^2 + b(1-u)^2}, \tag{10}$$

where  $b$  is a parameter of the problem (Leveque, 1997).

**The system of conservation laws** is, as obvious example, constructed from linear systems  $U_t + AU_x = 0$  with constant coefficient matrix  $A$ . The required conservation-law form is obtained defining the flux function as the product of the Jacobian matrix  $A$  and the vector  $U$ , namely

$$U_t + F(U)_x = 0, F(U) = AU. \tag{11}$$

The **isothermal equations of Gas Dynamics** are one example of non-linear system of conservation laws. These are

$$\left. \begin{aligned} U_t + F(U)_x &= 0, \\ U &= \begin{bmatrix} u_1 \\ u_2 \end{bmatrix} \equiv \begin{bmatrix} \rho \\ \rho u \end{bmatrix}, F = \begin{bmatrix} f_1 \\ f_2 \end{bmatrix} \equiv \begin{bmatrix} \rho u \\ \rho u^2 + a^2 \rho \end{bmatrix} \end{aligned} \right\}, \tag{12}$$

where  $a$  is the constant speed of sound. The Jacobian matrix is

$$A(U) = \frac{\partial F}{\partial U} = \begin{bmatrix} 0 & 1 \\ -(u_2/u_1)^2 + a^2 & 2u_2/u_1 \end{bmatrix} = \begin{bmatrix} 0 & 1 \\ a^2 - u^2 & 2u \end{bmatrix}.$$

The Eigenvalues of  $A$  are  $\lambda_1 = u - a$  and  $\lambda_2 = u + a$  and the right eigenvectors are

$$r^{(1)} = \begin{bmatrix} 1 \\ u - a \end{bmatrix}, r^{(2)} = \begin{bmatrix} 1 \\ u + a \end{bmatrix},$$

where the scaling factors have been taken to be unity.

A non-linear example of a system of conservation laws are the **isentropic equations of Gas Dynamics**:

$$\left. \begin{aligned} U_t + F(U)_x &= 0, \\ U = \begin{bmatrix} u_1 \\ u_2 \end{bmatrix} &\equiv \begin{bmatrix} \rho \\ \rho u \end{bmatrix}, F = \begin{bmatrix} f_1 \\ f_2 \end{bmatrix} \equiv \begin{bmatrix} \rho u \\ \rho u^2 + p \end{bmatrix} \end{aligned} \right\} \quad (13)$$

together with their closure condition, or equation of state (EOS)  $p = C\rho^\gamma$ ,  $C = \text{constant}$ . The eigenvalues are  $\lambda_1 = u - a$  and  $\lambda_2 = u + a$  and the right eigenvectors are

$$r^{(1)} = \begin{bmatrix} 1 \\ u - a \end{bmatrix}, r^{(2)} = \begin{bmatrix} 1 \\ u + a \end{bmatrix}.$$

## 2. NON-LINEAR SCALAR HYPERBOLIC CONSERVATION LAWS

### 2.1. The Initial Value Problem

The non-linear hyperbolic conservation laws have some distinguishing features such as wave steepening and shock formation. In what follows we restrict our attention to the IVP for scalar non-linear conservation laws, namely

$$\left. \begin{aligned} PDE : u_t + f(u)_x &= 0 \\ IC : u(x,0) &= u_0(x) \end{aligned} \right\} \quad (14)$$

A corresponding integral form of the conservation law is:

$$\frac{d}{dt} \int_{x_L}^{x_R} u(x,t) dx = f(u(x_L,t)) - f(u(x_R,t)) \quad (15)$$

The conservation law may be rewritten as

$$u_t + \lambda(u)u_x = 0,$$

where  $\lambda(u) = \frac{df}{du} = f'(u)$  is the **characteristic speed**. In the system case there are more than one characteristic speeds and these are the eigenvalues of the Jacobian matrix.

For the linear advection equation  $\lambda(u) = a$ , constant. For the inviscid Burger's equation  $\lambda(u) = u$ , that is, the characteristic speed depends on the solution and is in fact identical to the conserved variable. Finally, for the traffic flow equation  $\lambda(u) = u_m(1 - 2\rho)/\rho_m$ .

It is important to notice that the flux function  $f$  is assumed here to be a function of  $u$  only. Under certain circumstances, this is an inadequate representation of the physical problem. Relevant physical phenomena of our interest are shock waves in compressible media. Even the 'source' of the shock wave is captured by the inviscid flow assumption; these shocks also

have viscous dissipation and heat conduction, in addition to pure convection. A more appropriate flux function for a model conservation law would also include a dependence on the derivative of  $u$ , so that the modified conservation law would read:

$$u_t + f(u)_x = \alpha u_{xx} \tag{16}$$

with  $\alpha$  a positive coefficient of viscosity.

The behavior of the flux function  $f(u)$  has profound consequences on the behavior of the solution  $u(x,t)$  of the conservation law itself. A crucial property is **monotonicity** of the characteristic speed  $\lambda(u)$ . There are essentially three possibilities:

a) The characteristic speed  $\lambda(u)$  is a monotone **increasing** function of  $u$ , i.e.

$$\frac{d\lambda(u)}{du} = \lambda'(u) = f''(u) > 0 \text{ (convex flux)}$$

b) The characteristic speed  $\lambda(u)$  is a monotone **decreasing** function of  $u$ , i.e.

$$\frac{d\lambda(u)}{du} = \lambda'(u) = f''(u) < 0 \text{ (concave flux)}$$

c) The characteristic speed  $\lambda(u)$  has extrema, form some  $u$ , i.e.

$$\frac{d\lambda(u)}{du} = \lambda'(u) = f''(u) = 0 \text{ (non - convex, non - concave flux) .}$$

For the inviscid Burgers equation,  $\lambda'(u) = f''(u) = 1 > 0$  and thus the flux is convex. For the traffic flow equation  $\lambda'(u) = f''(u) = -2u_m/\rho_m < 0$  and the flux is concave.

**For the case of non-linear system of conservation laws the character of the flux function is determined by Equations of State.** One speaks of convex, or otherwise, equations of state. With this introduction done, we are going to study the **inviscid IVP** (14). For the moment, we assume that the initial data  $u(x,0) = u_0(x)$  is smooth. For some finite time the solution  $u(x,t)$  will remain smooth. We rewrite the IVP as

$$\begin{aligned} u_t + \lambda(u)u_x &= 0, \lambda(u) = f'(u), \\ u(x,0) &= u_0(x) \end{aligned} \tag{17}$$

One can see that the above PDE is here a **non-linear** extension of the linear advection equation. We construct therefore solutions to IVP (17) following **characteristic curves**, using the same procedure as we used for the linear advection equation.

## 2.2. General Solutions on Characteristics

Consider characteristic curves  $x = x(t)$  satisfying IVP

$$\frac{dx}{dt} = \lambda(u), x(0) = x_0. \tag{18}$$

Taking both  $u$  and  $x$  to be functions of  $t$  we find the total derivative of  $u$  along the curves  $x(t)$ , namely

$$\frac{du}{dt} = u_t + \lambda(u)u_x = 0. \tag{19}$$

This means that  $u$  is constant along the characteristic curve satisfying the IVP (17) and therefore **the slope**  $\lambda(u)$  is **constant** along the characteristic. Hence the characteristic

curves are straight lines. The value of  $u$  along each curve is the value of  $u$  at the initial point  $x(0) = x_0$ , i.e.

$$u(x, t) = u_0(x_0). \quad (20)$$

The slope  $\lambda(u)$  of the characteristic may then be evaluated at  $x_0$  so that the solution characteristic curves of the IVP are straight lines given by the equation

$$x = x_0 + \lambda(u_0(x_0))t. \quad (21)$$

The pair (20) and (21) may be regarded as **the analytical solution** of IVP (17).

There are some remarks to be made at this point. The first is that the point  $x_0$  depends on the given point  $(x, t)$  and thus  $x_0 = x_0(x, t)$ . The above solution is therefore given in implicit form, which is more evident if we substitute  $x_0$  to obtain

$$u(x, t) = u_0(x - \lambda(u_0(x_0))t). \quad (22)$$

Furthermore, since  $x_0 = x_0(x, t)$  we derive the  $t$  and  $x$  derivatives  $u_t = u'_0(x_0) \frac{\partial x_0}{\partial t}$  and  $u_x = u'_0(x_0) \frac{\partial x_0}{\partial x}$  and after some manipulations, we obtain the two derivatives:

$$\frac{\partial x_0}{\partial t} = - \frac{\lambda(u_0(x_0))}{1 + \lambda'(u_0(x_0))u'_0(x_0)t} \quad (23)$$

and

$$\frac{\partial x_0}{\partial x} = \frac{1}{1 + \lambda'(u_0(x_0))u'_0(x_0)t}. \quad (24)$$

Let us mention here that under some circumstances the denominator of the last two derivatives becomes zero. This leads to undetermined derivatives of  $u$  with respect the  $t$  and  $x$ .

### Wave Distortion and Shock Generation

In the case of the linear advection equation, in which the characteristic speed is constant, i.e.  $\lambda(u) = a$ , the solution consists of the initial data  $u_0(x)$  translated with speed  $a$  **without distortion**.

In contradistinction with the linear case, in the non-linear case the **characteristic speed  $\lambda(u)$  is a function of the solution itself**,  $\lambda(u) = f'(u)$ . The characteristic curve emanating from a point on the  $x$ -axis has a constant in time but variable in space slope. Therefore, we expect that distortions from the initial state to be produced in the solution. This is a distinguishing feature of non-linear problems.

For the moment let us assume that the flux function  $f(u)$  is convex, that is  $\lambda'(u) = f''(u) > 0$ . In this case, the characteristic speed is an increasing function of  $u$ . Given the assumed convex character of the flux, higher values of  $u_0(x)$  will travel faster than lower values of  $u_0(x)$ . Therefore, later the initial data in an interval where the initial condition is increasing will be transformed into a broader and flatter profile. This happens because the characteristic speed increases as  $x$  increases. We say that this is an **expansive region**. By contrast, in a region where the initial data is decreasing monotonically, the characteristic speed decreases as  $x$  increases. This region tends to get steeper and narrower as time evolves. This is called a **compression region** and the **distortion**

**phenomenon** just described is called **wave steepening**. The wave steepening mechanism will eventually produce folding over of the solution profile, with corresponding **crossing of characteristics** and thus with **multiple-valued solutions**. When the characteristics first intersect, we say that the wave breaks and thus the solution on characteristics make no sense anymore.

**Remark:** The compressive and expansive character of the initial data just described **reverses for the case of a concave flux**  $\lambda'(u) = f''(u) < 0$ .

Before crossing of characteristics, the single-valued solution may be found following the characteristic, as described previously. When characteristics first intersect we say that **the wave breaks**; the derivative  $u_x$  becomes infinite and this happens at a precise breaking time  $t_b$  given by

$$t_b = \frac{-1}{\lambda_x(x_0)}.$$

This is confirmed by equations (23) and (24). Breaking first occurs on the characteristic emanating from  $x = x_0$  for which  $\lambda_x(x_0)$  is negative and  $|\lambda_x(x_0)|$  is a maximum. **At the point where breaking occurs, the solution becomes discontinuous.**

**Remark:** This is an anomalous situation, which can be rescued by going back to the physical origins of the equations and questioning the adequacy of the model furnished by the inviscid equation. The improved model equation says that the time rate of change of  $u$  is not just due to the convection term  $f(u)_x$  but is a balance between convection and the diffusion term  $\alpha u_{xx}$ . The wave steepening effect of  $f(u)_x$  is opposed by the wave-easing effect of  $\alpha u_{xx}$ . This more complete description of the Physics of flow does not allow folding over of the solution. However, rather than working with the more complete, and therefore more complex, viscous description of the problem, we shall continue to use here the inviscid model. Further, this allows discontinuities to be formed as a natural **process of increasing compression**, namely **shock waves**.

**Shock waves** are in reality small transitions layers of very rapid changes of physical quantities as pressure, density and temperature. The transition layer for a strong shock is of the same order of magnitude as the mean free path of the molecules, that is about  $10^{-7}$  m. Therefore replacing these waves as **mathematical discontinuities** is a reasonable approximation.

In what follows, we will use for the IVP both its differential (14) and integral forms (15). The solution  $u(x,t)$  is assumed to be such that  $u(x,t)$ ,  $f(u)$  and their derivatives are continuous everywhere except on a line  $s = s(t)$  on the  $x - t$  plane across which  $u(x,t)$  has a **jump discontinuity**. If we select two fixed points  $x_L$  and  $x_R$  on the  $x$ -axis such that  $x_L < s(t) < x_R$ , then enforcing the conservation law in integral form on the control volume  $[x_L, x_R]$  leads to

$$f(u(x_L,t)) - f(u(x_R,t)) = \frac{d}{dt} \int_{x_L}^s u(x,t) dx + \frac{d}{dt} \int_{s(t)}^{x_R} u(x,t) dx. \quad (25)$$

The Leibnitz differentiation formula for integrals with variable boundaries

$$\frac{d}{d\alpha} \int_{\xi_1(\alpha)}^{\xi_2(\alpha)} f(\xi, \alpha) d\xi = \int_{\xi_1(\alpha)}^{\xi_2(\alpha)} \frac{\partial f}{\partial \alpha} d\xi + f(\xi_2, \alpha) \frac{d\xi_2}{d\alpha} - f(\xi_1, \alpha) \frac{d\xi_1}{d\alpha}$$

yields:

$$f(u(x_L, t)) - f(u(x_R, t)) = [u(s_L, t) - u(s_R, t)]S + \int_{x_L}^{s(t)} u_t(x, t) dx + \int_{s(t)}^{x_R} u_t(x, t) dx \tag{26}$$

where  $u(s_L, t)$  is the limit of  $u(s(t), t)$  as  $x$  tends to  $s(t)$  from the left,  $u(s_R, t)$  is the limit of  $u(s(t), t)$  as  $x$  tends to  $s(t)$  from the right and  $S = ds/dt$  is **the speed of the discontinuity**. As  $u_t(x, t)$  is bounded the integrals vanish identically as  $s(t)$  is approached from the left and right and we obtain

$$f(u(x_L, t)) - f(u(x_R, t)) = S[u(s_L, t) - u(s_R, t)] \tag{27}$$

This algebraic expression relating the speed  $S$  of the discontinuity and the two jumps

$$\begin{aligned} \Delta f &= f(u(x_R, t)) - f(u(x_L, t)) \\ \Delta u &= u(x_R, t) - u(x_L, t) \end{aligned} \tag{27}$$

is called the **Rankine-Hugoniot condition** and is usually expressed as

$$\Delta f = S \Delta u \tag{28}$$

For the **scalar** case considered here one can solve the equation for the speed  $S$  as

$$S = \frac{\Delta f}{\Delta u}$$

**Therefore, in order to admit discontinuous solutions we may formulate the problem in terms of PDEs, which are valid in smooth parts of the solution, and the Rankine-Hugoniot Conditions across discontinuities.**

In what follows we shall examine closely two typical examples of discontinuous solutions. Consider the following initial-value problem for the inviscid Burgers equation:

$$\begin{aligned} u_t + f(u)_x + 0, f(u) &= \frac{1}{2} u^2, \\ u(x, 0) = u_0(x) &= \begin{cases} u_L & \text{if } x < 0 \\ u_R & \text{if } x > 0 \end{cases} \end{aligned} \tag{29}$$

The two cases to be studied may mathematically occur depending on the relation between the left ( $L$ ) and right ( $R$ ) values of the initial solution.

**The  $u_L > u_R$  case**

Based on the discussion about the initial data in IVP, this assumption is the **extreme case of compressive data**. Due to the convexity of the flux,  $\lambda'(u) = f''(u) > 0$ , the characteristic speeds on the left are greater than those on the right, that is  $\lambda_L \equiv \lambda(u_L) > \lambda_R \equiv \lambda(u_R)$ . Crossing of characteristics takes place and single-valued solutions became impossible. This means that the discontinuous initial solution propagates in the  $x$ - $t$  plane and the actual discontinuous solution of the IVP (29) is therefore:

$$u(x,t) = \begin{cases} u_L & \text{if } x - S_t < 0 \\ u_R & \text{if } x - S_t > 0 \end{cases}, \quad (30)$$

where the speed of the discontinuity is found as

$$S = \frac{1}{2}(u_L + u_R). \quad (31)$$

**This discontinuous solution is a shock wave** and is compressive in nature. It satisfies the following condition

$$\lambda(u_L) > S > \lambda(u_R), \quad (32)$$

which is called the **entropy condition**.

### 2.3. Rarefaction Waves

Reconsider the IVP with general convex flux function  $f(u)$ :

$$\begin{aligned} u_t + f(u)_x &= 0, \\ u(x,0) = u_0(x) &= \begin{cases} u_L & \text{if } x < 0 \\ u_R & \text{if } x > 0 \end{cases} \end{aligned}$$

and **expansive** initial data  $u_L < u_R$ . As discussed previously, **the entropy-violating mathematical solution** to this problem is:

$$u(x,t) = \begin{cases} u_L & \text{if } x - S_t < 0 \\ u_R & \text{if } x - S_t > 0 \end{cases}, \quad (33)$$

For the inviscid Burgers equation, the rarefaction shock speed is:

$$S = \frac{\Delta f}{\Delta u} = \frac{1}{2}(u_L + u_R) \quad (34)$$

It is obvious that the shock speed given by (34) does not satisfy the entropy condition, since we have  $\lambda(u_L) = u_L < S < \lambda(u_R) = u_R$ .

Furthermore, we shall show that the solution (33) is unstable. By **instability** it is meant that **small perturbations of the initial data lead to large changes in the solution**. In other words, under small perturbations, the whole character of the solution changes completely. Amongst the various other reasons for rejecting this solution as a physical solution, instability stands out as a prominent argument.

Let us modify the initial data in by replacing the discontinuous change from  $u_L$  to  $u_R$  by **a linear variation** of  $u_0(x)$  between two fixed points  $x_L < 0$  and  $x_R > 0$ . Now the initial data reads

$$u_0(x) = \begin{cases} u_L & \text{if } x \leq x_L, \\ u_L + \frac{u_R - u_L}{x_R - x_L}(x - x_L) & \text{if } x_L < x < x_R, \\ u_R & \text{if } x \geq x_R, \end{cases} \quad (35)$$

The solution  $u(x,t)$  to this problem is found by following characteristics, as discussed previously, and consists of two constant states,  $u_L$  and  $u_R$ , separated by a region of **smooth transition** between the data values  $u_L$  and  $u_R$ . This is called a **rarefaction wave**.

The right edge of the wave is given by the characteristic emanating from  $x_R$ ,  $x = x_R + \lambda(u_R)t$  and is called the **Head** of the rarefaction. It carries the value  $u_0(x_R) = u_R$ .

The left edge of the wave is given by the characteristic emanating from  $x_L$ ,  $x = x_L + \lambda(u_L)t$  and is called the **Tail** of the rarefaction. It carries the value  $u_0(x_L) = u_L$ . As we assumed convex fluxes, i.e.  $\lambda'(u) = f''(u) > 0$ , larger values of  $u_0(x)$  propagate faster than lower values and thus **the wave spreads and flattens** as time evolves.

**The spreading of waves is a typical non-linear phenomenon not seen in the study of linear hyperbolic systems with constant coefficients, as well as the wave steepening is.**

Using the characteristics, the entire solution representing implicitly the rarefaction wave is given by:

$$\begin{cases} u(x,t) = u_L & \text{if } \frac{x - x_L}{t} \leq \lambda_L, \\ \lambda(u) = \frac{x - x_L}{t} & \text{if } \lambda_L < \frac{x - x_L}{t} \leq \lambda_R, \\ u(x,t) = u_R & \text{if } \frac{x - x_L}{t} \geq \lambda_R. \end{cases} \quad (36)$$

Now we are in the position to have two solutions of the IVP (29) expansive initial data. The first one is given by the **rarefaction shock** (33) and the second is the **rarefaction wave** (36). One can say that as  $x_L$  and  $x_R$  approach zero from below and above respectively, the smooth initial data at  $x = 0$  for the rarefaction wave (35) approaches the discontinuous initial data with  $u_L < u_R$ , for the rarefaction shock.

## REFERENCES

- [1]. Aftosmis M., Gaitonde D., Tavares T.S., **On the Accuracy, Stability, and Monotonicity of Various Reconstruction Algorithms for Unstructured Meshes**, AIAA Paper 94-0415, 1994
- [2]. Barth T.J., Jespersen D.C., **The Design and Application of Upwind Schemes on Unstructured Meshes**, AIAA Paper 89-0336, 1989
- [3]. Frink N.T., **Upwind Scheme for Solving the Euler Equations on Unstructured Tetrahedral Meshes**, AIAA Journal, 30, 1992
- [4]. Godunov S., Zabrodine A., Ivanov M., Kraiko A., Prokopov G., **Résolution numérique des problèmes multidimensionnels de la dynamique des gaz**, Editions MIR, Moscou, 1979
- [5]. Hirsch C. - **Numerical Computation of Internal and External Flows**, John Wiley & Sons, New York, 1988
- [6]. Liang S.M., Chen H., **Numerical Simulation of Underwater Blast-wave Focusing Using a High-Order Scheme**, AIAA Journal, 37, 8, 1999
- [7]. Toro E.F. - **Riemann Solvers and Upwind Methods for Fluid Dynamics**, Springer-Verlag, Germany, 1997

## MECHANICAL PACKING (AXIAL SEAL WITH SLIDING RINGS) STUDY USING FINITE ELEMENT METHOD – WITH “ANSYS 9 - WORKBENCH” PROGRAM

<sup>1</sup>GRIGORESCU LUCIAN, <sup>1</sup>ZIDARU NICOLAE

<sup>1</sup>Constanta Maritime University, Romania

Using computer software “Solid Works” to generate the geometric form of the seal's rings and “ANSYS-9 WORKBENCH” program for the FEM analysisi to calculate mechanical stresses and thermal loadings of a mechanical seals as a part of the centrifugal pumps working in an oil refinery.

The goal of this analysis is to improve the design of the seal.

**Keywords:** mechanical seal; thermomechanical analysis; mechanical and thermic stresses and strains; equivalent stress; finite element nets (mesh)

### 1. GENERAL PRESENTATION

The analysis was performed for the mechanical seals of the 100P3A and 100P3R pumps of an oil refinery.

Two “scenarios” was considered; each them is an “engineering” simulation. To define the simulations we considered as known: the type of material and the material properties; the behaviour of the contact surface of rings; the types and the magnitude of the loadings on the ring. As a variable are considered the geometric shape of the rings and loadings.

Type of the material of sliding rings: silicon carbide/graphite.

Mechanical and thermic characteristics of the slidings rinds

**Table 1: Graphite ring (fixed ring)**

Name	Value
Young's Modulus (E)	$1 \cdot 10^{10}$ Pa
Yield stress to compression ( $\sigma_c$ )	$10 \cdot 10^7$ Pa
Tensile stress (allowable) $\sigma_t$	$1,5 \cdot 10^7$ Pa
Thermical conductivity ( $\lambda$ )	104,7 W/m °C
Thermic elaongation factor ( $\alpha$ )	$5,25 \cdot 10^6$ ( $^{\circ}C$ ) <sup>-1</sup>
Maximum working temperature ( $T_{max}$ )	365 °C

**Table 2: Silicon carbide ring (mobile ring)**

Name	Value
Young's Modulus (E)	$4,8 \cdot 10^{11}$ Pa
Yield stress to compression ( $\sigma_c$ )	$105 \cdot 10^7$ Pa
Tensile stress (allowable) $\sigma_t$	$12,5 \cdot 10^7$ Pa
Thermal conductivity ( $\lambda$ )	100 W/m °C
Thermic elaoongation factor ( $\alpha$ )	$3,9 \cdot 10^6 (^\circ C)^{-1}$
Maximum working temperature ( $T_{max}$ )	2400 °C

**a)Scenario Nr. 1**

We consider that sliding rings operate in contact with the auxiliary liquid wich produce the lubrication and refrigera tion of the sliding rings. This is a normal working condition (state) of the seal.

The model of simulation:

- The computer program „SOLID WORK” define the geometric model of the assembly – Fig. 1.1
- The model has a total volume of  $1,23 \times 10^{-4} \text{ m}^3$
- Finite elements are Brick type – Fig. 1.2

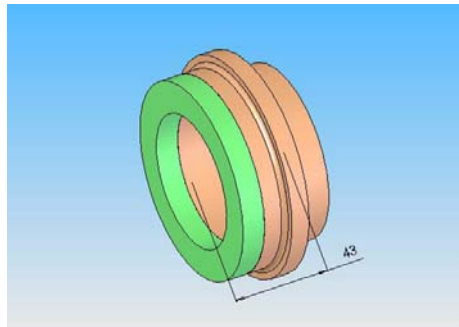


**Fig. 1.1. Mechanical packing fit:silicon carbide/graphite**

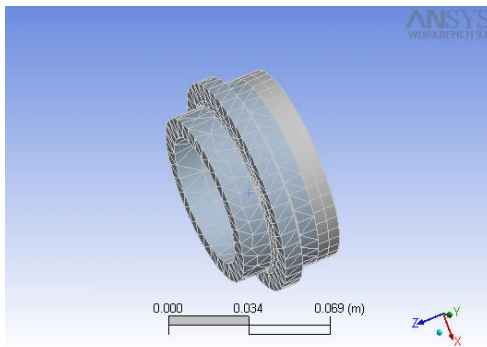


**Fig.1.2 Loadings and boundary condit**

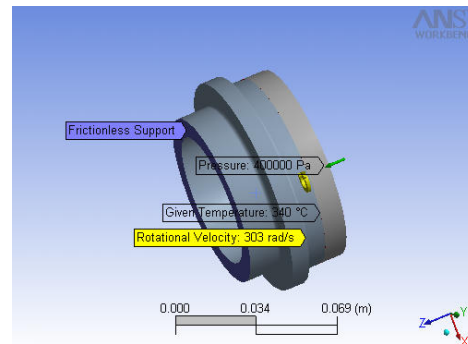


**Fig.1.3 Finite element net (brick type)**

Graphite sliding ring was divided in 162 Brick type finite elements with 1179 knots.  
Rotating silicon carbide slide ring was divided in 3929 Brick type finite elements with 6458 knots.

Loadings and border conditions are presented in Fig. 1.3.

Loadings: Contact axial pressure  $p_a=400.000$  Pa is realised by the springs and the auxiliary liquid.

- the auxiliary liquid is diesel fuel
- the temperature of the working liquid is  $T= 340^\circ$  C
- the angular speed of the rotating ring is  $\omega = 303$  rad/s

Border conditions: contact without fiction on the fixed ring surface.

#### b) Scenario Nr. 2

The auxiliary liquid circuit is damaged . The sliding rings run without auxiliary liquid, that is without lubrication and refrigeration. This is an abnormal working mode.

The model of the seal assembly is the same as in Scenario Nr. 1.

The loading and the border condition are presented in Fig. 1.4.

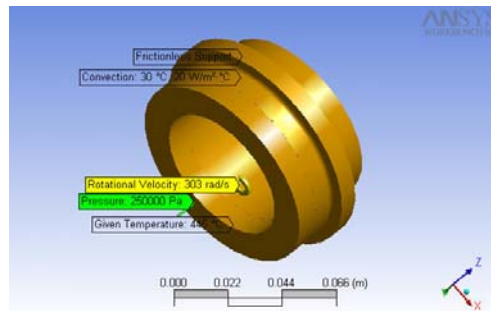


**Fig. 1.4. Loading and boundary conditions**

Loadings: Contact axial pressure  $p_a= 250.000$ Pa, is realised only by the springs, without auxiliary liquid;

- the temperature of working liquid is  $T = 340^\circ$  C.
- the angular speed of the rotating rings is  $\omega = 303$  rad/s.
- the temperature of contact area of the rings is  $445^\circ$  C.

Border conditions:

- contact without fiction on the fixed ring surface

heat transfer by air convection:  $T_{air} = 30^\circ$  C,  $\lambda_{air-rings} = 20$  W/m $^\circ$ C

## 2. SOLUTIONS

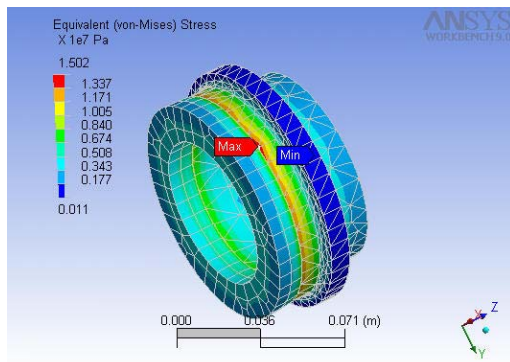
For the Scenario Nr. 1

- The type of sistem solving is selected by the program
- One or more bodies may be underconstrained and experiencing ring body motion. Weak springs have been added to attain a solution.
- Thermic deformations are calculated using a „reference” temperature, considered at  $22^\circ$  C. At this uniform temperature is considered that don't exist thermic deformation of the sliding rings.

The values of the stresses and strains are presented in Table 2.1

Table 2.1

Name	Scope	Referent system	Minimum	Maximum	Minimum Occurs On:	Maximum Occurs On:
Equivalent stress (Von Mises stress) – v. Fig. 2.1; 2.2; 2.3.	All Bodies in „model”	Global	112,464 Pa	$1,5 \cdot 10^7$ Pa	Silicon carbide ring	Silicon carbide ring
Elastic equivalent strain stress (Von Mises strain) – v. Fig. 2.4; 2.5; 2.6.	All Bodies in „model”	Global	$2,34 \cdot 10^{-7}$ m/m	$9,59 \cdot 10^{-4}$ m/m	Silicon carbide ring	Graphite ring



$$\sigma_{ech.max} = 1,5 \cdot 10^7 \text{ Pa (for the silicon carbide rings)}$$

Fig.2.1. Equivalent Stress von Mises (front view)

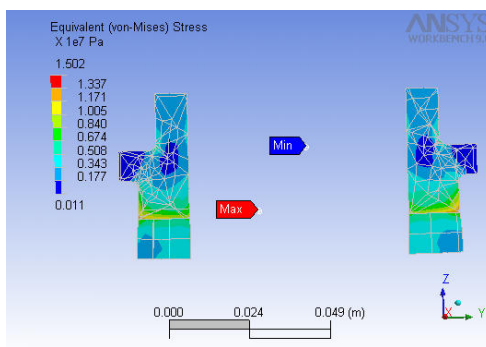


Fig. 2.2. Equivalent Stress von Mises (for cross section)

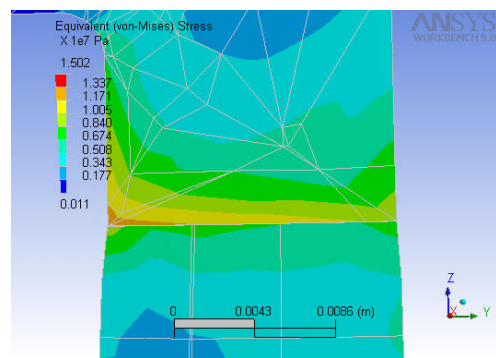
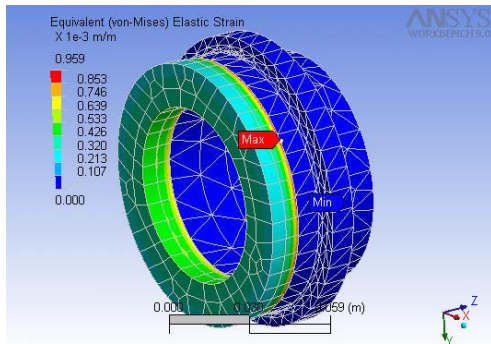


Fig. 2.3. Equivalent Stress von Mises (for contact zone)



$$S_{ech.max.} = 0,959 \cdot 10^{-3} \text{ m/m ( for graphite rings)}$$

Fig. 2.4. Equivalent Elastic Strain von Mises (front view)

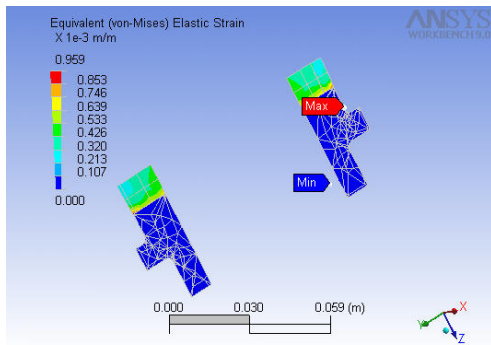


Fig. 2.5. Equivalent Elastic Strain von Mises (for cross section)

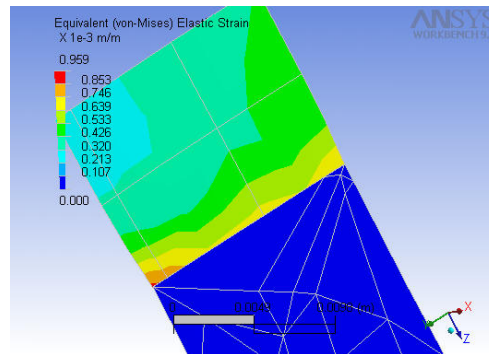


Fig. 2.6. Equivalent Elastic Strain von Mises (for contact zone)

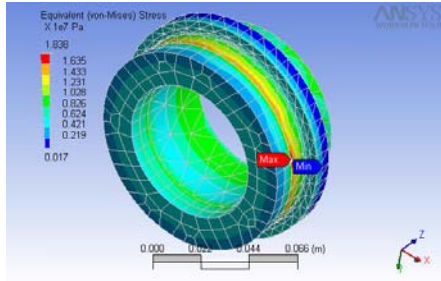
For the Scenario Nr. 2

- Solution are the same as of Scenario Nr. 1

It is different the values of the stresses and strains ( mechanical and thermic) –as in Table 2.2.

Table 2.2

Name	Scope	Referent system	Minimum	Maximum	Minimum Occurs On:	Maximum Occurs On:
Equivalent stress (Von Mises stress) – v. Fig. 2.7; 2.8; 2.9.	All Bodies in „model”	Global	167,110 Pa	$1,84 \cdot 10^7$ Pa	Silicon carbide ring	Silicon carbide ring
Elastic equivalent strain stress (Von Mises strain) – v. Fig. 2.10; 2.11; 2.12.	All Bodies in „model”	Global	$3,48 \cdot 10^{-7}$ m	$1,25 \cdot 10^{-3}$ m/m	Silicon carbide ring	Graphite ring



$$\sigma_{ech\ max} = 1,84 \cdot 10^7 \text{ Pa (for silicon carbide rings)}$$

Fig. 2.7. Equivalent Stress von Mises (front view)

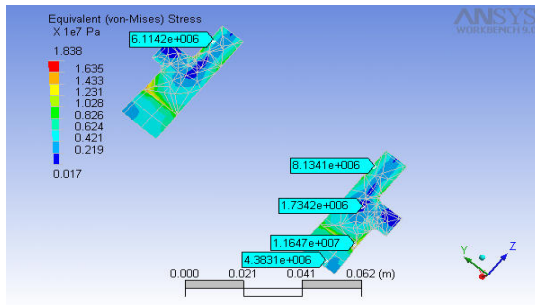


Fig.2.8. Equivalent Stress von Mises (for cross section)

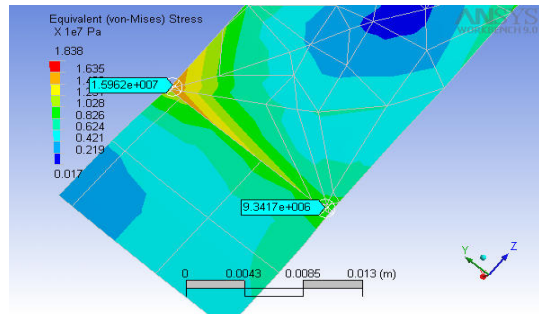
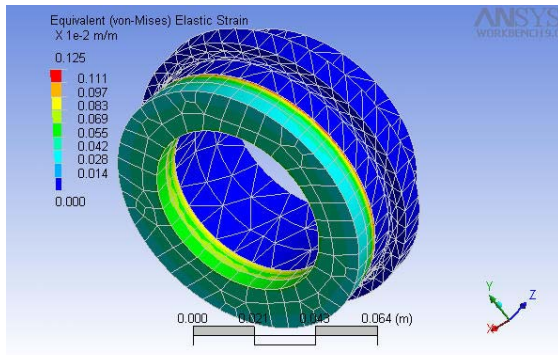
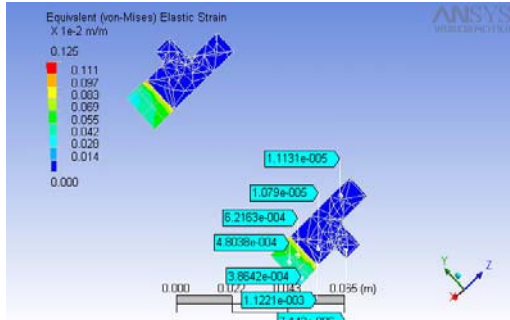


Fig.2.9. Equivalent Stress von Mises (for contact zone)



$$S_{ech.\ max.} = 0,125 \cdot 10^{-2} \text{ m/m ( for graphite rings)}$$

Fig. 2.10. Equivalent Elastic Strain von Mises (front view)



**Fig. 2.11. Equivalent Elastic Strain von Mises (for cross sections)**

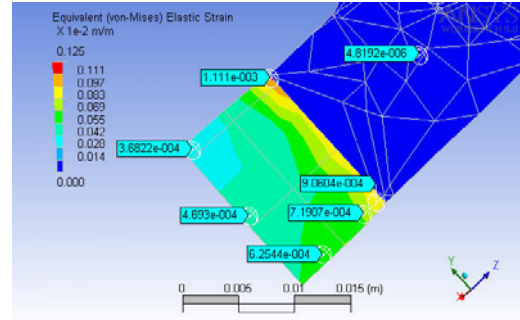


**Fig.2.12. Equivalent Elastic Strain von Mises (for contact zone)**

### 3. CONCLUSIONS

#### For the Scenario Nr. 1

The two sliding rings of the mechanical packing resist to compression stress in the normal running conditions (work in the presence of auxiliary liquid).

The maximum equivalent stress (Von Mises) appear in the silicon carbide ring.

$$\sigma_{echiv . max} < \sigma_{ac 1,2} \tag{1}$$

where:  $\sigma_{echiv . max} = 1,5 \cdot 10^7 Pa$

$$\sigma_{ac1} = \frac{\sigma_{c1}}{c} = \frac{105 \cdot 10^7}{5} = 21 \cdot 10^7 Pa \text{ (available stress to compression for the silicon carbide ring)}$$

$$\sigma_{ac2} = \frac{\sigma_{c2}}{c} = \frac{10 \cdot 10^7}{5} = 2 \cdot 10^7 Pa \text{ (available stress to compression for the graphite ring)}$$

$c = 5$  ( is the safety factor ).

- The maxim elastic equivalent strain is  $S_{ech} = 9,59 \cdot 10^{-4} m/m$  and it is greater that the maximum value  $S_{max} = 0,6 \cdot 10^{-4} m/m$ .

- The maximum strain is produced in the graphite ring.

#### For the Scenario Nr. 2:

The two sliding rings resists even in the damage conditions (in the absence of the auxiliary liquid).

The maximum equivalent stress (Von Mises) is produced in the silicon carbide ring.

$$\sigma_{echiv . max} < \sigma_{ac1,2} \tag{2}$$

where:  $\sigma_{echiv.max} = 1,84 \cdot 10^7 Pa$

$$\sigma_{ac1} = 21 \cdot 10^7 Pa$$

$$\sigma_{ac2} = 2 \cdot 10^7 Pa$$

- The maxim elastic equivalent strain is  $S_{ech.max} = 12,5 \cdot 10^{-4} m/m$  and it is greater than the maximum value  $S_{max} = 0,6 \cdot 10^{-4} m/m$ . The maximum equivalent strain is produced in graphite ring.

The final conclusion is that the sliding rings presents well strenght to compression. The equivalent stress (Von Mises) had a maximum value in the silicon carbide ring for the both scenarios. The maximum strain (deformation) is in the graphite ring and it is 1,3 times greater in the scenario Nr. 2 (damage running conditions).

## REFERENCES

- [1]. Aziz A.K. - *The Mathematical Foundations of the Finite Element Method with Applications to Partial Differential Equation*, Academic Press, New York, 1972
- [2]. Akin J.E. - *Application and implementation of Finite Element Methods*, Academic Press, New York, 1982
- [3]. Bathe K.J. - *Finite Element Procedures in Engineering Analysis*, Prentice Hall, Englewood Cliffs, N.J., 1982
- [4]. Davies, A.J. - *The Finite Element Method*, Clarendon Press, Oxford, uk, 1980
- [5]. Griffiths D.F. - *The Mathematical basis of Finite Element Methods*, Clarendon Press, Oxford, UK, 1984
- [6]. Grigorescu L. - *Contribution On Durability And Reliability Improvement Of Mechanical Axial Packings (Seals) Used In Petrochemical Industry*, Thesis Of Doctorate, Constanta Maritime University, 2007
- [7]. Mayer E. - *Garnitures mecaniques d'etancheité*, Paris. Dunod, 1977

## CLASSIFICATION OF THE MARINE SIMULATOR EXERCISES (WORKING SCENARIOS)

HINEV VALENTIN

*Nikola Vaptsarov Naval Academy, Bulgaria*

The exercises are classified on the basis of different quantitative and qualitative criteria. They provide information on the aims of exercise or which sphere or branch of the marine education it is designed for. Other criteria specify the number of the included objects as well as for the variables of the training environment and duration of the exercises. The classification of the exercises also takes into consideration the necessity of instructor-operators for operating the simulator sessions, the vessel traffic, special procedures in bridge management or the organization of the examination.

**Keywords:** classified, exercises, simulator, education, training.

### 1. INTRODUCTION

In the past few years, marine simulators have become some of the most effective instruments for education and training of marine staff (Maritime Education & Training [MET]). They are used with increasing success as means of training of cadets and students at marine colleges and academies. When trainees are introduced to an environment resembling real-life as closely as possible (6 main requirements of IMO to the simulators [3]), we make it possible for them quickly and easily to establish the main cause-effect relationships necessary to receive theoretical knowledge and gain the key practical skills to work onboard a ship. This makes simulator training the only alternative. The wide application of simulators in marine education is a positive fact. The wide range of training tasks and the need for their more effective management as training aids raise the central issue of the optimisation of the following activities: Planning of the educational and training process; Control and management of the educational process; Standardization of the curricula of the training centers.

#### 1.1 EXPERIMENTAL BASIS OF THE CLASSIFIER

The development of the model of the classifier, all the data and examples used in the paper are based on a number of experiments, conducted over the last 8 years during the standard operation of the two Transas Group navigational simulators, models Navy Trainer Professional version 3000 and version 4000 after 2005. The simulator system includes bridges of all classes, according to the IMSF classification, whereby the management of one of the simulators allows for one of the bridges to be modified [2] and acquire the functions and characteristics of each of classes, from Single Task Bridge (Category IV) to Full Mission Bridge (Category I). The bridges of the two simulators are used in classroom situations, to

train and assess the students' knowledge and skills in a large number of marine educational disciplines.

## **2. EXPOSE**

The establishment of a suitable and dirigible environment adapted to the specific aims of the training process is a task, the solution of which, to a great extent, determines the quality and volume of the simulator training

### **2.1. COMPONENTS OF THE ENVIRONMENT IN, WHICH SIMULATOR TRAINING IS CARRIED OUT**

For the purpose of the current analysis, the environment where simulator training is carried out is provisionally divided into two components. One of the components which is not a subject of the current article is the simulator with its hardware architecture and number and category of the simulators (according to IMSF). The second component is the simulation of reality. It is presented by the exercise scenario. Its format is an executable file, which manages the simulator during its session. The scenario contains all data and instructions necessary for the managing software to reproduce the situation necessary for the aims of the exercise and the assessment. For this reason, special attention is paid to this component.

### **2.2 MAIN STAGES IN THE DEVELOPMENT OF SIMULATOR EXERCISES**

The development of an exercise on the simulator includes the following activities: (1) Creation of a preliminary plan scenario (task); (2) Development of an executable file; (3) Exercise testing and correction of the (.exe) file until plan scenario objectives are met, and (4) Documentation of the exercise.

### **2.3 CONTENTS OF THE MAIN STAGES IN THE DEVELOPMENT OF SIMULATOR EXERCISE**

The plan-scenario of the exercise determines the aims and objectives of the training, or the assessment of the trainees. It must indicate the methods and means which trainees will use to solve the tasks assigned to them. The plan-scenario also determines: the games area, number and type of the own ships and bridge category. It contains the number, type and dynamics of the participating objects and parameters of the dynamic environment. The requirements to the operators and management of the vessel traffic and special objects (tugboats, helicopters, rescue boats and equipment etc.) must be specified in it. For the assessment of the trainees, the plan must clearly indicate the criteria, methods, means and instruments which the trainees can use to achieve the goal. In development of executable (.exe) file of the exercise, the information from the plan scenario is calculated and input using the input interface into the simulator. It is recorded there in the format of a software managing file and is used during the simulator sessions. At this stage passage planning of the moving aims, choice and introduction of the games area, outfitting of ports and fairways with the necessary equipment. Software for modification of the parameters of the environment in the games area is used at this stage also. At the third stage, the plan-scenario is tested for correspondence and validity. Exercises are tested by means of built-in test system by changing the time scale as well as "in real-life" conditions by a team of instructor and operator at the bridge. Both separate episodes and the exercise as a whole are tested. At this stage a test and a training of the subsidiary staff (steersman, pilots, operator etc.) necessary for the management of the traffic of the target vessels and other types of objects participating in the scenario. The actions of operators to back trainees

following a command from the bridge must be specified here. As a result of the tests, the (.exe) file or exercises scenario may be corrected if necessary. The last stage of the exercise preparation includes the preparation of the documentation. For the different educational institutions, the style and format of the documentation is different but generally speaking there should be three types of documents: general documents for the exercise, documents for the instructor and the managing team and documents for the trainees. For the general documentation, the most important documents are the syllabus and schedule of the exercise. The latter is a guiding document by means of which the overall management of the training process during the session is carried out. Different documents concerning the functions of the instructors and technical staff - instructions for the staff, for the specific settings of the simulator, the bridges and the trainees' work stations are prepared on the basis of the schedule. When traffic and bridges have to be managed by an operator, an exercise logbook must be created. General documents are also: lectures, training films, auxiliary and demonstration simulator exercises included in the curriculum, as well as documents specifying the norms and criteria for assessment of the students' knowledge and skills and registers containing students' scores. Documents designated for the students include: form with the aims and objectives of the exercise, instructions for use of the simulator and bridge, bridge checklist, list with bridge positions, starting parameters of the exercise and the ship, the logbook and report forms for the exercise and the voyage, as well as the various criteria for assessment set by instructors.

**2.4 CORRELATION BETWEEN THE DURATION OF AN EXERCISE IN TERMS OF THE EXERCISE SESSION AND THE TIME NECESSARY FOR ITS PREPARATION**

The detailed outline of the stages of creation and preparation of an exercise aims at illustrating the following conclusion: the time necessary for creation of an exercise exceeds by much its duration. The ratio between time needed for an exercise preparation and its session usually ranges from 3:1 to 5:1. For more complicated scenarios and for scenarios longer than 1 hour this ratio varies between 8:1 and 10:1. For the development and testing of (.exe) files for exercises with duration of over 4 hours, using dozens of moving objects and characteristics of the environment change greatly during the exercise, the ratio is in the area of 15:1 to 20:1.

**2.5 THE CLASSIFIER – A NECESSARY CONDITION FOR PLANNING AND MANAGEMENT OF SIMULATOR TRAINING**

The classifier is an instrument by means of which exercises created on the simulator can be compared using a set of criteria. It is a system of criteria where each exercise is subjected to analysis and comparison and the final result is a unique characteristic for each separate exercise

**Fig.1 Identification number of an exercise: "Bulk 1 Speed Testing Shallow Water", practical exercise No 68, discipline "Navigation for bachelors" - part I, semester IV.**

Navigation Simulator Identification Number of the Exercise

Cell	1	2	3	4	5	6	7	8	9	10	11	12	13	14	15	16	17	18	19	20	21	22	23	24	25
Code	0	1	0	F	1	S	E	1	0	1	0	4	0	2	0	0	0	0	5	0	0	6	8	0	2

For convenience and ease of processing, the exercise characteristic is represented as a 25-bit number (fig.1), consisting of Latin letters and digits. Under this number each exercise presented by an .exe file and a folder containing accompanying documentation can be stored as a database in the local network of the simulator or the training center. And vice versa: based on this 25 bit number by means of the classifier it is possible to decode the purpose and contents of each exercise and the conditions for its usage. stored as a database in the local network of the simulator or the training center. And vice versa: based on this 25 bit number by means of the classifier it is possible to decode the purpose and contents of each exercise and the conditions for its usage.

## 2.6 MAIN CRITERIA FOR EXERCISE CLASSIFICATION

Fig. 2 A table with criteria

Discrimination criteria	Cell	Code
Education Level	1	0, 1 or 2
Author	2	0, 1 or 2
Source	3	0, 1 or 2
Domain	4	F, N, E, M or D
Training phase	5	0, 1 or 2
Task, assignment	6	Latin Letter
	7	Latin Letter
Own Ships (pc.)	8	Dec. Digit
Targets & objects with/track (Sum)	9	00 – 99
	10	
Marine & Coast Objects & Bollards, fenders etc. (Sum)	11	00 – 99
	12	
Weather & Dept zones (Sum)	13	00 - 99
	14	
Traffic Services	15	0, 1 or 2
Bridges Services	16	0 or 1
Training Services	17	0, 1 or 2
Training Center Syllabus Items	18	Decimal Digit or/and Symbol
	19	
	20	
Training Center Syllabus Practical exercises	21	Decimal Digit or/and Symbol
	22	
	23	
Individual Number of the exercise	24	00 - 99
	25	

Criteria used in the classifier are 16. They are located in the left column of the table. Each criterion is represented by one, two or three cells (middle column of the table). In the right column of the table are shown codes for each criterion. For this purpose the criteria are combined into six sectors.

## **2.7 FIRST SECTOR. LEVEL OF THE SIMULATOR TRAINING**

In this classifier there are three levels of training of marine staff, depending on their level of qualification. Zero (0) marks all exercises intended for entry (primary) level. These are most of the exercises for students and cadets at Marine Academies and colleges. One (1) marks all the exercises intended for operation level of training, according the STCW'95 code. Two (2) marks all exercises designed for management level trainees.

## **2.8 SECOND SECTOR. TWO TECHNOLOGICAL CRITERIA**

The following two sectors of the classifier have technological purpose and denote: Cell 2 - author of the exercise and cell 3 - source. They indicate the origin of the scenario and the relation between the instructor team and the development of the exercise. The values of these cells are also: 0, 1 or 2. In Author cell zero (0) means that the exercise is developed by one person who is an instructor and an operator of the simulator. One (1) and two (2) mark the situation where the instructor and the operator are different persons [1]. One (1) means separation of the responsibility between the members of the team. In this case the operator on the basis of general instructions provided by the instructor develops the exercise. Two (2) is input when the instructor has developed a detailed plan-curriculum and scenario of the exercise, and the operator only input the data into the simulator. The third cell "source" indicates how the exercise is developed. Two (2) means that the exercise is new, one (1) means modification of an existing exercise or use of templates from other exercises and zero (0) marks a ready log file from another exercise.

## **2.9 THIRD SECTOR OF THE CLASSIFIER. PURPOSE OF THE EXERCISE. AREAS AND PHASES OF MARINE STAFF SIMULATOR TRAINING**

The main factor when classifying an exercise is its purpose in the training process. For this purpose, in developing the criteria mostly the STCW'95 code and various IMO model courses are used. Data from the curricula of some marine colleges and academies are also used. In the classifier the purpose of the exercise is marked with 3 criteria: domain (cell 4), Training phase (cell 5) and Task (cell 6 and 7). On next figure (figure 3) is shown domain "Navigation" (full name Maritime Navigation & Sea Operations Management), which contains 21 training directions. An exercise whose aims and objectives coincide with some of the domain training directions receives the code from the horizontal row where this direction is located.

**Fig. 3 Third segment from the classifier containing domain "Navigation" (code N) with training directions and phases and their codes.**

CELL4	CELL5	CELL6	EXERCISE TASK & ASSIGNMENT	CELL7
<b>DOMAIN N: MARITIME NAVIGATION &amp; SEA OPERATIONS MANAGEMENT</b>	<b>CODE 0 = EDUCATION PHASE</b>	P	Plan & Conduct A Passage & Determine Position.	C
		N	Maintain A Safe Navigational Watch.	W
		U	Use Radar & Arpa To Maintain Safety Of Navigation.	A
		V	Plan A Voyage & Conduct Navigation	P
		D	Determine Position & Accuracy Of Resultant Position Fix By Any Means.	A
		E	Determine And Allow For Compass Errors	D
		N	Determining & Taking Into Account Corrections Of The Principal Navigational Aids.	C
	<b>CODE 1 = TRAINING PHASE</b>	D	Maintain Safe Navigation Thought The Use Of Radar/Arpa & Modern Navigation System To Assist Command Decision-Making.	M
		W	Establish Watch Keeping Arrangements & Procedure	A
		M	Maneuver The Ship	S
		F	Fish Finding	F
		N	Ice Navigation	A
		N	River & River-Sea Navigation	R
		S	Maneuver & Handle Own Ship In All Conditions	H
	<b>CODE 2 = ASSESSMENT OF</b>	R	Respond To Distress & Emergencies Signals At Sea	D
		C	Co-Ordinate Search & Rescue Operations	S
		R	Operate Remote Controls Of Propulsion Plant & Engineering System & Services	C
		V	Scenarios To Vessel Traffic Management Simulators	T
		D	Dynamic Positioning Operator Training (Dps)	P
		M	Maneuvering & Perform Operations At The Sea In Accordance With Nato Standards	N
		A	Another Sea Operations & Actions	A

On Figure 4 there is an example for a classification of an exercise used in Bridge Team Management course. It is a new one, intended for management level trainees, developed by the operator. Its direction is "Maneuver & Handle own ship in all conditions", from domain

“Maritime Navigation & Sea Operation Management” and it is at a phase for training of the bridge team for sailing in hard conditions.

**Fig. 4 Identification number of an exercise entitled: “KOTC 6” – passage through Bosphorus strait, ship type Bulk Carrier 23000t, in heavy vessel traffic and strong following current**

Navigation Simulator Identification Number of the Exercise

Cell	1	2	3	4	5	6	7	8	9	10	11	12	13	14	15	16	17	18	19	20	21	22	23	24	25
Code	2	1	2	N	1	S	H	2	4	2	1	8	4	8	2	1	1	7	0	3	0	0	6	0	4

**2.10 EXTENDING THE SCOPE OF THE CLASSIFIER. INTRODUCTION OF MORE DOMAINS**

The contents of the domain “Navigation” is mostly taken from STCW’95 code, but the application of this content only would limit the use of the simulator. For that reason, more domains are used in this classifier. All domains in the classifier have similar structure. They differ from each other by number and content of training directions. Each exercise being classified can receive only one code included in all domains of the classifier.

Ship’s Navigation Equipment & Ship’s Signalling Systems domain, code E comprises 23 training directions. These directions contain the codes of all types of navigational and radio navigational equipment and systems for emission of all types and categories of signals. The Ships Handling & Ships Maneuvering, code M domain is the next one used in the classifier. At the moment it uses 27 training directions, related to the whole study of the ship manoeuvring management. The wide application of simulator training in marine colleges and academies is the reason for the inclusion of the following domain. This is the domain Fundamentals of Maritime Navigation, code F. At the moment this domain includes 11 directions. A characteristic feature of this domain is that the first digit from the ID number of an exercise classified with this domain cannot be assigned the value of two (2), i.e. these exercises are intended only for entry (primary) level. The ID shown on fig. 1 is for an exercise that received its code from domain F. The letter D in the fourth cell of the classifier encodes a specific exercise category – Demo exercises. These are auxiliary exercises where the trainees are above all observers. The content of domain D is formed as a sum of the directions included in all domains: N, E, M and F.

**2.11 FOURTH SECTOR: QUANTITATIVE PARAMETERS OF THE EXERCISES**

In the fourth sector of the classifier there are 4 parameters for comparability of the exercises. They are quantitative parameters and their dimension is number. In the cells 8, 9 and 10, 11, 12, 13 and 14 with digits are recorded respectively: the number of own ships, number of all moving objects (ships target, tugs, helicopters and others), the number of additional marine based or land based static objects, as well as the total number of weather zones and software for change of weather conditions. These parameters and objects have influence on its technological assessment. The values of the figures in cell 4 provide a general idea of the level of complexity of the scenarios and, to some extent, of the time needed for its development. For example, if we compare the values of cells in the fourth

segment of the exercises on fig. 1 and 4, we could see that the first exercise is comparatively simple. In the geographic area there is only one ship (cell eight contains value 1). There are no other moving objects, except for the Own ship (cell nine contains value 0, and cell ten contains value 1). There are also four additional objects (cell eleven contains 0, and cell twelve contains 4). There are also four buoys for organization of the speed polygon and 2 weather zones for simulation of current and wind influence in shallow and deep water conditions. (cell thirteen contains value 0, and cell fourteen contains value 2). The exercise on fig. 4 is a typical example of a complicated scenario. Except for two own ships there are also 42 moving objects, mainly ships causing heavy traffic, as well as 18 static ships in port piers and mooring places and 48 weather zones recreating the complicated current system in Bosphorus strait.

## **2.12 FIFTH SECTOR. ENSURING SIMULATOR SESSIONS**

The content of cell fifteen designates the necessity of maintenance of the traffic during the session. There are 3 codes: 0, 1 and 2. Zero means that the exercise does not need vessel traffic management. Such exercises require only one instructor. One in cell 15 means that the traffic must be managed. These exercises require an instructor and an operator. Two means that the operator has to be able to manage specialized ship models (tugboats, ast boats, helicopters) in real time. The contents of cell 16 signify the necessity for maintenance of the ship bridges during the session. There are two codes: 0 and 1. Code 0 means that the trainees execute all manipulations with the bridge equipment on their own. Code 1 means that the instructor or operator executes all manipulations following a command from the trainees. These include mooring operation, ship anchoring, tug operation, etc. The criterion from the fifth sector reflects the need for participation of highly qualified specialists in the training process. Zero in cell 17 means that such a specialist is not necessary. Code 1 means that training process requires the presence of qualified external specialists (pilots, masters of tug-boats or other special ships, marine rescue swimmers, military specialists, etc.). Code 2 in cell 17 means that more than one instructor teams manage the simulator during this session. The simulator may work jointly with other simulators, for example ERS, VTS, DPS simulators, and simulators for management of disasters, large-scale wrecks and crises.

## **2.13 THE SIXTH SECTOR OF THE SIMULATOR SHOWS ITS RELATION TO THE SYLLABUS AND CURRICULA OF THE COLLEGE OR ACADEMY**

There are 7 cells for this aim. Cells 18, 19 and 20 are intended for the code of the school subject of the exercise. On fig. 1 in these cell there are the digits 0 5 0. This is the code of the subject "Navigation" at the educational institution. The following three cells (21, 22 and 23) have the code of the practical exercise. In fig. 1 the code is 0 6 8 i.e. "Determination of the vessel's speed by means of observation and using measurement buoys lines." These codes are determined by the administration of the simulator academy or college. The last cells (24 and 25) mark the version of the exercise. For example on fig. 1 digits 0 and 2 in cells 24 and 25 mean second version of the exercise.

## **2.14 DEVELOPMENT AND INTRODUCTION OF THE CLASSIFIER**

The classifier reflects modern standards for usage of the simulators. The classifier is flexible and takes into account a possible future changes in its structure. The content of each segment and cell can be extended to include more criteria, if necessary. This may lead to the rise of new types of exercises. The same applies to adding extra domains. For example for the purposes of distance learning, it is expedient to use various animations, initially generated using the simulator. The exercises and their documentation differ from distance learning exercises. It is therefore essential for a new domain to be inserted. Such or similar changes to the structure of the classifier will not necessitate the re-initialisation of old exercises. This characteristic of the classifier is a crucial condition for its implementation as management tool. The classifier of the exercises, together with the method for change of the structure of bridges of the simulator [2], is an important tool for the efficient use of simulators for the training and the evaluation of the knowledge and skills of seafarers. For the successful implementation of the integrated classifier, regulations for its implementation and usage must be developed.

## **2.15 REGULATIONS FOR THE IMPLEMENTATION AND USAGE OF THE CLASSIFIER**

The regulations need to regulate the use of the classifier in the simulator or simulator training-center. The issues it must resolve are the following: (1)To regulate all types of documents, accompanying the example, and provide model forms for their development; (2)To regulate the use of codes in the classifier; (3)To regulate means for identifying the domain and the instructional direction of exercises; (4)To provide methods for determining the time needed for developing the exercises and the complexity of the scenario, of the exercises; (5)Requirements for the qualification of the instructors and simulator operators for the execution of the exercises with varying degree of complexity of the scenario; (6)The procedure and organization of simulator sessions and regulations for forming technical and instructor teams and the additional hired specialists; (7)Organization of database of documents, files and records of exercises, work regulations and access procedures; (8)The regulations and procedure for effecting changes in the classifier.

## **3. CONCLUSIONS**

The establishment of a database with classified exercises is a prerequisite for better management and exploitation of the resources of the simulator or simulator center. Information about the number, purpose and technical characteristics of exercises available provide data about the human, material and technical resources necessary for the realization of different simulator sessions. The management team of the simulator can assess the level and number of trainees and organize more effectively the training process. Data about the quantitative characteristics of the exercises allow us to do an impartial assessment of the simulator load and effectiveness, time and effort on behalf of instructors, and to determine the cost of the products created using the simulator. Availability of database with classified exercises would stimulate integration relations among simulation centers. Thus a possibility and later on necessity of active exercises and specialists exchange among training centers may arise.

## REFERENCES:

- [1]. Hinev Valentin – ***Teamwork at the Simulator – Organization of the Activities of Instructor Teams in Management of the Navigational Simulators*** - Proceedings of Naval Academy “N. J. Vaptsarov”, “Marine scientific forum”, volume 1, “Problems of academic education. Science about sea and vessels”, Varna, 2008.
- [2]. Hinev Valentin – ***Education and Training Capability Enhancement of the Navy Trainer Professional Simulators of the Transas Group Ltd.***- trans & MOTAUTO’06 Proceedings volume 5 “Training Theory and Scientific Researches”, Sofia, 2006
- [3]. S a n n a Sonniner & T a p i o Nyman – ***Use of Simulator Training” from Book collection - Human practice in the life cycle of complex systems. Challenges and Methods.*** Edited by Maaria Nuutinen & Juha Luoma. Espoo 2005. VTT Publications 582. 1
- [4]. STCW Convention 95;

## DECK CADET AND “ON-LINE TRAINING” ON BOARD OF THE SHIP

IORDANOAIA FLORIN

*Constanta Maritime University, Romania*

The paper is addressed to the marine officers from the Navigation section and to the students from the final year of studying who are in the training voyage, before the final exams and before obtaining the maritime certificate. The progress from the IT domain, communications and the techniques of leading the maritime ships allows nowadays the reduction of the determination time of the astronomical point of the ship. Due to the fact that IMO through STCW imposes the unification of the training way of the marine officers, no matter the country they come from, in this paper I introduce a series of notations and international standards. On their basis it can be accomplished the training of the students and of the deck officers from different countries for the on-line determination of the astronomical point.

**Keywords:** Computer, communication, navigation, international, on-line, training.

### 1. PROGRAMS OF IDENTIFYING THE HEAVENLY BODIES

The best-known computer programs used for identifying the heavenly bodies are: "Cyber Sky"[17] figure 1, "Sky Chart 3" [22], "Sky Globe" [21], etc. These programs can be used in the Astronomical Navigation offering a series of information about the used heavenly bodies so that, on the deck, the deck officer can choose the heavenly bodies or the type of calculation which he desires according to the problem which needs to be solved. The main facilities of the "Cyber Sky" are the following:

- it represents the dome of heaven after the type of the "Planetarium" as a whole, but it can be represented only as part of the dome of heaven.

- it accomplishes a series of very precise calculations according to: the astronomical refraction, the effects of the movements of precession and nutation, the disturbing effects due to the multiple gravitational forces of the heavenly bodies from our solar system.

- it can represent the celestial sphere for any moment of time chosen between: 4.000 BC. ÷ 4.000 A.C.

- it can accomplish the correction of time or hour through the introduction: of the local time or of the universal time or of the daily time, according to the "Julian" calendar.

- it allows the selection of the sunrise hour, of the sunset or of the passing to the meridian for Sun, Moon or planets.

- it presents the movement of the celestial sphere through the unrolling of the time "before" or "back", with different speed, through the following commands:

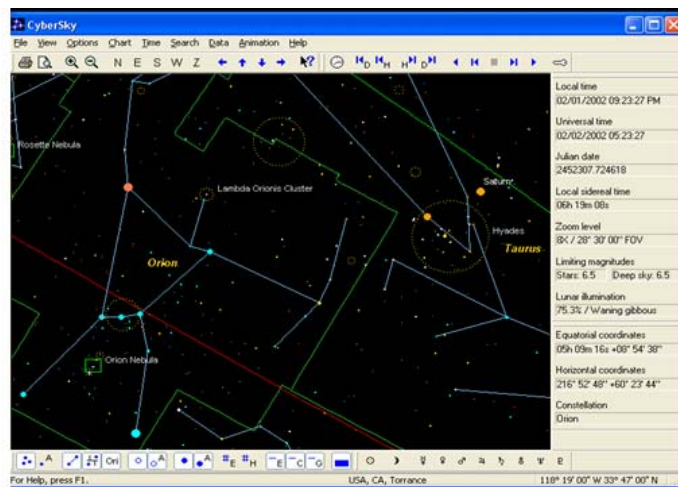


**Figure 1. "Cyber Sky" Program.  
Source: [www.cybersky.com](http://www.cybersky.com)**

-it allows the presentation of the celestial sphere from any point (place) of the 1,1156 places which are included in the data basis of the program.

-there can be added new points in the data basis of the program using the following commands:

-The image of the celestial sphere can be presented in different colour of blue (dark or light) according to the chosen moment of the day thus:

-it calculates the hours and the time durations for the civil, nautical and astronomical twilight:

-The program presents 8,403 stars which have the magnitude until the value of  $m_a=+6,5$  but the "shareware" variant of the program offers only the positions for a number of 1,629 of stars which have the magnitude until the value of  $m_a = + 5,0$ .

-it allows choosing the magnitude limit of the stars which are presented in the program.

-it can present the stars in different colours of white, grey or other colours according to their spectral type.

-The stars can be presented with their own name after the "Flamesteed" catalogue or after the literal notation of the "Bayer" stellar catalogue.

-The program contains detailed information about any of the stars found in the data basis. This information contains: the "Bayer" and "Flamesteed" numbering, the equatorial and horizontal coordinates, the distance, the magnitude, the name of the constellation from which it takes part, the sunrise time, the sunset time or the passing to the meridian, the spectral type, the class of luminosity.

-It presents the lines of the 88 constellations and the delimitations between them.

-It presents the name of all the constellations thus: the abbreviation, the name from the Latin language, the name from the English or German language.

-It represents the positions of the Sun, Moon and planets from our solar system and contains a series of detailed information about the Sun, Moon and Planets. This information refers to: the equatorial, ecliptic and horizontal coordinates, the distances, the elongations, the magnitudes, the name of the zodiacal constellation in front of it there is the sunrise hour,

the sunset hour or the passing to the meridian, the image of the disk of the chosen heavenly body and its illumination.

-It contains information about all the planets having the possibility of comparing the data referring to these.

-It allows the presentation of the net of lines and circle arcs of the systems of equatorial and horizontal coordinates.

-There can be presented the reference lines of the celestial sphere such as: the celestial meridian of the observatory, the celestial equator, the Sun ecliptic, the galactic equator.

-It presents the reference points of the celestial sphere: the celestial poles, the ecliptic poles and the galactic poles.

This program has a great use for the familiarity with the image of the celestial sphere for different positions of it, at different latitudes or at different hours of the day or of the night.

## **2. PROGRAMS WHICH EDIT NAUTICAL EPHEMERIDAE**

For the determination of the astronomical point of the ship with the help of the specialized IT programs there were accomplished a series of editing programs of the nautical Ephemerid, as a logical stage of the development or as an integrated part of a complex way of work. The best-known programs of editing The Nautical Ephemerid are the following: "The Navigator's Almanac" [15], "Interactive Almanac Ephemeris" [23], "Astro Nav PC" [16]. The program "The Navigator's Almanac" is between the first programs which offered the possibility of editing the information from the daily tablets of the Ephemerid. This has a relatively simple menu which can be used with the help of some keys pointed out by the red colour thus: the date of the observation day for a period of time between the years 1,900 ÷ 2,100; posting on the screen of the equatorial coordinates of the heavenly bodies (these allow the choice of the column of that heavenly body, which is posted on the screen, and from it, it can be chosen the corresponding value of the day and the observation hour); the beginning and the ending hours of the crepuscular, the hours of the sunrise or sunset for latitudes between 50° N ÷ 50° S.

## **3. SPECIALISED PROGRAMS FOR THE CALCULATION OF THE ELEMENTS OF THE HEIGHT RIGHT**

The calculation programs of the elements of the height right are between the most precise and extended from all the Astronomical Navigation programs. The programs used in this domain have an extensive menu which it isn't limited only to the problems of the Astronomical Navigation, there can also be solved problems of Estimated or Great Circle Navigation. Among the best-known professional programs of this type there are the following: "Sight Master" [20], "Astro-navigator" [24], and "Navstar System 2000" [19]. These programs accomplish the most part from the necessary calculations in the Astronomical, Estimated, Coastal, Great Circle or Mixed Navigation. They also allow the introduction of the specific data such as: the true road of the ship, the speed, "waypoints" [1]. These programs are easy to be used, the operator must only introduce the necessary data which are registered in the dialogue cassettes (corresponding marked). These are obtained after pushing the key pointed for all the necessary data thus: SHA, GHA, LHA, the declination, the sunrise and sunset hour, the hour of the beginning of the crepuscular, azimuth, the height, the correction for height. Besides these options, the programs also present those calculations of the data obtained from Nautical Ephemerid. On the maritime ship board, the

most used programs are the complex programs which offer multiple possibilities of calculations both for Nautical Astronomy and for Great Circle Navigation, using the mixed or the solving method of the calculated dead reckoning [1].

The calculation program "Sight Master" figure 2, is one of the most wide spread on the ship board due to the simple way of working with it, to the fact that it offers multiple possibilities of calculation, it means besides the calculations of astronomical navigation there can be accomplished a series of calculations of estimated navigation, the change of the ship route, etc. This contains Nautical Ephemerid with the possibility of calculation the heavenly bodies coordinates from 1583, until the year 2100. The precision of the program is from  $\pm 0'.1$  at stars, until 1' at the observations made for the Moon.



**Figure 2. "Sight Master" Program.**  
**Source: [www.sightmaster.com](http://www.sightmaster.com).**

#### 4. INTERNATIONAL STANDARDS OF TRAINING AND USED NOTATIONS IN THE ASTRONOMICAL NAVIGATION

On the basis of the students and marine officers training is found IMO-STCW. Inside this international standard of training there are used the following international notations:

- IMO = International Maritime Organization [3].
- STCW = Standards of Training, Certification and Watchkeeping [11].
- NA = Nautical Astronomy [4].
- Cadet = The student on shipboard for the maritime training.

For using the astronomical navigation for the determination of the astronomical point of the ship there are used the following international notations, presented in the table 1.

**TABLE 1. INTERNATIONAL SYMBOLS FOR CELESTIAL NAVIGATION**

<b>SYMBOLS AND NOTATIONS</b>	<b>SYMBOLS AND NOTATIONS</b>
$a_0$ = the first correction of Polaris	ISM = International Safety Management Code
$a_1$ = the second correction of Polaris	Lat. = latitude
$a_2$ = the third correction of Polaris	Long. = longitude

Ap.Alt. = apparent altitude	LHA = Local Hour Angle
BNA = Brown's Nautical Almanac	L.O.P. = Line of Position
C = chronometer	m = minute
CE = chronometer error	Mag. = magnitude
Corr. <sup>n</sup> = correction of "d" and "v"	Mer.Pass. = meridian passage
DUT = Difference between Universal Time	Mls. = miles
E = east	N = north
ET = Ephemeris Time	NA = Nautical Almanac
Eqn.of Time = equation of Time	NM = Nautical Miles
d = declination	Obs.Alt. = observed altitude
d = day.	Refr. = refraction
d = hourly variation of declination	S = south
d-correction = correction for the hourly variation of declination.	SD = semi-diameter
dec = declination.	SHA = sidereal hour angle
Dip = correction of horizon	UT = Universal Time
GHA = Greenwich hour angle	v = hourly variation of GHA
GMT = Greenwich mean time	v-correction = correction of the hourly variation of GHA
GPS = Global Positioning System	z = zenith distance
h = hour	Z = zenith
h =hour angle	Zn = True Azimuth
l = latitude	ZD = zenith distance
l̄ = Intercept (of Altitude, or zenith distance)	W = west

Source: Bibliographic references [2], [5], [6], [7], [10], [12], [13], [14].

## 5. ASTRONOMICAL NAVIGATION ON-LINE

Nowadays, the main problem on the maritime ships' board is represented by the lack of time for accomplishing all the activities. Due to the situation from the present navigation routes, during doing the navigation watch, the watch officer has no free time to be able to determine the astronomical point of the ship with the classical methods. Nowadays, this cannot leave his navigation command for very long time, especially for the ships with only one person in the watch service, without a cockswain [9]. In this situation the officer cannot leave his command, to stay on the deck in one of the stemmings or to go up on the standard deck to accomplish observations and measures for the heavenly bodies. Still for the determination of the astronomical point of the ship this can use the previously presented programs for preparing in time the astronomical observations. In this way this reduces the preparing time of the observations, of calculations and of staying on the deck besides the pilot house.

a). Preparing the observations on the ship board [1]. The astronomical observations are prepared thus:

- Preparing the working materials, which are used in observations: the star globe, the sextant, the chronometer (stop watch) and the observation sheet.

- It is calculated the point estimated for the moment of the civil and nautical crepuscular, according to: the position of the ship (latitude and longitude), the real route and the speed of the ship.

- It is calculated the helping elements thus: the sunset (the Sun rise) hour, the sidereal time at the meridian of that place.

It is orientated the star globe for the chosen moment, this can be: the Sun set hour, the ending hour of the night civil crepuscular, the beginning hour of the morning nautical crepuscular, the Sun rise hour.

- There are chosen the heavenly bodies according to: azimuth (Az), which must be between 60°-120° for the observations at three heavenly bodies and 90° for the observations at 2 heavenly bodies; the height (h), which must be between 30°-60°. These are registered in the table 2 and are drawn schematically the azimuths, in order to be chosen the best variants as in the figure 3.

**TABLE 2. THE CHOOSE OF THE STARS FOR OBSERVATIONS**

No.	STARS NAME	NOTATION AND CONSTELATIONS	Azimuth (Az)	Sight (h)
1.	VEGA	$\alpha$ LYRAE	041°	55°
2.	RASALHAGUE	$\alpha$ OPHIUCHI	087°	39°
3.	ALTAIR	$\alpha$ AQUILLAE	149°	31°
4.	ARCTURUS	$\alpha$ BOTEES	243°	58°
5.	DUBHE	$\alpha$ URSAE MAJORIS	305°	60°

Source: Author study

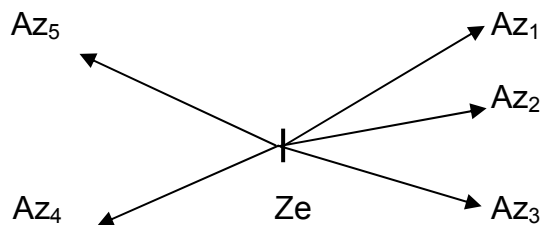


**Figure 3. Variants scheme.**

Source: Author study.

- It is calculated the left time until the moment of proceeding the observations thus:  $\Delta t = O_2 - O_1$ , where:  $O_2$  = the hour of the beginning of the measures,  $O_1$  = the hour of the moment of ending the preparations; then it is checked the weather forecast in order to see if this is favourable for proceeding the observations.

- It is calculated the height of the deck from which there will be made the observations or the height of the observatory eye (  $i$  ), from the sea level:  $i = hcp - T_p$ , where:  $hcp$  = the building height of the deck,  $T_p$  = the ship draught.

The proposed variants:  $V_1 = Az_1 + Az_3$ ,  $V_2 = Az_4 + Az_5$ ,  $V_3 = Az_1 + Az_2 + Az_3$ .

b). Proceeding the activities [1]. The determination of the astronomical point of the ship is done thus:

- At the time of the evening civil crepuscular, it is started the observation of the dome of heaven, in order to identify the chosen heavenly bodies.

- In the moment of their observation it is started the measurement of the height, simultaneously there are read: the medium time at Greenwich, in hours, minutes and seconds, the real route of the ship, the temperature, the pressure.

There are made calculations, determining the elements of the position lines.

- It is determined the point of the ship with the help of the lines of the height.

There are registered the values of the determined latitudes and longitudes, in the Board Diary.

-It is compared the astronomical point with the estimated one and there are analysed the differences.

c).The on-line training. In the Maritime University from Constantza it was created an astronomical group for students in 1995. In this group besides the speciality knowledge, the students were orientated towards the study of the astronomy and astronautics. A main aspect was represented by the creating a web site of the group on the internet (the address [www.cercastro.uv.ro](http://www.cercastro.uv.ro)). On this site there are found a series of useful information in the students training, from the syllabus of the course, the exercises and the navigation problems, the tests with variants of training and types of exam subjects, links towards different useful sites. For the training of the students and for the maintaining of the connections with those on the ship board, on the university site it was created a special page of the group. Through this page on the internet it will be accomplished the on-line training of the students and of the deck officers, but the students found in the university have also access on it. The way of organizing the connections is presented in the figure 4.

It is observed from the figure the fact that on the university server it is allocated a space for the page of the astronomy group. Through this page, there can be in touch the coordinate professor, the cadets and the students found in the country. Through the electronic computer of the astronomical group, the coordinate professor keeps in touch with the cadets or the students found in the country. On this computer there are installed the astronomical navigation programs and the data basis with the students from each year who attend or attended the theoretical course of astronomical navigation. These are the students from the II-nd year, the III-rd year and the IV-th year, because the students from the I-st year are not still familiarized with the basis notions of the astronomical navigation. The program is especially addressed to the III-rd and the IV-th year students found in the training voyage [11], but there can also take part into it the graduated students, cadet or found in the country. It is observed the fact that the connections are maintained through the internet, but in certain situations the cadet can call, using the mobile phone, the coordinate professor in order to get diverse information or even the help for training. The working program of the coordinate professor will be posted on the group page and this will be the time of the place, of the Constantza city, and the students found in long distance will calculate the time according to the medium time at Greenwich and the difference of the time zone.

The cadet, figure 5, will work in the following way: he will prepare the astronomical observations taking into account the algorithm, he will make the identification and then the measurement of the height of the heavenly bodies. After accomplishing these operations he will introduce the obtained data on the computer and he will obtain the astronomical point of the ship. If the error between the astronomical point and that read from GPS is bigger than  $\pm 3$  Mm, then this will make again the measurements and will introduce the data in the computer again. Both types of data he will send through e-mail in the data basis of the astronomical group. The coordinate professor will check the obtained data and he will send his observations to the cadet. The other students will be able to access the data basis and will observe the working way, the obtained values, the precision of determination of the astronomical point of the ship, after that they will be able to send their observations. The

cadet can present his results to the ship captain, to the first officer and to the other deck officers. These can offer him the support for improvement the measurement method of the height of the heavenly bodies, measuring in the same time with him the height of the heavenly bodies and then making comparison with the obtained results. The student is obliged through the training program to fill in a training notebook the IMO type [11], and in this notebook he will write all the obtained data, including the determination scheme of the ship point. The coordinate professor will receive by e-mail all the initial data and the final ones which he will introduce in the data basis of the astronomical group and which from that moment they can be accessed by each student. Then the professor on the same type of calculation programs will make the checking of the received data and according to the results he will send his response to the student. In the same way there can do the students found in the country who can ask further information or can send their own observations. Including these observations will be sent simultaneously in the data basis. In this way there is the possibility of feed-back of the cadet training and even of those who attend courses or are in holiday. The problems which can appear in this way of working are connected with the permanent functioning of the university server, of the board computer and of the general functioning of the internet. A problem is represented by the costs connected to the internet access at the ship board and to the communications using the mobile phones. These costs have still small values comparing to the benefits of the students training, of their improvement in this way.

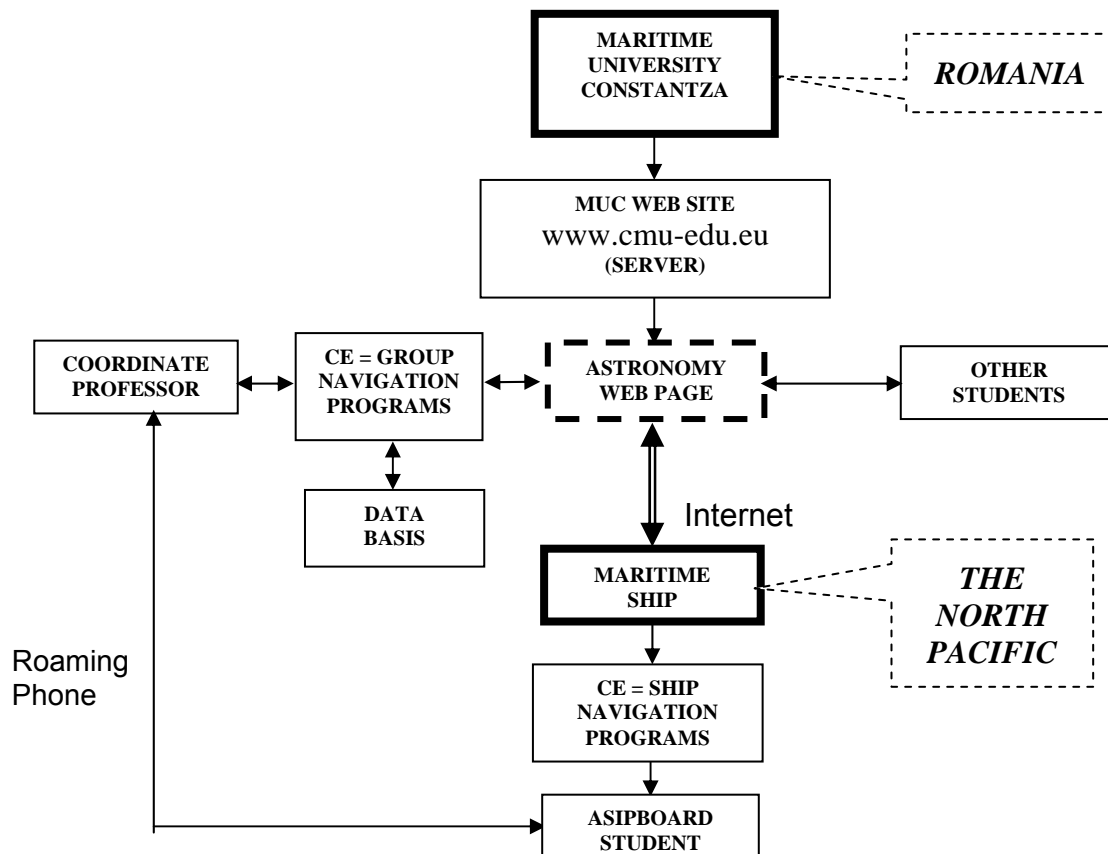


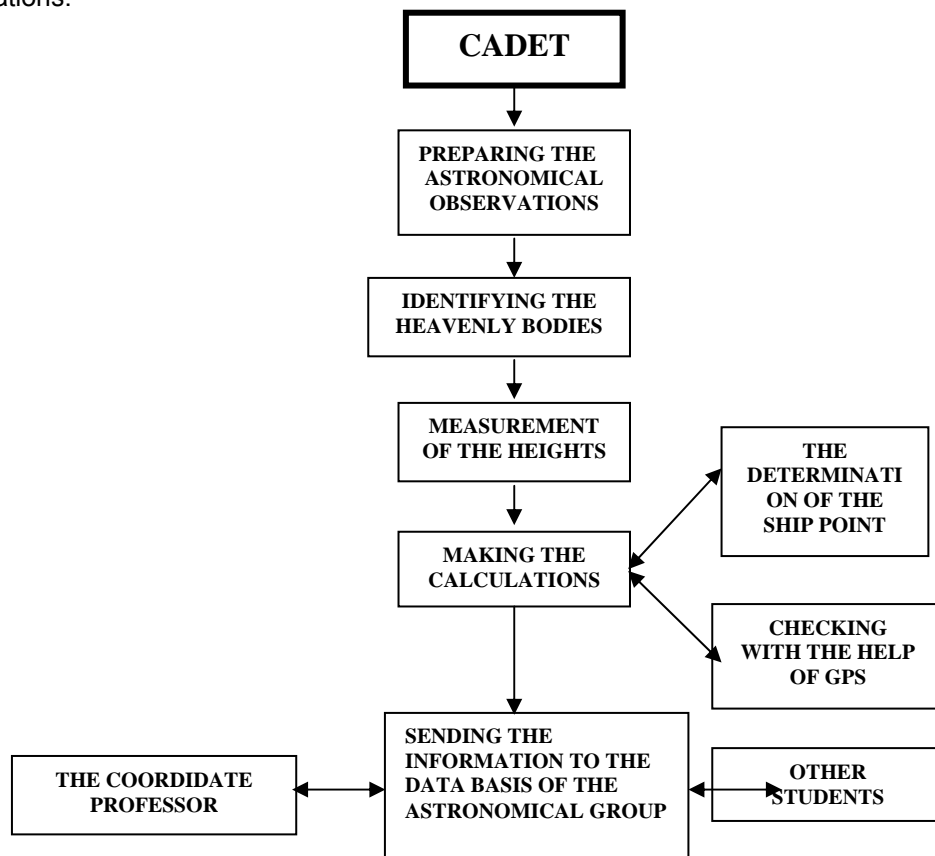
**Figure 4. The organization of the connections with the students.**  
 Source: The author's study, original

Legend:

- CE GROUP = the electronic computer of the group, with astronomical navigation programs
- CE SHIP = the electronic computer of the maritime ship
- MUC = Maritime University of Constanta.

## 6. CONCLUSIONS

The on-line training at the astronomical navigation has the following advantages: it helps the student found in the long distance from the university to be in touch with the speciality professors through an inter-active internet page; all his data can be checked and corrected by the coordinate professor and by his colleagues; it reduces very much the necessary time for the determination of the astronomical ship point through the classical calculations methods; it helps the student to get trust in his own forces necessary for the leading of a maritime ship. For students who still don't leave for the speciality training on the sea it has the advantage that these can see what their colleagues found on the sea are doing, they can use the data obtained by them for their theoretical training, for making the course projects and improving the speciality training. The coordinate professors will be able to follow in this way from the distance the students' activity and even to communicate with them for solving the problems connected to their training, which can appear on the ship board. On the basis of this program it appears for the first time in a university from Romania a modern method of training and education from the distance, with the help of the internet and of the mobile communications.



## REFERENCES

- [1] Iordanoaia F. ***Astronomy and Celestial Navigation***, „Nautica” Edition, Constanta, 2004.
- [2] Admiralty List of Radio Signals Volume 2, 1995, the Hydrographer of the Navy, Taunton, Somerset, USA, 1995.
- [3] Bridge Watchkeeping A Practical Guide, the Nautical Institute, O'Sullivan Printing Corporation, London, 1994.
- [4] Bridge Procedures Guide, International Chamber of Shipping, Witherby & Co. Ltd, London, 1990, 1998.
- [5] Brown's Nautical Almanac, Brown, Son & Ferguson Ltd, Glasgow, 2006, 2007.
- [6] Ephemerides Nautiques, Edinautic, Paris, 2002.
- [7] Guide du Navigateur, Service Hydrographique et Oceanographique de la Marine, Paris, 1992.
- [8] International Convention for the Safety of Life at Sea Solas-1974, Romanian Register of the Ships, Bucharest, 1995, 1997.
- [9] International Safety Management Code, I.M.O, London, 2002.
- [10] Sight Reduction Table, Hydrographic Department, Taunton, U.S.A., 1994.
- [11] S.T.C.W. - Standards of Training, Certification and Watchkeeping, London, 1978, 1995.
- [12] Symbols and Abbreviations, Hydrographic Department, Taunton, U.S.A., 1995.
- [13] The American Practical Navigator. Bowditch, Defense Mapping Agency Hydrographic/Topographic Center, Bethesda, U.S.A., 1995.
- [14] The Nautical Almanac, Her Majesty's Nautical Almanac Office, Aberdeen, UK, 2002.
- [15] <http://www.almanac.com/rise/>
- [16] <http://www.cybersky.com/>
- [17] <http://www.esa.net/>
- [18] <http://www.nasa.gov/vision/universe/stargalaxies/index.html>.
- [19] <http://www.sightmaster.com/>
- [20] <http://www.skyglobe.com/>
- [21] <http://www.skychart3.com/>
- [22] <http://www.skymap.com/>
- [23] <http://www.spacebox.org/>
- [24] <http://www.wfu.edu/~anderson/astronomy/labs/skyglobe.doc/>

## MULTISTATIC SONAR PULSE SIGNALS TIME DELAY ESTIMATION

<sup>1</sup>KOLEV N. ZH., <sup>1</sup>IVANOV P. VL., <sup>1</sup>KALOYANCHEV P., ST.

*Naval Academy – Varna, Bulgaria*

An application of a multistatic sonar concept is presented. Signal excess areas were simulated for a given configuration of one active source and two passive receivers for different sonar, target and sound speed profile parameters. Time delay estimation algorithm based on convolution in frequency domain is developed. Experimental results are given with real sonar measurements and time delay estimation in test tank and at sea trial.

**Keywords:** multistatic sonar, time delay estimation, digital signal processing

### 1. THE MULTISTATIC SONAR CONCEPT

In the beginning of sonar systems development the needed sonar range is acquired with powerful sources and monostatic systems. An increased sonar detection range with more power is not always the best solution in modern systems. An alternative way for increasing the range is proposed with the multistatic sonar concept which draws its origin from passive sonobuoys introduced during the second world war. It is based on area distributed or line arranged sensors forming a network [2]. Tactical scenario of a contemporary multistatic underwater surveillance system is shown on Fig.1.

In a multistatic system theoretically with less power the signal excess formulas give the same area as with more powerful monostatic source for the sake of distributed sensor area extension [2]. One or more buoys are active sources (actuators for the detection process) of sound waveforms with specific parameters. The target reflected signal is received by passive buoys under constant reverberation and noise fields. The adaptive depth positioning, sound propagation model based algorithms and coherent signal processing can increase total signal to noise ratio.

Critical technology parameters according to MTCL<sup>1</sup> is “Real-time processing of acoustic data from fixed, deployed or mobile arrays operating in the bi-static or multi-static mode to increase target signal-to-noise ratio by over 6 dB in order to increase detection range by over 10%, increase probability of correct decisions and reduce false alarms.”

---

<sup>1</sup> MILITARILY CRITICAL TECHNOLOGIES LIST, MCTL DATA SHEET 11.5-2. SIGNAL AND DATA PROCESSING FOR MULTI-SENSORS AND MULTI-PLATFORMS

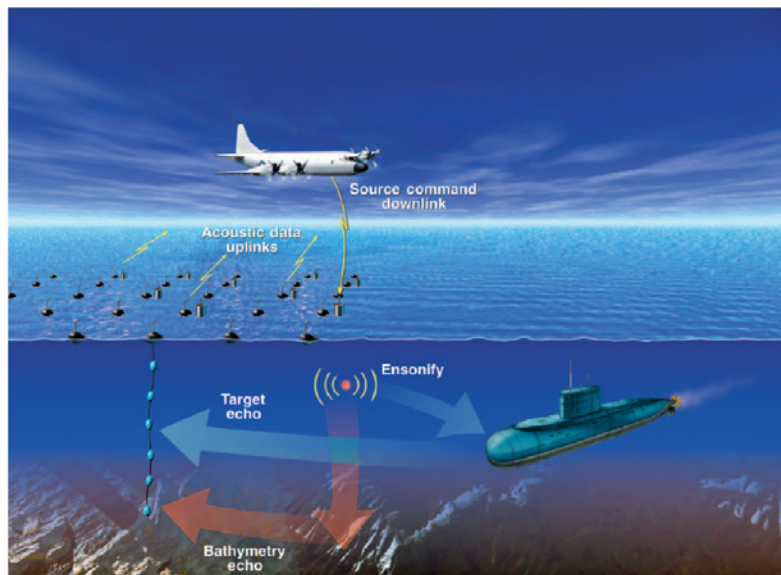


**Fig. 1. Tactical scenario of a multistatic underwater surveillance system [3].**

A preliminary concept is developed at the academy of a minimal multistatic system which is investigated partially – Fig.2. The minimal multistatic sensor network has the following components:

- Active sonar source comprising sensor node with power amplifier and transducer;
- Sensor node end devices comprising hydrophones and receivers;
- Computer with access point sensor node and software for sensor network control;
- The system if fixed at the bottom of the sea or a ship hull or a pier.

Simulated signal excess areas of a multistatic system with one active and two passive nodes are given on Fig.3. They are simulated for different sound speed profile, given active node signal parameters, channel depth and configuration.

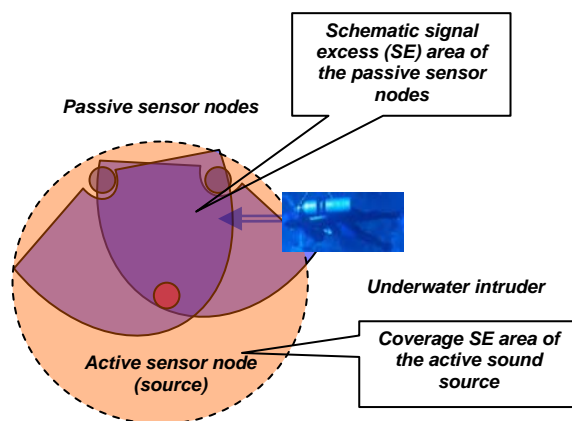


**Fig. 2. A multistatic system for diver detection - schematic concept.**

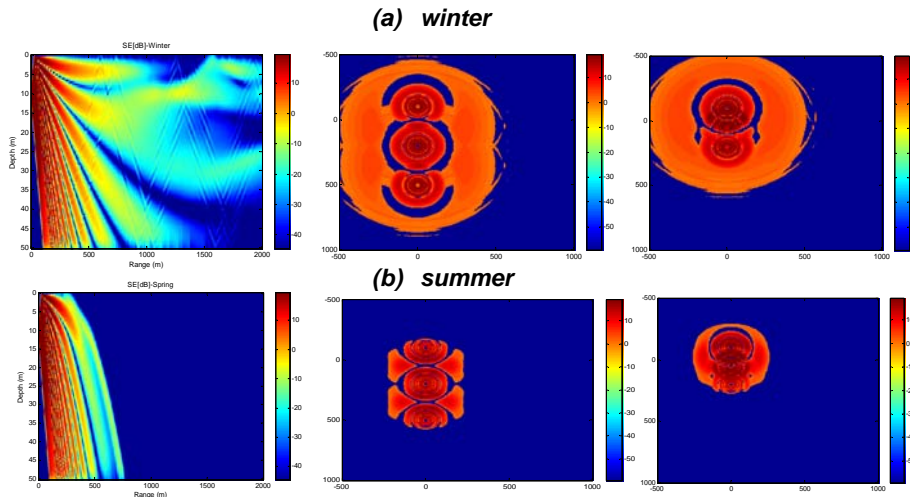


**Fig.3. Modeled signal excess for winter (a) and summer (b) sound speed profiles for one active source (center and end positioned) and two passive receiving nodes.**

At the moment investigations are going on at the naval academy for establishing the feasibility of the multistatic concept for detection of underwater moving objects in shallow waters. It is closely related with modern sensor network concept. In active multistatic sonar systems a source transducer ensonifies the area of the target and distributed hydrophones (End Nodes) receive and coherently process the scattered signals. After that preprocessed and compressed signals from receiver nodes is transferred to cluster unit (Access Point) where association, target racking and classification is applied. In this case it is expected that the performance of the distributed sonar system will be improved due to the increased signal to noise ratio in consequence of possible coherent signal processing in the distributed sonar.

## 2. IMPULSIVE SONAR SIGNALS TIME DELAY ESTIMATION

Impulsive sonar signals time delay estimation (TDE) is needed for underwater objects localization in active monostatic and multistatic sonar systems. Shallow waters are rich of ambient noise and replicas of the emitted signal caused by surface and bottom reverberation. This implies some difficulties in the detection of the signals. One of the main tasks in these sonar systems is time delay estimation of signals at different receivers. In order to process signals and to do TDE in a wireless system the problems of time synchronization and precise positioning of nodes have to be solved.

If  $S_1(t)$  is the source signal in time domain,  $n_1(t)$  and  $n_2(t)$  are additive independent noise components, then the expressions for signals at the two distant receiver nodes are:

$$\begin{aligned} x_1(t) &= s_1(t) + n_1(t) \\ x_2(t) &= as_2(t - t_D) + n_2(t) \end{aligned} \quad (1)$$

Where  $t_D$  - time delay between the two signals due to difference in positions.

For automatic measurement of TDE it is possible to use convolution (cross correlation) in the time or frequency domain (2). At the output of this function there is maximum for discrete offset corresponding to discrete TDE between the two signals.

$$x_1 \otimes x_2 = \sum_{m=0}^{N-1} x_1(m)x_2(n-m) \quad (2)$$

Implications arise in case of surface and bottom reverberation (Fig. 4).

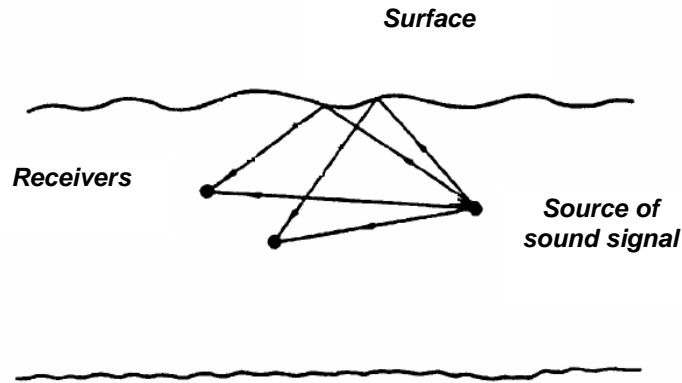


Fig. 4. Direct and surface reflected beams.

### 3. EXPERIMENTAL RESULTS

For multistatic system concept performance evaluations and TDE several experiments were carried out at BU naval academy test tank and also at sea.

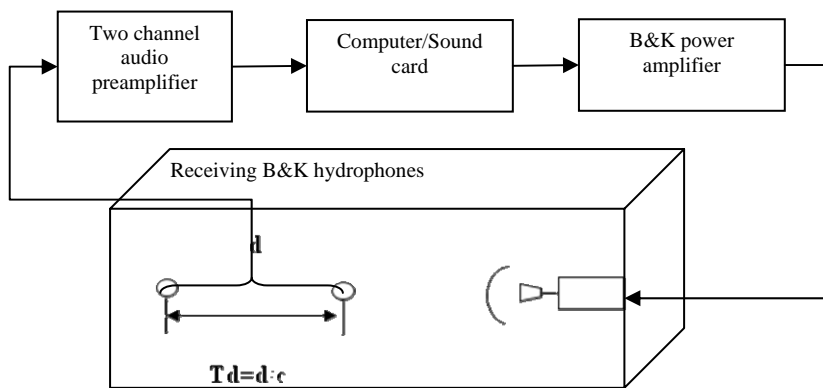
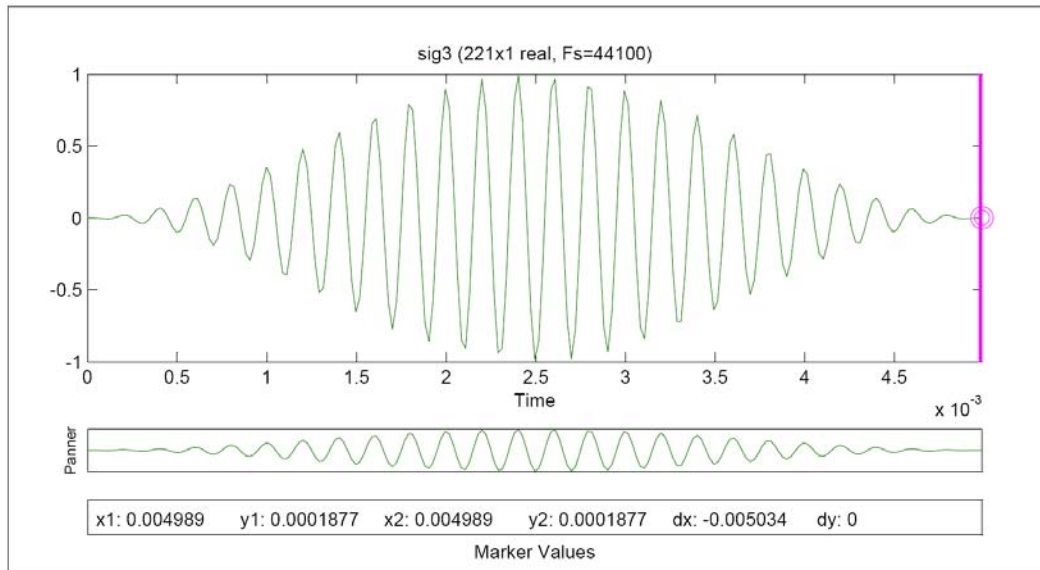
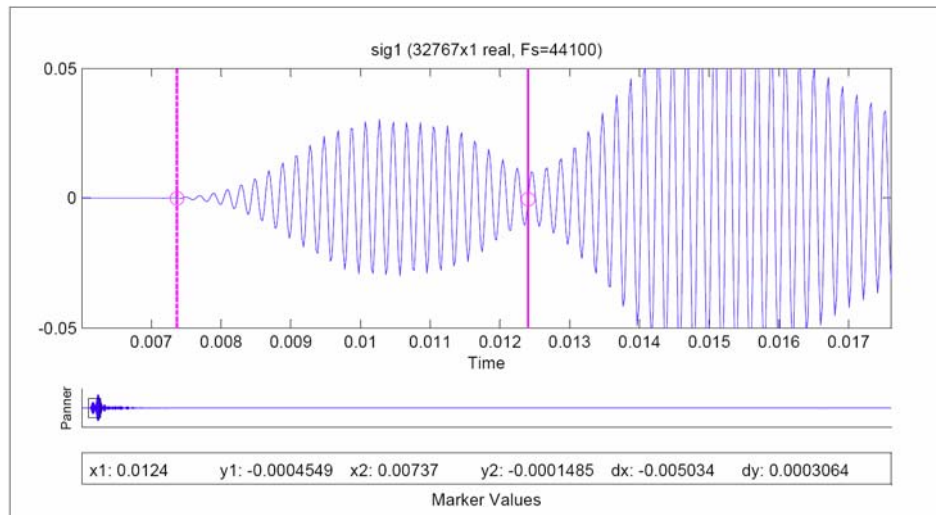


Fig. 5. Test tank experimental setup.



**Fig. 6. Synthesized and transmitted signal waveform with parameters – frequency  $F=5$  KHz and pulse width –  $T_i = 5$  ms. The signal is sampled at the output of the power amplifie with frequency  $F_s=44100$  Hz.**

On Fig.7 the received signals from the two hydrophones are shown. The hydrophone which is near to the source receives the signal  $X_1(t)$  in the time frame 0.0075 s - 0.0125 s . The signal at the second hydrophone  $X_2(t)$  is received 1 ms after ensonification of the first hydrophone in consequence of the distance between hydrophones –  $d$ . This TDE corresponds to the real distance between the two hydrophones which is 1,5 m.



**Fig. 7 (a).**

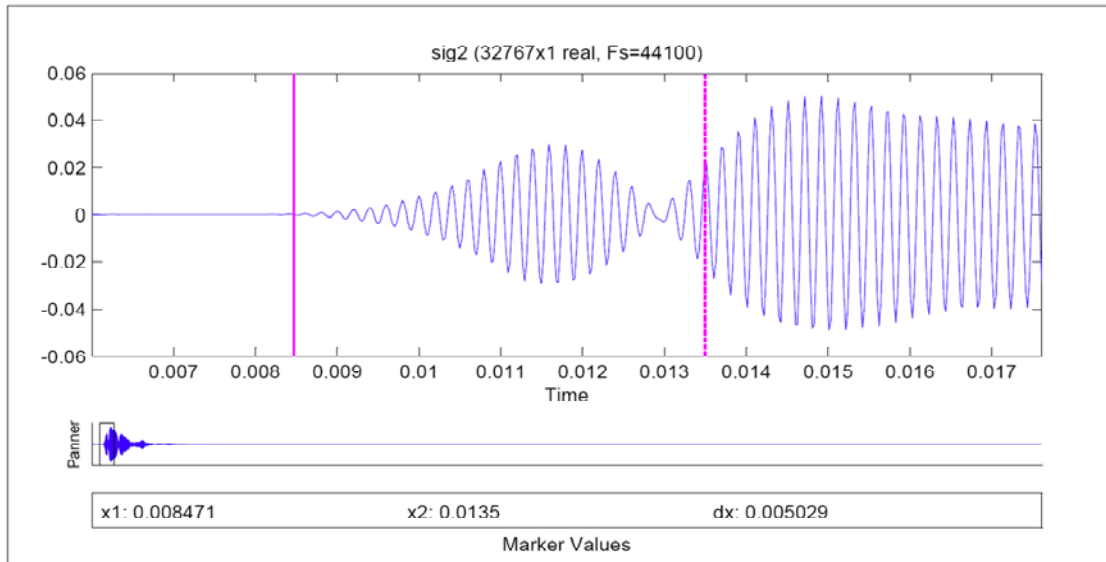


**Fig. 7 (b). Analysis of received short sound waveforms which shows possibility for separation of direct and reflected test tank signals and TDE – (a) - signal at first hydrophone; (b) – signal at second hydrophone.**

On the 19 and 20-th of august 2008 a sea trial took place near the island of St. Anastasia.



**Fig. 8. Island of St Anastasia during the experiment.**

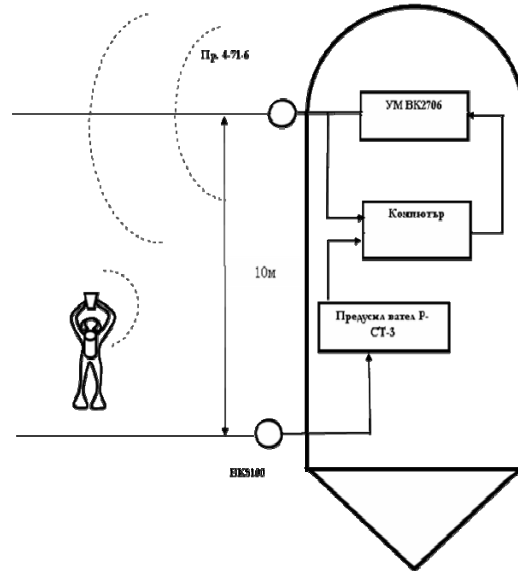
The aims of the bistatic experiment for diver detection were:

- Bistatic tests in passive and active mode;

- Synchronized non directional sound waveform generation and data storage with hydrophone on a given distance from the source;

The following types of signals were used in active mode:

- Simple pulse;



- LFM pulse;
- CW.
- Initial signal database forming;
- Database signals digital signal processing and parameters estimation.

Schematic of the experimental set up is given on Fig. 7. Some results are given on Figs 8-11.

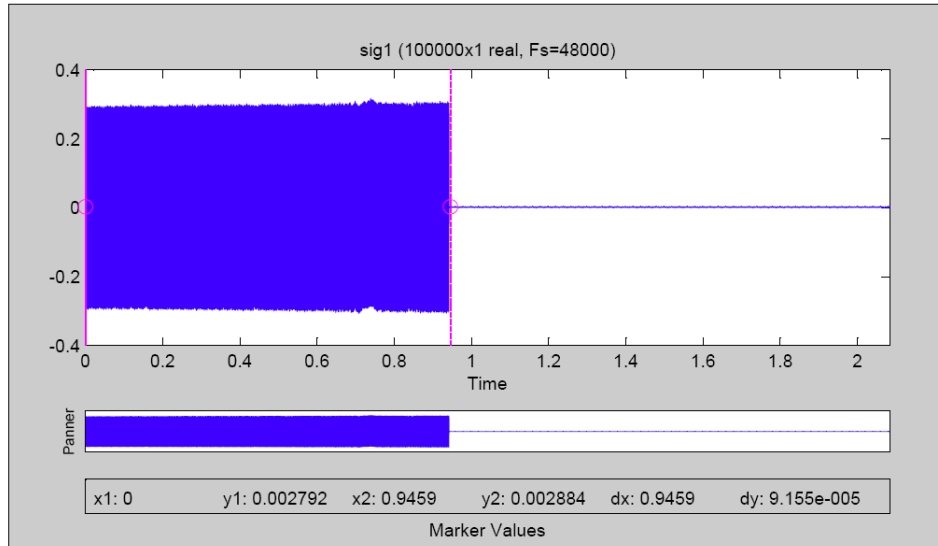


**Fig. 10 (a).**

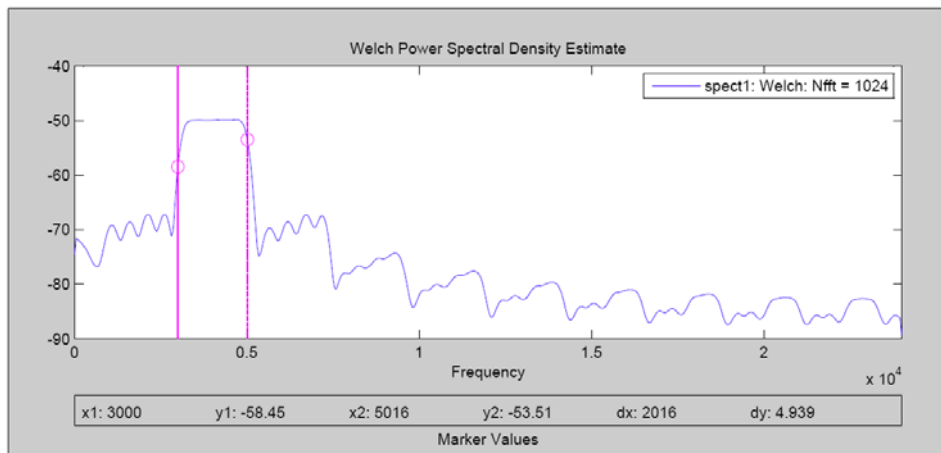


**Fig. 10 (b).**

**Fig. 10. Synthesized LFM pulse with bandwidth (3000 – 5000 Hz) and duration 1 s, sampled at the output of the power amplifier - (a). Estimation of power spectrum - (b).**

The preliminary signal processing of the received signal includes digital filter bandpass filtering which is needed to lower different noises (Fig. 12) .

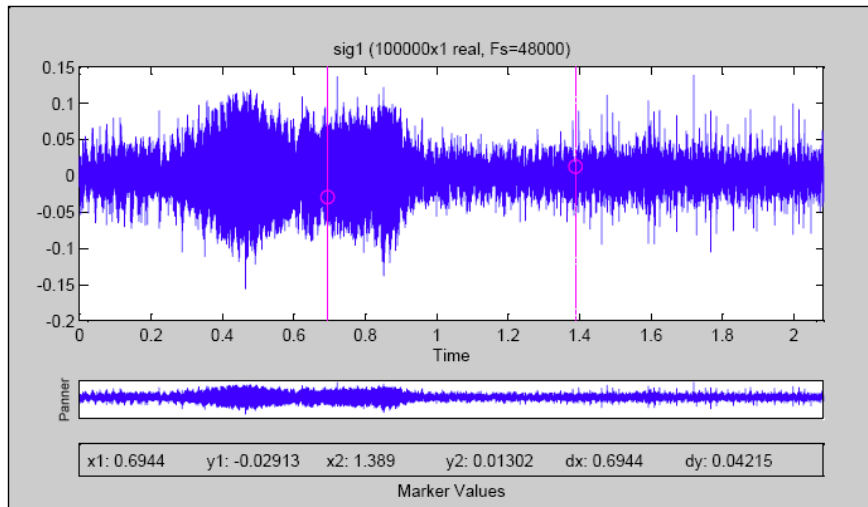


*Fig. 11 (a).*

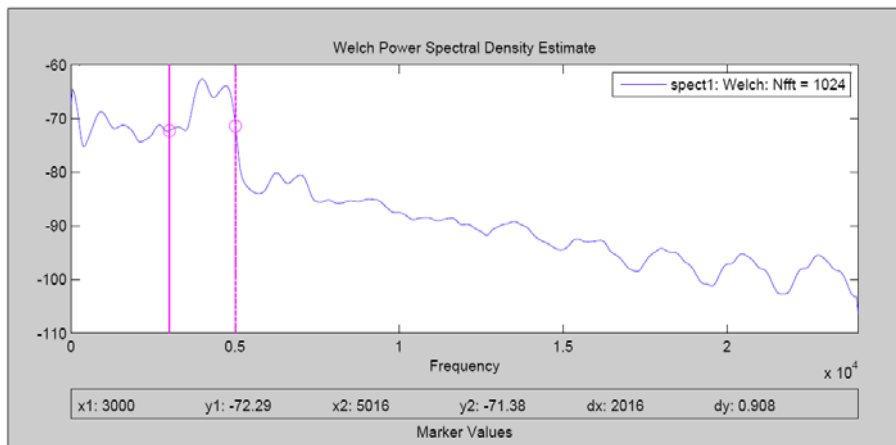


*Fig. 11 (b).*

**Fig. 11. LFM sampled pulse at the hydrophone after preamplification:  
 (a) – time domain waveform;  
 (b) – power spectrum estimation.**

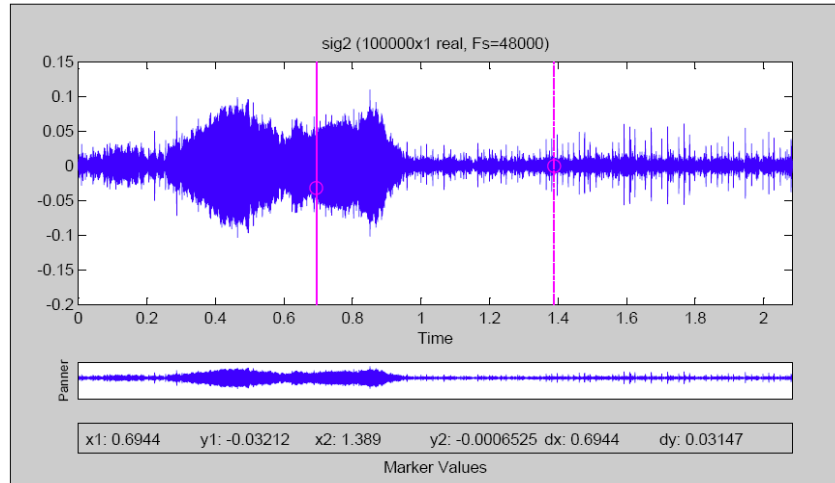


*Fig. 12 (a).*

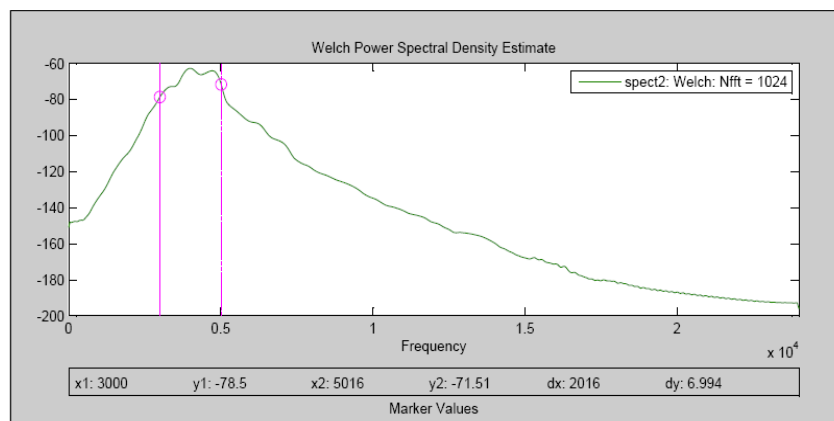


*Fig. 12 (b).*

**Fig. 12. LFM sampled pulse after band pass filtering:  
(a) – time domain waveform;  
(b) – power spectrum estimation.**

In Fig. 13 are shown transmitted and received signals sampled synchronously respectively at the output of the power amplifier and at the hydrophone.

The MATLAB algorithm for TDE by means of cross spectrum processing is given on Fig. 14.

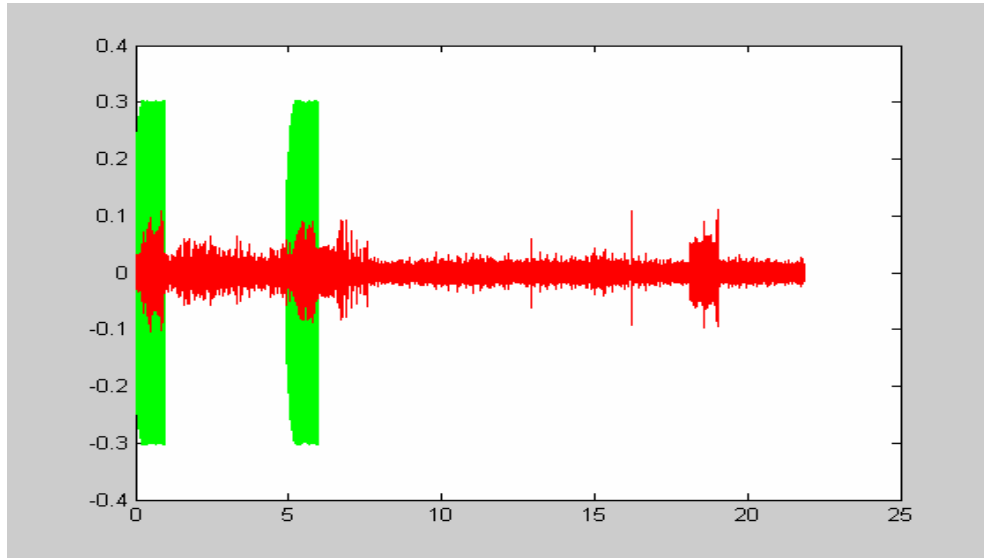


**Fig. 13. Waveforms in time domain of two consecutive transmitted (green) and received (red) LFM pulses.**

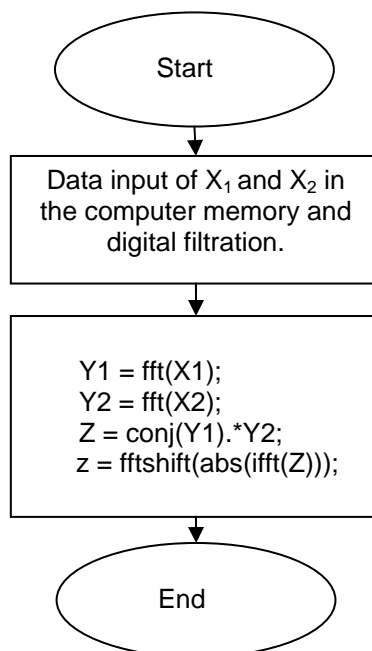


**Fig. 14. A Matlab algorithm for optimal processing.**

The first peak is due to the direct pulse signal and corresponds to distance between the transducer and hydrophone – 10 m. The other peaks are due to reflected beams from sea surface and bottom- Fig. 15.

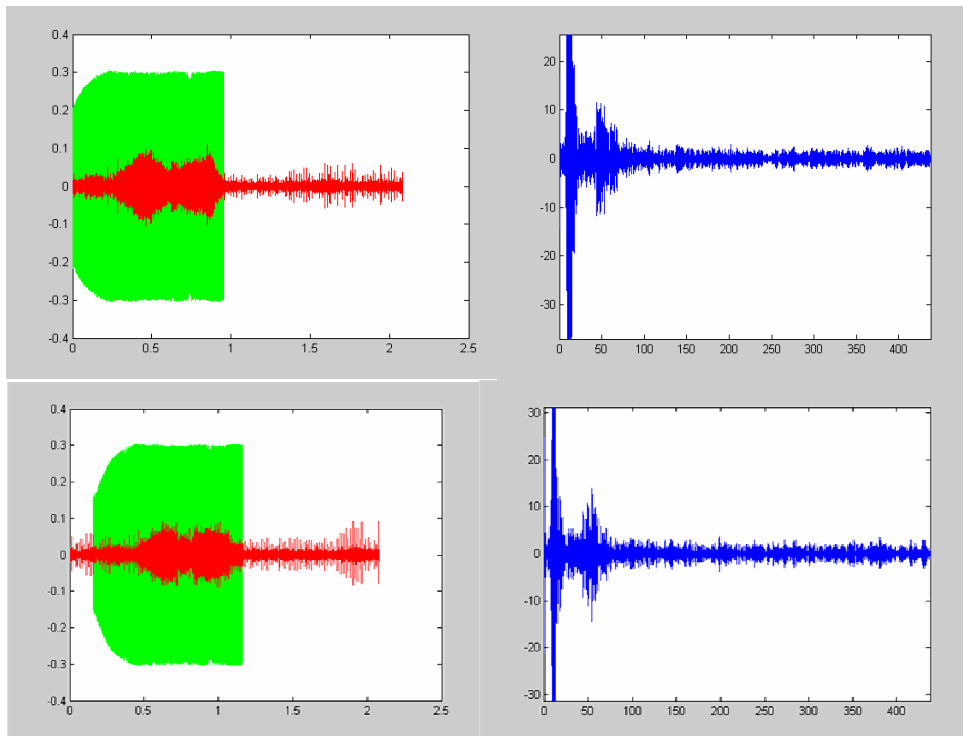


**Fig. 15. Optimal signal processing of the first and the second LFM pulses.**

#### 4. CONCLUSIONS

1. Time delay estimation is key factor for signal processing and target position estimation of underwater objects in monostatic and multistatic sonar systems.

2. In real sea shallow water conditions there are numerous reflected signals due to surface and bottom reverberation which implicates signal processing and TDE.

3. TDE experimental trials are useful for further understanding and pointing out the most important shallow water, sonar and transducer parameters influencing signal detection and towards improving signal processing algorithms and especially dereverberation.

4. There is a need for precise channel impulse response modeling and taking into account in the models of the transducer pattern and depth in the water column.

#### REFERENCES

- [1]. Coon A., *Spatial Correlation of Detections for Impulsive Echo Ranging Sonar. Johns Hopkins APL Technical Digest*, Volume 18, Number 1, 1997
- [2] Kolev N., Kaloyanchev P., Iliev I. *A concept for underwater port protection. Conference "Port protection", Sofia, 2008.*
- [3] Pihl J., Dalberg E., Hegethorn J., Ivansson S., et al. *Multistatic Sonar for Shallow Water Surveillance. Methodology Report. FOA Defense research establishment.* ISSN 1104-9154. 2000.

## THERMODYNAMIC AND ECOLOGICAL ANALYSIS OF INTERNAL COMBUSTION ENGINES

MEMET FEIZA

*Constanta Maritime University, Romania*

Ships are important air pollution sources since their high powered main engines often use heavy fuels. Internal combustion engines are widely used in the shipping sector. Shipping emissions cause significant effects on the environment.

In this paper is made an analysis of the thermodynamic efficiency of the Otto Cycle. The eco analysis is made by introducing the efficiencies under maximum power conditions and maximum ecological conditions, and also the heats rejected to the environment under these conditions.

**Keywords:** engine, cycle, efficiency, environment

### 1. INTRODUCTION

Internal combustion engines are equipments largely used by transportation sector. Emission reduction is an essential problem of this sector having in view that considerable contribution to the total emission of toxic substances falls to transportation.

The energy efficiency of internal combustion engines is not higher than thermal efficiency of the ideal engine working after the Carnot cycle. New designs of internal combustion engines are related to some issues like:

- emission of pollutants in the environment,
- efficiency of energy conversion processes occurring in the engine,
- reliability and correctness of the used working system.

The best of the cycles from a thermodynamic point of view is the Carnot cycle. It includes two isotherms and two isentropes. The Carnot cycle efficiency is an ideal one. No other cycle is able to equalize it for the same minimum and maximum temperatures.

Toxic constituents of the exhaust gas are known as exhaust emissions. The exhaust gases from internal combustion engines contain chemical substances which have a negative impact on the environment in the form of acidification, ozone formation, carcinogenic emissions etc.

In the last years is registered an intensive concern regarding effects of emissions from shipping. The Kyoto Protocol imposed measures for CO<sub>2</sub> reduction and other greenhouse gases (GHG). Among GHG, CO<sub>2</sub> is the most prevalent, that is why reduction emissions policies focus on this pollutant, since the climate change threatens life in many ways. This pressure made IMO to urge the Marine Environment Protection Committee (MEPC) to initiate a tool for the assessment of the GHG efficiency of ships in terms of GHG emission index (Koutovas and Psaraftis, 2009).

The most important method of CO<sub>2</sub> emissions reduction consists in the use diminishing [Kim et al, 2002]. The overall evaluation of energy savings and CO<sub>2</sub> emission reduction might be done in the following steps:

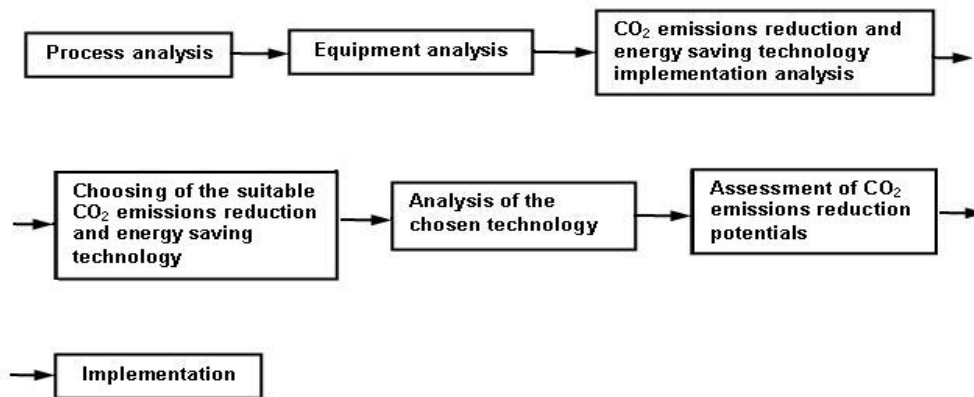


**Fig. 1. Evaluation of CO<sub>2</sub> emissions reduction and energy saving technology**

## 2. CYCLE ANALYSIS

The theoretical cycle of internal combustion engines is the Eichelberg cycle, where the combustion process happens during three transformations: isochoric, isobaric and isothermal.

Heat supplying during the Eichelberg cycle is given by the sum of the three components developed isochorically (2–3), isobarically (3–4) and isothermally (4–1), as seen in Figure 2.

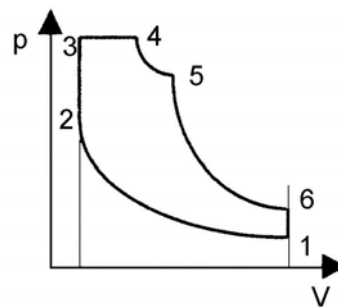


**Fig. 2. Eichelberg cycle**

$$Q_d = Q_{d,v} + Q_{d,p} + Q_{d,T} \quad (1)$$

The efficiency of the cycle is given by:

$$\eta = \frac{Q_d - Q_w}{Q_d} \quad (2)$$

where  $Q_w$  is the heat output, realized once and isochorically (6-1).

The efficiency of Eichelberg cycle results as:

$$\eta_E = \frac{c_v(T_3 - T_2) + c_p(T_4 - T_3) + RT_4 \ln \frac{V_5}{V_4} - c_v(T_6 - T_1)}{c_v(T_3 - T_2) + c_p(T_4 - T_3) + RT_4 \ln \frac{V_5}{V_4}} \quad (3)$$

By introducing the parameters: pressure ratio, volume ratio and combustion degree,  $\gamma, \varphi, \delta$ , and also using thermodynamical equations of specific heat capacity at constant pressure and individual gas constant, is obtain an other form of the Eichelberg cycle efficiency.

$$\gamma = \frac{P_3}{P_2} \quad (4)$$

$$\varphi = \frac{V_4}{V_3} \quad (5)$$

$$\delta = \frac{V_5}{V_4} \quad (6)$$

$$c_p = k \cdot c_v, \text{ J/(kg}\cdot\text{K)} \quad (7)$$

$$R = c_v(k - 1), \text{ J/(kg}\cdot\text{K)} \quad (8)$$

$$\eta_E = 1 - \frac{\gamma \varphi^k \delta^{k-1} - 1}{\varepsilon^{k-1} \{(\gamma - 1) + \gamma [k(\varphi - 1) + \varphi(k - 1) \ln \delta]\}} \quad (9)$$

where:

$k$  – isentropic ratio,

$c_v$  – specific heat capacity at constant volume, J/(kgK),

$\varepsilon$  – compression ratio.

The theoretical cycle for spark ignition engine (Otto) is presented in Figure 3. Its efficiency is obtained by making in equation (9)  $\varphi = 1$  and  $\delta = 1$ :

$$\eta_0 = 1 - \frac{1}{\varepsilon^{k-1}} \quad (10)$$

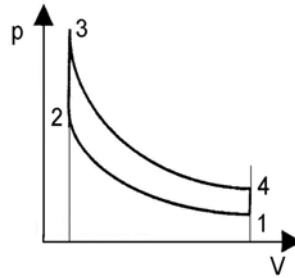


Fig. 3. Otto cycle

For the maximum compression ratio,  $\varepsilon_{max}$ , Otto cycle efficiency becomes equal to the Carnot cycle efficiency,  $\eta_c$ .

$$\eta_c = 1 - \frac{T_1}{T_5} = 1 - \frac{1}{\varphi \cdot \gamma \cdot \varepsilon^{k-1}} \quad (11)$$

Unlike the efficiencies of other internal combustion engines, the Otto cycle efficiency depends only on the compression ratio, some values being given in Table 1.

Table 1: Relation  $\eta_0 - \varepsilon$

$\varepsilon$	$\eta_0$
8	0,565
10	0,598
12	0,633
14	0,658
16	0,673
18	0,678
20	0,694
22	0,716
24	0,719
26	0,728

### 3. ECOLOGICAL ANALYSIS

The amount of heat rejected to the environment,  $Q_w$ , is proportional with  $CO_2$  emissions to the atmosphere. Thus, by using the Novikov model, it is possible to make work the engine in a more environmental way.

The Novikov model depicted below consists in a high temperature reservoir of  $T_h=const$ , a low temperature reservoir of  $T_l=const$ , a reversible Carnot engine with a hot isotherm of  $T=const$  and a thermal conductor of conductance  $g$ .

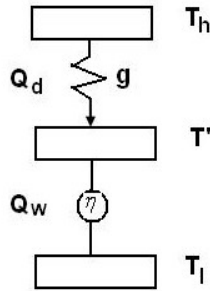


**Fig. 4. The Novikov model**

The heat rejected to the environment by the Otto engine at maximum power conditions,  $Q_W^{MP}$  and the one at maximum ecological conditions,  $Q_W^{ME}$  are given by:

$$Q_W^{MP} = gT_h(1 - \eta_{MP}) \left( 1 - \frac{T}{1 - \eta_{MP}} \right) \quad (12)$$

$$Q_W^{ME} = gT_h(1 - \eta_{ME}) \left( 1 - \frac{T}{1 - \eta_{ME}} \right) \quad (13)$$

where:

$\eta_{MP}/\eta_{ME}$  – efficiency at maximum power conditions / maximum ecological conditions,

$T$  – temperature ratio,  $T = \frac{T_l}{T_h}$ .

Efficiency are calculated as:

$$\eta_{MP} = 1 - \frac{f}{2}T - \frac{\sqrt{4(1-f)T + f^2T^2}}{2} \quad (14)$$

$$\eta_{ME} = 1 - \frac{f}{2}T - \frac{\sqrt{(1-f)T^{1,5} + f^2T^2}}{2} \quad (15)$$

In the above equations,  $f$  is the fractional fuel cost which depends on  $a$  and  $b$ , both measured in E/Joule:

$$f = \frac{\frac{a}{b} \left( 1 - \frac{T}{1 - \eta} \right)}{\left[ (1 - T) + \frac{a}{b} \left( 1 - \frac{T}{1 - \eta} \right) \right]} \quad (16)$$

The fuel fractional cost is given by the ratio between the cost of the fossil fuel and the cost of the engine. It is possible to get the heat rejected to the environment for different values of the function  $f$ .

In table 2 are seen some values of the efficiencies at maximum power conditions at maximum ecological conditions for same values of the function  $f$ .

**Table 2: Efficiencies under maximum power and ecological conditions**

$f$	$\eta_{MP}$	$\eta_{ME}$
0,1	0,288	0,414
0,2	0,309	0,420
0,3	0,327	0,422
0,4	0,344	0,426
0,5	0,348	0,434
0,6	0,356	0,440
0,7	0,372	0,444
0,8	0,378	0,465
0,9	0,407	0,478
1	0,500	0,500

For given values of the fuel fractional cost are obtained better efficiencies under ecological conditions. In these terms, the heat rejected to the environment is reduced in about 53% compared to the maximum power regime. CO<sub>2</sub> emissions related to the fossil fuel consumption must be connected to the performance of the engine operating in the two mentioned conditions.

#### 4. CONCLUSIONS

From the thermodynamic point of view the optimum cycle is Carnot cycle. Referring to the Otto cycle, the same efficiency as the Carnot cycle is reached for the maximum value of the compression ratio. This situation may occur only theoretically having in view the restrictions related to the inflammability of the air-fuel mixture and limits of the material.

The ecological analysis is imposed by the considerable contribution to the total emission of toxic substances emitted to the atmosphere by the maritime transport activity.

Was focused the heat rejected by the Otto engine. Were found better values of efficiencies at maximum ecological conditions that the ones at maximum power conditions. The heat rejected is diminished with 53% compared to the maximum power regime. Was assumed that this energy is directly proportional to CO<sub>2</sub> emissions.

#### REFERENCES

- [1]. Barranco-Jimenez M.A., Angulo-Brown F. – **Possible future scenarios for CO<sub>2</sub> atmospheric concentration: A thermodynamic approach**, Proc. of ECOS 2007, vol. I, pp. 659-666, June 25-28, 2007, Padova, Italy
- [2]. Kim H.Y., Park Y.G., Park M.H. – **Establishing the evaluation method for CO<sub>2</sub> emission reduction potentials in the industrial sector in Korea**, Proc. of ECOS 2002, vol. II, pp. 1272-1279, July 3-5, 2002, Berlin, Germany
- [3]. Kontovas C.A., Psaraftis H.N. – **On line ship emissions calculator as a decision making aid and policy evaluation tool**, Proc. of IMAM, vol. III, pp. 867-874, October 12-15, 2009, Istanbul, Turkey
- [4]. Postrzednik S., Zmudka Z. – **Advanced thermodynamic cycle of internal eco-engine**, Proc. of 28<sup>th</sup> International Symposium on Combustion, 2000, Edinburgh, Scotland

## A POINT OF VIEW ON THE REGASIFICATION OF LNG

MEMET FEIZA

*Constanta Maritime University, Romania*

LNG business started in the '60s and since then evolved quite fast. The high natural gas demand the existence of receiving terminals. The most significant function of a terminal is the LNG conversion through the vaporization process. In the last years, improvements of the LNG technology focused on the liquefaction process and shipping.

This paper deals with the regasification of LNG, which traditionally is done by taking heat from the sea water. Is analysed how the integration of the cryogenic heat sink in the situation of a  $H_2/O_2$  cycle affects the exergy efficiency.

**Keywords:** LNG, regasification, cryogenic, exergy efficiency

### 1. INTRODUCTION

The need of natural gas seems to be the fastest growing energy source over the next two decades. Worldwide natural gas consumption is expected to grow with an average rate of 2,4%/year starting with 2003 till 2030.

The significant role of natural gas as a primary fuel in the international energy sector justifies the massive shipping of this fuel.

The transport of natural gas on board the ship is mainly in the form of Liquefied Natural Gas (LNG), specialized vessels being known as LNG carriers. These are equipped with cryogenic tanks.

Having in view the last trends of fuel market, the focus on environmental issues and the existence of natural gas reservoirs in places where the construction of land gas pipelines is impossible, the LNG shipping sector is in development.

The interest for LNG marine transport result in the increase registered in LNG carriers orders. New LNG vessels are designed for major cargo capacities, like about 200 000 m<sup>3</sup>, and speeds of over 20 knots.

Natural gas demand imposes the existence of receiving terminals. The key activity on an import terminal is the regasification of LNG.

For LNG preparation is consumed power for compression and liquefaction, while an important portion is preserved as cryogenic exergy in LNG, which has a final temperature of about 110 K, significant under the one of environment or seawater.

LNG vessels have not refrigerating plants on board. The natural gas is preserved in liquid form by the thick insulation of their cryogenic cargo tanks.

LNG is shipped using insulated tankers till receiving terminals. Here is off loaded and pumped to a definite pressure, then heated and vaporized by taking heat from environment (sea water or ambient air). After that it is transported by pipelines to consumers. It is a better option to withdraw the LNG cryogenic exergy before its delivery to consumers, otherwise

cryogenic exergy from the LNG evaporation is wasted by the commonly seawater heating. The improvement might be done with a power cycle with heat sink integration.

## 2. EXERGY ANALYSIS

The exergy method is a powerful tool for analyzing and understanding industrial processes. It can be used to identify where and how process improvements can be done. Exergy analysis, derived from first and second law of thermodynamics, offers an energy quality measure, allowing the assessment of the most effective use of energy.

According to the first law, energy may not be created or destroyed, its quantity being constant in all processes. In a steady state process, energy quantity is defined by the thermodynamic function called “enthalpy”. The second law affirms that energy is degraded in all processes and its quality decreases. The quality of energy is expressed by other thermodynamic function called “exergy”.

Total energy is composed by two parts: the useful energy, which is utile for the accomplish of an action (exergy), and the useless energy (anergy). The useful part of the energy can be found by taking the system to thermodynamic equilibrium with the environment. When the environment conditions are reached, the useful energy to develop the action disappears. This state is named the Dead State, for which the exergy is zero.

$$Ex = (H - H_0) - T_0(S - S_0) \quad (1)$$

where:

- Ex – exergy
- H – enthalpy
- T – temperature
- 0 – standard state (25°C, 1 atm)

According to the exergy balance method, the exergy balance is written as:

$$\sum_j Ex_{j,in} - \sum_j Ex_{j,out} = \Delta Ex_{DL} \quad (2)$$

Above equation giving the sum of exergy destruction and loss for every component of a cycle.

The exergy efficiency is calculated by:

$$\eta_{ex} = \frac{\sum_j Ex_{j,out}}{\sum_j Ex_{j,in}} = 1 - \frac{\Delta Ex_{DL}}{\sum_j Ex_{j,in}} \quad (3)$$

The total exergy of a matter flowing under steady state, is calculated as the sum of the physical, chemical, kinetic, potential and mixing exergy:

$$Ex_i = Ex_i^{PH} + Ex_i^{CH} + Ex_i^{PT} + Ex_i^{KN} + Ex_i^{MIX} \quad (4)$$

On a per mass basis, the specific exergy of a stream, written as “e”, is defined like:

$$ex_i = ex_i^{PH} + ex_i^{CH} + ex_i^{PT} + ex_i^{KN} + ex_i^{MIX} \quad (5)$$

For mixtures, specific chemical exergy is calculated as [Manfrida et al, 2008]:

$$ex_i^{MIX} = TR_0 \sum_k x_{ik} \ln x_{i,k} \quad (6)$$

In equation (6),  $R$  is the gas constant and  $x_i$  is the number of moles. For a single element, the specific chemical exergy is represented only by the product between the number of moles and the chemical exergy of the element.

### 3. RESULTS AND DISCUSSIONS

Natural gas is shipped in liquid state being regasified (by heating with sea water) at the import terminal, in order to be transported by pipeline.

Having an view the important temperature difference between deposit conditions and supply condition of LNG (about 160°C) is useful to convert its cryogenic exergy into power for the improvement of the energy utilization. The regasification is analysed on the basis of a modified  $H_2/O_2$  power plant. The  $H_2/O_2$  cycle with heat integration for vaporization of the cryogenic reactants provides the heat needed to vaporize the reactants inside the condenser, instead of taking heat load from the sea water. A schematic diagram of the cycle is given in Figure 1.

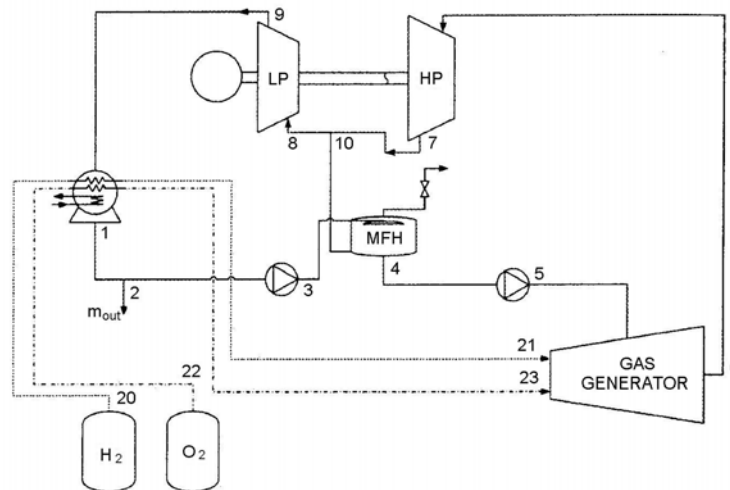


**Fig. 1. Improved reactive  $H_2/O_2$  cycle**

In the situation of the  $H_2/O_2$  vaporization within the condenser, having a net power output of 58600 kW, are founded values of exergy destruction and loss in the condenser and the

overall exergy efficiency of the two cycles: cryogenic H<sub>2</sub>/O<sub>2</sub> cycle and H<sub>2</sub>/O<sub>2</sub> cycle with heat integration for vaporization of the reactants (see Table 1).

**Table 1: Exergy analysis results**

H <sub>2</sub> /O <sub>2</sub> cycle		Modified H <sub>2</sub> /O <sub>2</sub> cycle	
$(\Delta E_{DL})_{condenser}$	$\eta_{ex}$	$(\Delta E_{DL})_{condenser}$	$\eta_{ex}$
6439,6	37,1	16742,86	38,7

Were presented values of exergy destruction and loss for the condenser having in view that in the case of the modified cycle the heat sink provides cooling to the condenser. Also, exergy analysis showed different values for the exergy efficiency due to the fact that for the two cycles, the inlet exergy differs by the value of the exergy appeared together with the vaporization of H<sub>2</sub>/O<sub>2</sub>. Still, the difference is slight.

#### 4. CONCLUSIONS

In the case of the cryogenic H<sub>2</sub>/O<sub>2</sub> cycle the heat for vaporization is available inside the condenser. The exergy analysis indicates an improvement if the H<sub>2</sub>/O<sub>2</sub> cycle is modified in the way of a heat sink integration. For the situation in which the net power output is of 58600 kW, the overall exergy efficiency of the modified cycle is of 38,7%, while for the typical H<sub>2</sub>/O<sub>2</sub> cycle is of 37,1%. Due to the inlet exergy value, the difference is minor.

#### REFERENCES

- [1]. Angelino G. – *The use of Liquid Natural Gas as Heat Sink for Power Cycles*, ASME Journal of Engineering for Power, 100, pp.167-177,1978
- [2]. Kim C.W. et al. – *Analysis of the power cycle utilizing the cold energy of LNG*, International Journal of Energy Research, 19, pp.741-749, 1995
- [3]. Manfrida G. et al. – *Simple ways to improve power plant performance and environmental compatibility through cryogenic fuel utilization*, Proc. of ECOS 2008, pp.551-557, June 24-27, 2008, Cracow, Poland
- [4]. Szargut J. – *Exergy method: technical and ecological applications*, WIT press Southampton, 2005
- [5]. Zhang N., Cai R. – *Principal power generation schemes with LNG cryogenic exergy*, Proc. of ECOS 2002, vol.I, pp.334-341, 2002, Berlin, Germany

## FPGA IMPLEMENTATIONS OF CONSTANT FALSE ALARM RATE DETECTORS (CFAR)

<sup>1</sup>MILANOV PETER, <sup>2</sup>ALEXANDROV CHAVDAR

<sup>1</sup>ZMD Bulgaria, <sup>2</sup>N. Vaptsarov Naval Academy, Bulgaria

FPGA implementations of CFAR detectors in different scenarios and environments are described in this paper. Possible combinations with other modules to improve performance and functionality, implemented in different classes FPGA's are discussed

**Keywords:** Radar, CFAR Detector, FPGA

### 1. INTRODUCTION

Radar operating in sea clutter environment has to adapt constantly the threshold to maintain a constant false alarm rate (CFAR) over the whole range of conditions that may be encountered. Dynamic range of power backscattered to receiver is very wide and statistical parameters of clutter can also vary widely – from thermal noise (no clutter return) trough spiky clutter with very non-Gaussian statistics. To make appropriate target detection, the threshold should be constantly adapted to the mean value of the clutter return. The local mean value of clutter is estimated from the mean of the surrounding cells in a certain range around the cell under test. The threshold is derived from the mean level, modified by a multiplier. A guard interval is incorporated in order to avoid targets that are close each other to affect noise estimation. Block diagram of basic CFAR detector is shown on Fig. 1

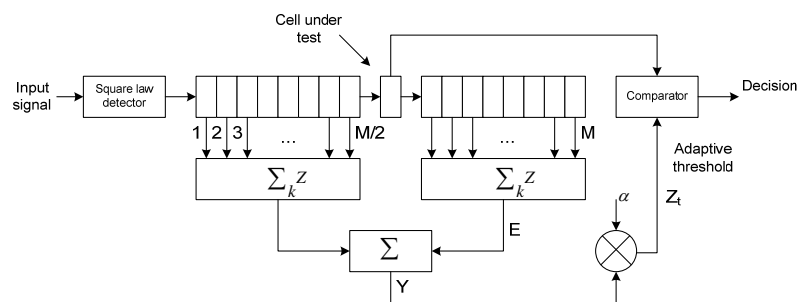


**Fig. 1. Block Diagram of a Cell Average (CA) - CFAR Detector**

A reference window is formed of M cells that surround the cell under test. The threshold is estimated by the mean value of the cells in the window. The multiplier  $\alpha$  is separately

delivered. The Cell – Average Constant False Alarm Detector (CA-CFAR) processor adaptively sets the threshold by estimating the mean value in window of M range cells. The CA-CFAR is the optimum CFAR processor (maximizes detection probability) in a homogeneous background.

**Table 1: CA-CFAR Average Detection Threshold (ADT) and optimal ADT of optimum fixed threshold processor**

P <sub>fa</sub>	Optimum ADT	M = 8		M = 16		M = 24		M = 32	
		A	ADT	A	ADT	A	ADT	α	ADT
1.00E-04	9.210	2.162	17.300	0.778	12.450	0.468	11.230	0.334	10.673
1.00E-06	13.800	4.623	37.000	1.371	21.940	0.778	18.680	0.540	17.278
1.00E-08	18.420	9.000	72.000	2.162	34.600	1.154	27.710	0.778	24.905

Table 1 shows relation of false alarm probability P<sub>fa</sub>, the multiplier α, Average Detection Threshold (ADT) and M, where, when M increases, α decreases and ADT also decreases for different values of P<sub>fa</sub>. A compromise must be adopted to choose the value of M without detection losses.

Based on previous results the following parameters are chosen for operation of the system shown on Fig. 1 and discussed in [9]. These parameters are M = 16, P<sub>fa</sub> = 10E-6 and α = 1.371.

The detection rule is as follows:

- If {Y > αy} target is present and the threshold αy is loaded in the cell under test before shifting the contents of all the cells.
- If {Y < αy} target is not present and the contents of all cells is shifted ahead by one.

## 2. FPGA IMPLEMENTATIONS OF CFAR

A CA-CFAR processor, described in [9] is implemented using XILINX chip XC9600 and consists of the following sub-circuits:

- Storage circuit
- Sixteen 8-bit shift registers
- An 8-bit data register ( CUT )
- Two accumulator circuits
- Eight 8-bit adders
- A multiplier
- An 8-bit comparator

Authors conclude that CA-CFAR does not estimate clutter mean level exactly, in shorter length M detection losses increases. The CA-CFAR processor operates with small losses only under clear environment but is not efficient in non-homogeneous environments. FPGA appears to be an excellent tool that provides simple implementation and high reliability.

Other implementations of CFAR processor in FPGA are discussed in [4]. The same assumption is made that received signals with higher levels are due to targets. Tested structure is similar to that, shown on Fig. 1. The average computational module sums up separately the data samples of both sides of the cell under test and computes their average, SL and SR, left and right respectively. Three modalities, the average, the minimum and the maximum, are used for this purpose and they are defined according to:

- Cell-Average CFAR  $Y_{ac} = \frac{1}{2}(SL + SR)$ ,

- Smallest-Of CFAR  $Y_{ac} = \min(SL + SR)$  and

- Greater-Of CFAR  $Y_{ac} = \max(SL + SR)$ .

Let  $X$  is the raw data samples of the signal to be processed and  $n$  is the number of reference cells in the CFAR detector. Guard cells are not included in the explanation. Data samples around the cell under test are presented as one-dimensional window shown as rectangle on Fig. 2. The data dependencies and sharing can be exploited to reuse previous result. Once a window has been processed, preceding result can be used to compute the result of the next window without the need of recalculating partial results over the entire domain just by inserting and deleting values from the window boundaries.

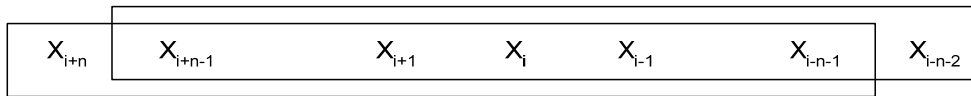


**Fig. 2. Graphical view of dependencies for adjacent reference data**

Fig. 3. shows a block diagram of the proposed structure. The main components are: a shift register, two processing elements for accumulating partial results, called Accumulating Processor Elements (APE), and a processing element that performs the threshold comparison, called CTPE.

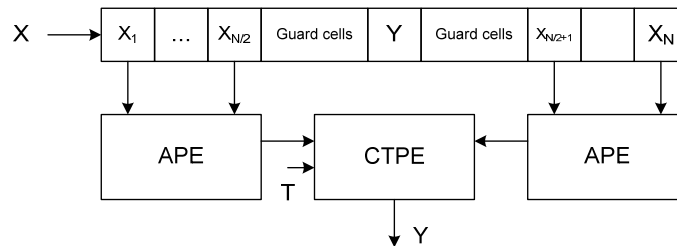


**Fig. 3. Main core structure of a CFAR detector**

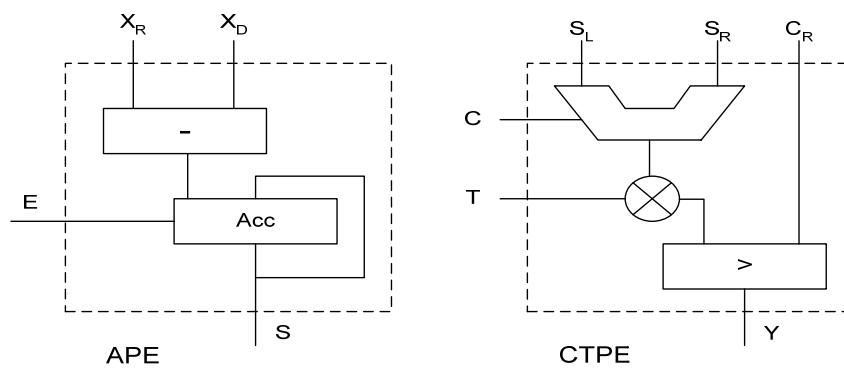


**Fig. 4. Internal structure of processing elements**

The internal structure of the processing elements APE and CTPE is shown on Fig. 4. The APEs computes  $SL$  and  $SR$  values and consist of accumulator and a subtractor. These

blocks have three inputs: XR - the data that is entered the new reference window, XD – the data that is deleted from the previous accumulation, and E – the signal that disables the activity of the accumulator in the latency period.

The CTPE block consists of an ALU-like sub-module and provides three modalities for computing the threshold: the average, the minimum and the maximum partial sums of SL and SR. The multiplier scales accumulated data and provides data to comparator. In proposed structure, on each cycle, data moves rightwards and after a latency period, the APEs accumulate data of the reference cells.

The structure above is developed using VHDL Hardware Description Language and is synthesized using Xilinx ISE targeted for a XC2V250 Virtex-II device. Table 2 summarizes total utilization of the FPGA resources and timing performance.

**Table 2: Synthesis summary and timing for the FPGA implementation of a CFAR processor for Xilinx Virtex-II XC2V250 – 6F456**

Slices	331(21%)
Flip Flops	540(17%)
4 Input LUTs	177(5%)
FPGA Occupation	21%
Max Clock Frequency	120MHz

The default CFAR configuration operates over 12-bit data, 32 reference cells and 8 guard cells. This configuration is common for most of radar applications with a good performance-accuracy trade-off. The internal temporal data in the accumulator can be extended to 18-bit precision, limited by the capacity of Virtex chip.

The proposed architecture provides an output result on each clock cycle and performs seven arithmetic operations concurrently. About 840 Millions of Operations per Second (MOPS) performance is reached. For instance, the execution time to perform CFAR processing on a data set of 4096x4096 samples takes 140ms, using 32 references and 8 guard cells respectively. The performance is about 18 times faster than the required theoretical processing time of 2.5s. The software implementation of CFAR algorithm, programmed in Visual C++ and executed on a personal computer with a Pentium IV processor running at 2.4GHz and 512MB main memory, takes 1.2s. DSP implementation of CFAR algorithm targeted to TMS320C6203 takes about 420ms.

The performance improvement of the discussed architecture is about 10 times compared to the software implementation on a CISC processor, but a lesser extent improvement is obtained compared to the DSP implementation. The architecture exploits the parallel nature of CFAR signal processing and it can be extended to more complex CFAR algorithms such as the statistic ordered algorithms.

In radar applications CFAR detectors are combined with other processing modules. Such application is described in [5]. The main processing chip is also Virtex-II Pro family member - XC2VP20-FF1152. Virtex-II Pro is a high performance FPGA that includes a large amount of high speed logic and fast multi port block RAM, but also a RISC processor – PowerPC 405. Block diagram of such system is shown on Fig. 5. Processed data are represented in 16-bit format for integer numbers and 32-bit for complex numbers. Dual port RAM additionally improves the overall performance of the system.

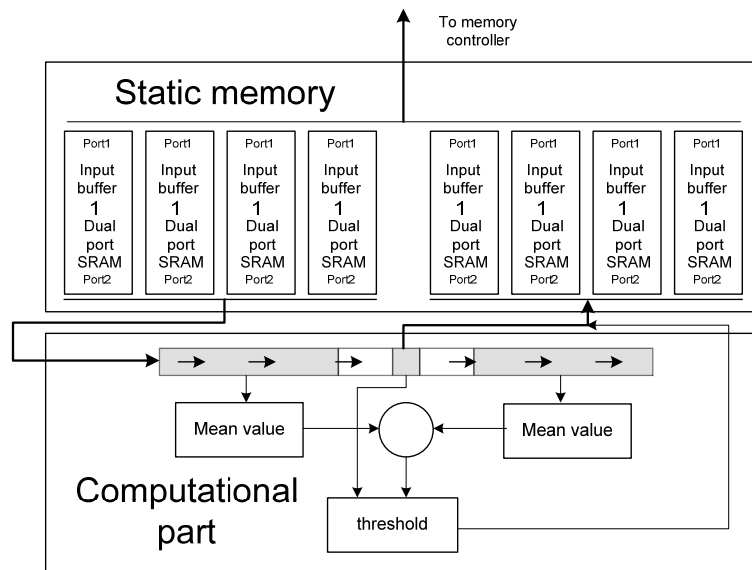


**Fig. 5. CFAR detector structure implemented using IC Virtex – II**

Resources used for implementation are summarized in Table 3. An additional SDRAM controller allows access to the radar image stored in the external memory.

**Table 3: Utilized resources summary of Radar CFAR co-processor implemented on a Xilinx Vetrex – II Pro based system**

Parameter	Value	Description
Ranges	1024	Range dimension of data cube
Pulses	128	Pulse dimension of data cube
Channels	16	Channel dimension of data cube
Proc. Frequency	100MHz	PowerPC/co-processor engine clock frequency
Memory frequency	125MHz	Memory clock frequency
Net frequency	250MHz	RapidIO clock frequency
Maximal system size	2	Max number of FPGA used experimentally
Proc. SRAM size	32KB	Max SRAM internal to each proc.
FIFO size	8KB	Size of FIFOs to/from SDRAM

**Table 4: CFAR detector co-processor resources**

Resource	Available	Used	%
Occupied slices	19392	1094	5
BRAMs	192	16	8
Equivalent Gate Count	1076386		

Higher complexity of algorithms requires increasing of computational resources, but high-performance FPGA costs a lot. An efficient alternative to Virtex family is budget class FPGA of Spartan series. Spartan does not include hardware processors, the number of hardware multipliers and multiport block RAM is reduced, the overall speed is lower, but the excellent performance/price ratio worth to optimize designs to Spartan family. Simple modules such as Sensitivity Time Control (STC), Fast Time Constant (FTC) and Gain modules that can be added to CFAR processors can be easily implemented in non-speed critical FPGA.

STC – this module is used to attenuate received signals, echoed from near objects. On case of calm sea, this value is set to minimum.

FTC removes visualization of unwanted constant echoes e.g. from rain. FTC acts like high-pass filter.

Gain is an Automatic Gain Control.

**Table 5: Resources used in FPGA implementation of STC, FTC, and Gain Modules in XSA – 50 board based on XILINX FPGA XC2S50TQ144-5**

Resource	Available	Used	%
Slices	768	101	13
Slice Flip Flops	1536	88	5
4 Input LUTs	1536	161	10
IOBs	96	51	53
BRAMs	4	3	75
GLKs	4	1	25

These three modules operate over 12-bit data and 2048 samples. The system outputs data on each clock pulse. Maximal clock speed is 102,176MHz.

System performance improvement of CFAR processor is discussed in [3]. CA-CFAR shows good performance in constant parameters regions. Pre-defining these regions and estimations of their parameters is needed to improve processor performance. The block-diagram of such architecture is shown on Fig. 6.

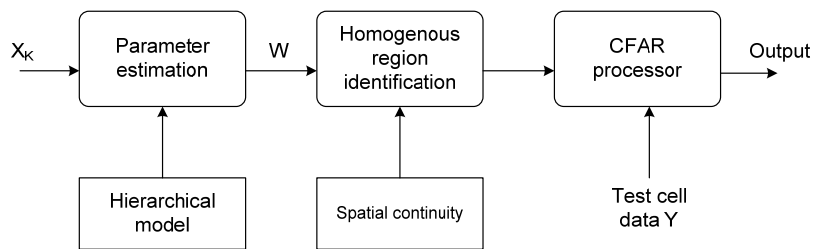


**Fig. 6. Block diagram of a two-stage CFAR algorithm**

The programmable nature of FPGA makes possible flexibility of the implemented algorithms. In contrast to fixed structures as CA-CFAR, an adaptive version of CFAR is discussed in [1]. The system combines ordering with arithmetic averaging and is inspired by the opportunity offered by the FPGA. Such a detector, known as Trimmed Mean (TM) CFAR,

has the advantage that it is reduced to the CA-CFAR and ordered statistics (OS)-CFAR detectors for specific trimming values. The main task for the TM-CFAR processor is to adjust

the false alarm probability to a desired level in a varying background environment through averaging after trimming the stray ordered samples from both maximum and minimum sides of the window containing reference cells.

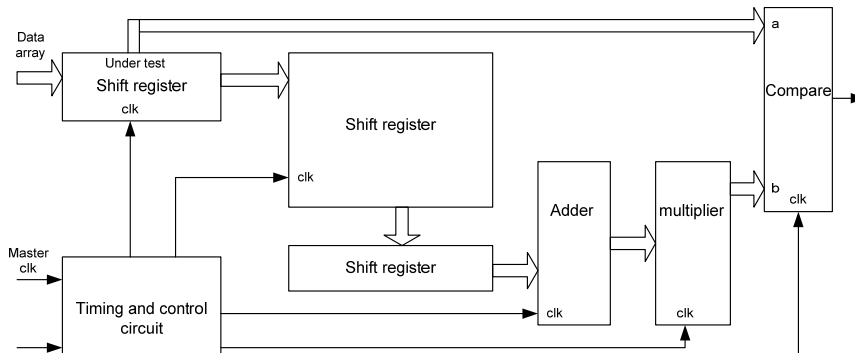


**Fig. 7. Generalized block diagram of a CFAR processor**

Structure of the proposed architecture is shown on Fig. 7. It consists of a shift register, sorting and trimming module, parallel adder, multiplier circuit, comparator and control/timing unit. The trimming operation is beneficial in minimizing the estimation error of the background, and is performed according to predetermined configuration. The control and timing module is responsible for initializing the process. It consists of counters and registers. The sorting module implements the bubble sorting algorithm and consists of a comparator, multiplexer and output latches.

The proposed TM\_CFAR processor is designed, synthesized and simulated using Altera Quartus II platform. The processor uses hardware resources such as Memories, Arithmetic Logic Units, Counters and Registers. The chip that the design is targeted to is Stratix EP1S10F484C45. In the simulation additional structures are included – 256x16 ROM and 256x1-bit RAM. The compilation report for the worst case of propagation delay shows that maximum operation frequency can reach 102MHz.

**Table 6: Statistics for the FPGA hardware resources utilization and timing performance**

Resource	Available	Used	%
ALUT	48352	4644	10
Total Registers		4394	5
Total Memory bits	2 544 192	4360	1
Clock frequency		100MHz	

Another way to improve the system performance is parallelism and it is very easy to implement in FPGA platforms. Such parallel processing unit is discussed in [7]. High computational throughput is a way to answer the increased requirements of signal computation in radar technology. If assumption is 16-bit input data, the sampling frequency of the input signal can lead to few Gbps total system throughput. A single CA-CFAR

processor can reach throughput of 947Mbps for 16-bit data and 60MHz clock, since 32 parallel CA-CFAR processors implemented on Virtex-II Pro technology can provide 31Gbps. Resource utilization as a function of k-parallel structures suggests between 1.4% for single and 37.5% for a 32 parallel design considering XC2VP30 chip. Visualization of proposed parallel structure for 2 processors is shown on Fig. 8.

A significant problem with number of parallel structures is power consumption of the chip that makes a compromise between performance and power requirements.

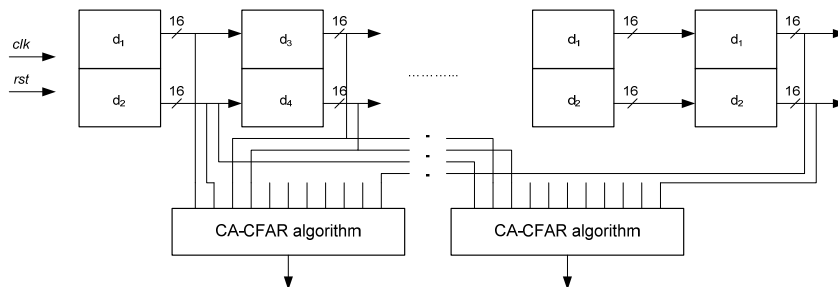


Fig. 8. Hardware data structure of two parallel CA - CFAR detectors

### 3. CONCLUSIONS

By their large amount of programmable logic and computational resources FPGAs offer very good opportunity for implementation of computational-intensive algorithms like these in radar processing. Especially suitable are CFAR processors that can be parallelized. Increasing the total amount of resources in one FPGA chip makes possible implementation of more complex CFAR processors. Future development of CFAR detection can be incorporation of memory controller (e.g. DDR2) and perform multi-dimensional CFAR over whole radar image, stored in external memory. By adding secondary processing modules to CFAR target detection it is possible to build a System-On-a-Chip solution for radar applications.

### REFERENCES

- [1]. Alsuwailem A. M., S. A. Alshebeili and M. Alamar - *Design and Implementation of a Configurable Real-Time FPGA-Based TM-CFAR Processor for Radar Target Detection*, (<http://www.oldcitypublishing.com>)
- [2]. Andraka, R., A. Berkin, *FPGAs Make a Radar Signal Processor on a Chip a Reality*, (<http://www.andraka.com/>)
- [3]. Biao Chen, Pramod K. Varshney, *Adaptive CFAR Detection for Clutter-Edge Heterogeneity Using Bayesian Inference*, IEEE Transactions on Aerospace and Electronic Systems Vol. 39, No. 4 October, 2003
- [4]. Torres-Huitzil César, R. Cumplido-Parra, S. López-Estrada, *Design and Implementation of a CFAR Processor for Target Detection*, (<http://ccc.inaoep.mx/>)
- [5]. Conger Chris, D. Bueno, and A. D. George, *Experimental Analysis of Multi-FPGA Architectures over RapidIO for Space-Based Radar Processing*, (<http://www.ll.mit.edu/>)
- [6]. García Joaquín, G. Viveros, R. Cumplido, *FPGA Based Architecture for Radar's STC, FTC and Gain modules*, (<http://ieeexplore.ieee.org/>)
- [7]. Kyovtorov V., G.Kuzmanov, H.Kabakchiev, and G.Gaydadjiev, *Parallel FPGA Design of CA-CFAR Algorithm*, (<http://ce.et.tudelft.nl>)
- [8]. Skolnik M., *Introduction to Radar Systems*, Editorial McGraw-Hill, 2000
- [9]. Saed T. R., Jawad K. Ali and Ziad T. Yassen *An FPGA Based Implementation of CA-CFAR Processor*, (<http://www.medwelljournals.com/>)

## MARINE DIESEL ENGINE ENERGY AND ECONOMICAL PARAMETERS DETERMINATION AFTER INDICATOR DIAGRAM DIGITAL PROCESSING

<sup>1</sup>MOSKOV JULIAN, <sup>1</sup>ZARKO ILIEV

<sup>1</sup>Naval Academy – Varna, Bulgaria,

In this paper determination of a marine diesel engine indicative diagram, taken by mechanical indicator, problem is reviewed. On the basis of recognition of images and analysis of the resulting database energy economical parameters (EIP) are collected, which completeness and accuracy exceed those obtained by modern mean indication pressure (MIP) systems. The software used for processing and generating the database in Flash environment is also described.

**Keywords:** Indicator diagram, Mean indicated pressure, Planimetric calculation, Digital recognition

### 1. INTRODUCTION

The objects dealt with by engineering have infinitely numerous of properties and are characterized with numerous links as in the objects, as well as with other objects and with the environment itself. Transition to the corresponding models appears to be the most complicated and responsible stage in the use of mathematical models in engineering practice. Largely a successful resolution of this task is determined from the experience and the intuition of the specialist in a specific area. At this stage in the operation of the modern marine diesel engine (MDE) still great place occupy mechanical indicators for determination of performance by cylinders[1,8]. Planimetric and subsequent calculation of the received indicator diagrams, appears to be unusually difficult with the available appliances in shipping conditions and very often contribute to an increase of over 10% error.

Technology of processing and purpose of the research. The indicated diagram drawn by a mechanical indicator has to be scanned in black and white format. The software part includes indPro, for digital recognition of diagrams of the cylinders accurately on the basis of the theory of recognition of the images. The program product deduces the necessary standard EIP on each cylinder of MDE and gives the opportunity for comparison as between individual cylinders and the reference data from the factory producer or obtained from the watch tests. The purpose of the study is to develop an algorithm and a software program, which recognize digitized indicative diagram drawn by a mechanical indicator. The resulting EIP are similar to those realized in modern MIP systems.

The following tasks are completed to achieve the designated purpose:

Analyzing of the modern MIP systems for diagnosis and control was carried out.

- Modern methods for processing of data bases, selection of an appropriate method to present the results obtained in a similar type of the MIP.
- Creating the algorithm for generating a database of digitized indicator diagram for Low force & speed (LFMDE).
- Creating a software module for obtaining and comparing EIP for each cylinder of the slow speed main diesel engine (SLSMDE).

## 2. ADVANCED MATHEMATICAL MODEL OF SLSMDE AND TC COMMON WORK. SCHEME STRUCTURE

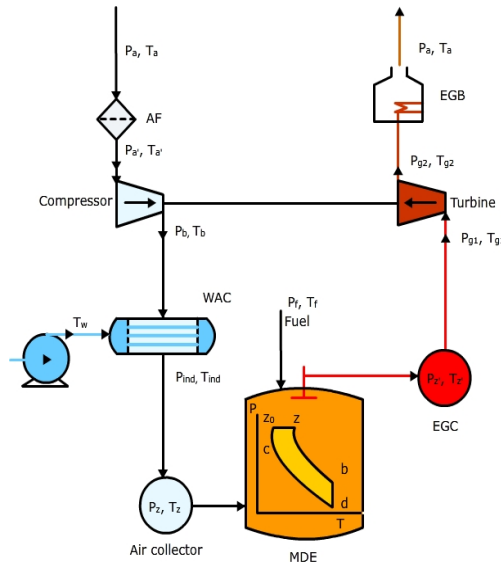


**Fig. 1. Combined MDE principle scheme.**

Figure 1 presents schematic diagram of a combined main MDE thermodynamic parameters. With the help of these parameters analysis of the processes that occur in the energy converters is made, respectively MDE and turbocharger(TC) constant pressure. They give quantitative assessment of the common work between the two heat machines. Indicator diagram, obtained by mechanical indicator, digital processing. Image storage system is bitmap. All the graphic data or part of it chosen by the user, in order to shorten processing time and prevent errors from soiled paper, is being processed pixel by pixel. A selectivity algorithm is calculating the number of pixels in the contour of the diagram, and then are converted into square millimetres subjected to the resolution.

Degree of accuracy:

The degree of accuracy at calculating the indicator diagram is straight proportional to the resolution of the scanner, since the contour of the image is considered the midpoint of the graphic line. Indpro precision is unreachable with hand tools - up to 0.5% error. If more diagrams are loaded(tries), calculating the average, error becomes close to zero. Active process calculation algorithm. Indicated work. The closed area of the indicative diagram in PV coordinates system is the indicated work [3,4]. The area received in cubic millimetres, after calculating, divided to the diagram length "l" in mm and multiplied by the spring coefficient (k pressure scale in mm / bar). The result is mean indicated pressure  $p_{mi}$  in bars. Multiplied by the cylinder volume  $V_s$  we get work indicator  $W_i$ . If we have an evolved indicator diagram it is necessary to redraw it so that the abscise of the crankshaft angle can be described volume by the piston.

Continue with measure of  $P_z$ ,  $P_c$  of the indicated diagram and calculation of  $\lambda$ .  $P_z$ - maximum pressure in the combustion chamber, and  $P_c$ - compression pressure. Identifying specific fuel consumption. Program algorithm.

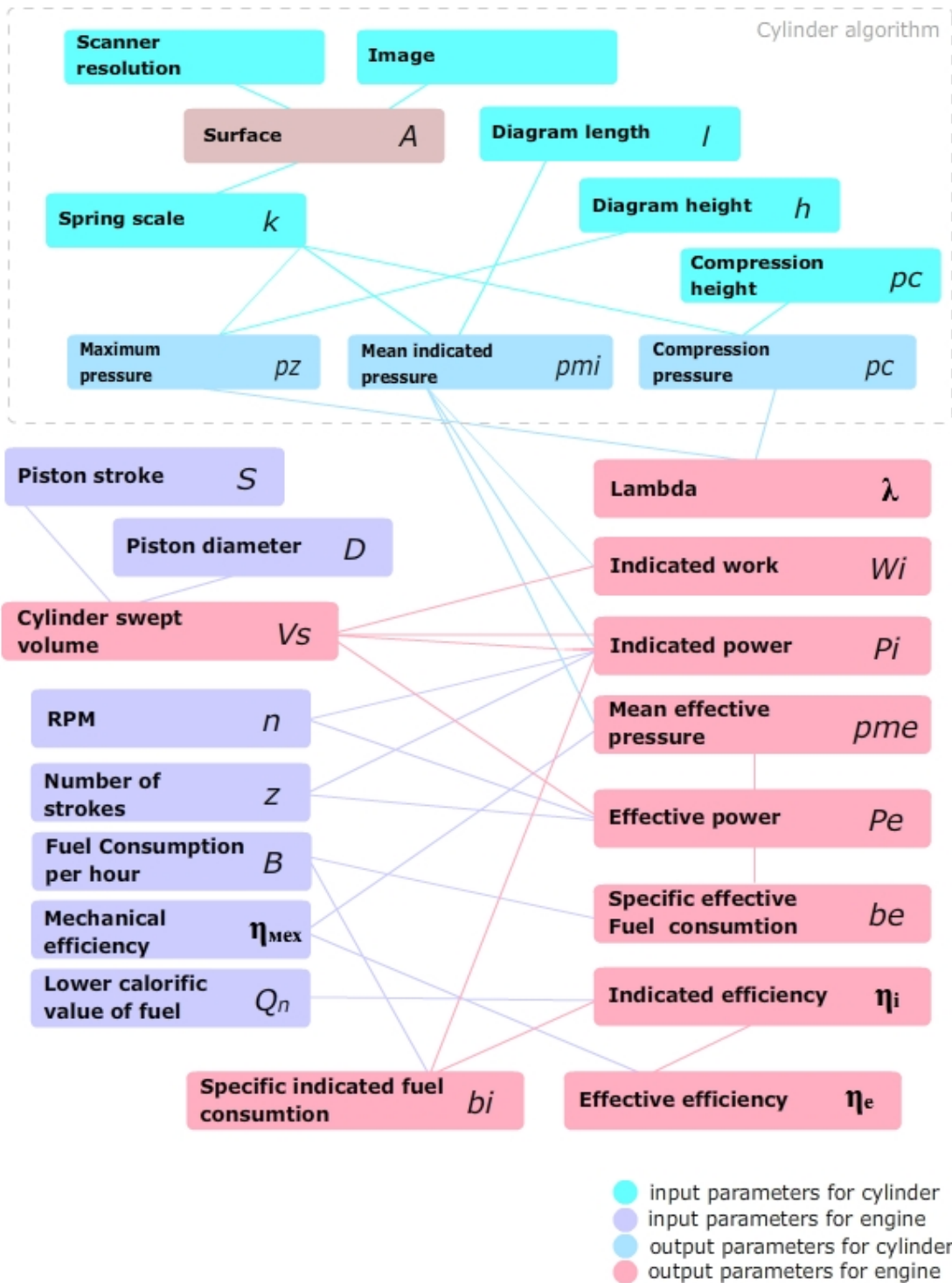
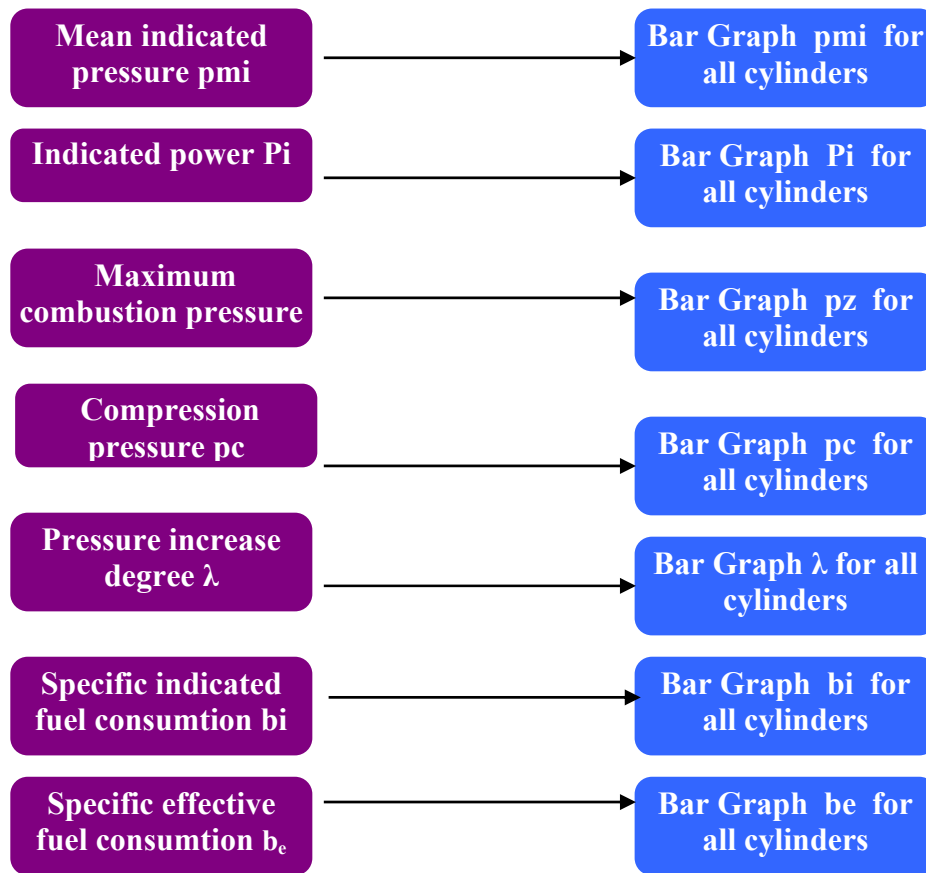


Fig. 2. Program cylinder algorithm.



**Fig. 3. Accuracy assessment, calculating MDE EIP obtained similarly to MIP system, was made.**

Core model is the indication process. Accuracy assessment of the graphical visualization of the indication process was made, through software [2,3,5] (Grafula3; LABFit). The methodology of evaluation is essentially bringing the graphic image of the procedure factors in digital form. The obtained result is transformed to a function. General information about the program. Principle of operation. The name of the program is "IndPro". Software program is written in Action Script3, Language Code UI8 in AdobeFlash CS4 in SWF file format was developed for numerical analysis and computation of ID[6.7]. Appropriate work environment for the program is Flash Player 10 or later. Once the program "INDRO" estimates the maximum combustion pressure (Pz), compression pressure (Pc), the cylinder mean indicated pressure (pmi), on the same page we input the initial data for the engine. The results are presented on the 2nd part of the program. After entering the input, push button "NEXT": 2nd page opens where the output data for each cylinder individually and the arithmetic average values are presented in a table. There is a panel, in the right side of the page, which is divided into bar graph visualization and active buttons. For each button pushed the bar graph is recalculated with the new parameter included. Pressing the button again makes it inactive and excludes its parameter from the bar graph. This allows dynamic use of bar graph and comparison of selected parameters.

Different dimensions are standardized by the proportional algorithm for maximum clear presentation of many parameters in common bar graph. Default standard value is the average for each parameter but can be manually assigned for a specific case. Button "CALCULATE": used before the button "NEXT". Calculates on the same page common engine parameters to make sure that we have entered the data correctly.

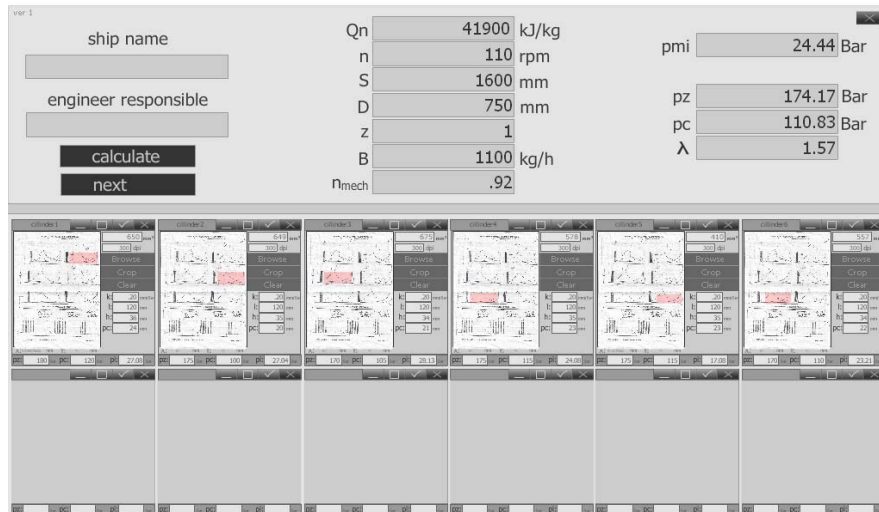


Fig. 4. Input table, obtained similarly to MIP system, was made.

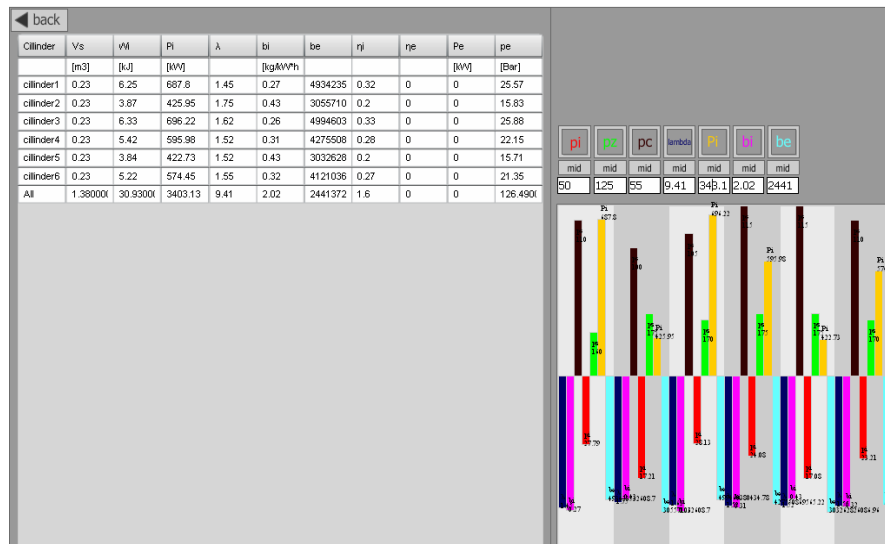


Fig. 4. Output table, obtained similarly to MIP system.

Identifying specific fuel consumption.  
 $bi = 3,6.106. B / P_i$ , kg / kWh B- fuel hourly  
 bi- fuel consumption specific indicator

Defining indicated efficiency.

$$\eta_i = 3600/Q_n \cdot b_i$$

Q<sub>n</sub> - lower calorific value of fuel is set to  
Q<sub>n</sub> = 41,900 kg / h

Calculation of the effective efficiency.

$$\eta_{ef} = \eta_i \cdot \eta_{mech}$$

η<sub>mech</sub> - mechanical efficiency of engine  
η<sub>mech</sub> = 0,78 - 0,82 sets a

Identifying specific effective fuel consumption.

$$BE = 3600/Q_n \cdot \eta_{ef}$$

kg / kWh BE-effective fuel consumption

Engine effective power.

$$RE = B / BE$$

kW

Minimum system hardware requirements for sustainable operation of the software.

**Table 1:** Recommended hardware and standard video playback and high-definition (HD).

Windows®	Macintosh	Linux®
Intel® Pentium® II 450MHz, AMD Athlon™ 600MHz or faster processor (or equivalent)	PowerPC® G3 500MHz or Faster processor  Intel Core™ Duo 1.33GHz or faster processor	Modern processor (800MHz or faster)
128MB of RAM	128MB of RAM	512MB of RAM, 128MB of graphics memory

## 2. CONCLUSIONS

1. Modern MIP calculators and system for technical diagnosis are not always available for reference diagnosis, which is needed to assist the personnel in decision-making.
2. Digital diagram calculating methodology is developed, and the output data is presented in a similar way as MIP systems.
3. The software is easily accessible and has a modular structure which enables upgrade.
4. Standard parameters compare is available for the EIP to support the development of the heat-technical statement of the chief engineer.
5. As guidelines for future development opportunity for creating a system generating expert advices for technical operation is realized.

## REFERENCES

- [1]. Malev K. – *Toplotechnicheski kontrol, diagnostica I regulirane na korabni dizelovi dwigateli. Izdatelstvo* “Slavena”, Varna, 2002r.
- [2]. Prodanov S., Yanev S., Malev K. – *Technicheska diagnostika na glavni korabni dizelovi dwigateli*, WUC SO“Woden Transport.”-VARNA, 1985r.
- [3]. Yanakiev W.H. – *Korabni dwigateli s wytreshno gorene – Teoriq I eksploataciq*. Izdatelstvo “Sv. Georgi Pobedonosec”, Sofia, 1996r.
- [4]. Prawila za eksploataciq na korabni dizeli – Technika, 1990
- [5]. [www.lemag.de/24.0.html](http://www.lemag.de/24.0.html)
- [6]. [www.kistler.com/KR\\_kr-kr/2222\\_EnginesPeakMeter/Engines-Peak-Meter.html](http://www.kistler.com/KR_kr-kr/2222_EnginesPeakMeter/Engines-Peak-Meter.html)
- [7]. [www.malin.co.uk/?page=products](http://www.malin.co.uk/?page=products)
- [8]. [www.manbw.com/files/news/files/1810/037.pdf](http://www.manbw.com/files/news/files/1810/037.pdf)

## ENGINE ROOM SIMULATOR ERS4000 USE FOR ANALYSIS OF ENERGY EFFICIENCY OF INTEGRATED SHIP ENERGY SYSTEM

<sup>1</sup>NEDEV MARIN, <sup>1</sup>ANGELOV NIKOLAJ, <sup>1</sup>PETKOV PETKO

<sup>1</sup>*Nikola Vaptsarov Naval Academy, Varna, Bulgaria*

The fuel consumption and GHG emissions from shipping are directly associated with energy efficiency of integrated ship energy system. In this paper, there are considered gas emissions from shipping, compared with other ways of transportation and on the basis of Engine Room Simulator ERS4000 are made an example for modeling and optimization of processes of energy producing and distribution. There are described some sources of gas emission and facilities to analyze possibilities to decrease of gas emissions and increasing of energy efficiency (technology-technical means for increasing energy efficiency with exploitation of ship energy system) and using different scenarios in education and examination of students, cadets and engine teams.

**Keywords:** energy efficiency, greenhouse gases emissions, engine room simulator, education, estimating of energy efficiency, integrated ship energy system.

### 1. INTRODUCTION

It is known, that the ships are autonomous energy and power systems and of this point of view, the optimal use of energy sources is of special priority, combined with other requirements, according to ship type.

The fuel consumption and fuel price influence directly on trade and other operations on the sea. But, in the contemporary world, excepting fuel price, the problem of air pollution by exhausted gases from diesel engines is of grate importance.

On this way, the requirement for higher energy efficiency have to meet not only requirements to the fuel price, but also to saved energy and respectively noxious gas emissions.

In general, energy efficiency should include all parameters of ship activities. So energy efficiency may be formulated as a ratio

$$\text{Energy efficiency} = \frac{\text{Performance, service, goods, energy...}}{\text{Input energy}} \quad (1)$$

The quantities are in the metrical/measuring system and unit of measure. In such cases requirements for higher energy efficiency include not only fewer expenses, but fewer emissions as well.

The definition like (1) spreads our opinion and gives opportunity to extend the concept and permit more precise assessment of energy efficiency. (For example, at cogeneration, part of the energy is converted into electrical energy and another part is used for heating water, cooling air and so. The result is more then 90 percent energy efficiency).

According to some authors [6] the energy efficiency is the fifth energy: after coal, fuel, gas and nuclear.

The GHG emissions from world shipping are estimated by the world ship fuel consumption and are special subject of many research groups, institutes and conferences. The results vary in timescale, underlying assumptions and modelling techniques.

In the following Table 1 some estimations of the consumed fuel, the emissions of carbon dioxide and allegeable addition of those discharges [1] are shown.

**Table 1**

	Base year	CO2 million tons	Fuel million tons	% of world fuel combustion <sup>a</sup>	Projected growth
IMO Updated Study (2008)	2007	843	277	3.1	By a factor of 1.1–1.3 by 2020 & 2.4–3 by 2050.
IMO/Group of Experts (2007)	2007	1,120	369	4.1	+ 30% by 2020
IMO GHG Study (2000)	1996	419.3	138	1.6	--
IEA (2005)	2005	543	214	2.0	--
TRT Transporti e Territorio	2006	1,003	NA	3.7	--
Endressen et al., 2007b	2002	634	200	2.3	+ 100–200% by 2050
Eide et al., 2007b	2004	704	220	2.6	+ 100–200% by 2050
Eide et al., 2007b	2006	800	350	2.9	+ 100–200% by 2050
Corbett et al., 2003b	2001	912	289	3.1	--

a World CO2 emissions from fuel combustion, 2005 IEA data.

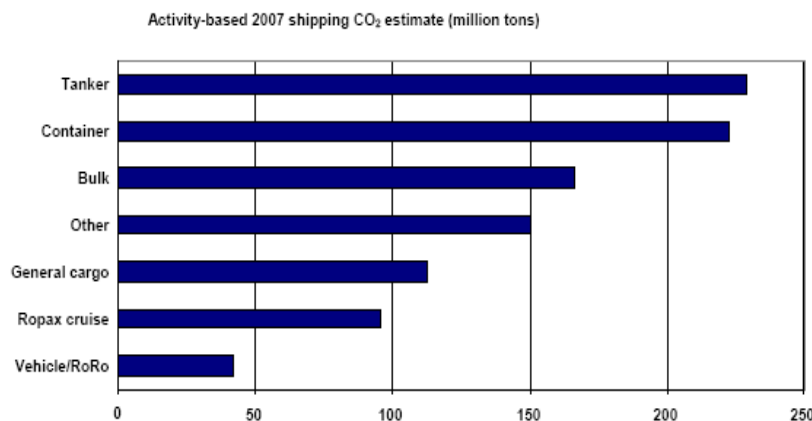
b From secondary sources including IMO Updated Study on GHG, 2008.

As follows in the Table 1 emission are received by ship fuel combustion in a world scale in the limits (1.6 – 4.1) % of the world emissions of carbon dioxide. The prognosis of IMO shows that those emissions in the period from 2007 to 2020 will increase (2.4 – 3) times.

In the year 2005 the shipping emissions have constituted 10% within the transport sector, the track/car transportation – 73%, air transport – 12%, railway transport – 3% and “pipe transport” – 2%. In case of lacking measures for limiting the transportation emissions they will be boosted doubly next 20 years.

Regardless of less shipping emissions of 10%, special attention was paid to CO<sub>2</sub> emissions from different types of ships. Data are given in Table 2

**Table 2**



Source: UNCTAD, based on IMO 2000 Updated Study on Greenhouse Gas Emissions from Ships, 2008 (IMO2008). Includes international and domestic shipping and excludes fishing and military vessels.

While GHG emissions from international shipping are significant in absolute terms, the relative share of the sea transportation is small compared with other types of transport. It has better indices about effective fuel consumption and treatment of the ecological shock on the environment. On a per ton kilometre (km) basis emissions from rail could be 3 to 4 times higher than emissions from tankers, while emissions from road and air transport could, respectively, be 5 to 150 times and 54 to 150 times higher.

The analysis shows that the extended use of the water/ship transport can ensure benefits on the carbon dioxide discharges and energy efficiency of a world scale.

Independently of the mentioned benefits, increasing the shipping energy efficiency remains important part of greenhouse gas reducing and consequently IMO, ship owners, ports and so have to take part with reducing the GHG gas emissions as well.

Regarding this the position of the European Commission is that all economy sectors must admit the activities for maintaining the earth climate. (KIOTO PROTOCOL TO THE UNITED NATIONS FRAMEWORK CONVENTION ON CLIMATE CHANGE).

Together with political, organizational and economical decisions the technical and educational activities are very important too.

The technical and technology improvements can reduce GHG emissions. For example, replacing the old ship equipment with new, more effective can reduce fuel consumption and GHG emissions from 3 to 30% for new ships and from 4 to 20% - for old ships. The new technologies for hull and propeller design reduce hull resistance, propeller power; the new engines are more effective too.

The use of alternative fuels and energy sources is not widely spread yet, because of technological difficulties to compete with diesel engines. Although some examples of switching from diesel to natural gas fuel take place (e.g. inland ferries in Norway and offshore supply vessels operating on the Norwegian Continental Shelf. Another project is LNG Fuelled Cargo Vessels [2] of company Sea-Cargo AS. In 2010 they will serve Baltic, Norwegian and British port.).

All those and other examples are connected with utilization of diesel engines. A biofuel is not recommended for use till now, because of some troubles associated with production, expending and safety in shipping. Solar panel sources, hydrogen propeller ships as well as carbon capture and storage technology could develop and applied to the ship transport. The solar panels are used as a slave sources. The Japanese companies Nippon Yusen KK and Nippon Oil Corporation [3] investigate photo solar panels, which produce about 0.2% power of the power system (40kW) of 60 000 DW tanker and decreases 6.5% of its fuel consumption and 1 – 2 % of CO<sub>2</sub> emissions. An important result will be decreasing emissions from such ships: CO<sub>2</sub> emissions about 20%, NO<sub>x</sub> – about 90%, sulfides oxides will be 0%.

The development of alternative energy sources is going on. One of the examples is the first German ferry with 48kW hydrogen fired battery in combination with lead gel battery [4], which gives 2 time's higher efficiency and zero emissions, named ZemShip. Other examples are produced in companies SkySails [8] and KiteShip Corporation of Alameda [7]. At the beginning in 2008 first cargo ship MS Beluga Skysail made cruise from Germany to Venezuela with computer controlled kite 160 m<sup>2</sup> could cut fuel consumption by 20% [8].

The sea ports as a part of sea transport chain can reduce emissions too. In that case in July 2008 was admitted the World Ports Climate Declaration. In a message to Media pool [5] in 10.12.2008 it is mentioned that the ships, visited the Italian port Civitavecchia could use the shore supply electrical energy for port maneuvering procedures. The Italian companies Enel and Fincantieri developed jointly energy project, connected to reduction of GHG emissions.

The Intergovernmental Panel on Climate Change (IPCC) developed guidelines for national GHG emissions inventories. The guideline divide emissions from water in two main categories: domestic and intentional.

CO<sub>2</sub> emissions from international shipping have been estimated both from activities and international fuel statistics. IMO Informal Cross Government/Industry Scientific Group of Experts agreed to a consensus estimate for CO<sub>2</sub> emissions in 2007, shown on Table 3

Consensus estimate 2007 CO<sub>2</sub> emissions (million tones CO<sub>2</sub>) **Table 3**

	Low bound	Consensus estimate	High bound	Consensus estimate % Global CO <sub>2</sub> emissions
Total ship emission <sup>1</sup>	854	1019	1224	3.3
International shipping <sup>2</sup>	685	843	1039	2.7

1 Activity based estimate including domestic shipping and fishing, but excluding military vessels.

2 Calculated by subtracting domestic emissions estimated from fuel statistics from the activity based total excluding fishing vessels.

The Intergovernmental Panel on Climate Change (IPCC) is not explicit regulations on CO<sub>2</sub> emissions from ships but they are predicted in base scenarios with increase by a factor of 2.4 to 3.0 by 2050 and factor of 1.1 to 1.3 for 2020.

The operational measures could reduce CO<sub>2</sub> and GHG emissions up to 40%. It is known that slowing down by 10% can lead to 25% [1] reduction in fuel consumption and emissions. Some shipping companies cut their operating costs during the 2008 only slowing down ship speed.

Some possible scenarios and results are showed in following Table 2 [1].

Table 2

Scope of intervention	Measure	Example
Technology and energy	<ul style="list-style-type: none"> <li>• Efficient and lower-emitting propulsion systems</li> <li>• Clean fuels and alternative energy sources</li> <li>• Ship design (structure, hull and machinery)</li> <li>• Emission control technologies (e.g. after exhaust treatment, carbon captures and storage)</li> </ul>	<ul style="list-style-type: none"> <li>• EU and IMO sulfur emission control areas</li> <li>• Solar Sailor 2006 and Skysails 2006</li> <li>• Switch from diesel to natural gas</li> </ul>
Operational	<ul style="list-style-type: none"> <li>• Speed reduction</li> <li>• Route selection</li> <li>• Monitoring of weather and sailing conditions</li> <li>• Collaboration among ports, carriers, other modes and other players in the supply chain</li> <li>• Cold ironing or onshore power</li> </ul>	<ul style="list-style-type: none"> <li>• NYK announcement in early 2008 to reduce the speed of all vessels in the fleet by 10% to cut fuel consumption by up to 25%</li> <li>• Vessel sharing agreement between Maersk MSC and CMA-CGM on transpacific trade</li> </ul>

The sea transport expenses depend most of all on fuel costs. Usually they reach 20 - 25%, but in 2008 they was 50% because of fuel prizes rise. So, reducing all fuel consumption and its expenses leads to GHG emissions going down too, and cutting shipping fuel expenses directly lead to decreasing of GHG emissions and improving of new reasons to increase energy efficiency. Following this conclusion companies are investing new

alternative and more efficient technologies with low GHG emissions. Some authors [6] point that every pound spent on energy efficiency avoids doubled investment in electricity supply.

## 2. OUR PROPOSAL

The optimal measures and maintenance of ship power systems and their new facilities is fully connected to education and study.

The simulators confirm investigate and produce new scenarios using existed software models of ship equipment.

In this case study optimal maintenance of ship energy systems gives facilities to raise energy efficiency as well.

The engine room simulator ERS – 4000 consist of 4 working places for education, investigations and analyzing the main engine and auxiliary ship systems by cadets, students, ratings, and engine officers too. One of the working places is shown on (Fig. 1). Computer models permit test/examination mode as well. The investigation and exploration advantages give opportunities to prepare doctoral and special projects.

Fifth working place includes real physicist models of power electrical plant (Fig. 2) and ship power plant (Fig. 3). The processes and software models could control from the computers or from real TRANSAS models, from buttons, potentiometers etc. There are available 3 types of ships: general cargo, tanker LCC and RO-RO with 2 types of main engines. Electric power plant includes 2 diesel generators, a shaft generator, turbo generator and emergency diesel generator. The development of different scenarios is available too. One of the main advantages is possibilities to provide education, trainee, tests, examines and different curses for engine team. Engine team may include engineers: chief engineer, second engineer, watch keeping engineers and electrical engineer. Engine team could solve different problems, connected with maintenance of power plants in different modes: stop, free engine, maneuvering, full ahead, could start, and preparing the power plants, shore power supply.



Ratings education is available too.

Drawing up a "Log Book" automatically gives opportunity to make a debriefing after after exercises. It is possible to do briefing before exercises.

Cameras and software make video and audio records automatically. The movies, records and log books could be use for briefing, debriefing, study and education.



**Fig. 2 Ship electrical power plant includes model of main switch board and auxiliary control board.**



**Fig. 3 Control board of ship power plant consists of panel for main engine control and auxiliary engines control panels.**

One of the main advantages is investigating power plants in different situations calculating efficiency, CO<sub>2</sub>, NO<sub>x</sub> emissions and so. We could calculate exhaust gases energy, convert it to steam energy and run the steam turbo generator. In mode "Full Ahead" utilization steam energy could speed up the ship, sourcing the shaft generator in motor mode from turbo generator, could decrease fuel consumption, low costs.

Other benefits are technical advantages: rising the power factor ( $\cos \varphi$ ) cut the electrical losses in the electrical distribution bars and systems, raising the efficiency factor. For example on fig.4 we could see benefit, calculated in 1080kW.

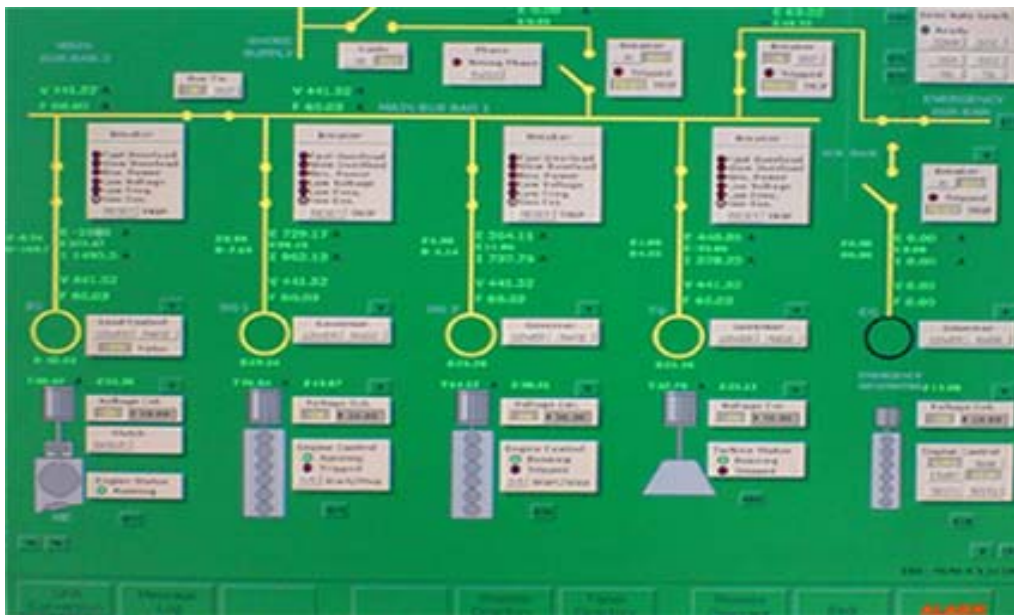


**Fig.4. All generators supply shaft generator, working in motor mode.**

There are other possibilities too. We could modify the situation and make an analysis with only turbo generator, with only diesel generator, diesel generators and so. All the examples give different results and conclusions. In comparison of all the results we could and see more opportunities to use and maintain the ship power plant and electrical power plant.

In comparison of the different situations we can calculate the reduced cost of fuels, safe engineering recourses of the equipment, calculate the recuperated energy.

A prime cost factor in future scenarios is fuel consumption, manicuring, cargo treatments, heating, cooling, ventilation and other vessel functions.

Advanced power management, monitoring and control systems in combination with intelligent power systems, generating concepts will contribute to substantial cost and resource savings.

### 3. CONCLUSIONS

The simulators permit analysis and calculating of energy efficiency of ship power plants.

The analysis permit to solve optimization problems, connected to integrated ship power plants.

Different scenarios could be used for education, study, trainee, examination.

The opportunity to develop different scenarios is available too

## REFERENCES

- [1]. IMO Study on Greenhouse Gas Emissions from Ships 2008/2009 United Nations, Information by the International Maritime Organization (IMO), Multi-year Expert Meeting on Transport and Trade Facilitation: 16-18 February ,2009, **Maritime Transport and the Climate Change Challenge**
- [2]. LNG Fuelled Vessels  
([http://www.gallois.be/ggmagazine\\_2009/gg\\_03\\_05\\_2009\\_138.pdf](http://www.gallois.be/ggmagazine_2009/gg_03_05_2009_138.pdf).)
- [3]. Japanese firms to take solar power to sea  
([http://www.eneos.co.jp/english/press/e71\\_enpr\\_081219.html](http://www.eneos.co.jp/english/press/e71_enpr_081219.html))
- [4]. First fuel cell passenger ship launches in Germany  
([http://www.protonpowersystems.com/news0.html?&tx\\_ttnews\[pointer\]=4&tx\\_ttnews\[tt\\_news\]=49&tx\\_ttnews\[backPid\]=19&cHash=28729afad6](http://www.protonpowersystems.com/news0.html?&tx_ttnews[pointer]=4&tx_ttnews[tt_news]=49&tx_ttnews[backPid]=19&cHash=28729afad6))
- [5]. Ships will use ecoenergy in Italian ports, Mediapool 10.12.2008
- [6]. **The negawatt versus the megawatt, Gary Parke, Evolve Energy ([www.evolveenergy.com/](http://www.evolveenergy.com/))**
- [7]. Kite Ship Corporation of Alameda  
(<http://abclocal.go.com/kgo/story?section=local&id=5668625>)
- [8]. Kite to pull ship across Atlantic, Tuesday, 22 January 2008, 10.55 GMT  
(<http://news.bbc.co.uk/2/hi/europe/7201887.stm>)

## ANALITIC METHOD FOR THE TEMPERATURE DISTRIBUTION INSIDE THE CILINDER WALLS

<sup>1</sup>OMOCEA ION, <sup>2</sup>TURCOIU TITI

<sup>1</sup>Constanta Maritime University, Romania, <sup>2</sup>Romano-Americana University of Bucharest, Romania

Is important to determine the temperature distribution inside the cylinder walls as well as on the two faces of the cylinder. It's necessary to be able to predict any deterioration of the material due to thermal stresses.

**Keywords:** temperature oscillations, amplitude of gas temperature, temperature distribution.

### 1. INTRODUCTION

Temperature determination on the inside of cylinder and outside temperature (on the cooling liquid side) it is very important to determine temperature distribution inside the cylinder walls.

With this it is possible to predict any deterioration of the material due to thermal stresses. We use the following terms:

- $T_{mg} = 1300$  [K] –average gas temperature;
- $T_{fr} = 340$  [K] –cooling liquid temperature;
- $\bar{\alpha}_{gp} = 400$  [W/m<sup>2</sup>K] –average heat coefficient from gas to cylinder;
- $\lambda = 55$  [W/mK] –thermal conductivity of the cylinder;
- $\bar{\alpha}_{pfr} = 1500$  [W/m<sup>2</sup>K] –thermal convection coeff. from cyl. to cooling liquid;
- $\delta = 40$  [mm] – cylinder thickness

### 2. THEORY

Heat flow can be computed using:

$$q = k(T_{mg} - T_{fr}) \left[ \frac{W}{m^2} \right] \quad (1)$$

where:

$$k = \frac{1}{\frac{1}{\alpha_{gp}(m)} + \frac{\delta}{\lambda} + \frac{1}{\alpha_{pfr}}} = \frac{1}{\frac{1}{400} + \frac{40 \cdot 10^{-3}}{55} + \frac{1}{1500}} = 256 \left[ \frac{W}{m^2 K} \right] \quad (2)$$

$$q = 256 \cdot (1300 - 340) = 254400 \left[ \frac{W}{m^2} \right] \quad (3)$$

Temperature determination on the inside of cylinder:

$$q = \alpha_{gp}(m) [T_{mg} - T_p(x=0)] \quad (4)$$

$$T_{p1} = T_p(x=0) = T_{mg} - \frac{q}{\alpha_{gp}} = 1300 - \frac{254400}{400} = 664 \text{ [K]} \quad (5)$$

Outside temperature (on the cooling liquid side) can be determined by:

$$q = \frac{\lambda}{\delta} (T_{p1} - T_{p2})$$

$$T_{p2} = T_p(x=\delta) = T_{p1} - q \frac{\lambda}{\delta} = 664 - 254400 \frac{0,04}{55} = 478 \text{ [K]} \quad (6)$$

To be noted that compared to a thinner cylinder the temperature difference on the two side of the cylinder increases with the thickness and thus thermal stresses.

Pressure distribution inside cylinder walls can be determined by

$$\Delta T_{px1} = \varphi \Delta T_g e^{-x1 \sqrt{\frac{\pi}{az}}} \text{ [m]} \quad (7)$$

where:  $\Delta T_g$  - temperature difference to  $T_{mg}$ .

This relation allows the determination of the distance  $x_1$  where temperature oscillations can be sensed:

$$x_1 = \sqrt{\frac{az}{\pi}} \cdot \ln \frac{\Delta T_g}{\Delta T_{px1}} \cdot \varphi \text{ [m]} \quad (8)$$

here:

$$\ln \frac{\Delta T_g}{\Delta T_{px1}} = \frac{2200 - 1300}{573 - 473} = 2,19 \quad (9)$$

Using known and computed values it can be determined that distance to which temperature oscillations take place is 0,0

**Table1.Oscillations depth function of engine rotations**

Nr crt	RPM	Temperature oscillations depth function [m]
1	50	0,037
2	60	0,032
3	70	0,028
4	80	0,025
5	90	0,023
6	100	0,020
7	110	0,018
8	120	0,017

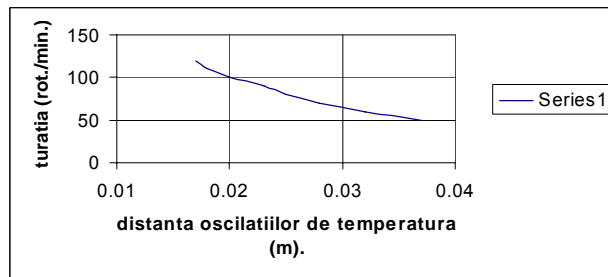


**Fig.1. Oscillations depth function of engine rotations**

Duration of a two stroke engine cycle at 120 RPM is:

$$z = \frac{60}{n} = \frac{60}{120} = 0.5 \text{ [s]} \quad (10)$$

$$\varphi = \frac{1}{\sqrt{1 + 2 \frac{\lambda}{\alpha_{gp}} \sqrt{\frac{\pi}{az}} + 2 \left( \frac{\lambda}{\alpha_{gp}} \right)^2 \frac{\pi}{az}}} = 0,185$$

$$a = \frac{\lambda}{\rho c_p} = \frac{55}{7 \cdot 680} = 0,011 \left[ \frac{m^2}{s} \right] \quad (11)$$

Temperature oscillations on the inside face of a cylinder can be obtained with:

$$\Delta T_p(x=0) = \varphi \Delta T_g \cos(2\pi \frac{\tau}{z} - \psi) \text{ [K]} \quad (12)$$

where:  $\tau$  - time

when  $\cos(2\pi \frac{\tau}{z} - \psi) = 1$  - the amplitude is maximum

$$\Delta T_p(x=0) = \varphi \Delta T_g = 0,185 \times 900 = 166,5 \text{ [K]} \quad (13)$$

**Table 2. Temperature oscillations function of RPM**

Nr crt	RPM	Temperature oscillations for $\Delta T_g = 900 \text{ K}$	Temperature oscillations for $\Delta T_g = 1200 \text{ K}$
1	50	234	312
2	60	225	300
3	70	207	276
4	80	198	264
5	90	189	252
6	100	180	240
7	110	171	228
8	120	166	216

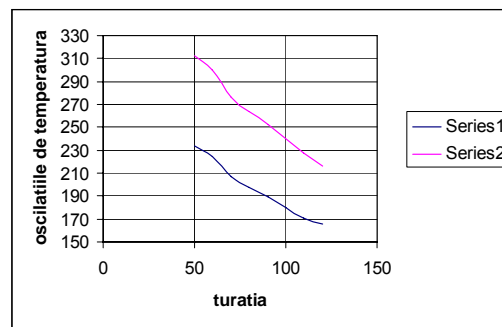


**Fig.2. Temperature Oscillations Function Of Rpm**

### 3. CONCLUSIONS

It is to be noted from the figure 1, that a decrease in engine rotation, causes the oscillation depth to increase towards the cooling liquid.

From the figure 2 it can be notated that temperature amplitude for  $x = 0$  decreases with rotation, but for the same rotation increases with amplitude of gas temperature.

Superposition of temperature oscillations over existing temperature field can had to increase in thermal stresses over admissible values.

### REFERENCES

- [1]. \*\*\* *Documentația motoarelor Sulzer.*
- [2]\*\*\* *Documentația motoarelor M.A.N.*
- [3]. Omocea I. – *Procese in motorul cu aprindere prin comprimare, tratate cu ajutorul termodinamicii ireversibile* - Ed. Paideia, Bucuresti, 2003.
- [4]. Popa, B., s.a. *Solicitări termice în construcția de mașini* - Ed. Tehnică, București, 1978.

## THE SEAFARERS'S LONELINESS; A FACTOR OF RISK FOR MARITIME SAFETY

RODRÍGUEZ-MARTOS RICARDO

*Universitat Politècnica de Catalunya, Spania*

Very often, when speaking about reduction of crews the shipping industry just thinks about the technical possibilities for such reductions. Unfortunately it will be paid less attention to the sociological and psychological impact, which can put into risk the vessel and the crew. There are several human consequences of crew reduction that should be taken in account according to the different kind of trips and also to the general possibility of crews to communicate among themselves. The communication language and the availability of somebody to speak are both, very important. Boredom can also affect concentration and attention. The loneliness feeling can, on the other hand, propitiate the consume of drugs in the case of people with some tendency to addictions. In this paper we will analyze these factors and suggest also some guidelines for the future.

**Keywords:** reduction of crews, loneliness, communication, safety, boredom, drugs, new technologies.

### 1. THE SOLITUDE OF THE SEAMAN

The solitude of the seamen is practically a cliché. In speaking of a seaman's hard life, the first problem that usually arises is that of solitude, a factor closely bound up with the seafaring profession. We will now go on to look at some aspects of seamen's solitude and to try to find ways of reducing it.

Although seamen are in the company of other crew members, companions, with whom they spend a lot of time, their distance from their homes and families, and being unable to go home at the end of the day, undoubtedly induce a feeling of solitude.

Solitude can be however worst when the seafarer has neither the possibility to share his free time with other colleagues because there is no body available or perhaps because the people around him speak another language.

This solitude can be more or less severe, depending upon both the situation of the individuals themselves and the atmosphere on board. Individuals with no strong affective links on land will not suffer from solitude except in the sense of limitation of their chance of speaking to other people or relating to society in general. Young, single men with a desire to see the world, though they may at times think of their family and friends, will experience solitude in a different way from the married men with children. And sometimes it will, of course, depend on a person's character; some people feel perfectly content alone, while others cannot bear it.

These are factors about which little can be done. Men with strong affective links will not stop having them, and men who cannot stand solitude will continue to suffer its

consequences. And there will in any case be a certain element of simply getting used to it, which also plays an important role.

As for the atmosphere aboard, this can depend on diverse factors such as:

- total number of crew;
- design of the vessel;
- individualizing tendencies;
- new technologies
- personal affinity;
- communication
- type of voyages.

## 2. REDUCTION OF CREWS AND INCREASED SOLITUDE

### Number of crew members

This is a factor with considerable influence on the other factors.

On a ship with a large crew there will be a larger proportion of similar professional and cultural level and, if there is a diversity of languages, there are more likely to be several crew members who speak the same language. Furthermore, on large ships a large crew will provide a sensation of Pmore company than would the same ship with a small crew.

And a further two cases can arise: a) vessels designed for example for a crew of thirty, where the crew is reduced to twenty, and b) vessels designed from the outset for a crew of twenty.

Even if the size of the vessel is the same, and the feeling of solitude depends partly on the space-crew ratio, solitude will be more noticeable in case a), because of empty spaces.

### Design of the vessel

If the ship has been designed for a crew of twenty, the cabins will be in line with this, as will the dining room and communal areas. There will be twenty or twenty-one cabins, all the crew will eat in one dining room or maybe two and the lounge will be of the right proportions for the number of people it has to accommodate.

If a vessel has been designed for a crew of thirty and that crew is then reduced to twenty, we will find from the outset that the cabins will be distributed by zones or decks, according to the professional category of the crew members, but in such a way as to always have a number of cabins together. Where the crew is reduced, without undertaking any refurbishment work, there would in this example be ten cabins left empty and, added to that, the twenty crew members would probably be divided into smaller groups per cabin zone. Seeing empty cabins of itself tends to increase a feeling of solitude. And if the vessel had three dining rooms and only two or even one are now used, the unused spaces, unless converted to other uses, will also create a greater feeling of solitude.

If, on the other hand, the vessel was actually built for a crew of twelve, spaces will be well used, with none left empty, and the sensation of solitude will not be so acute.

### Individualizing tendencies

Anthony Stringfellow of the Apostleship of the Sea in Liverpool asserted in relation to solitude: *I think perhaps the problem has got worse than it used to be. Nowadays, of course, everyone has his own cabin, and more and more of them carry their own stereos and now videos too. Then he has his own duty-free drinks and increasingly, I'm sorry to say, his own drugs. But I think with all this personal technology there is a tendency for people to isolate themselves more than they used to do. On top of that, ships today have much smaller crews, and that means the men have fewer chances of being together, of even meeting each other just in passing in different parts of the ship. This aspect of the problem has even been*

*officially recognised - naval architects and shipowners are now thinking of ways of designing the accommodation so that in the normal course of moving about they can ensure that people have a chance of meeting each other"*

Similarly, Rodney Wilson, an English ex-cook, commented: *Sometimes you're sitting there in your cabin when a companion comes down off his watch and all you hear is the gurgling of a tap being turned on and then a little music.*

It should not be deduced from this that if cabins are shared the crew members feel less alone. Indeed, crew members need a space to themselves in which they can commune with themselves in privacy. The problem arises when a person shuts himself away inside himself, as if trying to flee from the ship, as if trying to forget he was in the middle of the ocean.

#### New technologies

In the last years the number of seafarers with their own laptop is quickly increasing. This means that they can not only watch films, but also play many different games. So people spend less time in common areas and more time in their own cabins.

The fact that internet connection at sea is still very expensive has until now avoid that seafarers spend time chatting or navigating through the net, but this will probably change in the future.

Internet connection, like telephone calls, is something that seafarers use to do from seamen's clubs, where they can easily have access to such facilities.

However, there is a phenomenon that the author of this article has observed in the last times, when ships with Chinese crews arriving in Barcelona port: Almost every seafarer comes to the seamen's club with his own laptop, they ask for the wifi code and during the 3 or 4 hours they have free, they don't speak, they don't go for a walk, they just seat, everyone concentrated in his own laptop chatting or navigating through the net. This is, of course a way to be in touch with their families or friends at home, but this is also a decrease of the possibilities to share free time with the colleagues or to speak with the people in port or even to see something from the city they are visiting.

#### Personal affinity

In order to be able to overcome isolation within the crew itself, there must exist certain affinities which cannot in principle be assessed but can be facilitated. People of common customs and languages will always find it easier to get on, and that affinity can be facilitated in broad terms by controlling the composition of crews.

There are, of course, other factors, such as the character of each individual and his personal circumstances, which are truly difficult to foresee. The entire personnel department of a shipping company should nevertheless bear in mind, in addition to the professional aspect of each crew member, his personality in terms of enhancing a good atmosphere on board. This is of course totally impossible when shipping companies do not have their own crews, but rather have them supplied by manning agencies, an increasingly common situation especially on ships flying flags of convenience.

#### Communication

Communication among crew members is important for the functioning of the crew and for the way it affects the daily life of each crew member.

From the standpoint of the crew as a whole, we can see that with international crews a further and important source of division - language - is added to the circumstances of isolation and having to share a daily routine.

For work and life to run smoothly on board, for the ship to be safe and to perform its allotted task without risk, good relations aboard and good mutual understanding are necessary. When the crew members have difficulty in understanding each other, the crew cannot act as a team.

Difficulties in understanding put the ship's safety in danger when the crew members fail to understand each other.

A side of the important technical problems that can arise, difficulty in understanding also has other negative repercussions, such as mistrust, misunderstandings, and the isolation of the subgroups. This may increase the solitude feeling of some people.

#### Type of voyage

The longer the voyage the more time the crew spends far from home and the more influence the atmosphere on board will have on the sensation of solitude. On a ferry covering, for example, the Barcelona to Palma de Mallorca route, the crew will hardly have any chance to decide whether they get on well together, for they will often spend their free time off the ship and during the eight-hour journey each one will be getting on with his/her own job. Crew members will of course feel more or less content depending on what their workmates or immediate bosses are like, but that will be only the same as in any job, both on land and at sea.

On long voyages, on the other hand, a lack of affective ties and progressive isolation of a person can have harmful effects.

### **3. BOREDOM**

Martin Dyer-Smith has taken a close look at this subject. There is a conundrum implicated in smooth running systems and high levels of training. The expectation that something untoward will happen reduces with system reliability. Confidence increases with training and experience. These two factors can coincide with lethal effect. The bored are a danger to themselves, and others, since their behavior may become increasingly erratic. Mean performance may improve, but fluctuations become more and more pronounced.

Dyer-Smith feels that boredom is the problem most difficult to confront in modern industrial society. It has consequences at individual level (depression, alienation, suicide, etc.) and on a general level (accidents due to inattention, drowsiness, slow reflexes, etc.). Experience of boredom varies from one person to another, and the boredom of listening to a monotonous speaker is not the same as the boredom of the unemployed person or a man on lookout at sea.

Dyer-Smith quotes the remark of a captain: On the bridge you are on half-brain. Most of the time it's like being in a dream ... I don't need a brain anymore.

Dyer-Smith carried out a three-month study into the behavior of the watch aboard a small cargo vessel, observing that:

- watch keepers find day watches more boring than night watches;
- bored watch keepers avoided rather than sought compensating stimulation.

From this Dyer-Smith drew the following conclusions:

- boredom is a form of adaptation to low levels of stimulation;
- stimulation does not alleviate boredom but rather makes it worse;
- in the absence of other resources, a bored person cannot be held by stimulation;
- boredom is really a protection against depression.

Boredom is revealed as a factor of increasing importance, resulting in a steady loss of interest.

Tony Lane explains how a seaman on lookout perched perhaps 60 ft or 70 ft above the water might feel alone in the universe. At that height and on a clear night the eye can take in 170 square miles of ocean in a circular sweep. And it is empty. Lane adds that this seeing nothing in the middle of the ocean, not even any lights, makes the task indescribably tedious.

### **4. DRUGS AND ALCOHOLISME**

Consume of drugs and alcohol has become a concern for many shipping companies and international organisations. On board many ships is alcohol forbidden or controlled.

It is known that for falling in dependence of drugs there are 3 things necessary:  
Drug, person and the environment.

Drug: The addictive capacity of the drug is dependent on his (her, your) pharmacological action (share), on the dose, frequency and time of consumption.

Person

1.) The hereditary load. (So much physics as (like) of education)

2.) The personality of the individual:

- The low tolerance to the frustration.
- The feelings of insecurity and inferiority.
- The impulsiveness and the search of immediate satisfactions.
- The trend to the escapism.
- The difficulty for establishing interpersonal relations.

Environment: It determines the type of relation that is going to be established between the individual and the drug.

There exists an immediate environment or microgroup (family, group of friends) and a social, general, wide environment or macrogroup, of which all the members of a community take part.

This all means that, being available drug or alcohol, if the person fits in someone of the described suppositions and the environment is propitious, the person can fall down in the addiction, with all the negative effects that it implies.

## 5. CONCLUSIONS

We have in the ships two important objective factors of loneliness, which add to the traditional being away from home:

1.) The crew members' reduction, in general, that limits the possibility of human relation and increases the isolation and the loneliness.

2.) The mixture of cultures and languages, which impedes the communication among the crew.

These objective factors, will meet influenced, since it has been said for:

- The whole number of crew;
- The design of the vessel;
- Communication
- Type of voyages.

Additional we will have a subjective factor: the personality of the person, his (her) major or minor introversion.

What can be done?

The number of crew members stipulated should take account of human communication needs and the need for company as well. Everybody should have somebody else to talk to. Here the number of people is not the only factor: having a language in common and some cultural points of contact too, are also necessary. The food should not be too alien, and it should be possible to share customs and practices. People need to live in a social nucleus. Sociocultural habits lose their meaning at the individual level.

Other important factors needing monitoring are alcoholism and drugs. The solitary life of seamen, their easy access to cheap drinks and the availability of drugs in certain ports, all make them particularly vulnerable to these. The starting point, of course, is solitude, lack of communication, and personal frustration.

T. Munk stresses that a ship must be designed and fitted out to reduce the workload for the crew and to reduce the risk of accidents and equipment break-downs and that the crew must be instructed and trained accordingly.

Regarding the social life on board Munk considers that the crew member, as a person, has social needs, and if they are not met his psychic balance will be affected, and consequently his professional performance too may suffer.

Solitude is a terrible burden for a crew member when he has nobody to talk to, either because there really is nobody, or because he does not get on with the people there are around him. Feeling alone is very hard to cope with.

While it is inherently important for any crew that the make-up of the crew and the layout of the space available be conducive to good social relations between crew members, it becomes still more important on a ship with a reduced crew.

Many psychologists and sociologists have studied this matter and agree on the importance of common areas such as mess rooms, day rooms and games rooms being comfortable enough to induce the crew to use them, making them places for meeting and thus avoiding isolation in the cabins.

Mealtimes are important. On ships with traditional crews (20 to 40 people), as we said when talking about the crew in general, there are usually two or three mess rooms, divided along professional-category lines.

This custom is questionable, and present-day social-living patterns may possibly be tending to do away with such distinctions in favor of a better communal spirit among the entire crew.

On ships with crews of six or ten, this problem becomes much more acute, since then we would find that only three to five people would be sharing a mess room, and of them there would probably be one or two who would have to have their meals at a different time on account of the watch keeping schedule. The result is that they would end up having their meals virtually alone. And if on top of this people of different nationality and language are brought together, the results can be really catastrophic.

To make a reduced crew viable in human terms, it must be ensured that its members can communicate without difficulty, that they are all compatible in terms of habits, that they have adequate common areas to meet in, and that life and work on board are organized in such a way that no crew member is permanently condemned to seeing nobody and talking to nobody for days on end.

Undoubtedly, a change in the social attitude of the crew is needed in this. Up to now, owing to traditional reasons and cultural differences, the hierarchical pattern of ships went way beyond what was prompted by labor considerations, and it permeated every aspect of life on board.

In addition to the social evolution of our own times, which perforce leads to a change in such patterns, change becomes urgent and essential on ships with reduced crews. Such a cut-down group must necessarily change its outlook, and links as colleagues and members of the same team must weigh more heavily in human terms than differences in post or role on board.

## REFERENCES

- [1]. Deyer-Smith, M.B.A. *Boring work*. IMLA. Portugal, 1994
- [2]. Klemperer, E. *Reduction of Ships' Crews. Factors to be considered*. Rijeka, 1988
- [3]. Lane T., *Grey Dawn Breaking – British Merchant seafarers in the late twentieth Century*. Manchester, 1986
- [4]. Munk T., Lauritzen J., *Safety considerations in the design and operation of a six-man refrigerated vessel*. London, 1991
- [5]. Perry N., Wilkie R., *Social theory and shipboard structure*. UK, 1973
- [6]. Rodríguez-Martos R., *The merchant vessel; a sociological analysis*. Edicions UPC. Barcelona, 2009

## ANALYSIS OF TRANSIENT DIESEL-ENGINE

<sup>1</sup>SABAU ADRIAN, <sup>1</sup>BARHALESCU MIHAELA, <sup>1</sup>DUMITRACHE CONSTANTIN

<sup>1</sup>Constanta Maritime University, Romania

A computer analysis has been developed for studying the energy and exergy performance of a direct-injection, naturally-aspirated diesel engine operating under transient load or speed conditions. The model is validated at steady-state operation and incorporates many novel features for simulating the transient response and analyzing all of the engine availability terms. The analysis reveals via multiple diagrams how the exergy properties of the diesel-engine subsystems vary according to the engine cycles for various speed and load changes. The diagrams also show the current-speed response. In addition, the effects of operating parameters such as the intensity of the applied change or heat loss to the walls are described from first- and second-law.

**Keywords:** transient, energy, exergy, analysis, engine, load

### 1. INTRODUCTION

Diesel-engine simulation modeling has long been established as an effective tool for studying engine performance and contributing to evaluation and new developments. Thermodynamic models of the real diesel-engine cycle have served as a sound basis for complete analysis of engine performance and sensitivity to various operating parameters. Transient response, especially of turbocharged and naturally aspirated compression-ignition (diesel) engines, forms a significant part of their operation; it is characterized by short but serious off-design functions, requiring careful and proper modeling for successful study of the (speed) response. By contrast, second-law (exergy or availability) analysis with detailed study of what is happening during a process has contributed a new way of thinking about and studying thermodynamic processes.

In the present study, we describe improved simulation of transient operations. Simulation includes detailed analysis of thermodynamic and dynamic differential equations which account for the continuously changing character of transient operations.

Experimental results have been used under a variety of steady-state operating conditions to obtain calibration constants. An exergy balance is applied to all subsystems of the diesel engine such as the cylinder for both the closed and open parts of the cycle and the inlet and exhaust manifolds. We describe how the exergy changes (work, heat transfer, exhaust gas, irreversibilities) develop during a transient event. Only load-change operating schedules have been studied. Furthermore, the effects of important operating parameters such as the intensity of the applied (load) change and heat losses to the walls are investigated with the help of explicit multiple diagrams which show the speed profiles of transient events together with the most significant energy and exergy changes in the engine.

## 2. THEORETICAL BACKGROUND

There is spatial uniformity of pressure, temperature and composition in the combustion chamber at each instant of time (single-zone model). The fuel is dodecane ( $C_{12}H_{26}$ ) with an LHV = 42,500 kJ/kg. We assume perfect gas behavior. Polynomial expressions proposed by Krieger and Borman are used for each of the four species ( $O_2$ ,  $N_2$ ,  $CO_2$ , and  $H_2O$ ) considered in evaluations of internal energy and specific heats for first-law applications to the engine cylinder contents [11].

### Fuel pump and injection

To simulate the fuel-injection rate  $m_n$  (kg/s), the following expression proposed by Ferguson is used:

$$\frac{\dot{m}_{fi}}{M_{tot}} = \frac{\omega(\varphi)}{\varphi_d \Gamma(n)} \left( \frac{\varphi - \varphi_s}{\varphi_d} \right)^{n-1} \exp\left( -\frac{\varphi - \varphi_s}{\varphi_d} \right) \quad (1)$$

where  $\ln \Gamma(n) = (n - 0.5) \ln(n) - n + 0.5 \ln(2\pi) + 1/(12n) - 1/(360n^3) + 1/(1260n^5)$  with  $n = 3.6$ . Here,  $\varphi_s$  is the crank angle where injection begins,  $\varphi_d$  the duration of injection, and  $M_{tot}$  the total amount of injected fuel per cycle, which is found by using experimental data under steady-state conditions for the applicable engine-speed and fuel-pump rack position.

### Combustion

For the study of combustion processes, the model proposed by Whitehouse and Way is used [8], i.e we include preparation-limited and reaction-limited combustion rates. The corresponding equations are:

$$P = K_1 M_i^{1-x} M_u^x p_O^y \quad (\text{kg of fuel } / ^\circ\text{CA}), \quad (2a)$$

for the preparation rate, which controls the rate of burning of most of the fuel, and

$$R = \left( K_2 p_O / N \sqrt{T} \right) e^{-E_{act}/T} \int (P - R) d\varphi \quad (\text{kg of fuel } / ^\circ\text{CA}), \quad (2b)$$

for the rate responsible for the early part of combustion. Here,  $M_i = \int_{\varphi_i}^{\varphi} (dm_{fi} / d\varphi) d\varphi$  is the total mass (kg) of injected fuel up to the crank angle  $\varphi$  and  $\varphi dm_{fi} / d\varphi$  is the injection rate known from Eq. (1). Also,  $M_u = M_i - \int P d\varphi$  is the total mass (kg) of unprepared fuel, act is the reduced activation temperature (K) which accounts for the ignition delay, and  $p_O$  is the partial pressure of oxygen (bars). The constants  $x$ ,  $y$ ,  $K_1$ , and  $K_2$  are found from calibrations against experimental data under steady-state conditions.

It is vital for proper simulation of transient responses that combustion modeling takes into account the continuously changing character of the operating conditions. The constant

$K_1$  in the (dominant) preparation-rate equation is correlated with the Sauter mean diameter (SMD) of the fuel droplets by the relation  $K_1 = 1/(SMD)^2$ . The empirical expression of Hiroyasu is used, i.e.

$$SMD = 23.9(\Delta p)^{-0.135} \rho_g^{0.12} V_{tot}^{0.131} \text{ (}\mu\text{m)} \quad (3)$$

where  $\Delta p$  is the mean pressure drop across the injection nozzle in MPa,  $\rho_g$  the air density in kg/m<sup>3</sup> at the beginning of injection, and  $V_{tot}$  (in mm<sup>3</sup>) is the amount of fuel delivered per cycle per pump stroke.

### Heat transfer

The model of Annand is used to simulate heat loss to the cylinder walls, is,

$$dQ_L / dt = F \left[ a(\lambda / D) \text{Re}^b (T_w - T_g) + c(T_w^4 - T_g^4) \right] \quad (4)$$

where  $F = \pi D^2 / 4 + \pi D x$  is the surface and  $x$  the instantaneous cylinder height in contact with the gas;  $\lambda$  is the gas thermal conductivity (W/mK) and the Reynolds number  $\text{Re}$  is calculated with a characteristic speed equal to the mean piston speed and a characteristic length equal to the piston diameter  $D$ . For transient engine operation, a hysteresis expression is used to update the wall temperature  $T_w$  at each consecutive cycle, which changes as a result of the increase in speed and/or fuelling [10].

### Mechanical friction

To calculate the friction inside the cylinder, the following expression of Millington and Hartles [8] is used:

$$(f_{mep})_{st} = 0.123CR + 4.774 \cdot 10^{-4} N, \quad (5)$$

where  $(f_{mep})_{st}$  is the friction mean effective pressure (bar) at steady-state conditions and  $CR$  is the engine compression ratio.

For transient operations, we use the relation:

$$(f_{mep})_{tr} = (f_{mep})_{st} \left[ 1 + \varepsilon_{fr} \left| \varepsilon / \varepsilon_{\max} \right| \right], \quad (6)$$

where  $\varepsilon$  stands for the current angular acceleration (mean value over the engine cycle) and  $\varepsilon_{\max}$  is the maximum angular acceleration (or deceleration) which is experienced due to a 0-100% load increase (or decrease) during one cycle. The constant  $c_{fr} = 0.5$  to make the results agree with a proposal by Winterbone.

### Engine dynamics

If  $G_{tot}$  (in  $\text{kg}\cdot\text{m}^2$ ) represents the total system moment of inertia (engine, flywheel, and load), then the conservation of energy principle applied to the total system (engine plus load) is [2]

$$T_e(\varphi, \omega) - T_L(\omega) - T_{fr} = G_{tot} (d\omega / dt) \quad (7)$$

Here,  $T_e(\varphi, \omega)$  stands for the instantaneous value of the engine torque, which is the sum of the gas and inertial forces torque, i.e. [2]

$$T_e(\varphi, \omega) = [p_g(\varphi)F_p R_1 + N_{Tm}]r \quad (8)$$

where  $p_g(\varphi)$  is the instantaneous gas pressure,  $F_p$  the piston cross-sectional area =  $\pi D^2/4$ ,  $R_1$ , a measure of the instantaneous piston velocity [2], and  $N_{Tm}$  the force acting on the piston due to the inertia of the moving parts (piston and a part of the connecting rod) with the complex movement of the rod taken into consideration [2]. In Eq. (7), the load torque is

$$T_L(\omega) = \tau - k\omega^2. \quad (9)$$

For the cases that will be analyzed, the load is either linear (electric brake) so that  $\tau = 0$ ,  $s = 1$  and  $k > 0$  or rigid (automotive applications) with  $\tau \neq 0$  and  $k = 0$ .

In Eq. (7),  $T_{fr}$  stands for the friction term, which is constant during each cycle and is related to the transient friction mean effective pressure (fmep)<sub>tr</sub> by the expression

$$T_{fr} = [(fmp)_{tr} / 2\pi]F_p r. \quad (10)$$

### Governor dynamics

A mechanical governor is simulated in the present analysis. It operates according to Watt's principle. During transient operation, Newton's second law of motion for the sensing element of the governor (on a °CA basis) is [10]

$$m_{gov}\omega^2 (d^2 z / d\varphi^2) + f\omega(dz / d\varphi) + (k - b_{se}\omega_{gov}^2)z = a_{se}\omega_{gov}^2 - ky_0, \quad (11)$$

Where:  $z$  is the current displacement of the governor clutch (equal to the spring deformation),  $f$  the clutch friction coefficient (Ns/m),  $\omega_{gov}$  the combined mass of die clutch and flyweights,  $k$  the governor spring stiffness (N/m),  $a_{se}$  and  $b_{se}$  are characteristic properties of the governor sensing element [10], and  $y_0$  is the prior governor spring strain (also known as the governor setting).

### 3. ANALYSIS

The availability or exergy of a system in a given state is defined as the maximum reversible work that can be produced through interaction of the system with its surroundings as it reaches thermal, mechanical and chemical equilibrium [6,9]. In this study, only thermal and mechanical availability terms are taken into account, while chemical availability is involved only in the reactions of fuels to form products.

Application of the exergy-balance equation to diesel-engine subsystems, on a °CA basis, yields the relations given in the three succeeding paragraphs [6,9]:

For me cylinder,

$$dA_{cyl} / d\varphi = (\dot{m}_2 b_2 - \dot{m}_3 b_3) / 6N - dA_w / d\varphi + dA_L / d\varphi + d \quad (12)$$

The terms on the r.h.s. of Eq. (12) have the following meanings:

$$dA_w / d\varphi = (p - p_0)(dV / d\varphi) \quad (13)$$

is the work transfer, where  $dV / d\varphi$  is the rate of change of cylinder volume with crank angle [2,10];

$$dA_L / d\varphi = (dQ_L / d\varphi)[1 - T_0 / T_g] \quad (14)$$

is the heat transfer to the cylinder walls with  $dQ_L / d\varphi$  given by the Annand correlation (Eq.(4)), and  $T_g$  the instantaneous cylinder gas temperature;

$$dA_f / d\varphi = (dm_{fb} / d\varphi) a_{fch}, \quad (15)$$

where  $a_{fch}$  is the availability associated with burning for liquid hydrocarbon fuels of the type  $C_m H_n$  and is given by [1]

$$a_{fch} = LHV[1.04224 + 0.011925(n/m) - 0.042/m]. \quad (16)$$

For the present analysis,  $m = 12$ ,  $n = 26$  and  $a_{fch} = 1.064 LHV$ . The fuel burning rate  $dm_{fb} / d\varphi$  is given by the Whitehouse-Way model (Eq. (2a) or (2b)). The term on the l.h.s. of Eq. (12) is represented explicitly by

$$dA_{cyl} / d\varphi = dU / d\varphi + p_0(dV / d\varphi) - T_0(dS / d\varphi) - dG_0 / d\varphi \quad (17)$$

and is the change in availability of the cylinder contents, with  $U$  denoting the internal energy (J),  $S$  the entropy (J/K),  $G$  the Gibbs free enthalpy (J), and  $V$  the instantaneous cylinder volume (m<sup>3</sup>). Details concerning the derivation of the terms  $U$ ,  $S$  and  $G_0$  may be found in Refs. [1] and [2]. The terms  $m_2 b_2$  and  $m_3 b_3$  in Eq. (12) refer to the inflowing and outflowing exergy, respectively, where the flow availability is [11]

$$b = h - h_0 - T_0(s - s_0). \quad (18)$$

The term  $dI/d\varphi$  in Eq.(12) is the rate of irreversibility production within the cylinder which consists mainly of the combustion term, while inlet-valve throttling and mixing of the incoming air with the cylinder residuals contribute a little [2].

For the inlet manifold, the exergy-balance equation is [6]

$$dA_{im}/d\varphi = (\dot{m}_1 b_1 - \dot{m}_2 b_2)6N - dI_{im}/d\varphi, \quad (19)$$

where  $b_1$  is the flow availability at the intake-manifold inlet evaluated at atmospheric conditions. The term for irreversibilities  $dI_{im}/d\varphi$  accounts for mixing of atmospheric air with the intake manifold contents.

For the exhaust manifold, the exergy-balance equation is [10]

$$dA_{em}/d\varphi = (\dot{m}_3 b_3 - \dot{m}_4 b_4)6N - dI_{em}/d\varphi + dA_{Lem}/d\varphi, \quad (20)$$

where the index 3 denotes exit conditions from the engine cylinder and the index 4 identifies the exhaust manifold state. The term  $dA_{Lem}/d\varphi = (dQ_{Lem}/d\varphi)[1 - T_0/T_{em}]$  accounts for heat losses at the exhaust manifold, where  $T_{em}$  is the instantaneous temperature of the manifold contents. The term  $dI_{em}/d\varphi$  is the irreversibility rate in the exhaust manifold, which arises from throttling across the exhaust valve, mixing of cylinder exhaust gases with manifold contents and friction along the manifold length. The terms  $dA_{em}/d\varphi$  and  $dA_{im}/d\varphi$  Eqs. (20) and (19), respectively, are evaluated according to Eq. (17); for unsteady operations, they do not sum to zero (as they do for steady-state operation) at the end of a full

cycle of the working medium. Their respective cumulative values  $\int_0^{720} (dA/d\varphi)d\varphi$  are, however, small compared to the other availability terms, due to the natural aspiration operation of the engine.

#### 4. RESULTS AND DISCUSSION

Equation (7) describes the energy balance at the crankshaft and Eqs. (12), (19) and (20) describe the exergy balances in the cylinder, inlet and exhaust manifolds, respectively. They have been applied for various schedules of load changes and the results are given in Figs. 1-3. The engine under study is a naturally aspirated, indirect injection, T684 diesel engine

Figures 1-3 refer to load changes which are characterized by the following data: the initial load is 15% of the full engine load at the initial speed of 1500 rpm; (b) the full engine load (100%) at 1500 rpm is applied within 0.2 s; and (c) the load type is linear with a total moment of inertia  $G_{lot} = 1.5\text{kg}\cdot\text{m}^2$ .

Figure 1 is a presentation of predicted engine responses for speed, injected fuel, engine and load torques, and maximum cylinder pressures (main chamber and prechamber) to nominal load changes. At the initial condition, the engine and load torques are equal. As soon as the new load is applied, the engine speed drops because the load torque becomes considerably greater than its engine counterpart. This imbalance leads to a movement of the governor towards a position of more fuelling. Because the load type is linearly related to speed, the load torque decreases with speed, resulting in a rapid counterbalance between engine and load.

Figure 2 shows the responses of the exergy terms, indicated work, heat loss to the walls, exhaust gas from the cylinder, exhaust-manifold gas to the ambient, cylinder irreversibilities, and inlet and exhaust manifold irreversibilities as functions of the cycles. All of these terms are cumulative values over each cycle, divided by the chemical availability of the current

cycle fuel. The exergy terms for heat losses to the walls increase as functions of the number of engine cycles because of increases in the charge temperatures resulting from increases of the injected fuel quantities and accompanying fuel-air equivalence ratios  $f$ , similar results hold for the two exhaust-gas terms. All of the specified properties have profiles similar to the fuel term in Fig. 1.

Cylinder (combustion) irreversibilities decrease as the transient events proceed due to the fact that combustion irreversibilities fall with increasing loads. Greater loads result in less degradation of fuel chemical availability when transferred to the exhaust gases and also less mixing of exhaust gases with the air. The inlet-manifold irreversibilities constitute a very small percentage of the fuel chemical availability, whereas those for the exhaust manifold increase substantially between cycles 10 and 30 for which the main increase in injected fuel quantity occurs.

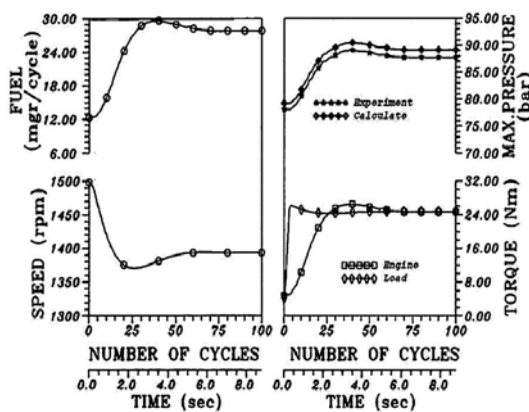


Fig. 1. Predicted engine energy response to an increase in load.

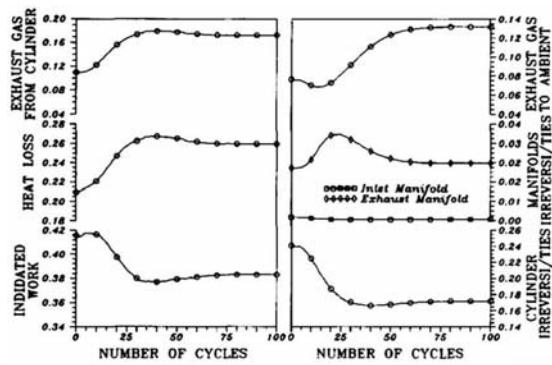


Fig. 2. Predicted engine exergy response to an increase in load.

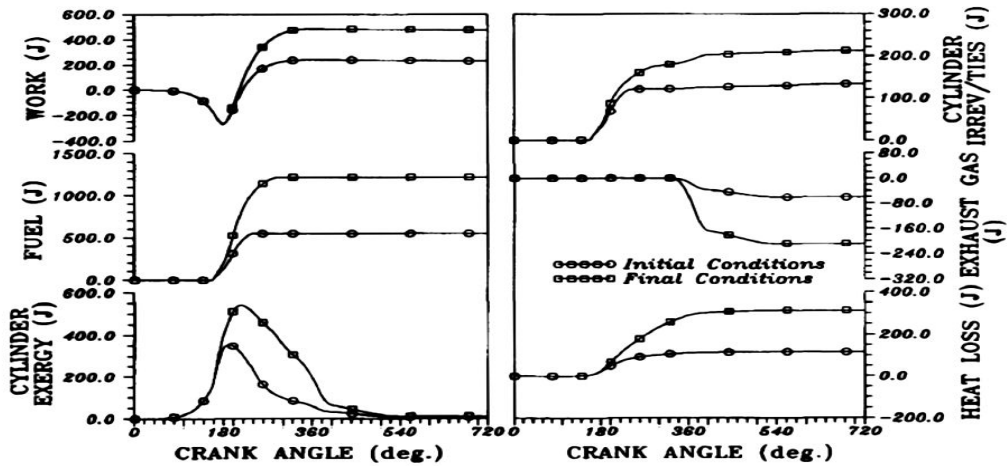


Fig. 3. Developments in the cumulative exergy terms of diesel engine at the initial and final steady-state conditions, after an increase in load.

Figure 3 is focused on the first and last cycles of the particular transient operation and shows the differentiation in the development of the various cumulative exergy terms.

## 5. CONCLUSIONS

A detailed first- and second-law analysis has been performed on a single-cylinder, naturally-aspirated, indirect-injection diesel engine to study the energy and exergy performance of engine subsystems during various transient operating schedules comprising changes in speed and load. We conclude that combustion irreversibilities decrease after a ramp increase in load, whereas the intensity of the heat lost to the walls has a minimal effect on the combustion irreversibilities. The indicated work decreases after both speed or load increases. Furthermore, the exergy terms for the heat losses to the walls increase after an increase in load, which becomes especially clear the greater the heat loss to the walls becomes. However, an increase in speed under a constant load reduces the relative value of the exergy terms for heat losses. The exergy terms for the exhaust gases from the cylinder and for the exhaust-manifold gas to the ambient increase with increasing load or speed and also with decreasing heat loss to the walls. The exhaust-manifold irreversibilities vary strongly during a load or speed change, while the inlet-manifold irreversibilities are insignificant.

## REFERENCES

- [1] Bazari, Z., *Diesel exhaust emissions prediction under transient operating conditions*. SAE paper No. 940666, Society of Automotive Engineers, Inc., Warrendale, PA, 1994.
- [2] Bejan, A., Tsatsaronis, G. and Moran, M., *Thermal Design and Optimization*. Wiley, New York, 1996.
- [3] Benson, R. S. and Whitehouse, N. D., *Internal Combustion Engines*. Pergamon Press, Oxford, 1979.
- [4] Bozza, F., Nocera, R., Senatore, A. and Tuccillo, R., *Second law analysis of turbocharged engine operation*. SAE Paper No. 910418, Society of Automotive Engineers, Inc., Warrendale, PA, 1991.
- [5] Dunbar, W. R. and Lior, N., *Teaching power cycles by both first-and-second law analysis of their evolution*. Proc. ASME-WAM, AES Vol. 27, Anaheim, CA, November, 1992.
- [6] Gyftopoulos, E. P. and Beretta, G. P., *Thermodynamics: Fundamentals and Applications*. Macmillan, New York, 1991.
- [7] Heywood, J. B., *Internal Combustion Engine Fundamentals*. McGraw-Hill, New York, 1988.
- [8] Millington, B. W. and Hartles, E. R., *Frictional losses in diesel engines*. SAE Paper No. 680590, Society of Automotive Engineers, Inc., Warrendale, PA, 1968.
- [9] Moran, M. J. and Shapiro, H. N., *Fundamentals of Engineering Thermodynamics*. Wiley, New York, 1992.
- [10] Rakopoulos, C. D., Hountalas, D. T., Mavropoulos, G. C. and Giakoumis, E. G., *An integrated transient analysis simulation model applied in thermal loading calculations of an air-cooled diesel engine*. SAE paper No. 970634, Society of Automotive Engineers, Inc., Warrendale, PA, 1997.
- [11] Sabau, A., Buzbuchi, N., Șoloiu, V.A.: *Combustion Numerical Modelling in Diesel Engines*. In Volumul "A XI-a Conferință Națională de Termotehnică", 8 pag., Galați, 2001.
- [12] Van Gerpen, J. H. and Shapiro, H. N., *Trans. ASME, J. Engng Gas Turbines Power*, 1990, **112**, 129.

## SIMULATION OF FUEL INJECTION PIPE PRESSURE

<sup>1</sup>SABAU ADRIAN, <sup>1</sup>DUMITRACHE CONSTANTIN, <sup>1</sup>BARHALESCU MIHAELA,

<sup>1</sup>Constanta Maritime University, Romania

Fuel injection pipe pressures are measured and simulated to study the effect of fuel injection pipe length on the injection system characteristics in a direct injection diesel engine. The fuel injection simulation is based on a linear model. The governing equations are solved by the finite difference method.

**Keywords:** injection, nozzle, finite difference method, fuel pipe

### 1. INTRODUCTION

Diesel engine is one of the power generation devices which convert chemical energy to mechanical energy. Due to its high thermal efficiency, diesel engines have been applied more and more to the vehicles and power plant. Due to the pollution of the environment and the shortage of energy sources, many diesel engine researches are carried on to improve the performance and to reduce the toxic emissions such as NO<sub>x</sub> and Particulates [11]. Many of these researches are focused on the optimization of the fuel injection system. This is because the diesel combustion processes are characterized by non-homogeneous diffusion flame and auto-ignition. The fuel injection system affects the diesel engine combustion process through the control of injection time, injection quantity and injection rate [6]. Many simulations of the diesel engine fuel injection system are carried out to understand the fuel injection system characteristics[8].The method of characteristics and the finite difference method have been used to solve the governing equations. Recent studies show that finite difference method is more advantageous than the method of characteristics concerning computation time and nonlinearity [7]. A simple linear model solved by the finite difference method is developed in this study which is programmed in Matlab language. An one-zone heat release calculation [5] is carried out using the measured cylinder pressure to analyze the combustion process.

### 2. SIMULATION

#### Fuel injection system modeling

The task of the fuel injection system is to meter the appropriate quantity of fuel for given engine speed and load, and to inject that fuel at an appropriate time. A fuel injection system is divided into pump, pipe and nozzle component to model the entire system. Following assumptions are made to develop a model [8] The variation of fuel bulk modulus and density is negligible.

The flow in the fuel injection pipe is one dimensional laminar flow. The convective term in the momentum equation can be neglected. The steady flow friction coefficient is used for the transient flow friction coefficient. The discharge coefficient is constant everywhere in the fuel injection system. As a result of above assumptions, a linear equation of state for the pressure can be formulated as Eqs. (1) and (2).

$$P = \beta_0 S \quad (1)$$

$$S = \frac{\rho - \rho_0}{\rho_0} \quad (2)$$

### Fuel injection pump

The volume of the pump component can be divided into 3 control volumes such as plunger chamber, delivery chamber, and spill port as shown in Fig. 1. The continuity of flow in 3 control volumes and the equilibrium of forces on the delivery valve give three governing equations.

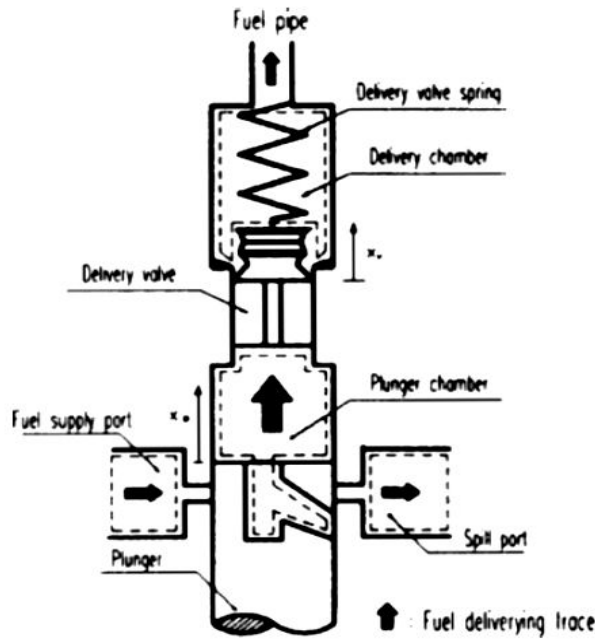


**Fig. 1 Schematic diagram of a fuel pump modeling**

An orifice model is used as a flow model for the interfacing control volume.

$$A_p \frac{dX_p}{dt} = \frac{V_p}{\beta_0} \frac{dP_p}{dt} + A_v \frac{dX_d}{dt} + Q_{pd} + Q_{ps} \quad (3)$$

$$A_v \frac{dX_d}{dt} + Q_{pd} = \frac{V_p}{\beta_0} \frac{dP_p}{dt} + \frac{dW_1}{dt} \quad (4)$$

$$M_d \frac{d^2 X_p}{dt^2} + k_d X_d = A_v (P_p - P_d) - f_d \quad (5)$$

### Fuel injection pipe

The continuity equation, momentum equation and the equation of state (Eq. (1)) are taken into account to calculate the flow and the pressure in the fuel injection pipe. The momentum equation can be expressed by Eq. (6) in the form of a cumulative flow equation.

$$\frac{d^2 W}{dt^2} = -\frac{A_{pipe}}{\rho_0} \frac{\partial P}{\partial x} - \frac{32\nu}{D^2} \frac{\partial W}{\partial t} \quad (6)$$

### Fuel injection nozzle

The fuel injection nozzle volume can be separated into two control volumes, i. e. nozzle chamber volume and sac volume as in Fig. 2. It is assumed in the process of constructing governing equations that the injection rate into the combustion chamber is the same as the fuel flow rate from the nozzle chamber to the sac volume. By considering of the continuity equation and the equilibrium of force on the needle valve, Eqs. (7) and (8) can be obtained.

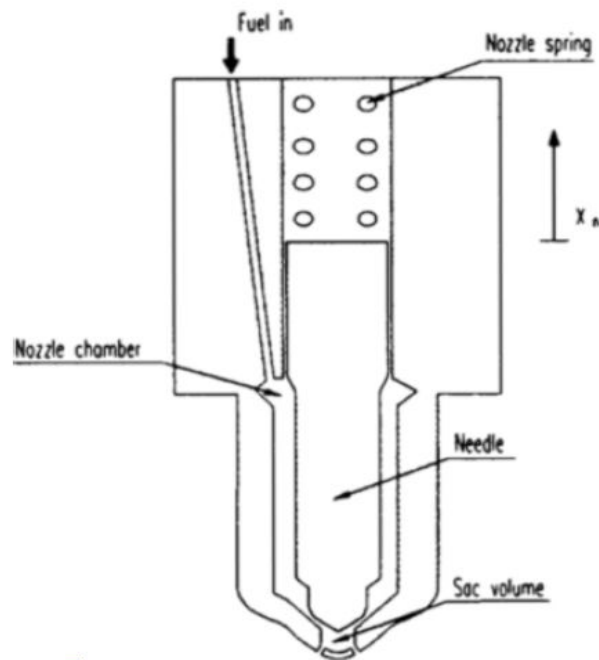


Fig. 2 Schematic diagram of a nozzle

### Boundary conditions

Fuel is delivered into the cylinder through the injection pump, the injection pipe, and the injection nozzle. Fuel is compressed by the plunger lift in the pump and injected into the cylinder. For that reason, the plunger lift and the cylinder pressure are used as the boundary condition. The plunger lift is calculated from the cam profile and roller's diameter in the in-line pump. The cylinder pressure is measured by the pressure transducer mounted in the cylinder head. As mentioned above, the entire fuel injection system is modeled as a three-component model i. e. pump, pipe, and nozzle. In order to calculate the whole system, it is assumed that the delivery chamber pressure is identical to the first node pressure of the injection pipe. Similar assumption is also applied to another boundary section where the last node of the fuel pipe meets the nozzle chamber.

### Calculation method

When Eqs. (3), (4), and (7) are discretized by the finite difference method, they are nonlinear equations. To find solutions for these nonlinear simultaneous equations, Newton Raphson method is employed. The fuel injection pipe governing equations are turned into a finite difference form by the Leap-Frog scheme. This explicit scheme converges when Eq. (9) is satisfied. [1]

$$\frac{\Delta X}{\Delta t} \geq C_0 = \sqrt{\frac{\beta_0}{\rho_0}} \quad (9)$$

## 3. EXPERIMENT AND ANALYSIS

The experiment is carried out to measure the cylinder pressure and the fuel injection pipe pressure four tow length of fuel pipe.

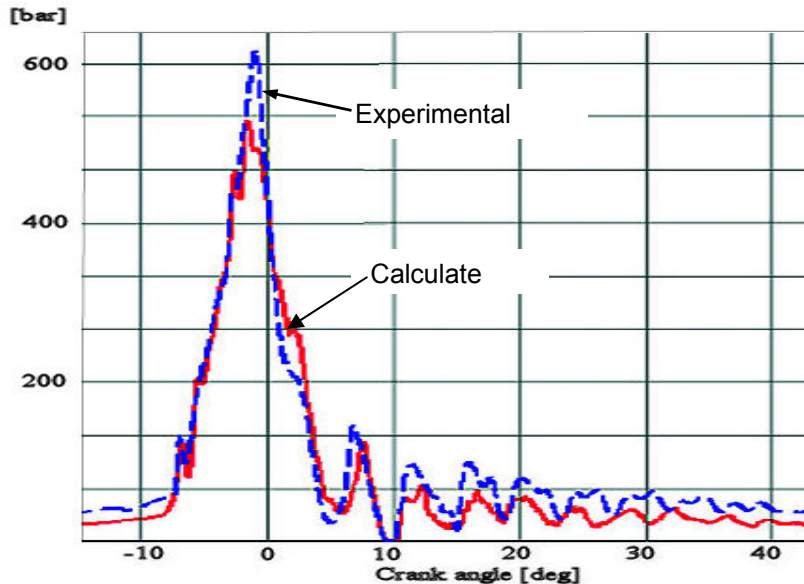


**Fig.1 Measured and simulated fuel pipe pressure and cylinder pressure at 1000 rpm, full load (opening pressure : 215 bar, pipe length 460 mm)**

The experimental set-up includes a 4 stroke cycle 4 cylinder diesel engine T684, a dynamometer, data acquisition system, pressure transducers, and etc. Table 1 shows the specifications of the injection system of engine.

**Tabel 1 Specification of fuel injection system**

Pump type Bosch	in-line pump
Plunger diameter	10.5 mm
Prestroke	3.2 mm
Fuel pipe diameter	2 mm
Nozzle type	Hole type
Nozzle hole number	4
Nozzle hole diameter mm	0.24
Nozzle hole angle	90

Figures 1 and 2 show the measured and simulated fuel pipe pressures for the engine speeds of 1000 rpm and 1500 rpm at full load. The maximum fuel pipe pressure of the simulation is similar to that of the measurement with slight

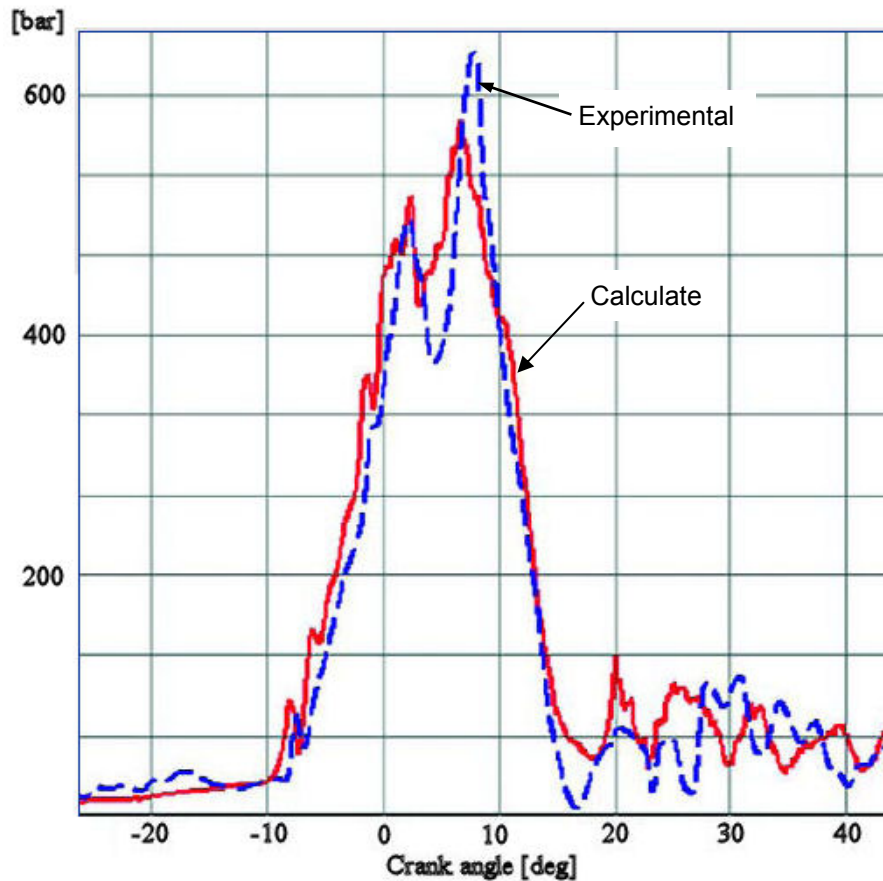


**Fig. 2 Measured and simulated fuel pipe pressure and cylinder pressure at 1500 rpm, full load (opening pressure : 215 bar, pipe length 520 mm)**

#### 4. SUMMARY AND CONCLUSION

A study is carried out to investigate the effects of the fuel injection length pipe pressure variations on the combustion of a direct injection diesel engine.

The fuel injection pressure and cylinder pressure are measured at the same time.

The following conclusions are derived from this study.

1. The measured fuel pipe pressures and the simulated fuel pipe pressures matched well to each other except for the later stage of the injection when cavitation might be occurring.
2. The longer fuel pipe length causes the retarded fuel injection timing. These variations affect the injected fuel quantity and the injection pipe pressure profile after the injection.

#### REFERENCES

- [1] Anderson, D A., Tannehill, J. C. and Pletcher, R. H., 1984, **Computational Fluid, Mechanics and Heat Transfer**, Hemisphere Publishing Corporation, pp. 87--178.
- [2] Arcoumanis, C. and Fairbrother, R. J., 1992, **Computer Simulation of Fuel Injection Systems for DI Diesel Engines**, SAE Paper 922223.
- [3] Cheng, Wai and Gentry, Richard, 1986, **Effects on Charge Non-Uniformity on Diesel Heat Release Analysis**, SAE Paper 861568
- [4] Cheung, Hon M. and Heywood, John B., 1993, **Evaluation of One-zone Burn-Rate Analysis Procedure Using Production SI Engine Pressure Data**, SAE Paper 932749.
- [5] Chun, Kwang Min and Heywood, John B., 1987, **Estimating Heat-Release and Mass-of -Mixture burned from Spark-Ignition Engine Pressure Data**, Combust. Sci. and Tech. Vol. 54, pp. 133--143.
- [6] Heywood, John B., 1988, **Internal Combustion Engine Fundamentals**, McGraw-Hill, pp. 491 562.
- [7] Kumar, K., Gaur, R. R., Garg, R. D. and Babu, M. K. Gajendra, 1983, **A Finite Difference Scheme for the Simulation of a Fuel Injection System**, SAE Paper 831337.
- [8] Lee, Hang-kyung, 1994, **Effects of Injection Pressure and Nozzle Geometry on D. I. Diesel Emissions and Performance**, SAE Paper 950604.
- [9] Shin, Bum-sik, Lee, Suk-Young and Chun Kwang Min, 1996, **An One-zone Heat Release Analysis of a 6 Cylinder Compression—Ignition Engine**, KSAE 96370013 Transaction Vol. 4, No. 1.
- [10] Sabau, A., Buzbuchi, N., Şoloiu, V.A.: **Combustion Numerical Modelling in Diesel Engines**. In Volumul "A XI-a Conferință Națională de Termotehnică", 8 pag., Galați, 2001.
- [11] Sugiyama, G., Ryu, H. and Kobayashi, S., 1994, **Computational Simulation of Diesel Combustion with High Pressure Fuel Injection**, COMODIA 94, pp. 391--396.

## APPLIED RESEARCH AIMED AT DESIGNING THE OPTIMAL SOLUTION FOR A SUBMERSIBLE ELECTRIC GENERATOR

<sup>1</sup>SAMOILESCU GHEORGHE, <sup>2</sup>SERGIU NICOLAE, <sup>2</sup>DORIAN MARIN, <sup>3</sup>SERGHEI RADU, <sup>1</sup>BARBU ALINA

<sup>1</sup>"Mircea cel Batran" Naval Academy, Romania, <sup>2</sup>National Institute for Research and Development in Electrical Engineering, Romania, <sup>3</sup>Zodiac Company, Romania

The paper presents a laboratory model of a submersible electric generator operating at relatively low speed values, synchronous, tri-phased, average built-in structure. The generator was conceived as a tightly sealed device, inner bearing coating and a driving shaft provided with tightening rings. The inductor is the fixed coil and the rotatable inductor with cylindrical permanent magnets Nd-Fe-B sintered and claw poles.

**Keywords:** electric generator, excitation, permanent magnets, claw poles

### 1. PRESENTATION OF THE LAB MODEL

In Fig. 1, we present an explanatory axial section of a generator produced by INCDIE ICPE-CA

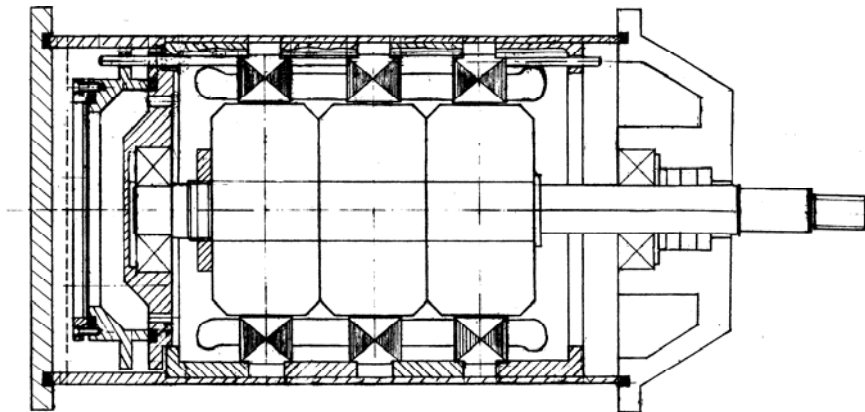


**Fig.1. Axial section through the generator**

The construction embeds three fixed coil subassemblies (with indentures), lined up within the encasing with intermediary spacing clamps and coiled together (the coils go through the three fixed coils), as well as the three rotatable subassemblies with claw poles sustained by the common shaft.

The inductive excitation flux is achieved with permanent magnets (Nd-Fe-B,  $B_r \approx 1\text{T}$ ,  $\mu_r \approx 1$ ) of a cylindrical shape directed along an axial anisotropic line, interposed one by one among the claw poles slots of the three rotatable subassemblies (the number of pole pairs  $p=6$ ) [1,2].

The entrefer between the claw poles and the stator core teeth is relatively small, of about 0,5mm. On the frontal surface (towards the entrefer) of the claw poles of  $\frac{1}{2} \times 25 \times 25 = 312,5 \text{ mm}^2$  (each) and a dispersion between the claws along a winding trajectory having a length of  $(25+25) \times 6$ , average width of 4mm and of an entrefer height of about 5mm, resulting for an optimal speed, straight to the shaft of the hydraulic turbine of about 450 rot/min, the tension on the idle Y-voltage outlet terminals of about 24 V, an effective value experimentally confirmed (see the table below). For a winding pertaining to the fixed coil of a 0,6mm diameter we rely on an effective maximal power of approx. 80 W.

For the construction of the electric generator with a lubricated bearing coating form the river water, we have given up on the standard built-up, given the selected perfectly sealed frame – because of the serious consumption noticed for the sliding bearing coatings made of a special sintered brass. Thus, we have retorted to two classic bearings, these being tightly salad together with the stator coil with the help of three oil retainer ring set-up at the exit of the operating shaft from the carcass.

The excitation was achieved by means of the rotor made of permanent magnets of rare fields, manufactured by INCDIE ICPE-CA.

The optimization and design of the stator coil was achieved with the help of a special calculation program of the magnetic field generated by the rotor assembly.

## 2. EXPERIMENTS ON THE LAB MODEL

On the lab model of the submersible electric generator we have performed idle and on-load measurements in order to raise its specific power depending on the rotation speed. The set of measurements was performed with INCDIE ICPE-CA. The generator sustained in a console was set in gear by means of an elastic hitch and operated with the help of a continuous current electric motor, of a variable rotation speed. We have taken into account the characteristic of the submersible electric generator both idle and on-load. (Table 1)[3].

The rotation speed was measured with an electronic revmetre type MSP 01.

We have measured the tension for each phase of the generator and for the driving motor as well.

**Table 1: Tri-phased synchronous generator**

n {rot/min}	<i>Tri-phased synchronous generator</i>						
	U <sub>line</sub> [V]	U <sub>phase</sub> [V]	I <sub>phase</sub> Idle Measurements	P <sub>phase 1</sub> [W]	P <sub>phase 2</sub> [W]	P <sub>phase 3</sub> [W]	P <sub>tot</sub> [W]
570	65.70	37.45					
495	56.00	32.3					
307	34.80	19.84					
158	17.70	10.09					
450	40.66	23.50	1.27	25.00	27.50	31.25	83.75
350	31.14	18.00	1.00	12.50	17.50	18.00	48.00
200	17.30	10.00	0.60			5.75	cca 15
100	8.65	5.00	0.25				
415	36.33	21.00	1.32	20.00	25.00	27.50	72.50
350	30.28	17.50	1.11	10.00	17.50	20.00	47.50
222	19.90	11.50	0.71			8.00	cca 21

### 3. ELEMENTS OF ELECTROMAGNETIC CALCULUS FOR THE DESIGN OF A SUBMERSIBLE ELECTRIC GENERATOR

The solution concluded upon and designed is a synchronous electric micro generator in immersion. We take into account a variant for which we make use of stator subassemblies with indentures and rotor with claw poles, in special construction [4,5,6].

The stator (induced) regroups three subassemblies: steel sheet package form the auto alternator, lined up with intermediary spacing clamps. The steel sheet presents 36 semi-closed indentures. The axial fastening is made with three tyrants between the traction shield and the spacing clamps on the one hand, and the opposite traction inner shield with the spacing clamp on the other hand. The rotor (inductor) regroups on the shaft three subassemblies of claw poles pairs ( $n_{sub}=3$ ) in special construction, adapted for excitation with permanent magnets, of a cylindrical shape and are placed inside the claws (instead of the coil) with ferromagnetic spacing clamps. The centering and consolidation on the shaft is made with the help of interior non-ferromagnetic sockets. The axial centering is achieved with a bolt nut along a screwed section of the shaft. The traction bearing assures the position towards the stator. The end of the traction shaft goes through two tightening oil-retainer rings. The opposite traction shaft is axially free. The entire construction is tightly sealed with a glass shaped carcass with a tightening collar flange joint to a traction shield by bolts.

Dimensional and coiling elements:

- Interior diameter of the package of stator steel sheet:      The exterior diameter of the magnet:

$$D = 89mm;$$

$$D_{em} = 70mm$$

- The axial length of a steel sheet package (of the three):      The interior diameter of the magnet:

$$l = 23mm;$$

$$D_{im} = 45mm;$$

- The size of the entrefer :

$$\delta = 0.5mm;$$

The height of the magnet:

$$h_m = 7mm;$$

The useful surface of a claw pole:

$$S_p = 312mm^2;$$

The number of stator indentures:

$$Z = 36;$$

The dispersion entrefer between claws :

$$\delta_\sigma = 5mm;$$

The number of pole pairs:

$$p = 6;$$

The average lateral surface of equivalent dispersion for a pair of poles:

$$S_\sigma = 300mm^2;$$

The number of phases:

$$m = 3;$$

The number of indentures on pole and phase:

$$q = 1$$

The number of spires on phase :

$$w_1 = 216$$

(12 coils with 18 spires).

- permanent sintered magnets NdFeB, with a remnant induction  $Br \cong 1T$  (considered as coverage) and the relative reversible permeability:

$$\mu_r = 1.$$

Calculus elements:

- The frontal surface of the magnet :

$$- S_m = \frac{\pi(D_{em}^2 - D_{im}^2)}{4} = 2258 \cdot 10^6 [m^2]; \quad (1)$$

The calculus of the electromotor tension (idle tension at the terminals) on phase voltage (effective value)

As shown before, the construction incorporates three stator subassemblies of auto alternator ( $n_{sub}=3$ ).

In order to establish the value of the electromotor tension we have taken into account a surface of the claw poles  $S_p=312mm^2$  and a magnetic dispersion between poles along a winding trajectory between claws with an equivalent surface for a pair of poles  $S_\sigma = 300mm^2$  and an average entrefer  $\delta_\sigma = 5mm$ . The reference rotation speed taken into account is  $n=150$  rot/min, to which we relate a frequency of the phase electric tension;

$$f_1 = \frac{p \cdot n}{60} = \frac{6 \cdot 150}{60} = 15Hz ; \quad (2)$$

The shape and dimensions of the stator indentures imply an increment factor of the equivalent entrefer  $\delta'$  (Carter factor) of  $K = 1.18$ , resulting  $\delta' = \delta \cdot K = 0.59mm$ .

Applying the calculus formula for magnetic circuits we obtain the following relations and values:

- average magnetic induction inside the magnet

$$B_m = \frac{B_r}{1 + \frac{1}{\mu_r} \cdot \frac{2\delta'}{h_m} \cdot \frac{S_m}{p(S_p + \frac{2\delta'}{\delta_\sigma} \cdot S_\sigma)}} = 0.959T \quad ; \quad (3)$$

- Magnetic induction in the entrefer :

$$B_\delta = B_m \cdot \frac{S_m}{p\left(S_p + \frac{2\delta}{\delta_\sigma} \cdot S_\sigma\right)} = 0.943T ; \quad (4)$$

- Idle electric tension (effective value):

$$U_0 = 4 \cdot f_1 \cdot w_1 \cdot B_\delta \cdot S_p \cdot k_{w1} \cdot n_{sub} = 11.4V ; \quad (5)$$

( $k_{w1} = 1$  - winding factor).

#### 4. CONCLUSIONS

The research undertaken have enabled us to achieve the submersible generator and implement it while a drill on the river Prut; we have also come up with an ecologic craft powered by the energy of the river Danube.

#### REFERENCES

- [1]. Cazacu, M.D.; Nicolaie, S. – *Micro-hydroturbine for run-of-river power station*, the 2-nd Conference of Romanian Hydro-energy specialists, 24 – 25 may 2002, Polytechnics University, Bucharest, Vol.II, 443 – 448
- [2]. Samoilescu, Gh. ș.a. – *Sistem cu autonomie energetica destinat supravegherii paselor de trecere pe Dunare*, Editura ANMB, 2006
- [3]. Samoilescu, Gh. ș.a. – *The analysis of the buoys used on the river for making a non-conventional energetic system*, ICATE 2006 - 8<sup>th</sup> Intenational Conference on Applied and Theoretical Electricity, Băile Herculane, oct. 26-28, 2006
- [4]. \* \* \* ICPE-CA – *Instalatie de conversie neconventionala de mica putere bazata pe integrarea unor materiale avansate si solutii tehnologice noi*, project RELANSIN / 2003
- [5]. \* \* \* Colectiv ICPE-CA (Mihăiescu, Gh.M.; Kappel, W.; Nicolae, S.; Seghianu, R.; Hondrea, M.), UPB (Cazacu, I.M.) si BERIMPEX S.R.L. (Berar, C.) – *Hidrogenatoare de mica putere, Atelierul. Actualitati si perspective in domeniul masinilor electrice*, ICPE-ME-SA, 2004
- [6]. \* \* \* Colectiv ICPE-CA (Kappel, W.; Codescu, M.M.; Stancu, N.; Mihaiescu, Gh.M.; Nicolae, S.; Hondrea, M.; Seghianu, R.) – *Magneti permanenti pe baza de NdFeB pentru hidrogenatoare de mica putere*, Conferința Naționala de surse noi si regenerabile, CNSNRE, Târgoviște, 2004

## ANALYSIS OF ASYNCHRONOUS TRIPHASE ELECTRIC MOTORS USED IN AC PROPULSION SYSTEMS

<sup>1</sup>SAMOILESCU GHEORGHE, <sup>2</sup>SAMOILESCU ADELINA, <sup>3</sup>RADU SERGHEI,  
<sup>1</sup>CIZER LAURA

<sup>1</sup>*“Mircea cel Batran” Naval Academy, Romania*, <sup>2</sup>*Politechnic University of Bucharest, Romania*, <sup>3</sup>*Zodiac Company, Romania*

Seen from the perspective of electromechanics, propulsive engines can be asynchronous, synchronous and synchronous - asynchronous, can have low rotation frequencies for direct coupling to the screw shaft, whereas at high rotation frequencies the coupling is performed through a reducer. With respect to asynchronous engines used in the electrical propulsion of ships, several features have been subject to our close examination: the moment when sliding, the mechanical characteristic between motor speed and coupling as well as between coupling and sliding in accordance with the rotor speed, and finally the coupling characteristics of asynchronous engines and the related mechanisms.

**Keywords:** asynchronous, synchronous, coupling, propulsive engines

### 1. INTRODUCTION

Electro motors used in ship propulsion have the following features [1, 2]:

- high values of induction and loads;
- small dimensions and weights;
- high quality material for components;
- ventilation done by coupling and also artificially in order to avoid overheating in case of reversing;
- increased resistance against elements (humidity, salts, oils and impurities);
- perfect insulation against high voltage and poor working conditions for windings;
- rotor diameter – total length ratio is 2/2.2 for asynchronous motors and 2.5-3.5 for synchronous motors.

The synchronous engine is made up of a physical component – the stator, and a mobile one – the rotor. The stator has a casing, shields and a core made up of electro technical iron sheets in the shape of a cylinder, with inner slots for the stator windings. These are made up of coils with active sides located in the slots.

The distribution of phase coils in several sides has a series of advantages:

- a better cooling of windings;
- magnetic fields with a space distribution closer to sinusoidal shapes;
- deletion of several harmonics from the electromotor phase voltage;

- use of shorter pitch windings in a two-layer arrangement done by including the two active sides from different coils of the same or various phases in each slot.

The windings are made up of copper bars and the insulation of the bar winding between the spires and against the slot walls is done according to the voltage, temperature while permanent operation, shape and dimension of windings.

The rotor has a cylinder-shaped core made up of electro technical iron sheets mounted on the shaft and provided with peripheral slots for applying the rotor windings. According to the types of windings, the rotors are in short-circuit – single caged, equipped with high bars, double caged – or can have windings connected to the stator or speed-adjusting rheostat by means of rings and brushes –the collecting rings are on the rotor shaft.

Wound rotors have corrugated windings made up of copper bars with two -layer active sides. The phase heads are connected to the rings located on the rotor shaft which is in contact with the brushes that are galvanically connected to the terminals of the stator or speed-adjusting rheostat. The three rings are isolated, separated one from another

Wound motors can be equipped with a ring shorting device and a brush lifting device – the motor are at a constant rotation frequency.

The motors equipped with a short-circuit rotor have the rotor circuits in the shape of single or double cage. The motors ensure the start and automatic reversal and develop high overload momentum.

The double caged motor is equipped with a peripheral cage made up of brass or previously treated bronze to allow a better resistance and a small dispersal reactance; it is also equipped with an inner copper cage with small resistance and relatively high reactance.

## 2. ELECTRIC MOTORS USED IN ELECTRIC PROPULSION

At the start of propulsive double caged electro motors, the frequency  $\nu_2$  of the current in the rotor - in the first moment and till the electric motor reaches a significant angular speed - is almost equal to the frequency in the stator. [2, 3, 4].

$$\nu_2 = s \times f_1 = \frac{n_1 - n_2}{n_1} \times \nu_1 \cong \nu_1 \quad (1)$$

where:  $s$  – sliding;

$n_2$  – number of rotations (rotor);

$n_1$  – number of rotations (synchronous rotating field);

$\nu_1$  – stator frequency;

$\nu_2$  – rotor frequency.

Since the bars of the inner cage are arranged in the iron of the rotor and the space between the cages is narrow, the cage inductance ( $L_R$ ) is relatively high. As a result, at significant rotor frequencies, the resistance of the inner cage becomes:

$$R = 2\pi\nu_2 L_R \quad (2)$$

The high resistance of the outer cage and its reduced reactance improve the rotating momentum in the first starter or reversal momentum, the sliding varies from  $s = 0,5$

to  $s = 2$ . Therefore, the peripheral cage plays an important part at the start, whereas the inner one while operating.

When the propulsive electromotor reaches the nominal number of rotations and the sliding is reduced, the number of magnetic lines crossed by the outer cage bars within the time limit is smaller. Since the electromotive voltage which has been induced in both cages is in direct proportion with the number of crossed magnetic lines, when the sliding diminishes up to  $s = 0,01$ , the current within the outer cage is greatly diminished as well, and its spinning momentum reaches an insignificant value at the nominal angular speed of the propulsive electromotor. Once the sliding is diminished, the spinning momentum of the inner cage increases and reaches a dominant value at nominal frequency.

Thus, at the start of the double caged propulsive electromotor, at the initial stage the outer cage is mainly operational whereas the inner one operates in working conditions. In figure 1,  $M_L$  and  $M_P$  curves show the trajectory of rotation momentum while in operation and at the start, the momentum have been created by the two cages.

The  $M_{LP}$  curves define the total momentum that has been developed by the rotor of the propulsive electromotor which is equal to the sum of the momentum of the two cages.

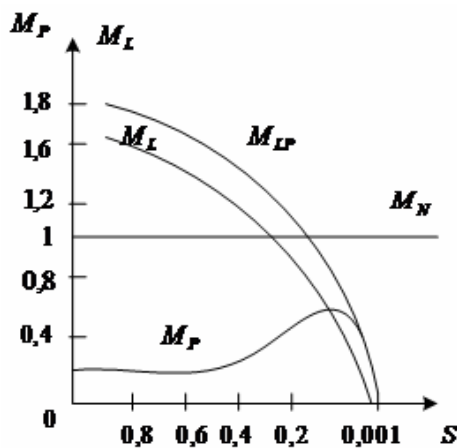


**Fig.1. Characteristics of the sliding function couple**

The characteristic of the sliding function couple or rotation function couple, the characteristic of the sliding function current (load), the characteristic of the efficiency and the power factor as actual output at constant voltage and feeding frequency are the most important features that define the running of the asynchronous motor.

The stator windings in the case of the asynchronous motor are charged at symmetrical sinusoidal electric voltages, crossed by symmetrical currents and develop a spinning magnetic field with sinusoidal distribution within the split core. Inside the rotor windings connected in short-circuit electromotive voltages are induced – provided that the rotation speed is different from the speed of the spinning speed of the stator currents (speed of synchronism).

The rotor currents develop their own spinning magnetic field – the reactive field of the inductor, with the rotation speed that equals the difference between the speed of the

spinning field developed by the rotor currents and the speed of the rotor. Operated by the rotor, as opposed to the stator, this field has the very speed of the inductive spinning field developed by the rotor currents. A resulting magnetic spinning field is developed and it induces rotation electromotive voltages during the stator and rotor phases. When the speed of rotor is lower than the synchronism speed, the spinning field develops an electromagnetic field around the rotor which is moved. At the synchronism rotation there are no more electromotive voltages and currents in the rotor circuits and the electromagnetic couple is null.

Wound rotor asynchronous motors can have:

- brush lifting and ring short-circuit devices – used when the operating mechanism (screw shaft) needs a higher starting couple. The natural characteristics lift when the starting is done at full load and the rotation adjustment is not needed.
- no brush lifting devices – used for operations which do not need frequent on/off's, at full load and rotation adjustment by means of the rheostat in the rotor circuits.

For the propulsive electro motors of the screw shaft system that are continuously operating, the equation of the relative electromagnetic field is as follows:

$$\frac{M}{M_{\max}} = \frac{2}{\frac{s}{s_m} + \frac{s_m}{s}} \quad (3)$$

where:  $s_m$  – is the kinetic sliding which corresponds with the maximum value of the couple.

The maximum couple is direct proportional to the square feeding power and in indirect proportion with the load reactance of the corresponding scheme - Fig.2:

$$M_{\max} = \frac{3\rho}{2\omega_1} \frac{\left(\frac{v_1}{c_1}\right)^2}{x} \quad (4)$$

The overloading coefficient  $\left(\frac{M_{\max}}{M_n}\right)$  has values between 1, 5 ÷ 3, 5.

At lower sliding values as opposed to the critical value, the result is a linear portion of the couple – sliding characteristic around the origin. The equation (3) becomes:  $\frac{M}{M_{\max}} \cong 2 \frac{s}{s_m}$ ,

when:

$$\frac{s}{s_m} \ll 1 \quad (5)$$

At higher sliding values as opposed to the critical value, the result is a portion with hyperbolic variation of the couple-sliding characteristic. The equation (3) becomes:

$$\frac{M}{M_{maz}} \cong 2 \frac{s_m}{s}, \text{ and } \frac{s_m}{s} \gg 1 \quad (6)$$

In the case of asynchronous high power motors the resistance of the motor phase is disregarded, and only the dispersal reactance is retained. The equation of the electromagnetic couple becomes:

$$M = 3 \frac{\rho}{\omega_1} \frac{\frac{U_1^2}{c_1^2 x}}{\frac{x}{R_2} s + \frac{R_2}{x_s}} \quad (7)$$

however, its maximal value is obtained for  $\frac{dM}{ds} = 0$ , when  $s = s_m = \frac{R_2'}{x}$

$$M_{max} = \frac{3\rho}{2\omega_1} \frac{\left(\frac{U_1}{c_1}\right)^2}{x} \quad (8)$$

where:  $\rho$  - number of pole pairs;

$\omega_1$  - pulsation of currents in the stator phases;

When  $\frac{R_1}{c_1}$  ration cannot be disregarded

$$\frac{M}{M_{max}} = \frac{2 \left(1 + \frac{R_1 s_m}{c_1 R_2'}\right)}{\frac{s}{s_m} + \frac{s_m}{s} + 2 \frac{R_1 s_m}{c_1 R_2'}} = \frac{3\rho}{2\omega_1} \frac{\left(\frac{U_1}{c_1}\right)^2}{\frac{R_1}{c_1} + \sqrt{\left(\frac{R_1}{c_1}\right)^2 + x^2}} \quad (9)$$

where:

$$s_m = \frac{R_2'}{\sqrt{\left(\frac{R_1}{c_1}\right)^2 + x^2}}$$

The mechanical rotation-couple characteristic is accomplished following the replacing of the sliding in accordance with the rotor rotation.

$$n = \frac{60}{2\pi} \Omega_2 = \frac{60}{2\pi} \Omega_1 (1 - s) = n_1 (1 - s) \quad (10)$$

where:

$$s = 1 - \frac{n}{n_1}$$

$$n_1 = \frac{60\omega_1}{2\rho\pi}$$

$\Omega_1$  – speed of stator spinning field;

$\Omega_2$  – speed of rotor spinning field;

$n_1$  – synchronism rotation (rotation of spinning field).

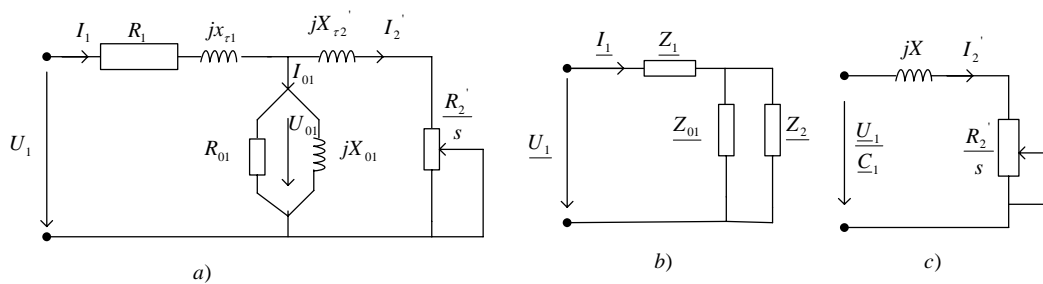


Fig. 2.

In fig. 2, the expressions have the following significations:

$R_{01}$  – resistance of iron losses;

$x_{01}$  – magnetization reactance;

$U_1$  – input voltage at network terminals when idle (before connecting the motor);

$U_{01}$  – voltage induced in the stator phase by the actual magnetic flux;

$\Phi_m$  – maximal value of coil developed flux.

The voltage and current equations of the asynchronous motor are:

$$\underline{U}_{01} = \left( \frac{R_2'}{s} + jx'\sqrt{2} \right) \underline{I}_2'$$

$$\underline{I}_{01} = \frac{U_{01}}{R_{01}} + \frac{U_{10}}{jx_{01}} \tag{11}$$

$$\underline{U}_1 = \left( R_1 + jx_{\sqrt{1}} \right) \underline{I}_1 + \underline{U}_{01}$$

Following the balancing of the electromagnetic couple and the mechanical one the permanent working status is established at constant rotational speed of electric motors [2, 5].

The couple characteristics of asynchronous motors are crossed by the ones of the operating mechanisms and they meet in one or two points - Fig. 3.

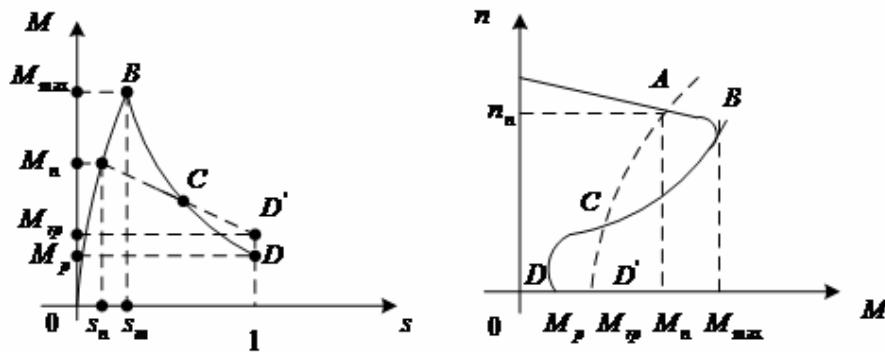


Fig. 3.

The OAB portion represents the characteristic of motor stable function. Wherever A is between O and B, at an impulse of the sliding variation, the resulting dynamic couples re-establish the equilibrium – an accelerator couple appears when slowing down whereas a braking couple appears when speeding up.

The dynamic couples operate over the BC portion, amplifying the impulse of speed variation

The BCD portion does not allow the motor to permanently operate as the load currents exceed nominal values. In the case of asynchronous motors, the rotation is slightly modified at load change. The starting couple is higher than the screw shaft. In order to produce the starting couple ( $M_p$ ) the particular case in which  $s = 1$  is taken into account.

$$\frac{M_p}{M_{max}} = \frac{2}{s_m + \frac{1}{s_m}} \quad (13)$$

The starting couple can be increased by means of the starting rheostat which modifies the value of the equivalent resistance as opposed to the stator, and it represents a specificity of the wound rotor motors using higher starting couples. For this particular type of electric motors, the power factor is increased by the motor charging as the consumed active input increases faster than the reactive one on the stable portion of the couple characteristic [2,4,5].

### 3. CONCLUSIONS

For asynchronous triphase short-circuit rotor motors the equations determined for the wound rotor motors are also applicable, provided that the current distribution over the rotor bars is uniform from the  $s = 1$  interval to  $s = 0$ .

Taking into account the fact that the asynchronous short-circuit rotor normal built-up motors have a low starting couple and can only start operating in free motion or at low loads, motors with mixed rotor resistance have been designed to ensure a higher starting couple that matches with a lower rotor current (ameliorated starting motors, motors with peculiar effect, with high bars and double caged motors). The parameters of these motors vary

according to the sliding; therefore the natural mechanical characteristic cannot be expressed in analytical configuration as for the wound rotor motors.

From the functional perspective, the short-circuit double caged rotor motor does not allow the same improvements in the starting conditions as the wound rotor motor and its natural, maximal and starting couple has low values ( $1,8 \div 1,2$ ), whereas the starting current is high  $(6 \div 8)I_n$ . The asynchronous double caged rotor motor has one peripheral high resistance starting cage and one inner low resistance working cage that can be used to allow the permanent running of this motor type when they reach their highest inertia momentum. These motors have high couples at low sliding (the outer cage determines a mechanical high couple characteristic at the start, whereas the inner cage has a mechanical low sliding characteristic.)

The asynchronous high bar rotor has an increased mechanical starting characteristic due to the effect of uneven peripheral distribution (peculiar effect) of the electric current in the massive conductor at high frequencies – this case was noticed at the start. As a result, the apparent resistance increases whereas the dispersal reactance decreases at the start. The motor with increased sliding is a variant of the high bar motor (deep slots) and its starting couple has been increased while its starting current is decreased.

## REFERENCES

- [1]. Alf Kare Adnanes - ,*Maritime Electrical Installations and Diesel Electrical Propulsion*, Oslo ABB AS, Marine, 2003
- [2]. Leidi, G. et alii. - ,*Quality of power in ships with electric propulsion*, Proc. of ICHQP. 7<sup>th</sup> International Conference on Harmonics and Quality of Power, 1996
- [3]. Nanu, D. - ,*Sisteme Electromagnetice Navale*, Constanța, Editura Muntenia, 2004
- [4]. Samoilescu, G. et alii. - ,*Exploatarea Sistemelor Energetice Navale*, Constanta, Editura Academiei Navale „Mircea cel Batrân”, 2004
- [5]. Samoilescu, G. et alii. - *Instalatia de propulsie electrica a navei*, Constanta, Editura Academiei Navale „Mircea cel Batrân”, 2006

## CONCEPTS OF REFRIGERATION CYCLES AND CRYOGENICS FOR LNG TANKERS

<sup>1</sup>STAN LIVIU, <sup>1</sup>BUZBUCHI NICOLAE, <sup>2</sup>BERESCU SERBAN

<sup>1</sup>Constanta Maritime University, Romania, <sup>2</sup>Romanian Naval Authority, Romania

This paper represents an overview about cryogenics applications in the maritime field and onboard commercial vessels. Basics thermodynamics in general and cryogenic refrigeration in particular are theoretical knowledges which become compulsory when we are dealing with complex processes like liquefaction, re-liquefaction and boil-off. The papers aim is to familiarize the students/crew members onboard LNG tankers with the basic concepts of refrigeration cycles and cryogenics.

**Keywords:** cryogenics applications, refrigeration cycle, thermodynamic processes

### 1. INTRODUCTION IN CRYOGENICS

Cryogenics (from a Greek word “κρυος” = icy cold), deals with phenomena occurring at very low temperatures. Several arbitrary bounds on the “low temperatures” may be established [2]:

- <120 K was adopted by the XIII Congress of the Intl' Institute of Refrigeration,
- <173 K, (-100 °C) is a more rounded figure,
- <200 K seems a better choice because, in current practice, there is no much interest in the range from the traditional refrigeration applications (i.e. from ambient temperature to some -55 °C (218 K)), and the nearest colder technique: dry ice, at -78 °C (195 K).

First centigrade temperature scale was proposed in 1742 by prof. A. Celsius. The Celsius, Kelvin, and Fahrenheit temperature scales are shown in relation to the phase change temperatures of water. The Kelvin scale is called absolute temperature and the Kelvin is the SI unit for temperature. The temperature scales relations are well known:  $TC = TK - 273,15$  [K] and  $TF = 9/5 TC + 32$  [ F]. Temperatures and temp. scales are based on the Zero-th law of thermodynamics, which states that „If two objects are at the same time in thermal equilibrium with a third specified object, they are in thermal equilibrium with each other” (I.C. Maxwell) – and in fact they have the same temperature.

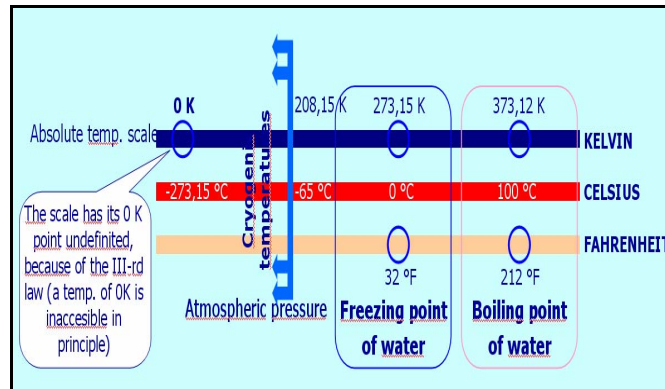


**Fig.1. Cryogenic region on temperatures scales**

The lower limit for cryogenics is 0 K, a value that may be approached but not attained (Nernst theorem-3-rd law of thermodynamics, 1918). The general applications of cryogenics (i.e. below 210 K) are:

- At some 195 K, dry ice production and use;
- At~ 112 K, liquefied natural gas (LNG) production and transport;
- At ~ 90 K, liquid oxygen/nitrogen production by liquid air fractional distillation;
- At ~ 80 K, high - temperature superconductors (HTS);
- At ~ 20 K, liquid hydrogen, deep vacuum space simulators (at 20 K the vapour pressure of nitrogen is some  $10^{-8}$  Pa);
- Below 10 K, various low temperature space (LTS) applications;
- Below 5 K it is basically scientific research, but also infrared and microwave detectors cooled to decrease thermal noise of electrons (Johnson/Nyquist noise).

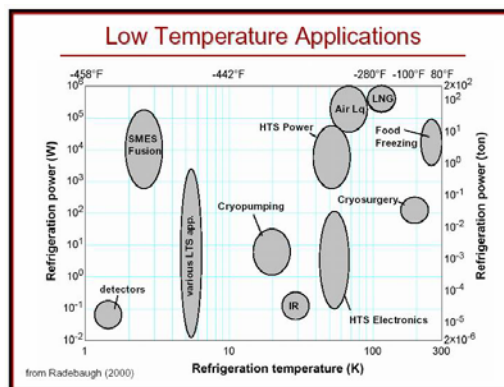


**Fig.2. Main cryogenics applications**

Temperatures down to 0,5 K may be reached by evaporative cooling of <sup>3</sup>He, and below that, demagnetisation of paramagnetic salts are used to achieve  $10^{-6}$  K.

The maritime field applications of cryogenics are referring to all cargo which is normally carried at temperatures below  $-65\text{ }^{\circ}\text{C}$  (208, 15 K):

- All gases, including natural gas (methane) can be liquefied at extremely low temperatures.
- Such liquid gasses are commonly called “cryogenic fluids“: Oxygen, Helium, Argon, Methane, Hydrogen, etc. Once liquefied, the gases will remain in a liquid phase even at atmospheric pressure, provided that it is kept at its saturation temperature.
- On board ship (Gas Carriers), all gases are always carried in liquefied state (to be transport efficient).

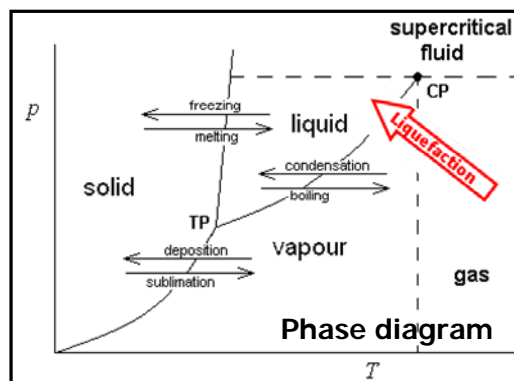


**Fig. 3. Phase diagram – Pressure/Temperature diagram for varying states of matter**

Cryogenic gas liquefaction represents the conversion of a gas to the liquid phase by cooling or compression (industrial Terminals process ashore); first cryogenic liquefaction was made in 1780 by G. Monge, a teacher of S. Carnot.

Cryogenic gas re-liquefaction and boil-off control represent the process happening on board Gas Carriers when the gas vapours returns to liquid phase being then drawn back into the cargo tanks.

## 2. THERMODYNAMIC PROCESSES APPLIED IN CRYOGENICS

### 2.1. Basic concept of refrigeration

The aim of refrigeration is to get temperatures below that of the local environment, therefore be able to draw heat from a load by normal heat transfer. Any endothermic process lowers the temperature of the system and is able to produce a refrigeration effect.

#### Refrigeration cycles

- Take in work from the surroundings and transfer heat from a low temperature reservoir to a high temperature reservoir. Schematically, they look like the diagram from heat engines, but with the direction of the arrows reversed.

#### Second law of thermodynamics – Refrigerators:

*“It is not possible for heat to flow from a colder body to a warmer body without any work having been done to accomplish this flow”.*

The statements about refrigerators apply to air conditioners and heat pumps, which embody the same principles. This is the "second form" or Clausius statement of the second law. For a refrigerator, the useful quantity is the heat extracted,  $Q_C$ , not the heat exhausted.

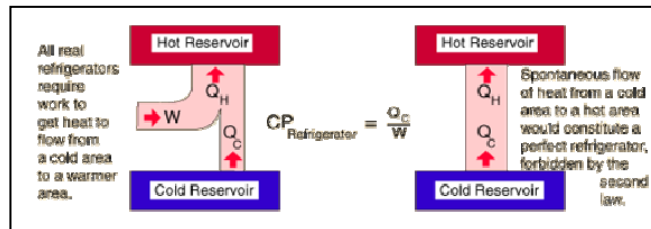


**Fig.4. Second law of thermodynamics applied to refrigerators**

## 2.2. Carnot cycle and inverted carnot cycle

The Carnot cycle (from Sadi Carnot, 1824) is known as the most efficient heat engine cycle allowed by physical laws, consisting of two isothermal and two adiabatic processes.

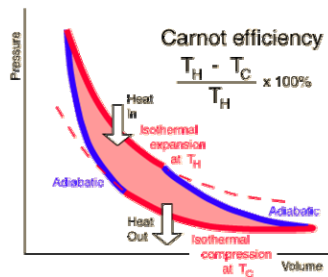


**Fig. 5. Operation of a Carnot heat engine**

**(1 to 2)** - Adiabatic (isentropic) compression, to change temperature without heat transfer.  
**(2 to 3)** - Isothermal expansion (heat input), from the hot reservoir at the hot-source temperature  $T_H$ .

**(3 to 4)** - Adiabatic (isentropic) expansion, to change temperature without heat transfer.

**(4 to 1)** - Isothermal compression (heat rejection) to the cold source (usually the environment), at the cold-source temperature  $T_C$ .

NOTE: To approach the Carnot efficiency, the processes must be reversible and involve no change in entropy.

The Carnot cycle can also run in reverse and it is called refrigeration cycle. The cycle works now as a refrigerator or a heat pump. The heat and work transfers are indicated in the figure below.

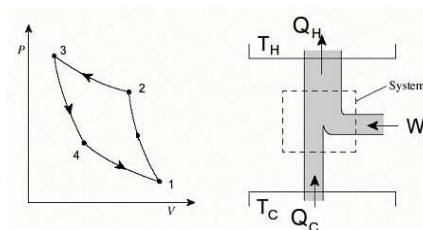


**Fig. 6. Operation of a Carnot refrigerator**

The processes in the cycle are as follows:

- (1 - 2) - Adiabatic (isentropic) compression.
- (2 - 3) - Isothermal compression (at  $T_H$ ). During this compression, heat  $Q_H$  /per unit mass is rejected to the hot source at  $T_H$ .
- (3 - 4) - Adiabatic (isentropic) expansion lowers the temperature to  $T_C$ .
- (4 - 1) - Isothermal expansion (at  $T_C$ ). During this expansion a quantity of heat  $Q_C$  /unit mass is received from the cold source at temperature  $T_C$ .

### 2.3. Refrigeration methods

Theoretically, there are several ways to produce artificial refrigeration, and we can divide these processes into two main categories:

1. Thermodynamics processes;
2. Thermo electrical and magnetically processes.

The thermodynamics processes could take place in open (non-cyclic), respectively closed (cyclic) systems. The open (non-cyclic) thermodynamics cooling processes take place through the freezing mixtures or endothermic mixtures. In these methods, refrigeration can be accomplished by melting ice or by subliming dry ice. These methods are used for small-scale refrigeration such as in laboratories, workshops or in portable coolers. The closed thermodynamics cyclic refrigeration can be classified as:

- A. Vapour refrigeration cycle
- B. Gas refrigeration cycle

The vapour cycle refrigeration can be further be classified as:

- A.1. Vapour compression refrigeration:
  - A.1.1. Mechanical vapour-compression refrigeration (Mechanical compression-refrigeration machine);
  - A.1.2. Mechanical ejector vapour-compression refrigeration (Cold vapour ejection-refrigeration machine);
- A.2. Vapour (gas) absorption refrigeration - thermo chemical vapour-compression refrigeration (Absorption - refrigeration machine).

Other refrigeration methods consist of:

- C. Thermoelectric refrigeration, based on Peltier effect to create a heat flux between the junction of two different types of materials;
- D. Magnetic refrigeration (or adiabatic demagnetization), based on magneto-caloric Warburg effect;
- E. Vortex-tube refrigeration (Centrifugal expansion Ranque- Hilsch effect) used for spot cooling, when compressed air is available;
- F. Thermo acoustic refrigeration, using sound waves in a pressurized gas to drive heat transfer and heat exchange.

In the followings, the focus will be on the thermodynamic closed processes with emphasize on the gas expansion refrigeration cycles, which are used especially for cryogenic refrigeration.

When working fluid is a gas that expands, the refrigeration cycle is called a gas-expansion cycle. It works on the reverse Brayton cycle and is only used in special applications like cryogenic refrigeration. The Brayton cycle was developed in the 19<sup>th</sup> century by George Brayton. One major difference between a regular Brayton cycle (such as a jet-engine or a gas-turbine) and a reversed Brayton cycle is the working fluid.

Cryogenic temperatures can be achieved when using a regenerator - a heat exchanger that preheats the fluid before it enters the compressor and cools the fluid further down before

it enters the turbine. This way, the fluid is expanded to much lower temperatures, and more heat can be absorbed from the cooling compartment.

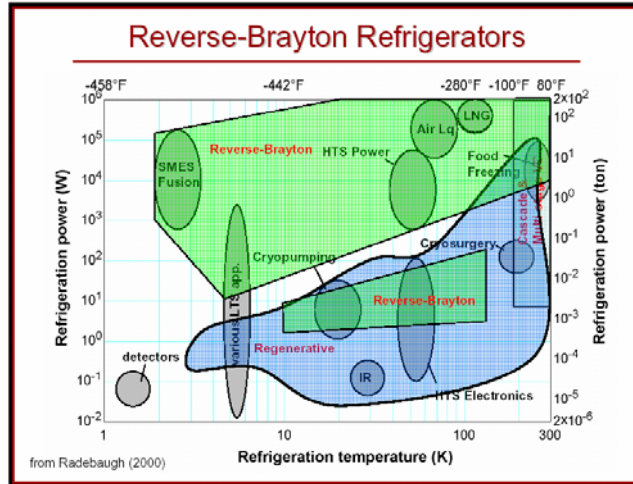


**Fig. 7. Main cryogenics applications based on reverse Brayton cycle**

In Cryogenics, reversed Brayton cycles are used to cool down systems where very low temperatures are required. The basic system components include:

1. Compressor
2. Expander (turboexpander) – cool the gas by non-isentropic expansion
3. Counterflow heat exchanger
4. Cold-end heat exchanger.

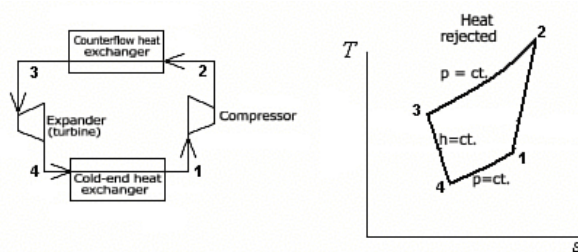


**Fig. 8. Gas expansion refrigeration cycle**

- (1-2) Gas non-isentropic compression
- (2-3) Isobar condensation (high pressure)
- (3-4) Isoenthalpic turbine expansion and
- (4-1) Isobar compression (Low pressure)

### 3. CRYOGENICS APPLICATIONS IN MARITIME SHIPPING

We have said that in maritime applications, we are talking about cryogenics when the cargo temperature is below  $-65\text{ }^{\circ}\text{C}$  (218,15 K). Ships which carry such kind of cargo are the Gas Tankers – LEG's and LNG's where all cargo is carried in liquefied state at different

temperatures. For instance, two of the most common cryogenic fluids carried in fully refrigerated containment system are the methane (carried on board LNG's at -162,2 deg.C) and ethylene, carried on LEG's at its boiling points of -104 deg.C. Of course, there are many other liquefied petroleum gases (i.e propane, butane, propylene, ammonia etc.) carried on board LPG's in different containment systems (fully pressurized or semi-pressurized /semi refrigerated), but we cannot classify them as cryogenic because they have the boiling point at a value that don't exceed -42 deg.C (for propane).

The ship cargo is kept cool by evaporating a fraction of the cargo which is referred to "boil-off", which means an increasing amount of vapor over the cargo liquid surface, due to boiling of the cargo. This happens due to cargo temperature variations. Boil-off from the cold LNG is typically used to power the ship while it is underway. Thus, the common feature of these ships are capturing the boiled-off LNG, and burning it as propulsion fuel. The gas can be burned directly as boiler fuel or mixed with fuel oil.

NOTE: The boil-off gas represents about 0.15% of the volume per day. The daily rate is depending not only on the ship loading condition (loaded voyage about 0.15% and ballast voyage about 0.10%) but also varies with changes in barometric pressure, ambient temperature or sea condition.

#### **Re-liquefaction and boil-off control**

Because every LEG's/LPG's are fitted with a re-liquefaction plant and boil-off control, these represent one of the common features of these ships. But why we need a re-liquefaction plant? Basically because we need:

1. To cool down the cargo tanks before loading;
2. To re-liquefy the cargo vapors generated by flash evaporation and boil-off during loading and
3. To maintain cargo temperature and pressure. There are two types of re-liquefaction plants used nowadays: the indirect cycle plant (limited use, only for chlorine and ethylene oxide) and direct cycle plant, which is the most common.

On the other hand, the boil-off control is accomplished through different methods:

1. Send cargo boil-off to the re-liquefaction plant and back into cargo tank;
2. Use cargo boil-off as fuel;
3. Cooled cargo boil-off in a heat exchanger;
4. Cooled cargo tank shell.

First method of boil-off control is accomplished in the direct cycle re-liquefaction plant, which can be classified as:

1. Single-stage direct cycle, suitable for semi-pressurized cargoes like propane at high suction pressures; In order to prevent the re-vaporization, the liquid/vapour mixture may be either distributed in the cargo tank by spray rail at the top or taken to the bottom of the tank.
2. Two-stage direct cycle, used for the liquefied gas tankers handling wide range of products (especially butadiene and vinyl chloride) and having in addition an inter-stage cooling; This cycle is suitable where suction pressures are low. The vapours in the first stage are compressed in compressor and then the vapours are taken to an inter-stage cooler where its superheat is reduced. The cooling medium is cargo liquid flashed down to intercooler pressure from the SW cooled condenser. The rest are similar with the previous cycle.
3. Cascade direct cycle, used for fully refrigerated cargoes like ethylene. This cycle is used especially on board LEG's. There are two refrigeration plants working with 2 different refrigerants (cargo and R22) coupled by a double role heat exchanger (evaporator and condenser).

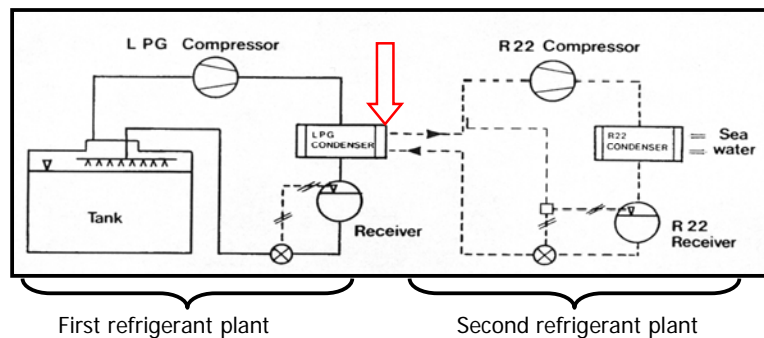


**Fig.9. Cascade direct re-liquefaction cycle**

The cycle is identical with single-stage direct cycle but the cargo condenser is cooled using R22 instead of sea water. We have to mention that, according to Montreal Protocol, R22 will be phased out in the near future (it is not an ozone friendly refrigerant).

#### 4. CONCLUSIONS

This paper represents an introduction to a very complex topic referring to thermodynamic processes and their application in cryogenics equipments. The paper was structured into 3 main chapters covering cryogenics, thermodynamic processes (basic concept of refrigeration, Carnot and inverted Carnot cycles and refrigeration methods) and cryogenic application in the maritime shipping (Gas Carriers) with emphasize on re-liquefaction process and boil-off control methods.

#### REFERENCES

- [1]. BEJAN A. - *Termodinamica Tehnică Avansata*, Editura Tehnica, București, 1996.
- [2]. MARTINEZ I. - *Thermodynamics of refrigeration and heat pumps*, Escuela Tecnica Superior Ingenieros Navales ETSIN UPM, Ciudad Universitaria, Madrid, 2004.
- \*\*\* IMO Model Course 1.06, 1999 and 2007 Edition – Specialised Training for Liquefied Gas Tankers, ISBN 92-801-6109-1.
- \*\*\* SIGTTO (Society of Intl' Gas Tanker and Terminal Operators), *Liquefied Gas Handling Principles on Ships and in Terminals*, Witherby Marine Publishing London, ISBN 1-85609-087-6, 3<sup>rd</sup> Edition, 1996.
- \*\*\* Note de Curs "Teoria și Construcția Navei", 2006, UMC.
- \*\*\* <http://www.solentwaters.co.uk/>
- \*\*\* <http://www.gastechnology.org/>
- \*\*\* <http://en.wikipedia.org/wiki/>

## INCOMPRESSIBLE MODELS AND LOW MACH NUMBER EXPANSIONS FOR SHALLOW WATERS

<sup>1</sup>VLADU GABRIEL, <sup>2</sup>GHERGHINA AUREL

<sup>1</sup>Research Center for Navy, Romania, <sup>2</sup>Military Staff, Romania

An asymptotic analysis starting from the Navies-Stokes equation derived for a compressible ideal gas shows that there is a lack of consistency between compressible models and 'incompressible' sub-models, in the presence of heat conduction. The paper presents three mathematical formulations of the governing equations and restricts our attention to the two-dimensional case.

**Keywords:** low Mach number, incompressibility

In the field of CFD, the incompressibility assumption is very important for applications since many common fluids (liquids) are incompressible or only very slightly compressible. Mathematically, **the incompressibility condition** means:

$$\operatorname{div}V = 0 \quad (1)$$

Therefore, the volume occupied by a group of fluid particles at the initial time remains constant during the flow. The continuity equation written as

$$\rho_t + u\rho_x + v\rho_y + w\rho_z + \rho(u_x + v_y + w_z) = 0$$

leads to

$$\frac{D\rho}{Dt} = \rho_t + V \cdot \nabla\rho = 0 \quad (2)$$

This means that if the density is initially constant and on the boundaries from where the fluid comes inside the domain under consideration it remains so. This is equivalent to say that the fluid is **homogeneous**.

Further, having in mind the previous derivation of the compressible models and their EOS and constitutive models, it could be useful to make a distinction between models obtained by:

1. **Incompressibility hypothesis.**
2. **Low Mach number expansions.**

We emphasize here that the incompressibility hypothesis does not impose an explicit restriction on the magnitude of the velocity. Moreover, the incompressible models aim to describe liquids where compression effects are neglected and **the density is taken as constant**. For example, it is not rational to expect from an incompressible model to describe

accurately the propagation of acoustic or pressure waves through liquids. This is due the fact that the incompressibility condition (1) is normally associated with other working hypothesis made on the EOS and on the fluid transport properties. Further, the energy equation is firmly 'decoupled' from the continuity and momentum equations, by stating that the temperature field can be calculated separately, after the velocity and pressure fields have been determined.

On the other side, the compressible models presented in the previous chapter are valid for gases. Starting from the compressible models it is rational to discuss about the low Mach number expansions. The precise definition of the Mach number is  $M = |V| \sqrt{\rho'(p)}$ . Therefore if we let  $M$  go to zero means that keeping constant values for density and temperature, the magnitude of the velocity is a small parameter. An asymptotic analysis starting from the Navies-Stokes equation derived for a compressible ideal gas shows that there is a lack of consistency between compressible models and 'incompressible' sub-models, in the presence of heat conduction. A possible physical explanation is the following assertion: compressible models are valid for gases and the low Mach number limit yields particular incompressible sub-models. These particular sub-models are definitively determined by the EOS and transport properties chosen for the gas. Further, such an asymptotic analysis reveals that the incompressible sub-model is very sensitive to the errors in the pressure calculation.

### 1. THE INCOMPRESSIBLE NAVIER-STOKES EQUATIONS IN PRIMITIVE VARIABLE FORM

The primitive variable formulation of the incompressible two dimensional Navier-Stokes equations is given by:

$$\begin{aligned}
 u_x + v_y &= 0 \\
 u_t + uu_x + vu_y + \frac{1}{\rho} p_x &= \nu [u_{xx} + u_{yy}] \\
 v_t + uv_x + vv_y + \frac{1}{\rho} p_y &= \nu [v_{xx} + v_{yy}]
 \end{aligned} \tag{3}$$

where the kinematic viscosity is:

$$\nu = \frac{\eta}{\rho} \tag{4}$$

Recall that  $\eta$  is the coefficient of shear viscosity. We have a set of three equations for the three unknown quantities  $\mathbf{u}$ ,  $\mathbf{v}$ ,  $\mathbf{p}$ , the primitive variables. This is a mixed elliptic-parabolic system. Due to the mixed nature of the mathematical model, the solution cannot be obtained directly via time-marching algorithms. In principal, given a domain along with initial and boundary conditions for the equations one should be able to solve this problem using the primitive variable formulation.

## 2. THE INCOMPRESSIBLE NAVIER-STOKES EQUATIONS IN STREAM-FUNCTION VORTICITY FORM

The stream-function vorticity formulation is another way of expressing the incompressible Navier-Stokes equations. This formulation is attractive for the two-dimensional case but not so much in three dimensions, in which the role of a stream function is replaced by that of a vector potential. The magnitude of the vorticity vector can be written as:

$$\zeta = v_x - u_y \quad (5)$$

Introducing a stream function  $\Psi$  we have for the velocity components:  $u = \Psi_y$ ,  $v = -\Psi_x$ . By combining the momentum equations so as to eliminate the pressure  $p$ , we obtain the **vorticity transport equation**:

$$\zeta_t + u\zeta_x + v\zeta_y = \nu[\zeta_{xx} + \zeta_{yy}] \quad (6)$$

This is an **advection-diffusion equation** of **parabolic** type. In order to solve it, one requires the solution for the stream function  $\psi$ , which is in turn related to the vorticity  $\zeta$  via:

$$\psi_{xx} + \psi_{yy} = -\zeta \quad (7)$$

This is called the **Poisson equation** and is of **elliptic type**. There are numerical schemes to solve (5)-(7) using the apparent decoupling of the parabolic-elliptic problem to transform it into the parabolic equation for the vorticity and the elliptic equation for the stream function. A relevant observation, from the numerical point of view, is that the convection terms of the left hand side of the equation can be written in conservative form and hence we have:

$$\zeta_t + (u\zeta)_x + (v\zeta)_y = \nu[\zeta_{xx} + \zeta_{yy}] \quad (8)$$

This follows from the fact that  $u_x + v_y = 0$ , which was also used to obtain.

## 3. THE INCOMPRESSIBLE NAVIER-STOKES EQUATIONS IN ARTIFICIAL COMPRESSIBILITY FORM

The artificial compressibility formulation is yet another approach to formulate the incompressible Navier-Stokes equations and was originally put forward by Chorine, for the steady case. Let us consider the two-dimensional incompressible Navier-Stokes equations written in non-dimensional form:

$$u_x + v_y = 0, \quad (9)$$

$$\begin{aligned} u_t + uu_x + vv_y + p_x &= \alpha[u_{xx} + u_{yy}] \\ v_t + uv_x + vv_y + p_y &= \alpha[v_{xx} + v_{yy}] \end{aligned} \quad (10)$$

where the following non-dimensionalisation has been used:

$$\begin{aligned} u &\leftarrow \frac{u}{V_\infty}, v \leftarrow \frac{v}{V_\infty}, p \leftarrow \frac{p}{\rho_\infty V_\infty^2}, \\ x &\leftarrow \frac{x}{L}, y \leftarrow \frac{y}{L}, t \leftarrow \frac{tV_\infty}{L}, \\ \alpha &= \frac{1}{ReL}, ReL = \frac{V_\infty L}{\nu}. \end{aligned}$$

Multiplying by the non-zero parameter  $c^2$  and adding an artificial compressibility term  $p_t$  the first equations reads:

$$p_t + (uc^2)_x + (vc^2)_y = 0 \quad (11)$$

The convective terms in the momentum equations can be written in conservative form, so that the modified system becomes:

$$\begin{aligned} p_t + (uc^2)_x + (vc^2)_y &= 0 \\ u_t + (u^2 + p)_x + (uv)_y &= \alpha[u_{xx} + u_{yy}] \\ v_t + (uv)_x + (v^2 + p)_y &= \alpha[v_{xx} + v_{yy}] \end{aligned} \quad (12)$$

The equations can be written in compact form as

$$U_t + F_x(U) + G_y(U) = S(U) \quad (13)$$

where the vectors of unknowns, fluxes and source terms are:

$$U = \begin{bmatrix} p \\ u \\ v \end{bmatrix}, F = \begin{bmatrix} c^2 u \\ u^2 + p \\ uv \end{bmatrix}, G = \begin{bmatrix} c^2 v \\ uv \\ v^2 + p \end{bmatrix}, S = \begin{bmatrix} 0 \\ \alpha(u_{xx} + u_{yy}) \\ \alpha(v_{xx} + v_{yy}) \end{bmatrix} \quad (14)$$

The above equations are called the artificial compressibility equations. Here  $c^2$  is the **artificial compressibility factor**, usually taken as a constant parameter. The 'source' term vector in this case is a function of second derivatives. Note that the modified equations are equivalent to the original equations in the steady state limit only. The left-hand side of the artificial compressibility equations forms a non-linear hyperbolic system.

More recently, new formulations have been proposed for the solution of steady and unsteady incompressible Navier-Stokes equations. Since time-marching methods cannot be applied directly, the system (12) must be transformed into a more convenient one. **The dual time approach** requires the addition of derivatives of a fictitious pseudo-time  $\tau$  to each of the three equations to give:

$$\begin{aligned} \frac{1}{\beta^2} p_\tau + p_t + (u)_x + (v)_y &= 0 \\ u_\tau + u_t + (u^2 + p)_x + (uv)_y &= \alpha[u_{xx} + u_{yy}] \\ v_\tau + v_t + (uv)_x + (v^2 + p)_y &= \alpha[v_{xx} + v_{yy}] \end{aligned} \quad (15)$$

where  $\beta$  is a parameter and the term added to the continuity equation has the same form as the basic artificial compressibility method. A steady-state solution in pseudo-time ( $\partial p / \partial \tau, \partial u / \partial \tau, \partial v / \partial \tau \rightarrow 0$ ) corresponds to an instantaneous unsteady solution in real time. A recommended value for the parameter  $\beta$  in the case the governing equations are written in dimensionless form is  $\beta \approx \Theta(1)$ . The convective part of the system (15) is of hyperbolic type and therefore a time-marching solution procedure is possible.

## REFERENCES

- [1]. Aftosmis M.; Gaitonde D.; Tavares T.S., *On the Accuracy, Stability, and Monotonicity of Various Reconstruction Algorithms for Unstructured Meshes*, AIAA Paper 94-0415, 1994
- [2]. Barth T.J.; Jespersen D.C., *The Design and Application of Upwind Schemes on Unstructured Meshes*, AIAA Paper 89-0336, 1989
- [3]. Frink N.T., *Upwind Scheme for Solving the Euler Equations on Unstructured Tetrahedral Meshes*, AIAA Journal, 30, 1992
- [4]. Godunov S.; Zabrodine A.; Ivanov M.; Kraiko A.; Prokopov G., *Résolution numérique des problèmes multidimensionnels de la dynamique des gaz*, Editions MIR, Moscou, 1979
- [5]. Stoia-Djeska M., *A Practical Introduction to Computational Fluid Dynamics*, EDP, Bucharest, 2005
- [6]. Hirsch C., *Numerical Computation of Internal and External Flows*, John Wiley & Sons, New York, 1988

## THE IMPACT ON EMISSIONS IN SW EUROPEAN SHORT SEA SHIPPING BASED ON MOPSEA EMISSION MODEL

<sup>1</sup>XAVIER MARTÍNEZ DE OSÉS F., <sup>1</sup>MARCEL-LA CASTELLS

<sup>1</sup>*Universitat Politècnica de Catalunya, Spania*

According to the mid-term review of the EU White Paper on Transport, Short Sea Shipping is expected to grow at a rate of 59% (metric tonnes) between 2000 and 2020. Even with Marpol Annex VI [1] in operation, the share of emissions from maritime transport can no longer be ignored because they would become increasingly important. There is an existing need to evaluate the impact of the maritime transport on emissions.

This paper analyses emissions of maritime transport in SW European Short Sea Shipping, considering actual routes and ships' particulars based on MOPSEA [2] emission model and the results of LAERTES [3] project carried out by TRANSMAR Research group. This paper will conclude proposing some results that would justify the need to reduce atmospheric emissions from sea-going vessels to compete with road transport mode. Policy makers have to be aware of the results and its effect on the current legislation for maritime transport.

**Keywords:** Euorepan short sea shipping, emission models, maritime environmental impact

### 1. INTRODUCTION

The European transport policy undertakes to enhance sustainability in transport in order to improve economic activities in the whole European Union. The reduction of pollutant emissions and a better equilibrium among modes of transportation to avoid road congestion are the pillars of the above policy. Although most developed countries boast a national network of roads to move freight despite road transport being the most expensive, pollutant mode, with the highest rate of fuel consumption per cargo unit, both public and private stakeholders have begun to use the freight rail and maritime options more extensively in search for a better alternative.

Maritime transport was and still is an environmentally friendly and safe mode of transport, especially compared to congested road transport. Additionally, it contributes to the reduction of traffic congestion on European roadways. In particular, Short Sea Shipping is considered the fastest way to sustainability. However, there is still considerable scope for improvement, especially with regard to NO<sub>x</sub> and SO<sub>2</sub> emissions.

Most of the international environmental legislation excludes guidelines with regard to emissions from vessels. The only internationally applied convention, is the Marpol 73/78 Convention that covers prevention of pollution of the marine environment by vessels from operational or accidental causes. The International Maritime Organization (IMO, 2005) adopted in 1997 (and entered in force on May 2005) Annex VI "prevention of air pollution from vessels". With this annex, worldwide limits have been placed on sulphur dioxide (SO<sub>2</sub>) and nitrogen oxide (NO<sub>x</sub>) emissions from vessels. Even with Marpol Annex VI in operation,

the share of emissions from vessels will increase in the future as the exhaust emissions of other transport modes decrease even more. This is due to the more severe emission standards and fuel specifications for road transport, railway traffic and inland navigation that came into force during the last decade. Recently, on a European level, a new EU Directive to reduce atmospheric emissions from vessels entered in force on 11 August 2005 (EU Directive 2005/33/EC).

The present paper is divided into four sections. First, we briefly discuss the state of art of the existing emission models for the assessment of emissions maritime transport used. Second, we explain in detail MOPSEA emission model, the data necessary and their methodology used in our calculations. In the next section, we explain in detail the LAERTES project. Finally, we obtain some results based in the MOPSEA model and some conclusions of this study.

## **2. STATE OF THE ART OF EMISSION METHODS FOR MARITIME TRANSPORT**

In this section we give an overview of the emission methods used for the assessment of maritime transport used in Europe. As far as environmental performance is concerned, several attempts have been made to estimate external costs in the transport sector. The most important results were obtained by some research projects, especially those within the 4th, 5th and 6th EU-framework programmes. Projects that conducted similar research are MEET (1999), RECORDIT (2001), ENTEC (2002), UNIT (2003), EMS (2003), TRENDS (2003), INFRAS (2004), ExternE (2005) REALISE (2005), MOPSEA (2006), EMMOSS (2007), EMSA (2007) and iTREN-2030 (2007), and IMO proposals.

MEET [4] stands for Methodologies for Estimating air pollutant Emissions from Transport. MEET is a methodology for calculating the emissions from maritime transport among the methodology for the other transport modes. RECORDIT [5] (and thus REALISE) results were expressed at emission factor costs.

ENTEC [6] is an analysis to quantify the ship emissions of SO<sub>2</sub>, NO, CO<sub>2</sub> and hydrocarbons in the North Sea, Irish Sea, English Channel, Baltic and Mediterranean Sea. EMS [7] stands for Emission registration and Monitoring for Shipping had as target to map the different emissions from sea-going vessels and inland shipping for the Netherlands. TRENDS [8] stands for TRAsnport and ENVironment Database System. TRENDS is a methodology to determine the emissions from the four most important transport modes: road, rail, shipping and aviation.

INFRAS [9] develops estimates of accidents, noise, air pollution, climate change risks, other environmental and non-environmental effects, and congestion for four modes (road, rail, air and water transport) in 17 European countries for 1995 and 2010 whereas ExternE [10] is a methodology, provides a framework for transforming impacts that are expressed in different units into a common unit –(monetary values).

The maritime transport emission model REALISE [11] determines both SO<sub>2</sub>, NO<sub>x</sub>, CO, nm-VOC y PM (local contamination), CO<sub>2</sub>, CH<sub>4</sub> and S (global contamination) and pollution, accidents and noise. On the other hand, the maritime transport emission model MOPSEA accounts for the energy consumption as well as the carbon dioxide (CO<sub>2</sub>), sulphur dioxide (SO<sub>2</sub>) (based on technology of the engine) nitrogen oxides (NO<sub>x</sub>), carbon monoxide (CO), hydrocarbons (HC) and particulate matter (PM) exhaust emissions (type of fuel) of transport activities from sea-going vessels.

EMMOSS [12] intends to determine emissions caused by railway, inland waterway and seagoing vessels, for transport of people as well as goods on Flemish territory, EMSA [13] treats about the revision of MarPol Annex VI in 2007 and finally, iTREN-2030 [14] is an

analysis tool for transport in the European Union, covering transport, energy, environment and economy in 2030.

### 3. MOPSEA EMISSION MODEL

MOPSEA is an activity-based emission model to determine emissions from sea-going vessel. In this section we have developed an emission model based on MOPSEA model for our specific area, European Short Sea Shipping. For our calculations, we have developed an Excel program with different spreadsheets.

The following criteria are considered:

- a) Is designed to calculate emissions and energy consumption for the different stages of navigation for every voyage and hotelling period. The percentage of MCR is dependant of the stage of navigation. For our purposes, the selected engine load was fixed to 85% of engine load for the cruise speed stage, 40% of engine load for the reduced speed stage, 20% for the manoeuvring stage [15].
- b) Provides two different types of main engine: 2-stroke engine and 4-stroke engine. The model uses different methodology for 2-stroke engine, 4-stroke engine and auxiliaries engines and is dependant of the year of construction of the engine.
- c) The used power of the main engines is dependant on the speed of the vessels and on rates of flow. This is taken into account through the combination of duration and used power for every stage of navigation.
- d) The model makes a distinction between technology related emissions and fuel related emissions.

For every voyage, the characteristics of the vessels and the characteristics of the route are known:

**Table 1: Calculation of initial data based on MOPSEA model**

Characteristics of the sea-going vessels
Ship type
Length (m)
Main engine type
Fuel type
Power main engine (kW)
Date of building
RPM Main engine
Speed (knots)
Power auxiliary engine (kW)
Date of building auxiliary engine
Auxiliary engine type
Characteristics of the route
Distance (km)
Duration of the total voyage
Cruising speed time (h)
Reduced speed time (h)
Manoeuvring time (h)
Hotelling time (h)

The above data allows assessment of the emissions for the maritime transport calculated from the MOPSEA model and are divided in fuel related emissions and technology related emissions.

The fuel related emission factors for CO<sub>2</sub> and SO<sub>2</sub> are modelled as a combination of the following factors:

**Table 2: Emission factors related on type of fuel**

Energy use (kW·h)
Basic emission factor
Correction dependant on the year of the vessels
Correction NOx restrictions

The technology related emission factors for HC, CO NOx and PM are modelled as a combination of the following factors:

**Table 3: Emission factors related on technology of the engine**

Energy use (kW·h)
Basic emission factor
Correction dependant on the year of the vessels
Correction NOx restrictions
Correction factor for % of MCR

With all these factors, we can develop a new spreadsheet with the results considering the different stages of navigation:

**Table 4: Table of results considering both type of emissions and different stages of navigation**

Cruise speed stage
Emissions Technology of the engine ( Tm )
Emissions Type of fuel ( Tm )
Reduced speed stage
Emissions Technology of the engine ( Tm )
Emissions Type of fuel ( Tm )
Manoeuvring stage
Emissions Technology of the engine ( Tm )
Emissions Type of fuel ( Tm )
Hotelling stage
Emissions Technology of the engine ( Tm )
Emissions Type of fuel ( Tm )
<b>Total Emissions ( Tm )</b>

#### 4. THE LAERTES PROJECT AND PREVIOUS RESEARCH

To estimate the emissions from maritime transport as good as possible, we have preferred to use the MOPSEA methodology than REALISE model because MOPSEA model uses more accurate parameters for the calculation of the emissions compared with REALISE model, data obtained in LAERTES project.

To use this methodology is necessary detailed statistical data relate on SW Short Sea Shipping routes for the year 2009. The data of SW Short Sea Shipping fleet and traffic in May 2009 between Spain and Europe is based on project “Análisis de la aplicación del ecobono, en los tráficos marítimos españoles” carried out for the TRANSMAR research group in the Department of Nautical Science and Engineering of the Universitat Politècnica de Catalunya in 2009.

We have selected a total of 29 routes between Spain and Europe These are the actual (May 2009) Short Sea Shipping routes and all of them leave from Spanish ports and have different destinations in Western Europe (Table 5).

**Table 5: Routes selected in our analysis**

<b>Route 1</b>	Barcelona-Civitavecchia
<b>Route 2</b>	Barcelona-Genoa
<b>Route 3</b>	Barcelona-Fos Sur Mer
<b>Route 4</b>	Barcelona-Livorno
<b>Route 5</b>	Valencia-Salerno
<b>Route 6</b>	Valencia-Livorno
<b>Route 7</b>	Valencia-Palermo
<b>Route 8</b>	Tarragona-Salerno
<b>Route 9</b>	Tarragona-Livorno
<b>Route 10</b>	Tarragona-Civitavecchia
<b>Route 11</b>	Vigo-Livorno
<b>Route 12</b>	Barcelona-Marseilles
<b>Route 13</b>	Valencia-Marseilles
<b>Route 14</b>	Valencia-Pireus
<b>Route 15</b>	Barcelona-Koper
<b>Route 16</b>	Barcelona-Pireus
<b>Route 17</b>	Bilbao – Zeebrugge
<b>Route 18</b>	Bilbao – Antwerp
<b>Route 19</b>	Pasajes-Vlissingen
<b>Route 20</b>	Santander-Zeebrugge
<b>Route 21</b>	Pasajes-Zeebrugge
<b>Route 22</b>	Vigo-Zeebrugge
<b>Route 23</b>	Vigo-Bremerhaven
<b>Route 24</b>	Santander-Emden

<b>Route 25</b>	Santander-Cuxhaven
<b>Route 26</b>	Vigo-Saint Nazaire
<b>Route 27</b>	Bilbao - Kotka
<b>Route 28</b>	Santander-Kotka
<b>Route 29</b>	Bilbao - Le Havre

These 29 selected routes are served, in May 2009, by a total of 35 Ro-Ro and Ro-Pax vessels. The selected Ro-Ro and Ro-Pax vessels' particulars are shown in Table 6:

**Table 6: Ro-Ro and Ro-Pax vessels' particulars selected in our analysis**

Vessels	Speed (knots)	Length (m)	Power ME (kW)	Year ME
Cruise Roma	27.5	225	55440	2008
Eurostar Barcelona	32	211.9	50424	2001
Eurostar Roma	27	173.7	31680	1995
Majestic	23	188,2	36000	1993
Splendid	23	214.14	36000	1994
Excellent	23	202,83	25952	1998
Excelsior	24	202	28944,8	1999
Fantastic	23	188	36000	1996
La Surprise	20	141.25	12960	2000
Florenzia	23	186	21600	2004
Eurocargo Valencia	20	195	12510	1999
Eurostar Salerno	24	186.4	18900	2003
Eurostar Valencia	24	186.4	18900	2003
Setúbal Express	17.8	169.4	9720	1992
Salerno Express	16	140.11	4487	1982
Malta Express	18	126.5	11032	1980
Sorrento	24	186.4	18900	2003
L'Audace	20	142	12960	1999
Arroyo Frío Dos	14	107.91	4796	1985
Arabian Breeze	18	164	7943	1983
Yohjin	18	164	7943	1983
Carlo Morace	18	135	11032	1981
Neptune Okeanis	20	164.4	12600	2005
Neptune Thelisis	20	164.4	12600	2006
Grand Benelux	20.1	176.7	11060	2001
Neptune Hellas	15.7	105.54	3884	1979
Valmont Express	17.5	122.8	7356	1982
Elisabeth Russ	20	153.43	11030	1999
Friedrick Russ	20	153.43	11030	1999

<b>Birka Carrier</b>	20	154.5	15600	1998
<b>Birka Express</b>	20	154.5	15600	1998
<b>M/V Autoprider</b>	20	126.9	9440	1997
<b>M/V Autoprogress</b>	20	126.9	9440	1998
<b>M/V Autoracer</b>	20	119.9	9000	1994
<b>M/V Autorunner</b>	20	119.9	9000	1994
<b>M/V Autosun</b>	20.9	140	16800	2000
<b>Australian Highway</b>	16.7	154.51	6840	1981
<b>Borden</b>	17	142.34	8780	1977
<b>Super Fast Levante</b>	22	158	25204	2001
<b>Birka Transporter</b>	16.5	122	5880	1997
<b>Misana</b>	20	165.75	15000	2007
<b>Misida</b>	20	165.75	15000	2007
<b>Repubblica Argentina</b>	20	208,82	17780	1998
<b>Grande Buenos Aires</b>	19.6	214	18280	2004
<b>Grande Francia</b>	19.6	214	18280	2002
<b>Grande San Paolo</b>	19.6	214	18280	2003
<b>Grande Basile</b>	18.5	214	15540	2000
<b>Repubblica del Brasil</b>	19	206	17771	1998

Some of these routes are served for different vessels, and some of these vessels sails in different routes. The following are the results for Route 1, i.e. between Barcelona port and Civitavecchia port with Cruise Roma Ro-Pax vessel considering both emission methods:

**Table 7: Emission parameters in selected route based on MOPSEA mode**

Emissions Technology of the engine ( Tm )		Emissions Type of fuel ( Tm )	
<b>Cruise speed stage</b>		<b>Cruise speed stage</b>	
HC	0.393	CO <sub>2</sub>	538.70
CO	3.469	SO <sub>2</sub>	0.70
NOx	10.363	<b>Reduced speed stage</b>	
PM	0.232	CO <sub>2</sub>	31.76
<b>Reduced speed stage</b>		SO <sub>2</sub>	0.04
HC	0.023	<b>Manoeuvring stage</b>	
CO	0.205	CO <sub>2</sub>	7.94
NOx	0.611	SO <sub>2</sub>	0.01
PM	0.014	<b>Hotelling stage</b>	
<b>Manoeuvring stage</b>		CO <sub>2</sub>	0.86
HC	0.006	SO <sub>2</sub>	0.00
CO	0.051		
NOx	0.153		
PM	0.003		
<b>Hotelling stage</b>			

HC	0.002
CO	0.009
NOx	0.048
PM	0.004

**Table 8: Global Emission in selected route based on MOPSEA model**

<b>Cruise speed stage</b>	
Emissions Technology of the engine ( Tm )	14.46
Emissions Type of fuel ( Tm )	539.40
<b>Reduced speed stage</b>	
Emissions Technology of the engine ( Tm )	0.85
Emissions Type of fuel ( Tm )	31.80
<b>Manoeuvring stage</b>	
Emissions Technology of the engine ( Tm )	0.21
Emissions Type of fuel ( Tm )	7.95
<b>Hotelling stage</b>	
Emissions Technology of the engine ( Tm )	0.06
Emissions Type of fuel ( Tm )	0.86

The results in the below tables allow estimation of the total emission with a vessel in one Short Sea Shipping route applying model above mentioned.

## 5. RESULTS FROM THE ANALYSIS

Routes	Vessel	MOPSEA RESULTS (Tm)
<b>Barcelona - Civitavecchia</b>	Vessel 1	595.59
	Vessel 2	470.95
	Vessel 3	346.6
<b>Barcelona - Genoa</b>	Vessel 1	372.25
	Vessel 2	372.25
	Vessel 3	267.19
	Vessel 4	286.7
	Vessel 5	370.66
<b>Barcelona - Fos Sur Mer</b>	Vessel 1	85.49
<b>Barcelona - Livorno Valencia - Salerno</b>	Vessel 1	244.62
	Vessel 1	295.04
	Vessel 2	375.09
	Vessel 3	375.09

	Vessel 4	232.35
	Vessel 5	120.04
<b>Valencia - Livorno</b>	Vessel 1	50.06
	Vessel 2	121.13
	Vessel 3	158.08
<b>Valencia - Palermo</b>	Vessel 1	335.65
	Vessel 2	207.71
<b>Tarragona- Salerno</b>	Vessel 1	307.76
<b>Tarragona - Livorno</b>	Vessel 1	96.45
<b>Tarragona - Civitavecchia</b>	Vessel 1	205.88
<b>Vigo - Livorno</b>	Vessel 1	389.73
	Vessel 2	389.73
	Vessel 3	540.92
<b>Barcelona - Marsella</b>	Vessel 1	83.13
	Vessel 2	83.13
<b>Valencia - Marsella</b>	Vessel 1	146.21
	Vessel 2	146.21
<b>Valencia - Pireo</b>	Vessel 1	497.91
	Vessel 2	497.91
	Vessel 3	435.04
<b>Barcelona - Koper</b>	Vessel 1	205.15
<b>Barcelona - Pireo</b>	Vessel 1	311.94
<b>Bilbao – Zeebrugge</b>	Vessel 1	251.31
	Vessel 2	251.31
<b>Bilbao – Antwerp</b>	Vessel 1	341.75
	Vessel 2	341.75
<b>Pasajes-Vlissingen</b>	Vessel 1	221.4
	Vessel 2	221.4
	Vessel 3	212.03
<b>Santander-Zeebrugge</b>	Vessel 1	208.46
	Vessel 2	208.46
	Vessel 3	199.64
<b>Pasajes-Zeebrugge</b>	Vessel 1	220.52
	Vessel 2	220.52
	Vessel 3	211.19
<b>Vigo - Zeebrugge</b>	Vessel 1	234
	Vessel 2	417.74
<b>Vigo-Bremerhaven</b>	Vessel 1	554.06
<b>Santander-Emden</b>	Vessel 1	215.59
<b>Santander-Cuxhaven</b>	Vessel 1	315.13
<b>Vigo-Saint Nazaire</b>	Vessel 1	377.95
<b>Bilbao - Kotka</b>	Vessel 1	435.05
<b>Santander-Kotka</b>	Vessel 1	905.56

	Vessel 2	905.56
<b>Bilbao - Le Havre</b>	Vessel 1	295.94
	Vessel 2	309.87
	Vessel 3	309.87
	Vessel 4	309.87
	Vessel 5	278.55
	Vessel 6	310.69

## 6. CONCLUSIONS AND FURTHER RESEARCH

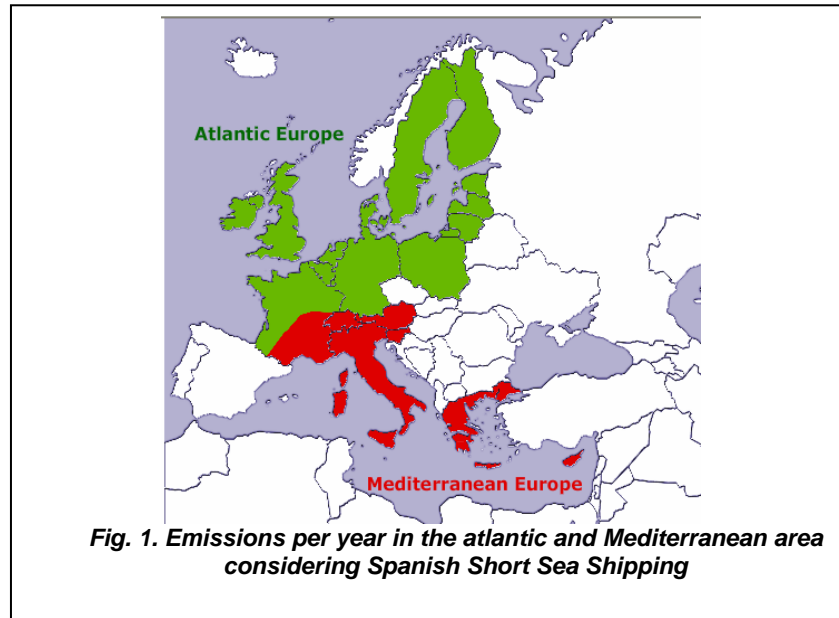
Table 10 gives an overview of what is considered in MOPSEA methods:

**Table 9: Parameters and differences considered in MOPSEA method**

	<b>MOPSEA model</b>
<b>Routes</b>	Actual routes in Mediterranean Short Sea Shipping between Spain and Europe.
<b>Vessels</b>	Actual Ro-Ro (and Ro-Pax) in Short Sea Shipping between Spain and Europe.
<b>Stages of navigation</b>	<ul style="list-style-type: none"> <li>- Cruise speed</li> <li>- Reduction speed</li> <li>- Manoeuvring</li> <li>- Hotelling</li> </ul>
<b>Emission parameters</b>	<ul style="list-style-type: none"> <li>- <b>Technology of the engine:</b> CO<sub>2</sub> and SO<sub>2</sub>.</li> <li>- <b>Type of fuel:</b> NO<sub>x</sub>, CO, HC, PM.</li> </ul>
<b>Engine</b>	<ul style="list-style-type: none"> <li>- <b>Main engine:</b> Type, fuel, power, rpm and date of building).</li> <li>- <b>Auxiliary engine:</b> Type, power and date of building).</li> </ul>

Table 11 shows the results of emissions of vessels for the year 2009 in Short Sea Shipping routes considering MOPSEA emission model. If we know all Short Sea Shipping routes in SW Europe (departing or arriving in a Spanish port), the characteristics of the vessels and the frequency of each route, we can calculate the total amount of emissions per year in this area obtaining a total amount of 1701775 Tm of emissions from maritime transport in this area.

Next figure shows the total amount of emissions from maritime transport if we are considering the Atlantic and the Mediterranean zones.



Emissions from maritime shipping become important and emission reductions from maritime transport and in harbours are to be considered. These results would justify the need to reduce atmospheric emissions from sea-going vessels to compete with road transport mode. Policy makers have to be aware of the results of such comparison and its effect on the current legislation for maritime transport.

Data obtained can be used for further research, affording prediction of emissions in the near future by keeping in mind the traffic and fleet evolution and the existing legislation.

## REFERENCES

- [1]. MarPol 73/78 Convention is the main international convention that covers prevention of pollution of the maritime transport. The International Maritime Organization adopted in 1997 Annex VI, prevention of air pollution from vessels.
- [2]. Gommers, A et al. *MOntoring Programme on air pollution from SEA-going vessels Project*, 2007, Belgium.
- [3]. Martínez F.X. and Castells M. *Análisis de la aplicación del ecobono, en los tráficós marítimos españoles*. Laertes Project funded by the Ministry of Spanish Public Works , 2009, Barcelona. (Spanish)
- [4]. MEET. *Methodology for calculating transport emissions and energy consumption*, Transport research, Fourth Framework Programme, Strategic Research, DG VII, 1999, ISBN 92-828-6785-4.
- [5]. RECORDIT. *Real cost reduction of door-to-door intermodal transport*. AMRIE, 2001.
- [6]. ENTEC. *Quantification of emissions from ships associated with ship movements between ports in the European Community*. Final report for the European Commission, July 2002.
- [7]. EMS. *Emission inventory and monitoring of shipping*. Dutch Adviesdienst Verkeer en Vervoer (AVV), 2003.
- [8]. TRENDS. *Calculations of Indicators of Environmental Pressure* caused by Transport. European Commission, 2003.

- [9]. INFRAS. **Report evaluating transport external costs**, funded by UIC, 2004.
- [10]. ExternE Project: **Externalities of Energy**. Supported by the EU, 2005. [www.externe.info]
- [11]. REALISE Project: Regional Action for Logistical Integration of Shipping across Europe. 2005, AMRIE. [http://www.realise-sss.org]
- [12]. EMMOSS. **Emission model for maritime, inland waterway and rail for Flanders**. Transport & Mobility Leuven, 2007.
- [13]. EMSA. **Air emissions from ships working paper to inform member states' discussions in relation to the revision of MARPOL Annex VI**, Workshops on air emissions from ships, 2007.
- [14]. iTREN-2030. **Network analysis tool for transport in the EU, scenario forecast for 2030 covering transport, energy, environment and economy**. EU project, 2007.
- [15]. These assumptions are taken from the project EMS, November 2003.



### **For Authors**

Are edited scientific papers in topics, written in English. Papers are selected after a peer review. Each participant is allowed to send maximum 2 papers as first author. Authors should make sure that the manuscripts submitted are ready for refereeing. The papers that are to be published must bring scientific contributions to the journal. The papers also have to contain the results of some of your work. It is strongly recommended an even number of pages, no longer than 6-10 pages. The papers that do not respect the publishing conditions and which are not integrated in the thematic of this journal will be rejected from the start by the Editorial Board. Authors submitting an article affirm that the same manuscript is not concurrently submitted to another publication. The authors are entirely responsible for the content of their papers.

**PUBLISHED SINCE 2008**

**ISSN:1844-6116**

**ON LINE SINCE: 2008**

**PUBLISHED BY: Editura Nautica/ Constanta Maritime University**